# Exploiting the Architectural Features of Various Macromolecules for Biomimetic Applications

## Georgia Mann

**Department of Chemistry**

**The University of Sheffield**

Submitted to the University of Sheffield

In fulfilment of the requirements for the degree of

Doctor of Philosophy

September 2013

## Declaration

I hereby declare that the research discussed has not been submitted, either entirely or partly, for this or any other degree. All the work presented in this thesis is the original work of the author, except where other sources have been acknowledged by references. This work was carried out at the University of Sheffield between October 2009 and September 2013.

Signature: ...................................................................................................

Georgia Mann

Date: ......................

# Acknowledgements

First and foremost I would like to express my sincere gratitude to my supervisor Dr. Lance Twyman. Thank you for your on-going support and expertise throughout the course of my studies. Without your guidance, patience and encouragement, this thesis would not have been possible.

This work would not have been possible without the help of many colleagues, so I would like to express my gratitude to the following people: Dr. Brian Taylor and Susan Bradshaw for help with NMR, Melanie Hannah for all the technical help over the years, Harry Adams for help with X-Ray, Keith Owen for Grubbs training and technical help, Paul Turner for his computer knowledge, Richard Bottomley for help with GC, Simon Thorpe for Mass spectrometry, Dan Jackson for glass repair, Svetomir Tzokov for TEM imaging, Amy Walsh and Tom Swift for help with fluorescence and Kate Kirkham and Mark Williams for colloidosome preparation. I would also like to express my thanks to Pauline Boulding, Pete Farran, Nick Smith, Louise Brown-Leng and Denise Richards, you have all shown me such kindness, made me laugh and helped me enormously over the years and I am extremely grateful to you all.

In addition, I would like to express my gratitude to everyone on F floor for providing an enjoyable and relaxed work environment. I have made many friends over the years and my experience working on F floor has been a thoroughly enjoyable one. A special thank you must go to Dr. Adam Ellis, your friendship and expertise over the last three years has helped me hugely and I am extremely thankful. Furthermore, I would like to convey my sincere appreciation to my friends and colleagues Jason Loader, Victoria Lovett, Lara James, Aj Cankut, Luke Cartwright, Mike Walker and Kuljit Dyal. Thank you all for your friendship, helping me preserve my sanity and for making my PhD a much more enjoyable experience.

My final thanks must go to my mum and dad and my sisters. Thank you for your continued love and support, without which none of this would be possible. Thank you for not only believing in me, but putting up with me through the difficult times as I know it could not have been easy. I love you all with all my heart and I am eternally grateful for all you have done for me.

*For Katrina,*


*You are the greatest friend I could have hoped for and I miss you every day*

# Abstract

This research has examined a variety of different macromolecules; namely dendrimers, hyperbranched polymers, di-block co-polymers and colloidosomes. The architecture of these materials has been exploited for a variety of applications.

The first area studied involved exploiting the peripheral groups of dendrimers. This project continued on from previous results within the group which showed a size based mechanism for dendrimer-protein interactions. The mechanism for complexation of a dendrimer and a protein was probed by CD spectroscopy and results revealed that, upon complexation, the protein's structure does not change and binding takes place at the active site entrance of the interfacial area.[1] Continuing on from this work, fluorescent labelled PAMAM dendrons (G1.5 and G2.5), provided by Professor Neil Mckeown of Cardiff University, were used in a direct binding assay with cytochrome-c. G1.5 and G2.5 both showed strong interaction, giving association constants of $4.2 \times 10^4$ ($\pm 2.5\%$) and $3.2 \times 10^4$ ($\pm 2\%$) respectively. However, unusual stoichiometries were observed.

The next area of study focussed on the interior properties of hyperbranched polymers. This work looked at controlling the environment surrounding a receptor and anion binding was the tool used to probe these properties. Hyperbranched poly 3, 5 diacetoxybenzoic acid of varying molecular weights was used to house an anion receptor and the effect upon binding affinities of a variety of anions was measured. The polymer had a negative effect upon binding the tetrahedral dihydrogen phosphate anion. A similar effect was also observed for the smaller spherical anions (fluoride and chloride). However, a different observation was made for the larger spherical anions (bromide and iodide), where binding appears to be stronger in the polymeric receptors than in the free receptor. For the non-spherical anions, benzoate and acetate, the binding was similar when the small and medium sized polymers were used (1,600 and 4,000 respectively), although, binding dropped significantly for the highest molecular weight studied (10,500).

For a water-soluble anion receptor system a different approach was employed. This consisted of a biocompatible di-block co-polymer micelle composed of poly (ethylene glycol) and poly ($\varepsilon$-caprolactone) (mPEG-b-PCL$_n$). A variety of hyperbranched polymers were encapsulated. Encapsulation was verified by particle sizing, UV/Vis spectroscopy and TEM imaging.

The final area studied continued the theme of encapsulation using di-block polymers. The work involved collaboration with Professor Steve Armes, where the encapsulation properties of colloidosomes were probed using catalysis. The reaction studied was the oxidation of cyclooctene using a porphyrin catalyst, which was situated within the oil phase of the colloidosome. Results showed an increase in the yield of products when the reaction took place within the colloidosome. Furthermore, a change in product distribution was also observed.

# Abbreviations

**AIST -** Integrated Spectral Database System of Organic Compounds

**Asp -** Aspartic acid

**APAF1 -** Apoptopic protease activating factor

**AP -** Alkaline Phosphatase

**AS -** Active site

**ATP -** Adenosine triphosphate

**Au DENPs –** Dendrimer encapsulated gold nanoparticles

**BNCT -** Boron Neutron Capture Therapy

**BTNA -** N-benzoyltyrosine-p-nitroanilide

**CD** - Circular Dichroism

**CDCl$_3$ -** Deuterated chloroform

**CMC** - Critical micelle concentration

**Cyt $c$ -** Cytochrome $c$

**Chy -** α-Chymotrypsin

**$^{13}$C-NMR** - Carbon Nuclear Magnetic Resonance Spectrometry

**D -** Dendritic unit

**DB -** Degree of Branching

**DDQ** - 2, 3 – Dichloro-5, 6-dicyano- $p$-benzoquinone

**DLS -** Dynamic Light Scattering

**d$^6$-DMSO -** Deuterated dimethyl sulfoxide

**DNA -** Deoxyribonucleic acid

**D$_2$O -** Deuterated Water

**EDA** - Ethylene diamine

**ES MS -** Electrospray Ionisation Mass Spectrometry

**EtOH -** Ethanol

**FDA** - Food and drug association

**FTIR -** Fourier Transform Infrared Spectroscopy

**G -** Generation

**GC** - Gas Chromatography

**Gd -** Gadolinium

**Gly** - Glycine

**GPC -** Gel Permeation Chromatography

**Hb -** Haemoglobin

**HBP -** Hyperbranched Polymer

**HCL** - Hydrochloric acid

**HLB -** Hydrophobic-lipophile balance

**$^1$H-NMR** - Proton Nuclear Magnetic Resonance Spectrometry

**HOMO -** Highest Occupied Molecular Orbital

**HPLC -** High-Performance Liquid Chromatography

**IL -** Interleukin

**iNOS -** Inducible nitric oxide synthase

**IR -** Infrared Spectroscopy

**$K_d$ -** Dissociation constant

**L -** Linear Unit

**LUMO** - Lowest Occupied Molecular Orbital

**MRI** - Magnetic Resonance Imaging

**MALDI-TOF-MS -** Matrix Assisted Laser Desorption Ionisation Time Of Flight Mass Spectroscopy

**Mb -** Myoglobin

**$M_n$ -** Number Average Molecular Weight

**MS -** Mass Spectrometry

**$M_w$ -** Weight Average Molecular Weight

**NLO -** Non-linear optical

**Nm -** Nanometre

**NMP -** 1-Methyl-2-pyrrolidinone

**NP -** Nanoparticle

**NSAID** - Non-steroidal anti-inflammatory drug

**NTA -** Nitro triacetate

**O/W -** Oil-in-water

**PAA -** Poly (acrylic acid)

**PAMAM -** Poly (amidoamine) dendrimer

**PCL** - Poly (ε-caprolactone)

**PDB -** Protein Data Bank

**PEG** - Poly (ethylene glycol)

**PEO** - Poly (ethylene oxide)

**PD -** Polydispersity

**PDMAEMA -** Poly(dimethylaminoethyl methacrylate)

**PEI** - Polyethyleneimine

**PG** - Phosphatidyglycerol

**PLA** - Poly (lactide)

**PMMA** - Poly (methyl methacrylate)

**PPG-TDI -** Polymeric diisocyanate (tolylene 2, 4-diisocyanate-terminated poly (propylene glycol)

**PPI -** Poly propylene immine

**Ppm -** Part per million

**PS -** Polystyrene

**RI -** Refractive index

**ROMP -** Ring Opening Multi-branching Polymerisation

**ROP** - Ring Opening Polymerisation

**RNA -** Ribonucleic acid

**SVCP -** Self-Condensing Vinyl Polymerisation

**T -** Terminal Unit

**TAPP -** Tetraacetoxyphenyl porphyrin

**TEA -** Triethylamine

**TEM -** Transmission Electron Microscopy

**THF -** Tetrahydrofuran

**TFA** - Trifluoroacetic acid

**TMODS -** Trimethoxy (octadecyl) silane

**TNF-α** - Tumour necrosis factor alpha

**TPP -** Tetraphenyl porphyrin

**UV/vis -** Ultraviolet-visible

**W/O** - Water-in-oil

**µM -** Micrometer

**NMR Abbreviations**

**s** - singlet

**d** - doublet

**t** - triplet

**q** - quartet

**m** – multiplet

**br** - broad

*o* *- ortho*

*m* *- meta*

*p* *- para*

# Table of Contents

# Chapter 1

## Introduction to Dendritic Polymers

# Chapter 1 - Introduction to Dendritic Polymers

## 1.1 General introduction to dendritic polymers

Dendritic polymers represent a moderately novel aspect of polymer chemistry which, up until around 25 years ago, focussed primarily on linear polymers. Linear polymers still remain a focal point in research today; however, present day research now directs a great deal of attention towards dendritic macromolecules. The interest in dendritic polymers has increased at an accelerated pace since the work by Tomalia[2], Vogtle[3] and Newkome,[4] with particular focus on dendrimers and hyperbranched polymers.

The study of dendritic polymers has developed over the years, ranging from synthesis and properties to potential applications. As a result, many dendrimers and hyperbranched polymers are available, with some specific dendrimers even being available commercially.[5] The main objective of this chapter is to supply the reader with the necessary information required to grasp the subjects' specific concepts, which will be employed in this area of research. This review is not an extensive account and for this the reader is directed to a number of recommended reviews in the literature.[2, 6-10]

### 1.1.1 Traditional polymer architectures

Primarily it was considered that there were three main structural classes for polymeric molecules; linear, branched and cross-linked (**figure 1**)**.** Linear polymers are comprised of monomer units that have been linked together in a continuous fashion, thereby generating a polymer molecule. A branched polymer is a molecule where linked monomer units form side branches; subsequently, these extend outwards from diverse branching points along the main polymer chain. Finally, a cross-linked polymer occurs when a bond is formed between individual polymer chains; either between parts of the same chain, or linking different chains together to create a polymer network.[11] With these structural classes of polymers, the process required to generate the necessary architectures is largely statistical. As a result, products

which display a high level of polydispersity and limited structural control are fabricated.

Linear Polymer                    Branched Polymer                    Cross linked Polymer
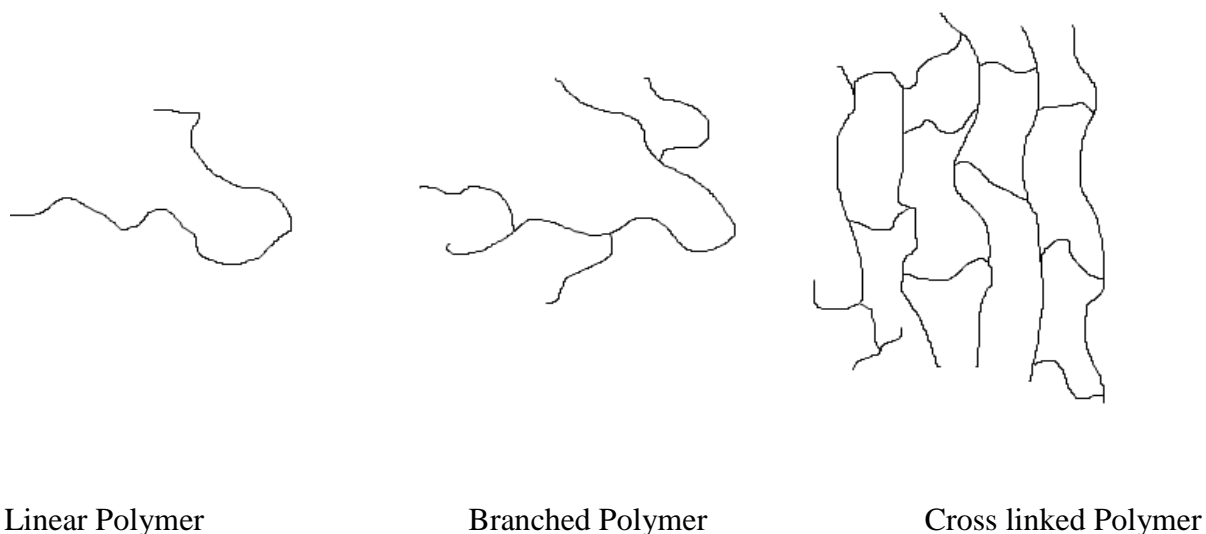
**Figure 1** − Figure to illustrate the three traditional classes of polymer adapted with permission from [Esfand, R.; Tomalia, D. A. *Drug Discovery Today* **2001**, *6*, 427]. Copyright [2001] Elsevier.[12]

### 1.1.2 Dendritic polymers

Synthetic strategies used to generate structure controlled macromolecules were discovered from as early as the 1970's, bringing to pass a novel class of polymer termed dendritic. There are a variety of different types of dendritic polymers; dendrons, dendrimers, linear-dendritic hybrids, dendrigrafts, dendronised polymers, hyperbranched polymers, star polymers and hypergrafted polymers. These subclasses can be seen overleaf in **figure 2**. It is apparent that there is a wide array of architectures which fall into this category.[12] However; this chapter will focus on dendrimers and hyperbranched polymers specifically, as they are used in the upcoming chapters.
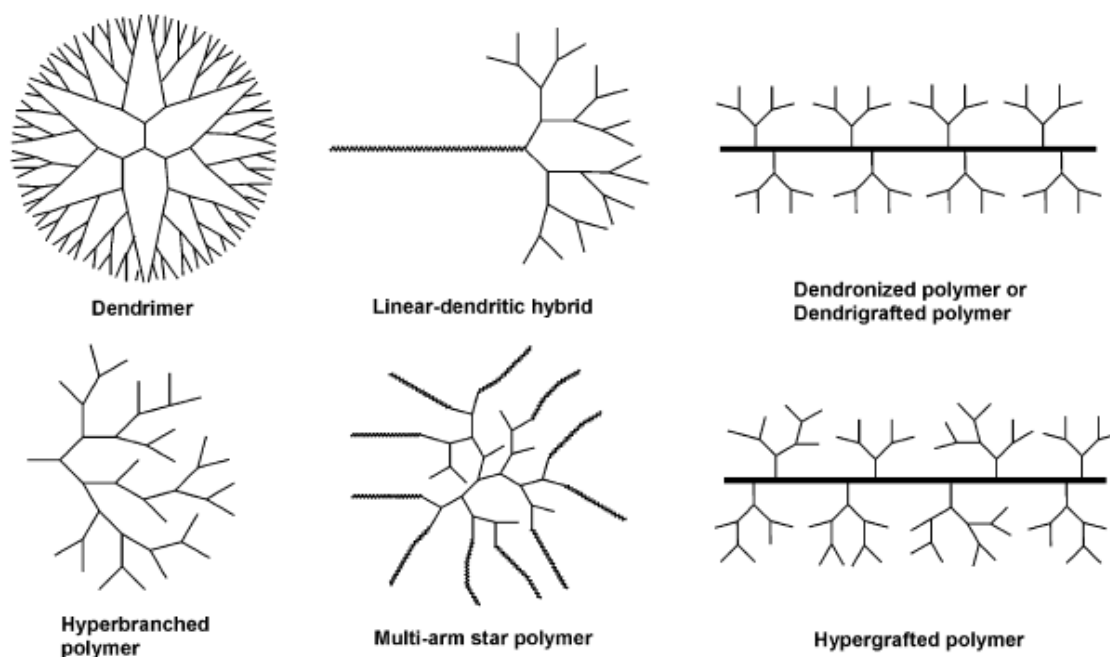
**Figure 2** – Figure to illustrate the subclasses of dendritic polymers, reprinted with permission from [Gao, C.; Yan, D. *Prog. Polym. Sci.* **2004**, 29, 183]. Copyright [2004] Elsevier.

Dendritic polymers are macromolecules which contain a high degree of branching, and the monomers used in their construction are multifunctional. They differ from conventionally branched polymers, such as linear polymers containing branched units, due to the possibility of branching at each and every monomer repeat unit. As a result, a large quantity of functionalised terminal groups is attained. In addition, the branching present within dendritic structures has a large influence on physical properties, such as viscosity and hydrodynamic volume. These properties differ from existing linear analogues and, as a result, there has been a high level of investigation into the potential of these architectures in a range of applications; including non-linear optics, mechanical property modifiers, coatings and even stretching to the field of medicine.[5]

### 1.1.3 Dendritic structure and terminology

The term 'dendrimer' stems from the Greek words 'dendron', meaning tree and, 'meros' meaning part.[13] Dendrimers are strongly recognised as polymeric molecules, despite their structural difference to linear polymers. Due to these differences, conventional polymer chemistry nomenclature is ineffective in describing these molecules adequately. Subsequently, this has given rise to new terminology, which has to be employed in order to best describe this novel class of materials. Both dendrimers and hyperbranched polymers fall

into the same class of polymer; however, they differ a great deal in structure. The varying nature in branching gives rise to their opposing architectures (**figure 3**).
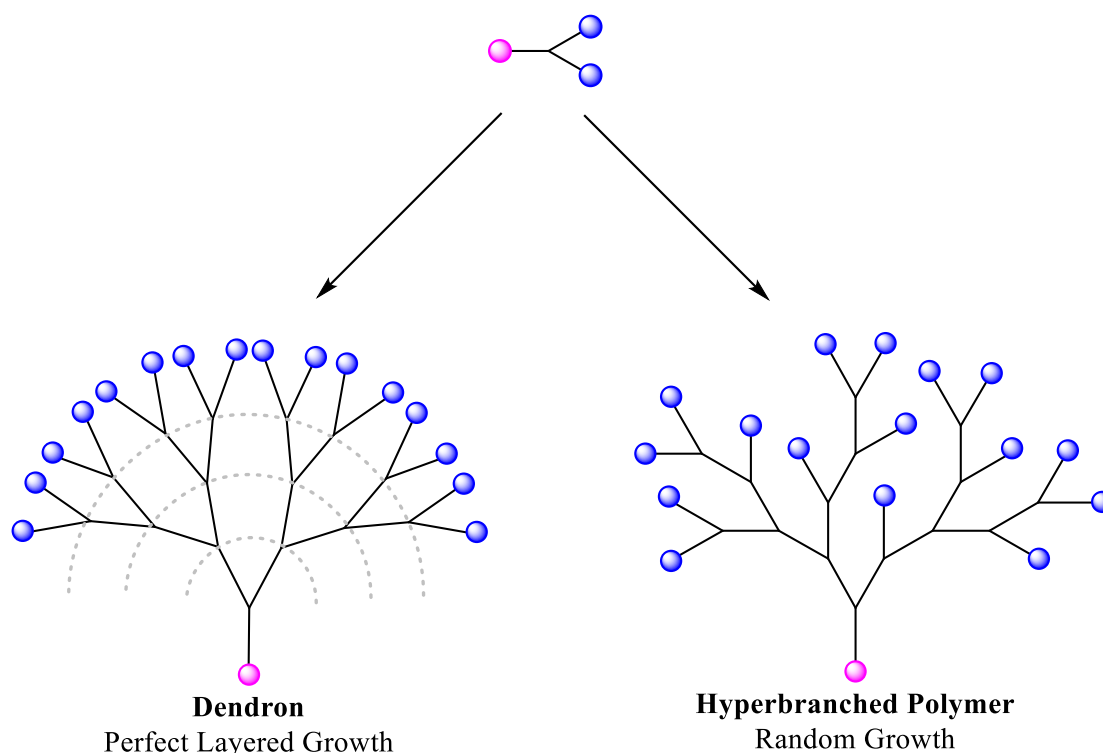


**Figure 3 –** Figure to illustrate the nature of branching within a dendron of a dendrimer and a hyperbranched polymer.

Dendrimers comprise of a series of regular branching monomers throughout their structure, surrounding an inner core. They are symmetrical and monodisperse, subsequently possessing an exact molar mass.[14] Dendrimers differ to classical polymers, due to their elevated degree of molecular uniformity and regularity.

Due to the highly controlled synthesis required in the preparation of a dendrimer, the overall molecular architecture consists of only two different types of monomer residue. The first type of residue is known as a *dendritic unit.* A dendritic unit is one which has fully reacted, and thereby able to contribute to branching. The second type of monomer residue is described as a *terminal unit*, and is located at the periphery of the macromolecule. Moreover, the structure of a dendrimer comprises of three divergent regions; an initiator core, repeat branching units and functionalised terminal groups **(figure 4)**, which are structural components unique to these macromolecules.
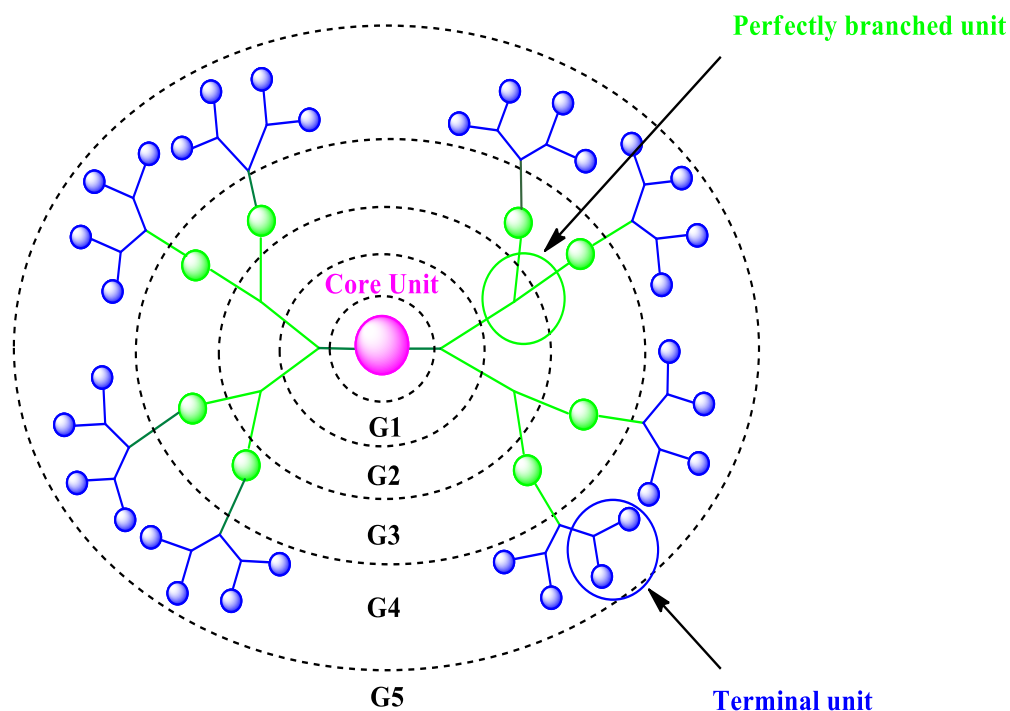
**Figure 4 –** Figure to illustrate the structural components of a dendrimer; a core unit, a perfectly branched unit and a terminal unit.

Dendrimers are composed of $AB_n$ monomer units, where every layer of repeat units generated with each stepwise reaction gives rise to a new 'generation' of branching units. These units are inter-reliant on each other, providing a dendrimer with its exclusive molecular shape.[5] The value of n determines the amount of terminal groups on the periphery of the molecule; if n=2 the number of terminal groups will double with each increasing generation and if n=3 the number of peripheral groups will triple.[14] As a general rule, low generation dendrimers form more open structures, with a higher molecular weight leading to a more globular and denser architecture. As is a result of increased branching, crowding of branches occurs, subsequently forcing a more closed structure.[10] Dendritic growth is mathematically restricted; therefore, at a specific generation there is a steric limit to growth which is known as De Gennes packing.[15] Growth may still occur past this critical point, but the result is the occurrence of structural flaws within the dendrimer.

Hyperbranched polymers, however, are polydisperse and adopt a far less ordered structure in comparison to dendrimers (**figure 3**). These dendritic polymers are generally produced using

a non-iterative polymerization process; consequently leading to unreacted branch points within their structure. [6]

Dendritic units and terminal units are common to both dendrimers and hyperbranched polymers. In addition to these units, there is also the possibility for the occurrence of partially reacted repeat units, more commonly known as *'linear units.'* The formation of these linear units gives rise to the structural imperfections within the hyperbranched polymer and as a result, structural control over layers of growth disappears.[5] The structural components of a hyperbranched polymer can be seen below in **figure 5**.
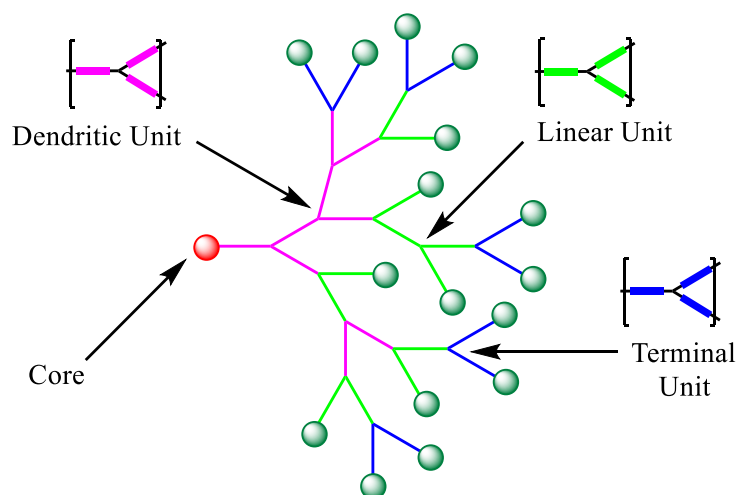


**Figure 5 –** Figure to illustrate the structural components of a hyperbranched polymer; a core unit, a dendritic unit, a linear unit and a terminal unit.

The degree to which branching occurs is dependent on the type of synthesis used, the type of monomer (i.e. $AB_2$ or $AB_3$) and also the reactivity of the individual functional groups present on monomer units. In order to best describe hyperbranched polymers, taking into account both linear and branched units, Fréchet introduced the degree of branching (DB) in the form of an equation (**equation 1**).[16] The degree of branching allows the quantification of linear and non-linear character within the polymeric architecture.

$$\text{Degree of Branching (DB)} = \frac{D+T}{D+T+L}$$

**Equation 1 -** Fréchet's equation for the Degree of branching (DB)

D represents the number of dendritic units, T represents the number of terminal units, and L represents the number of linear units. Following on from the work of Fréchet, Fray developed an equation (**equation 2**) which does not regard the core itself as a branching point as it is only influential to the level of branching at the initial stages of a reaction.[17]

$$DB = \frac{2D}{2D+L}$$

**Equation 2**- Fray's equation for the Degree of branching (DB)

This equation allows the degree of branching of a polymer to be realised by the actual number of growth directions. As a result, both high and low molecular weight polymers can be analysed, thereby deeming this equation highly useful within this field of chemistry.[18] The degree of branching for a hyperbranched polymer falls between 0 and 1, lying directly between the values of a linear polymer and a dendrimer respectively. There are two ways in which the degree of branching can be deduced; the first, which in turn is the most convenient, is the use of spectroscopy. This method makes use of peak area in nuclear magnetic resonance spectra and is relatively simple and effective. The second, which is less fitting, is via degradation of the polymer backbone.[5]

It is important to note that hyperbranched polymers can adopt numerous isomeric structures for any degree of branching it may possess. Isomerism is a vital difference between hyperbranched polymers, and either dendrimers or linear polymers, meaning that a hyperbranched polymer could theoretically display a degree of branching also equal to 1 without having a dendrimeric structure.[18]

### 1.1.4 Properties of dendritic polymers

The study of dendritic macromolecules has proceeded at an accelerated rate in recent years. Dendritic polymers are substantially different from analogous linear polymers, which has led to numerous noted differences in their physical properties.[19] As a direct result of the highly

13

branched structures, these macromolecules exhibit contrasting behaviour to linear analogues in solution.[20] With linear polymers, as the molecular weight increases so does the level of chain entanglement, producing an increase in viscosity. With dendritic polymers, viscosity increases with increasing molecular weight up until a certain point. This anomalous maximum in the relationship between intrinsic viscosity and molecular weight is a direct result of the globular structures dendritic polymers assume in solution. Dendritic macromolecules, with molecular weights higher than this maximum, exhibit a reduced solution viscosity, as the globular morphology inhibits chain entanglement.[21, 22] **Figure 6** is a graphical representation of this relationship; comparing linear polymers, hyperbranched polymers and dendrimers.[23]
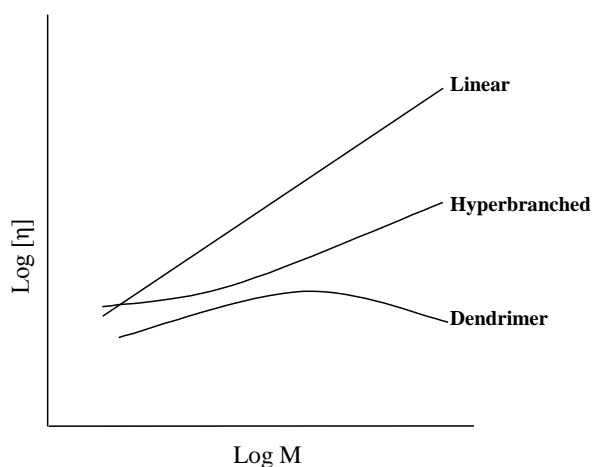


**Figure 6** – A Graphical representation of log[η] (intrinsic viscosity against log M (molecular weight) of the polymer, adapted with permission from [Jikei, M.; Kakimoto, M. Prog. Polym. Sci. **2001**, 26, 1233]. Copyright [2001] Elsevier.

The relationship between molecular weight and intrinsic viscosity can be illustrated by the Mark-Houwink-Sakurada equation given below.

$$\eta = kM^{\alpha}$$

Where η represents intrinsic viscosity, M the molecular weight and where k and α are constants, which are particular for the polymer-solvent system in question. In general, values of α fall within the range of 0.5 and 1.0 for linear polymers, whereas, dendritic polymers have been reported to have values of α lower than 0.5, providing evidence for the globular morphology they adopt in solution.[23]

14

In addition to reduced viscosity, another outcome of the compact globular morphology is that dendritic macromolecules possess smaller hydrodynamic volume compared to linear analogues.[19] This particular property can pose a problem when utilising analytical techniques based on size, such as gel permeation chromatography (GPC).[5] GPC is customarily calibrated with linear polymer standards, such as polystyrene, and the use of these polymers supplies a satisfactory estimate of molecular weight in the greater part of most cases. When non-linear polymers are analysed, the molecular weight values can be highly underestimated, due to misrepresentation of data. This effect becomes more pronounced for higher molecular weight polymers, due to an increase in the difference of hydrodynamic volume between linear and dendritic polymers. These analytical difficulties can be intensified further as a result of the high level of functionalised surface groups present on dendritic macromolecules. In linear polymers, peripheral groups play a small role in the overall determination of physical properties of the polymer. However, in dendritic macromolecules, the groups at the periphery of the molecule are extremely influential in determining solubility. In high molecular dendritic polymers, the surface groups protect the interior from circumferential solvent molecules, resulting in a more compacted structure and a greater level of underestimation. Contrary to this, the solubility can also be enhanced with appropriate functionalisation of the periphery.

## 1.2 Synthesis of Dendritic polymers

### 1.2.1 Synthesis of Dendrimers

Work by Flory in 1952[24] gave rise to the true breakthrough into the field of dendritic polymer chemistry. Flory's theory involves condensation between $AB_x$ (where $x \geq 2$) monomer molecules. Following the theoretical work by Flory, Vögtle *et al.*[3] published the first iterative synthetic procedure for the construction of a dendrimer. The synthesis involved aliphatic amine $AB_2$ type monomer molecules. Condensation gave rise to the synthesis of '*cascade*' polymers.[3]

Dendrimers are monodisperse symmetrical macromolecules, and to synthesise this class of polymer requires a high degree of synthetic control. This is accomplished via a highly controlled stepwise methodology, whereby the dendrimer is constructed one monomer layer at a time. The production of a dendrimer is a challenging task to perfect. The synthetic procedure involves numerous protection and deprotection steps at each stage of the synthetic

procedure. In addition to this, purification at each stage is both crucial and demanding. As previously stated, primary synthetic strategies were set in motion as early as 1978, by means of manufacturing these symmetrical and uniform macromolecules.[3] There are two major synthetic approaches, which are currently in operation, to generate this unique type of macromolecule. These two strategies differ considerably from one another, and are known as the divergent and convergent approach respectively.[25]

## 1.2.2 Divergent synthesis

The divergent approach (**figure 7**) has arisen from the influential work of Tomalia, Newkome and Vögtle's branched model. This particular approach involves building the dendrimer from an initiator core, increasing layers out towards the periphery of the molecule.[25] Growth is initiated using repetition of coupling and activation steps. The peripheral end groups of each subsequent generation are reacted with the complementary reactive group on the monomer unit.[11] Due to this, new branch points have been established at each site, leading to an increased number of terminal functionalised groups; this step is commonly referred to as a coupling step. Once the first coupling step is driven to completion, an activation step will take place. This is where the dormant functional groups can then be activated, so that further monomer can react, thus resulting in an increase in generation.[25] Activation and coupling proceed in a repetitious fashion, resulting in an increase in the number of reactions at the perimeter. Furthermore, it can also be stated that the number of active hydrogen's available will consequently establish the number of branches in the macromolecular intermediate. It can be noted at this point that these are sequentially connected to other interior generations.[2]
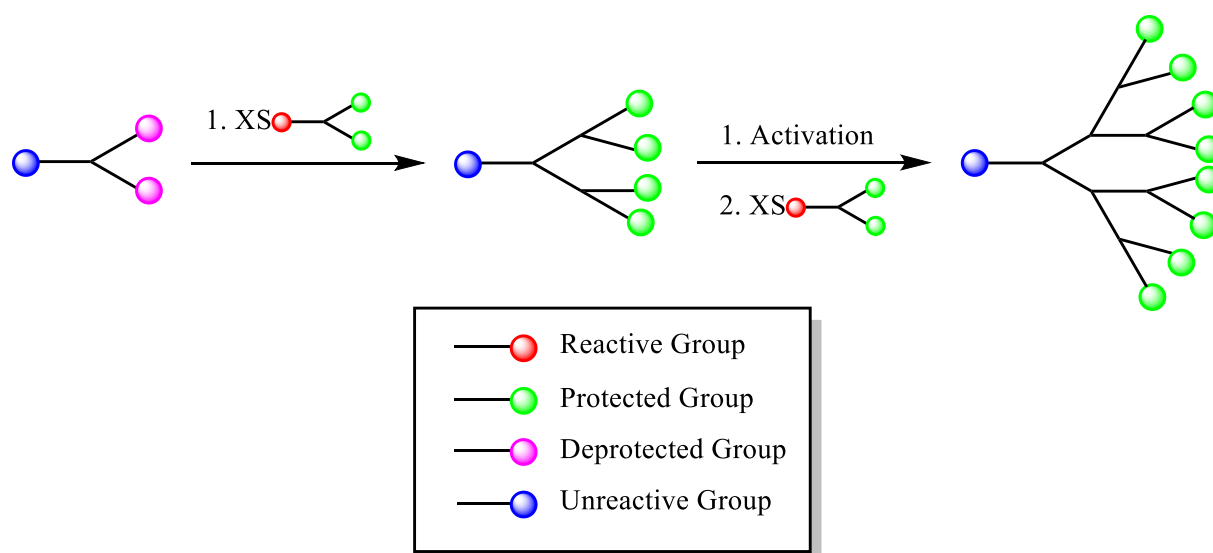
**Figure 7**- Growth of a dendrimer via the divergent approach, illustrative of one branching point of a multifunctional core.

An advantage associated with this particular type of methodology is that the divergent approach is a moderately clear-cut synthetic procedure and, on proviso that favourable reaction conditions are maintained and fitting reagents are used, this method is perfectly suited for the manufacture of dendrimers on an industrial scale. However, there are certain disadvantages linked to this methodology. For example, the result of repetition on activation and coupling reaction steps produces an exponential increase in the number of reactions at the perimeter. As a result, there is a need for a large excess of reagents, in order to ensure both reaction steps reach completion.

Another inconvenience to this synthetic route is due to the rise in the number of coupling reactions required with each increase in generation. This factor is accompanied by an increase in the probability of unwanted side reactions, and the formation of incomplete by-products. Should such unwanted side reactions take place, there is a possibility of architecturally similar by-products forming, which are extremely difficult to remove. It is also vital that the activating agent is fully eradicated, in order to prevent development of smaller, superfluous dendritic structures.[11]

The first family of dendrimers to be synthesised and commercialised were the Polyamido amines (PAMAM'S). This dendritic family has also been referred to as 'starburst' dendrimers and was first characterised by Tomalia et al in 1985.[2] This particular type of dendrimer has

17

received a great deal of attention in recent years and for more detailed information regarding this family of dendrimers, the reader is directed to numerous detailed pieces of literature.[2, 12, 26, 27]

### 1.2.3 Convergent synthesis

The convergent method for dendritic polymers (**figure 8**) was first accounted for in the work carried out by Fréchet and Hawker.[6, 25, 28] This synthetic approach commences with what will become the periphery of the end product and progresses inwards. By commencing at the periphery of the macromolecule and gradually working inwardly, a reactive dendron is generated. In order to create a globular dendritic architecture, several dendrons are further reacted with a polyfunctional core molecule.[12] Therefore, the convergent method deviates from the divergent approach, as the core is incorporated to the macromolecule in the ultimate reaction step.[29]
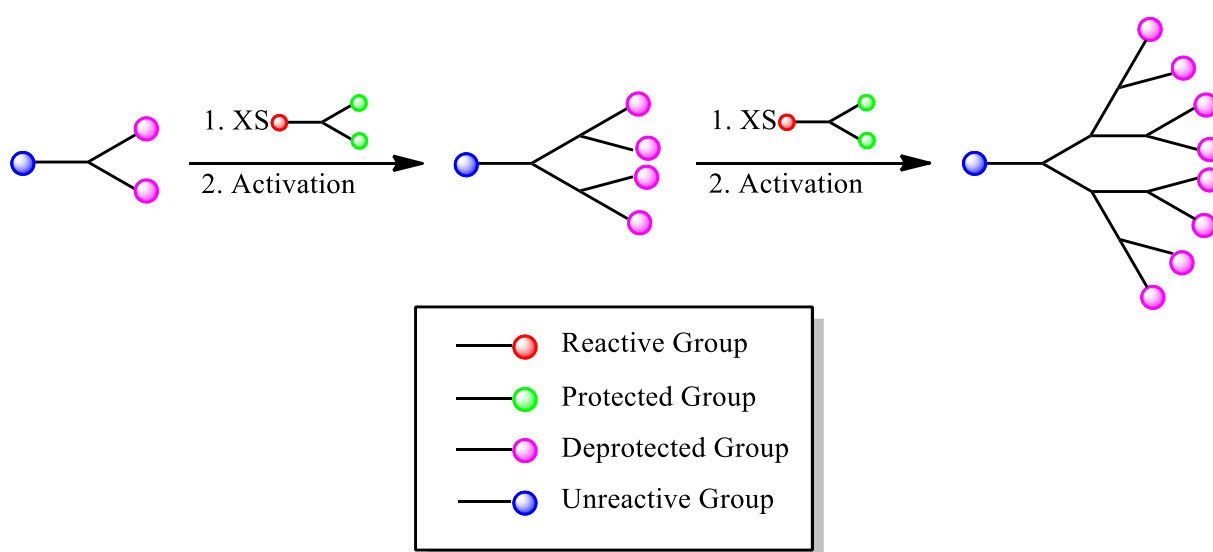


**Figure 8**- Growth of a dendrimer via the convergent approach.

After coupling, the focal point of the dendron can be triggered using an activation step, which is further coupled to functional surface groups on more available monomer units. Working from the peripheral layer to the interior provides greater architectural control, as there are fewer coupling reactions at each stage of dendrimer growth. As a result, only slight surplus reagents are required to drive the reaction to completion, which aids purification. Therefore, it can be seen that the convergent approach has numerous advantages over the divergent

method. One of the most appealing features to this type of synthesis is its capability in distributing functional groups throughout the architecture in a selective fashion. Consequently, it is a suitable method for manufacturing accurate, well defined, symmetrical and unsymmetrical dendritic structures.

There are also certain inconveniences to this methodology, such as steric crowding. This arises from construction of macromolecules from the perimeter towards the core. It is difficult to produce large generation dendrimers without an elevated level of defects within the structure.[11] The most widely applicable dendrimers created by this synthetic procedure are poly (benzyl ethers), which have been manufactured by Grayson and Fréchet.[6, 29]

### 1.2.4 Synthesis of Hyperbranched Polymers

In 1952, Flory built upon his previous work to develop a theory by which highly branched polymer molecules can be synthesised without gelation. Instead of utilising a bifunctional A monomer and a trifunctional B monomer in a polycondensation reaction, a monomer with one A functionality and two or more B functionalities was used.[24] Although work by Flory was the initial breakthrough into dendritic chemistry, the first example of a hyperbranched polymer was not synthesised until 1988 by Kim and Webster.[30]

In order to successfully synthesise dendrimers, an exhaustive iterative procedure involving numerous protection and deprotection steps is required. The synthesis of hyperbranched polymers does not require an exhaustive approach, as they can be conveniently synthesised in a one-pot process.[31] Although this synthetic approach is less time consuming than dendrimer synthesis, the one-pot method involves random polymerisation of monomer units, giving rise to an extensive molecular weight distribution.

The synthesis of hyperbranched polymers commonly involves the employment of one of three synthetic processes; step growth polymerisation, self-condensing vinyl polymerisation of AB* monomers and multi-branching ring opening polymerisation of dormant $AB_X$ monomers.[8]

### 1.2.5 Step growth polycondensation

Step growth polycondensation involves the polymerisation of $AB_x$ monomers ($X \geq 2$) in a one-step polycondensation reaction.[8] Usually the monomer of choice is $AB_2$ (**scheme 1**) however, it has been noted that monomers containing six B functionalities ($AB_6$) have been employed, not to mention the polycondensation of paired monomers such as $A_2$ and $B_3$.[32, 33] This specific route can withstand numerous diverse functional groups and has, therefore, been widely used in the manufacture of many hyperbranched polymers, including polyphenylenes[30, 34], polyesters[31, 35], polyethers[36] and polyamides[37]. An added advantage to this method is the low cost and commercial availability of $AB_x$ monomers. Although some features of this synthetic approach are beneficial, it is important to note the negative aspects associated with this particular method. Polymer gelation is a potential outcome, resulting in the need for a far more arduous purification process. A further disadvantage to step growth polycondensation is the potential occurrence of unwanted side reactions, such as cross linking. As a result, the $AB_x$ monomers selected must be synthesised before polymerisation can take place.[7,8]
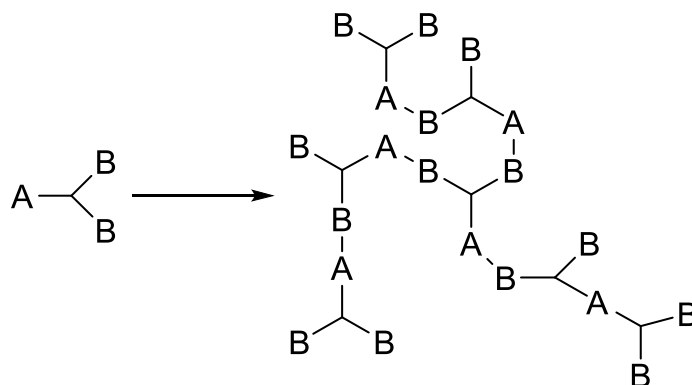


**Scheme 1** – Schematic representation of the process of step growth polymerisation of an $AB_2$ monomer.

### 1.2.6 Self-condensing vinyl polymerisation of AB* monomers

In 1995, Fréchet *et al.*[23, 38] documented a novel, resourceful approach to synthesising hyperbranched polymers, known as self-condensing vinyl polymerisation (SVCP). This approach proceeds via self-polymerisation of a vinyl monomer, if it possesses a side group which can be converted into an initiating moiety. Such side groups include; a 'living' free radical, an electrophilic cation or even a carbanion. This transformation occurs by the action of an external stimulus; such as heat, light or an external additive. This type of

polymerisation can be viewed as a fusion of both vinyl polymerisation and classical step growth polycondensation reactions, as it functions via iterative coupling of growing moieties involving steps which are characteristic of classical vinyl polymerisations.[23, 38]

The activated structural unit is most commonly denoted as an AB* inimer, where A represents the vinyl bond and B* represents the activated functional group. The term *'inimer'* is used to describe a monomer with the capability to initiate monomers. In an SCVP system, chain initiation occurs when an activated species, B*, is added to a vinyl group of another inimer, leading to the formation of a dimer with two active sites and a double bond. A newly generated propagating centre, A*, and the activated centre, B*, can then react with the vinyl group of another molecule resulting in the formation of a hyperbranched polymer (**scheme 2**).[39] This particular synthetic approach has been employed to manufacture polystyrenes, poly(methacrylate)s and poly(acrylate)s.[8]
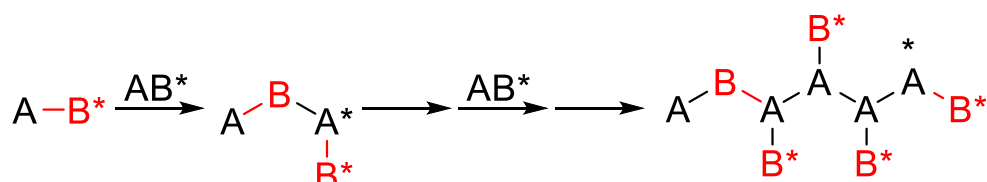


**Scheme 2 -** Schematic representation for self-condensing vinyl polymerisation of AB* monomers; chain initiation is shown in black and the initiator side groups are shown in red.

### 1.2.7 Multi-branching ring opening polymerisation of latent $AB_x$ monomers

The third major approach to hyperbranched polymer synthesis is called multi-branching ring-opening polymerisation. There has been less exploration into this method of polymerisation in comparison to the other strategies described beforehand. This approach, however, offers promise of a high level of control regarding synthesis of novel hyperbranched polymers.[40] This strategy was first introduced in 1992 by Suzuki, who reported the multi-branching polymerisation of cyclic carbamate with the aid of a palladium catalyst in order to generate polyamines. The idea Suzuki put across involved the initiator itself as the core, providing a dendritic macromolecule.[41] The monomers utilised in this method of polymerisation are latent $AB_x$ type monomers. The monomers do not contain any branching points; the branching points are created via propagation.[23]

Glycidol is a latent $AB_x$ monomer which has received a great deal of attention in the synthesis of hyperbranched polyglycerols. Frey and co-workers produced the first publication

involving this monomer in 1999 and, from this point, interest in this monomer grew at an escalated rate.[8, 40] Polyamines, polyesters[42] and other polyethers[44] have also been prepared successfully using this strategy.

## 1.3 Dendritic polymer applications

### 1.3.1 Applications of Dendrimers

The area of dendrimer chemistry has recently become one of the most quickly escalating areas of modern science, receiving a great deal of interest.[25] Over the years, dendrimers have been used in the field of nanotechnology, bio-mimicry, diagnostics, catalysis and an assortment of therapeutic agents. These macromolecules have received a large amount of curiosity extending a great deal beyond that of classical polymers. Such increased interest is largely due the unique characteristics dendrimers possess. The peripheral surface, interior cavities and core unit can all be exploited and tailored for a specific reaction (**figure 9**).



(i)  (ii)  (iii)
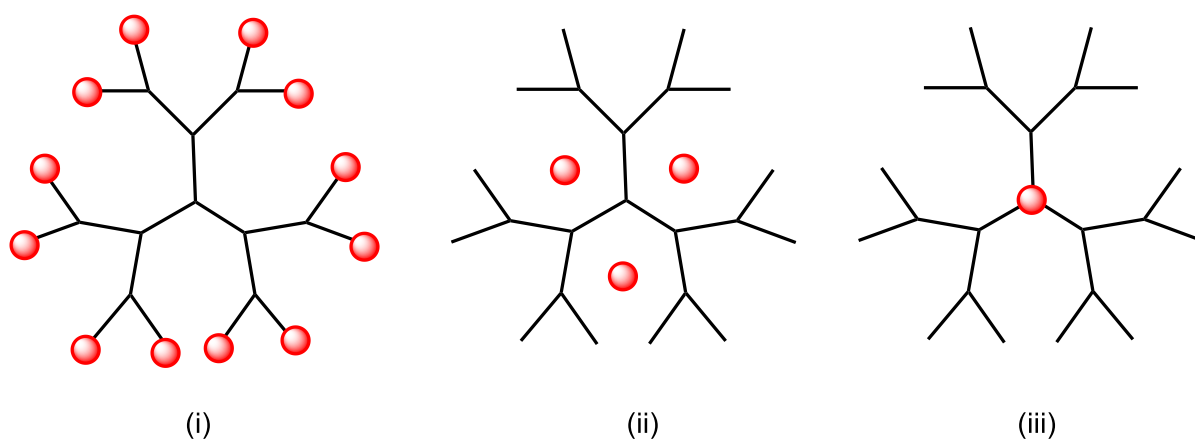
**Figure 9**– Figure to illustrate the structural elements of a dendrimer which can be exploited: (i) peripheral groups (ii) internal cavities and (iii) core unit

The surface of a dendrimer possesses a large amount of peripheral units, making it useful for applications involving covalent interactions of functional groups. An example of an application which profits from this approach is chemical sensing. A dendritic sensor, which was researched by Balzani, Vögtle and co-workers[44], was a fourth generation poly (propylene amine) dendrimer, possessing 32 dansyl units at the surface, demonstrating a fluorescence response to small $Co^{2+}$ ions. However, it is not only inorganic species which can be detected; sensors designed for recognition of organic species are also involved in a large amount of research.[25, 44] More recently, Akin *et al*.[45] reported an amperometric alcohol biosensor. The

sensor was developed by the immobilisation of alcohol oxidase, via a PAMAM dendrimer, onto a cyste-amine modified gold electrode. The determination of ethanol was achieved through the depletion of oxygen by an enzymatic reaction. The biosensor showed a response time of 100 s and a detection limit of 0.016 mM. The biosensor also displayed up to 67 % of initial activity after storage for a period of four months. Biosensors of this nature can be used in the analysis of ethanol in numerous alcoholic drinks and also in the observation of the generation of alcohol in yeast cultivation. For more information regarding the use of dendrimers in the area of biochemical sensing, the reader is directed to the following review by Satija.[46]

However, the most exciting prospect for the use of dendrimer surfaces is within medicine; with some areas including MRI contrast agents, gene delivery and drug delivery. There has even been research into the use of dendritic macromolecules as potential therapeutic drug molecules. MRI contrast agents are extremely important in medicine as diagnostic tools, which are used to generate anatomical images of high clarity of 'soft' tissue, such as organs or blood vessels. The process involves interaction of tissue with a defined magnetic field, resulting in a nuclear resonance signal of water; this signal itself is then allocated to its location of origin. The signals detected using this technique are then renovated and converted into the desired image. The role of a contrast agent is to improve sensitivity of this diagnostic approach, with Gadolinium (Gd) being a common element used.[25, 26] Common low molecular weight Gd chelates do not remain in the blood vessels long enough after injection; therefore, their main drawback is rapid extracellular diffusion, meaning they will be rapidly eliminated from the blood stream. Some examples of common imaging agents include $[Gd(DTPA)]^{2-,}$ $[Gd(DOTA)]^-$ and $[Gd(HP-do3a)]$.[47] The outcome of this resulted in research into utilization of dendrimers, which have been shown to have more extensive lifetimes in blood vessels when compared to lower molecular weight Gd chelates. Furthermore, they have demonstrated efficient acceleration in proton relaxation resulting in high quality tissue imaging.[25]

Dendrimers have also been considered for use in gene delivery to act as carriers for genetic material. Gene therapy is crucial in the medical industry, as there is the likelihood that it could have a positive effect on either hereditary or acquired genetic disorders. Nucleic acids are particularly complicated to transport, meaning that non-viral vectors are actively sought out in this industry. It is assumed that non-viral vectors are able to prevent DNA from undergoing enzymatic degradation.[14, 25] Polyamido amine and PPI dendrimers, possessing

amine surface groups, have been deemed potential non-viral carriers in gene therapy and have featured in numerous pieces of literature.[48-51] Under physiological conditions, the surface groups become protonated; therefore, enabling polyanionic DNA to bind to the polycationic dendrimer surface via electrostatic interactions, which signify their potential as a non-viral vector for effective gene transfer. They also have a considerably low toxicity and have a high attraction for genes possessing a negative charge.[52] The size of these molecules can be seen as added benefit, as it enables the transport of a high volume of genetic material.[25]

One of the most important biomedical applications, for which dendrimers are an ideal contender, is the area of drug delivery.[53] Owing to the toxicity of a dendrimer increasing with higher generation, the biological properties of dendrimers become crucial.[26] There are two proposed ways in which a drug can interact with a dendrimer; firstly it can be encapsulated within the dendritic cavities, or secondly, by electrostatic or covalent interactions to the periphery.[25] Dendrimers have flexibility to their structure, particularly around the core, making them ideal as hosts for molecule entrapment.[52] Dendrimers have therefore been considered to facilitate drug solubility and bioavailability, and also as vehicles which control release of drugs to their respective targets. In addition, they have been targeted for research for molecular entrapment, due to their open architecture. The drug which has been most frequently complexed to full generation PAMAM dendrimers is ibuprofen, a non-steroidal anti-inflammatory drug (NSAID) possessing carboxylate functional groups. Ibuprofen is able to interact with the amine groups on the surface of the dendrimer. A study by Kolhe *et al.* [54] involved the interaction of G3 and G4 PAMAM dendrimers, with 32 and 78 ibuprofen molecules respectively, via ionic interactions, and was later concluded by NMR and IR spectroscopy. Testing in vitro revealed that there was slower release of ibuprofen to cells, when complexed to the dendritic architecture, compared to free ibuprofen.[54]

In 2002, Fréchet *et al.*[55] developed three contrasting polyester based dendrimers. One macromolecule had hydroxyl peripheral groups, another had tri (ethylene glycol) monomethyl ether surface groups and the third, a star polymer type structure, had polyester units located on the surface. The star polymer exhibited the most potential in terms of cytotoxicity and half-life and, as a result, was used to covalently coordinate to the anticancer drug, doxorubicin. The drug was connected to the star polymer architecture by a hydrazone linkage. Results demonstrated a large reduction in the cytotoxicity of the drug and reports showed that doxorubicin was taken up within cancer cell lines sufficiently. This study shows

the promise of this type of material as a potential drug carrier. Dendrimers are preferable over classical polymers concerning polymer-drug interactions, as they are unique symmetrical molecules which are highly defined. As a result of their immense surface area, they can potentially accommodate high loadings of drugs.[52, 53]

Another therapeutic application, which dendrimers can be applied to, is Boron neutron capture therapy (BNCT). This type of therapy has been used to treat numerous diseases, in particular, the treatment of cancer. It involves intravenous admission of a pharmaceutical containing $^{10}$B (the stable isotope of boron) to patients, which journeys to cancer cells. This is subsequently followed by irradiation of the patient using a low energy neutron beam. BNCT functions well when adequate amounts of $^{10}$B are being transported to tumour tissue, as it can then be irradiated by neutrons. Irradiation results in the generation of highly energetic alpha particles and $Li^{3+}$ ions. The cations and energetic particles, which are formed, hinder the potential for tumour cells to replicate. A challenge associated with this technique is the select transportation and localisation of therapeutic agents, containing boron, inside tumour tissue. An important criterion of this is for agents to have a relatively low toxicity, and a potential solution was to create polymer scaffolds containing boron, in order to improve the selectivity and activity of it. PAMAM dendrimers have been used in research for preparation of immunoconjugates, yielding high concentrations of boron. Barth and co-workers synthesised the first PAMAM dendrimer containing Boron where they proclaimed that polyhedral borane [Na(CH$_3$)3B$_{10}$H$_8$NCO] was able to be complexed to 2nd and 4th generation PAMAM dendrimers, via conjugation to the surface of the dendrimers.[26, 47, 52, 56]

More recently, dendrimer encapsulated gold nanoparticles (Au DENPs) have been actively researched in the field of medicine. In 2012, Shan et al.[57] have synthesised Au DENPs using amine terminated dendrimers as templates for non-viral vectors for gene delivery. Au DENPs showed higher gene transfection efficiency in comparison to dendrimers without entrapped nanoparticles. In 2013, Wang et al.[58] have utilised Au DENPs for glutathione triggered release of anti-cancer drugs, both in vitro and also in live cells. These studies show the potential of these systems in the development of novel therapeutics.

It is not only biomedically where these unique macromolecules have been applied; they have also been used to improve numerous industrial processes. The blend of both high solubility and large surface area makes them attractive for use in catalysis, with dendrimers also being

involved in research as potential catalytic supports. Catalysis is an area of expanding chemistry with regards to the incorporation and newly found importance of dendrimers within industrial science. Due to their architecture, there are two main ways in which dendrimers can be modified to function as a catalyst.[26,52] Firstly, is the attachment of catalytic functional groups to the periphery of the dendrimer, and secondly, the introduction of a catalytic site at the central core of the dendrimer, giving the dendrimer nano-reactor properties. This occurs because of the internal cavities which lie in close proximity to the catalytic core being hidden from the external environment.[26,52] The dendritic catalyst exhibits advantageous characteristics of homogenous catalysts, as well as benefits inherent of heterogeneous catalysts. An advantage of a homogenous catalyst is that they have unproblematic accessibility of active sites, however, unlike heterogeneous catalysts, they are difficult to extract from the reaction mixture. Dendrimers are easily recovered by techniques such as ultrafiltration, and the vast peripheral surface is multifunctional, causing all catalytic sites to be exposed to the reaction mixture. They therefore combine advantages of both homogeneous and heterogeneous catalysts, which is consequently the main basis of their appeal in industry. The Van Koten group established the first catalytic dendrimer for use in addition reactions for polyhaloalkanes.[26] For more information regarding dendrimers in the area of catalysis, the reader is directed to the following reviews.[59-61]

### 1.3.2 Applications of Hyperbranched polymers

The development of hyperbranched polymers is intensifying a great deal within the field of macromolecular science. Hyperbranched polymers have similar capabilities to dendrimers, considering the core, periphery and branched interior all have the potential to be functionalised. There are a large number of suggested applications for these macromolecules; however, it is important to note how investigations into the use of hyperbranched polymers are still in their infancy when compared to dendrimers. In comparison to dendrimers, hyperbranched polymers are structurally imperfect. Nonetheless, despite the limited control, they provide a promising cost-effective alternative to dendrimers, being the primary motive for research into their commercial applications.

It is the original and novel properties belonging to these macromolecules which deem them as excellent contenders for numerous diverse applications. Characteristic properties of hyperbranched polymers are highly dependent upon the degree of branching. The structural differences present in hyperbranched polymers, compared to linear analogues, gives rise to

amorphous materials, as branching thwarts crystallisation. Moreover, these materials also display low viscosity both in solution and in bulk. This low viscosity combined with potential for high functionality can be employed for numerous applications, such as cross-linkers, additives, rheology modifiers, coatings[62] and tougheners for epoxy resins.[63, 64]

One of the most common bulk applications of hyperbranched polymers is the generation of polymeric blends. There is a lot of interest with blending hyperbranched polymers with linear polymers, as the result is generation of novel polymeric materials. An example of this is a blend of hyperbranched polyphenylenes with polystyrene by Kim and Webster. This fusion resulted in the improved melt viscosity and thermal stability. Furthermore, the mechanical properties were changed upon blending, such as the enhancement of the initial modulus.[8,34] Exploiting hyperbranched polymers as a blend component is widespread amongst research into applications of dendritic macromolecules. Research in polymeric blends has triggered interest in other applications. Voit *et al.* investigated blending amphiphilic hyperbranched polyesters with an array of linear poly (olefins), which has given rise to an amphiphilic polyester derivative capable of transporting polar organic additives, such as dye molecules.[9] This system is comparable to nanocapsules or the dendritic box.[65] The dye molecule is enveloped within the hyperbranched polyester and then blended with the linear poly (olefin) (**scheme 3**).[9]
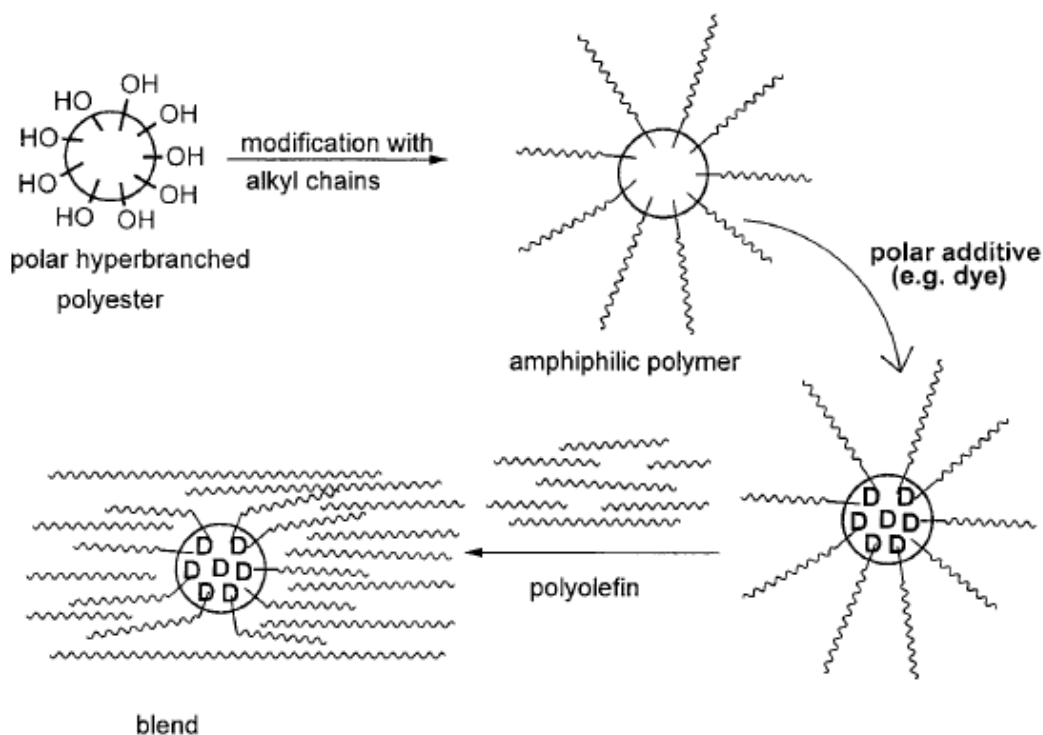
**Scheme 3**-A schematic diagram showing the diffusion of the diffusion of an organic dye molecule into an amphiphilic hyperbranched polyester, followed by the inclusion into a poly (olefin) matrix. Diagram reprinted with permission from [Voit, B. Journal of Polymer Science Part a-Polymer Chemistry **2000**, 38, 2505]. Copyright [2000] John Wiley & Sons, inc.

Frey and co-workers took an alternative approach and investigated the use of hyperbranched polyglycerols as nanocapsules used to transport dye molecules. The work carried out showed how the topology of the hyperbranched polymer was fundamental in the encapsulation of the dyestuff.[66]

Another application which has received attention is the use of hyperbranched polymers as surface coatings, especially polymer films. Möller produced ultra-thin films from arborescent graft polystyrenes. The films produced were of even thickness and the overall thickness was found to be dependent on the molecular weight and branching density of the hyperbranched polymer in question.[8, 67] Asif *et al.* investigated a waterborne coating using ultraviolet curing technology. Waterborne coatings have achieved a great deal of interest, as they are known to reduce air pollution, lower the risk of fire and improve numerous areas of occupational health and safety. A succession of waterborne hyperbranched polyurethane acrylates for aqueous dispersion based upon hydroxyl functionalised polyester Boltoron $H_2O$ were shown to display good dispersability.[68]

Hyperbranched polymers have been considered for use as non-linear optical (NLO) materials. The majority of research in this particular area has focussed primarily on one dimensional NLO polymers, such as main chain or side chain polymers. The NLO chromophore can align in numerous different ways in one-dimensional polymers, for instance, head to head, head to tail and shoulder to shoulder. Zhang *et al.* have synthesised hyperbranched polymers with carbazole NLO chromophores, which displayed reasonable NLO properties. Zhang and co-workers have also synthesised a novel hyperbranched polyester containing 4-(2-cyano-2-methoxycarbonyl) aniline as the polar chromophore. In this particular hyperbranched polymer the chromophores link at the cross site of the branches, giving rise to a head to tail main chain backbone. This formation removes centrosymmetry, which would essentially thwart the polymer displaying non-linear optic activity.[69]

The field of chemical engineering is a novel area which has exploited the use of hyperbranched polymers. Hyperbranched polymers can be used in extractive distillation, solvent extraction and membranes. Due to the intricate and multi-step synthesis required to generate structurally perfect dendrimers, the use of hyperbranched polymers offers a more cost effective alternative. Hyperbranched polymers display numerous properties which signify their promise as extraction solvents, and there are now hyperbranched polymers which are commercially available and approved by the FDA for this application. An alternative engineering application for these macromolecules is the separation of gases via absorption; however, research in this area is still in its infancy. Furthermore, the idea of using hyperbranched polymers as the stationary phase for preparative chromatography has also been put forward; thus, the potential of these polymers, for industrial purposes, is clearly recognisable.[70]

A great deal of research exists in utilisation of hyperbranched polymers as valuable drug carrier systems. A dendrimer remains the ideal competitor, due to its well defined architecture, large volume of functional groups and molecular uniformity. Dendrimers are thus considered as an attractive vehicle for drug delivery in modern science. Kolhe *et al.* have also investigated the use of the hyperbranched polymer Perstorp Polyol as a potential candidate. Perstorp polyol is a 5th generation aliphatic polyester, possessing surface hydroxyl groups. The architecture itself bears a resemblance to that of a dendrimer, but is not as well defined. The potential of these polymers within the medical field is unequivocal and has

triggered a lot of interest into the study of these polymers and their relative complexation ability to a wide array of numerous marketable drugs.[55] Due to their good solubility and excellent processability; three dimensional dendritic polymers have attracted much attention in numerous areas of science. They are therefore perfect for use in an ample range of applications, and the interest in these macromolecules is continuing to flourish.

## 1.4 References

(1)      Chiba, F.; Mann, G.; Twyman, L. J. *Org. Biomol. Chem.* **2010**, *8*, 5056.

(2)      Tomalia, D. A.; Baker, H.; Dewald, J.; Hall, M.; Kallos, G.; Martin, S.; Roeck, J.; Ryder, J.; Smith, P. *Polym. J. (Tokyo)* **1985**, *17*, 117.

(3)      Buhleier, E.; Wehner, W.; Vogtle, F. *Synthesis-Stuttgart* **1978**, 155.

(4)      Newkome, G. R.; Yao, Z. Q.; Baker, G. R.; Gupta, V. K. *Journal of Organic Chemistry* **1985**, *50*, 2003.

(5)      Inoue, K. *Progress in Polymer Science* **2000**, *25*, 453.

(6)      Grayson, S. M.; Frechet, J. M. J. *Chemical Reviews (Washington, D. C.)* **2001**, *101*, 3819.

(7)      Gao, C.; Yan, D. *Prog. Polym. Sci.* **2004**, *29*, 183.

(8)      Yates, C. R.; Hayes, W. *European Polymer Journal* **2004**, *40*, 1257.

(9)      Voit, B. *Journal of Polymer Science Part a-Polymer Chemistry* **2000**, *38*, 2505.

(10)     Bosman, A. W.; Janssen, H. M.; Meijer, E. W. *Chemical Reviews* **1999**, *99*, 1665.


(11)     Odian, G. *Principles of Polymerization*; McGraw-Hill, 1970.

(12)     Esfand, R.; Tomalia, D. A. *Drug Discovery Today* **2001**, *6*, 427.

(13)     Pandey, A. G.; Aggarwal, A.; Das, S. *Asian J. Biochem. Pharm. Res.* **2011**, *1*, 249.

(14)     Cloninger, M. J. *Current opinion in chemical biology* **2002**, *6*, 742.

(15)     De Gennes, P. G.; Hervet, H. *J. Phys., Lett.* **1983**, *44*, 351.

(16)      Hawker, C. T.; Lee, R.; Fréchet, J. M. J. *Journal of the American Chemical Society,* **1991**, 113, 4583

(17)     Hoelter, D.; Burgarth, A. J.; Frey, H. *Acta Polymerica* **1997**, 48, 30

(18)     Kim, Y. H. *Journal of Polymer Science Part a-Polymer Chemistry* **1998**, *36*, 1685.

(19)     Hawker, C. J.; Malmstrom, E. E.; Frank, C. W.; Kampf, J. P. *Journal of the American Chemical Society* **1997**, *119*, 9903.

(20)     Rathgeber, S.; Monkenbusch, M.; Kreitschmann, M.; Urban, V.; Brulet, A. *Journal of Chemical Physics* **2002**, *117*, 4047.

(21)     Farrington, P. J.; Hawker, C. J.; Frechet, J. M. J.; Mackay, M. E. *Macromolecules* **1998**, *31*, 5043.

(22)     Hawker, C. J.; Farrington, P. J.; Mackay, M. E.; Wooley, K. L.; Frechet, J. M. J. *Journal of the American Chemical Society* **1995**, *117*, 4409.

(23)     Jikei, M.; Kakimoto, M. *Prog. Polym. Sci.* **2001**, *26*, 1233.

(24)     Flory, P. J. *Journal of the American Chemical Society* **1952**, *74*, 2718.

(25)     Dykes, G. M. *Journal of Chemical Technology & Biotechnology* **2001**, *76*, 903.

(26)     Klajnert, B.; Bryszewska, M. *Acta biochimica Polonica* **2001**, *48*, 199.

(27)     Peterson, J.; Ebber, A.; Allikmaa, V.; Lopp, M. *Proceedings of the Estonian Academy of Sciences, Chemistry* **2001**, *50*, 156.

(28)     Hawker, C. J.; Frechet, J. M. J. *Journal of the American Chemical Society* **1990**, *112*, 7638.

(29)     Lee, J. W.; Kim, J. H.; Kim, B. K.; Shin, W. S.; Jin, S. H. *Tetrahedron* **2006**, *62*, 9193.

(30)     Kim, Y. H.; Webster, O. W. *Abstracts of Papers of the American Chemical Society* **1988**, *196*, 104.

(31)     Yamaguchi, N.; Wang, J. S.; Hewitt, J. M.; Lenhart, W. C.; Mourey, T. H. *Journal of Polymer Science Part a-Polymer Chemistry* **2002**, *40*, 2855.

(32)     Miravet, J. F.; Frechet, J. M. J. *Macromolecules* **1998**, *31*, 3461.

(33)     Emrick, T.; Chang, H. T.; Frechet, J. M. J. *Macromolecules* **1999**, *32*, 6380.

(34)     Kim, Y. H.; Webster, O. W. *Macromolecules* **1992**, *25*, 5561.

(35)     Turner, S. R.; Voit, B. I.; Mourey, T. H. *Macromolecules* **1993**, *26*, 4617.

(36)     Uhrich, K. E.; Hawker, C. J.; Frechet, J. M. J.; Turner, S. R. *Macromolecules* **1992**, *25*, 4583.

(37)     Scholl, M.; Kadlecova, Z.; Klok, H. A. *Prog. Polym. Sci.* **2009**, *34*, 24.

(38)    Frechet, J. M. J.; Henmi, M.; Gitsov, I.; Aoshima, S.; Leduc, M. R.; Grubbs, R. B. *Science* **1995**, *269*, 1080.

(39)    Zhao, Z. F.; Wang, H. J.; Ba, X. W. *Journal of Chemical Physics* **2009**, *131*.

(40)    Sunder, A.; Hanselmann, R.; Frey, H.; Mulhaupt, R. *Macromolecules* **1999**, *32*, 4240.

(41)    Suzuki, M.; Ii, A.; Saegusa, T. *Macromolecules* **1992**, *25*, 7071.

(42)    Trollsas, M.; Lowenhielm, P.; Lee, V. Y.; Moller, M.; Miller, R. D.; Hedrick, J. L. *Macromolecules* **1999**, *32*, 9062.

(43)    Sunder, A.; Mulhaupt, R.; Frey, H. *Macromolecules* **2000**, *33*, 309.

(44)    Balzani, V.; Ceroni, P.; Gestermann, S.; Kauffmann, C.; Gorka, M.; Vogtle, F. *Chem. Commun. (Cambridge)* **2000**, 853.

(45)    Akin, M.; Yuksel, M.; Geyik, C.; Odaci, D.; Bluma, A.; Hopfner, T.; Beutel, S.; Scheper, T.; Timur, S. *Biotechnol. Prog.* **2010**, *26*, 896.

(46)    Satija, J.; Sai, V. V. R.; Mukherji, S. *J. Mater. Chem.* **2011**, *21*, 14367.

(47)    Stiriba, S. E.; Frey, H.; Haag, R. *Angewandte Chemie-International Edition* **2002**, *41*, 1329.

(48)    Eichman, J. D.; Bielinska, A. U.; Kukowska-Latallo, J. F.; Baker, J. R., Jr. *Pharm. Sci. Technol. Today* **2000**, *3*, 232.

(49)    Shah, D. S.; Sakthivel, T.; Toth, I.; Florence, A. T.; Wilderspin, A. F. *Int. J. Pharm.* **2000**, *208*, 41.

(50)    Richardson, S. C. W.; Pattrick, N. G.; Man, Y. K. S.; Ferruti, P.; Duncan, R. *Biomacromolecules* **2001**, *2*, 1023.

(51)    Ferruti, P.; Marchisio, M. A.; Duncan, R. *Macromol. Rapid Commun.* **2002**, *23*, 332.

(52)    Jang, W. D.; Selim, K. M. K.; Lee, C. H.; Kang, I. K. *Prog. Polym. Sci.* **2009**, *34*, 1.

(53)    D'Emanuele, A.; Attwood, D. *Advanced Drug Delivery Reviews* **2005**, *57*, 2147.


(54)    Kolhe, P.; Misra, E.; Kannan, R. M.; Kannan, S.; Lieh-Lai, M. *International Journal of Pharmaceutics* **2003**, *259*, 143.

(55)    Padilla, D. J. O. L.; Ihre, H. R.; Gagne, L.; Frechet, J. M. J.; Szoka, F. C., Jr. *Bioconjugate Chem.* **2002**, *13*, 453.

(56)    Barth RF, Adams DM, Soloway AH, Alam F, Darby MV., *Bioconjug Chem.* **1994**, 5,58–66

(57)    Shan, Y.; Luo, T.; Peng, C.; Sheng, R.; Cao, A.; Cao, X.; Shen, M.; Guo, R.; Tomas, H.; Shi, X. *Biomaterials* **2012**, *33*, 3025.

(58)    Wang, X.; Cai, X.; Hu, J.; Shao, N.; Wang, F.; Zhang, Q.; Xiao, J.; Cheng, Y. *J. Am. Chem. Soc.* **2013**, *135*, 9805.

(59)    Astruc, D.; Chardac, F. *Chem. Rev. (Washington, D. C.)* **2001**, *101*, 2991.

(60)    Twyman, L. J.; King, A. S. H. *J. Chem. Res., Synop.* **2002**, 43.

(61)    Twyman, L. J.; King, A. S. H.; Martin, I. K. *Chem. Soc. Rev.* **2002**, *31*, 69.

(62)    Sunder, A.; Heinemann, J.; Frey, H. *Chemistry-a European Journal* **2000**, *6*, 2499.

(63)    Varley, R. J.; Tian, W. *Polymer International* **2004**, *53*, 69.

(64)    Boogh, L.; Pettersson, B.; Manson, J. A. E. *Polymer* **1999**, *40*, 2249.

(65)    Jansen, J.; Meijer, E. W.; Debrabandervandenberg, E. M. M. *Journal of the American Chemical Society* **1995**, *117*, 4417.

(66)    Stiriba, S. E.; Kautz, H.; Frey, H. *Journal of the American Chemical Society* **2002**, *124*, 9698.

(67)    Sheiko S. S.; Gauthier M.; Möller M.; *Macromolecules* **1997**, 30, 2343.

(68)    Asif, A.; Huang, C. Y.; Shi, W. F. *Colloid and Polymer Science* **2004**, *283*, 200.

(69)    Zhang, Y. D.; Wada, T.; Sasabe, H. *Polymer* **1997**, *38*, 2893.

(70)    Seiler, M. *Fluid Phase Equilibria* **2006**, *241*, 155.

# Chapter 2

# Inhibition of protein-protein interactions using polyamidoamine (PAMAM) dendrimers

# Chapter 2 – Inhibition of protein-protein interactions using polyamidoamine (PAMAM) dendrimers

## 2.1 Introduction

### 2.1.1 Preface

At the start of my PhD, I worked alongside Dr. Fumiko Chiba in the area of protein-protein binding. This chapter will highlight my contribution towards this project within the group, and the results presented are reported in the literature.[1]

### 2.1.2 Introduction to Protein-Protein interactions

Proteins can interact with other proteins, resulting in the formation of protein-protein complexes, of which there are two types; namely homocomplexes and heterocomplexes. Homocomplexes are normally stable and enduring, whereas heterocomplexes can also exhibit durability, as well the ability to be formed or broken apart by external factors. Therefore, a prerequisite for heterocomplexes is the involvement of a protein which can exist independently. Protein-protein complexation is involved in practically all biological functions; including signal transduction[2], cytoskeletal remodelling[3], cell regulation[4] and many others.[4-6] Therefore, when two proteins interact with one another, it is neither a random nor unsystematic occurrence. Protein-protein association is meticulously scripted to accomplish a particular aim.[2]

As formerly stated, protein-protein interactions are of fundamental importance in numerous biological processes; some examples include hormone-receptor, protease-inhibitor and antibody-antigen complexes. The roles of these particular complexes are well known and understood. There are also numerous complexes which are not well known, but are of no less significance. Abnormal protein-protein interactions can also take place, which can play a significant role in a variety of disease processes. The condition drepanocytosis (more commonly termed sickle cell anaemia) is a disease brought about by the oligomerisation of mutant haemoglobin. This ailment highlights the negative effect of these undesirable protein-protein interactions. There are also protein-protein interactions which are less specific, occurring when proteins form aggregates. Misfolded protein aggregates, amyloid fibrils, are connected with numerous illnesses such as Alzheimer's and numerous forms of rheumatoid arthritis.[7]

**2.1.3 A Protein-protein binding interface**

As previously indicated, protein-protein interactions are extremely important in a vast array of biological processes, thereby triggering a large level of interest in the comprehension and potential manipulation of these interactions. In order to design molecules to interrupt protein-protein interactions, it is essential to gain understanding of the nature of protein-protein interfaces.[8] The protein-protein interface can be defined as the area of surface available on both protein partners in question, which become inaccessible upon interaction, and are predominantly hydrophobic in nature.[9]

There are often conformational changes involved with protein-protein complexation and numerous different models have been proposed to explain the mechanism involved. In 1894, Emil Fischer brought about the concept of the 'lock and key' model, assuming some kind of shape selectivity. This model indicates that one protein has a crevice into which its ideal partner fits, with practically no conformational change. However, it is important to understand that this proposal is not suitable for interactions of proteins with substances varying in shape. This dilemma was overcome by Daniel Koshland in 1958, by the introduction of the 'induced fit' model. This particular model assumes that the active site has a certain element of elasticity, enabling it to accommodate a ligand, and thereby leading to a change in conformation. Finally, the last idea proposed is the idea of a pre-existing equilibrium. This hypothesis indicates that the native state of the protein in question, displays an assembly of conformations at the active site, resulting in the ligand being drawn to an active conformation.[10]

The mechanism behind protein-protein interactions is complicated as a result of the large surface area involved. However, this is not the only factor to consider, electrostatics and hydrophobicity also play a crucial part. It is the cooperative effect from the combination of these numerous parameters which result in successful interactions.[4] The mechanism itself is highly specific; a protein selects a partner with an interfacial area comparable in size, of three dimensional shape, and with complementary intermolecular forces and amino acids in the correct location. **Figure 10** is a schematic representation for a simplified mechanism for protein-protein interaction, indicating the specificity of partner selection.
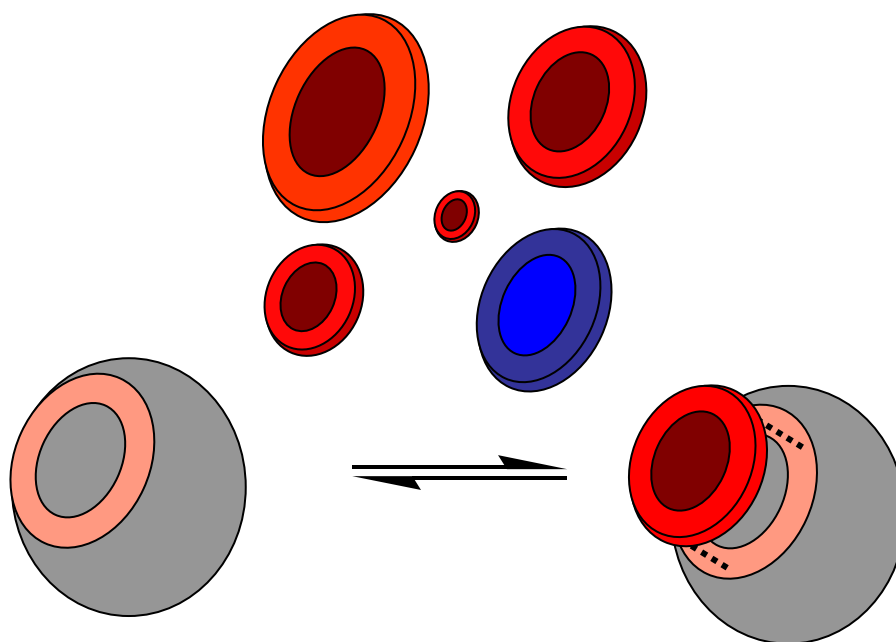
**Figure 10**- Schematic representation for the mechanism of protein-protein binding, illustrating the selection of a compatible partner.

The principles behind these specific interactions of proteins are not fully realised and, to gain a better understanding, Bogan and Thorn combined the techniques of alanine screening with kinetic and thermodynamic measurements.[5] These techniques were used to determine the contribution of individual residues to the key binding region, more commonly known as the 'hot spot.' The idea of the hot spot was first pioneered by Clackson and Wells[4, 11], and it originated from the discovery that the free energy of binding was not uniformly spread across the interface of a protein, but rather comprised of a small area of amino acid residues. It is the residues within this region which play a part in the stability of the protein complex.[8] The hot spot is therefore a critical feature of the protein-protein interface.

Bogan and Thorn demonstrated that 'hot spots' of binding energy are located near the centre of the interface, whereas residues located at the periphery rarely contribute to binding. Research also demonstrated that the surrounding residues of the hot spot most likely work by keeping bulk solvent away from interacting residues. The omission of bulk solvent from interacting residues has been shown to be a necessary condition for favourable interactions.[4] Bogan and Thorn also looked into amino acid preferences within the hot spot region, finding that the hot spots are enriched with three types of amino acid with a frequency larger than 10%, namely; tryptophan (21%), tyrosine (12.3%) and arginine (13.3%). As the amino acid

composition present in hot spots was not random, it showed that there was a preference towards certain amino acids with regards to the high energy interactions between two specific proteins in a heterodimer.[5]

Examining the structures of proteins at this level provides knowledge into the workings of protein-protein association; thereby enabling research into the design of synthetic agents which could disrupt unwanted interactions, which result in disease.

### 2.1.4 Inhibition of protein-protein interactions

Due to their fundamental role in biological systems, the interference and disruption of these interactions can result in the potential unearthing of new therapeutic agents. Research into the design of synthetic agents to interrupt these interactions has advanced over the years, and there has been a great deal of investigative work into the design of both small and large molecular weight molecules as prospective protein-protein binding inhibitors.[6]

When protein-protein complexation occurs, non-covalent interactions prevail; namely Van der Waals forces, electrostatic interactions, hydrogen bonding and hydrophobic effects. There are two different strategies which can be employed to inhibit protein-protein binding; firstly targeting the interior active site of the protein which is shielded from bulk solvent, and secondly, by targeting the exterior surface of the protein which is exposed to bulk solvent.

## 2.2 Protein-protein inhibition using low molecular weight synthetic agents

### 2.2.1 Small molecule inhibitors

The majority of research within the pharmaceutical industry in this area has involved designing small molecules as potential inhibitors. Traditionally, small molecules are designed specifically to interact with the active site or a specific site of the enzyme. The interactions within a protein active site which predominate include hydrogen bonding, electrostatic interactions and salt bridges. Consequently, small 'drug like' molecules, which possess hydrophilic motifs and hydrogen bond donor groups, could prove effective.[12] However, it is important to note that there are various challenges involved in the design of synthetic agents which are tailored to target protein-protein interactions. Firstly, the area required for recognition is quite sizeable (ranging between approximately 700-1500Å$^2$ per protein).[4] This creates a problem for small molecule inhibitors. Furthermore, interacting surfaces have been

ascertained as shallow cavities possessing no specific features, making selective targeting difficult to accomplish. Another drawback arises from the nature of the binding region of the protein partners in question. The binding site of the two proteins is frequently referred to as non-contiguous; thereby, meaning mimicry using straightforward synthetic peptides would be ineffective.[12] In addition, unlike enzyme-ligand interactions, protein-protein interaction surfaces are more complicated. Instead of one partner possessing a pocket and the other occupying said pocket, both proteins could contribute protrusions and sub pockets, thwarting inhibitor design.[13] Furthermore, when considering using small molecules as potential drug molecules, they need to be effective when in vivo. Not only must they demonstrate a high efficacy against the target protein, they must also reveal low toxicity and superior bioavailability. In general, molecules which exhibit these 'drug like' qualities have a tendency towards molecular weights less than 500.[14]

In the late 1990's, there were some advances in the development of small molecule inhibitors. In 1999, Quershi and co-workers developed a non-peptide antagonist **1** (**figure 11**). This molecule was discovered through the screening of a chemical library of inhibitors of human erythropoietin, binding to the extracellular region of the erythropoietin receptor. This led to the discovery of a biphenyl indole derivative, which showed competency as an inhibitor of interaction, with a maximal inhibitory concentration of 60μL.[14,15]
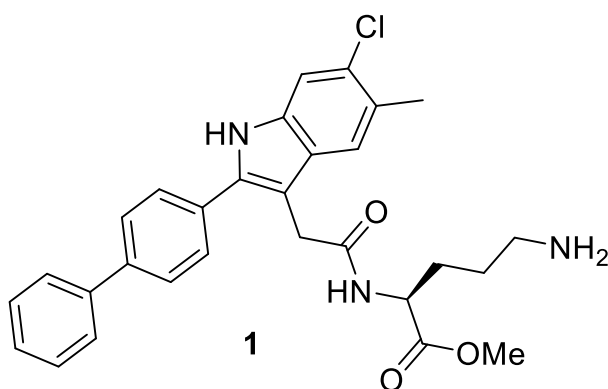


**Figure 11** – Figure to show the chemical structure for the non-peptide erythropoietin antagonist developed by Quershi and co-workers.[14, 15]

In addition to this, Tilley *et al.*[16] identified small molecules with the capability to block cytokine receptor signalling. Interleukin-2 (IL-2) is a cytokine which plays a crucial role in

growth activation and differentiation of T cells.[13] Initially, the small molecule **2** (**figure 12a**) was designed as a mimic for arginine and phenylalanine side chains of interleukin-2, which has crucial involvement in binding to the α subunit of the interleukin-2 receptor (IL-2Rα). Use as a mimic failed, but research has shown that it has subsequently been found to be a potent inhibitor of interleukin-2, binding to its receptor.[13, 14, 16] This provided the first example of a small molecule inhibitor of protein-protein interactions, where the inhibitor bound to the protein partner, as opposed to the receptor. Braisted *et al.*[17] expanded on this work to develop a more potent analogue **3**(**figure 12b**). This compound had an $IC_{50}$ of 60mM and bound to IL-2 with a 1:1 stoichiometry and a $K_d$ of 100nM. In 2005, Waal *et al.*[18] continued on from these advances and fabricated a nonpeptidic, potent inhibitor **4** (**figure 12c**). Continuing on from the work discussed beforehand, Waal and co-workers used chemical modification of previous analogues to enhance the ability of the inhibitor. Studies showed that the incorporation of furanoic acid resulted in a 23-fold improvement in the activity of the inhibitor.
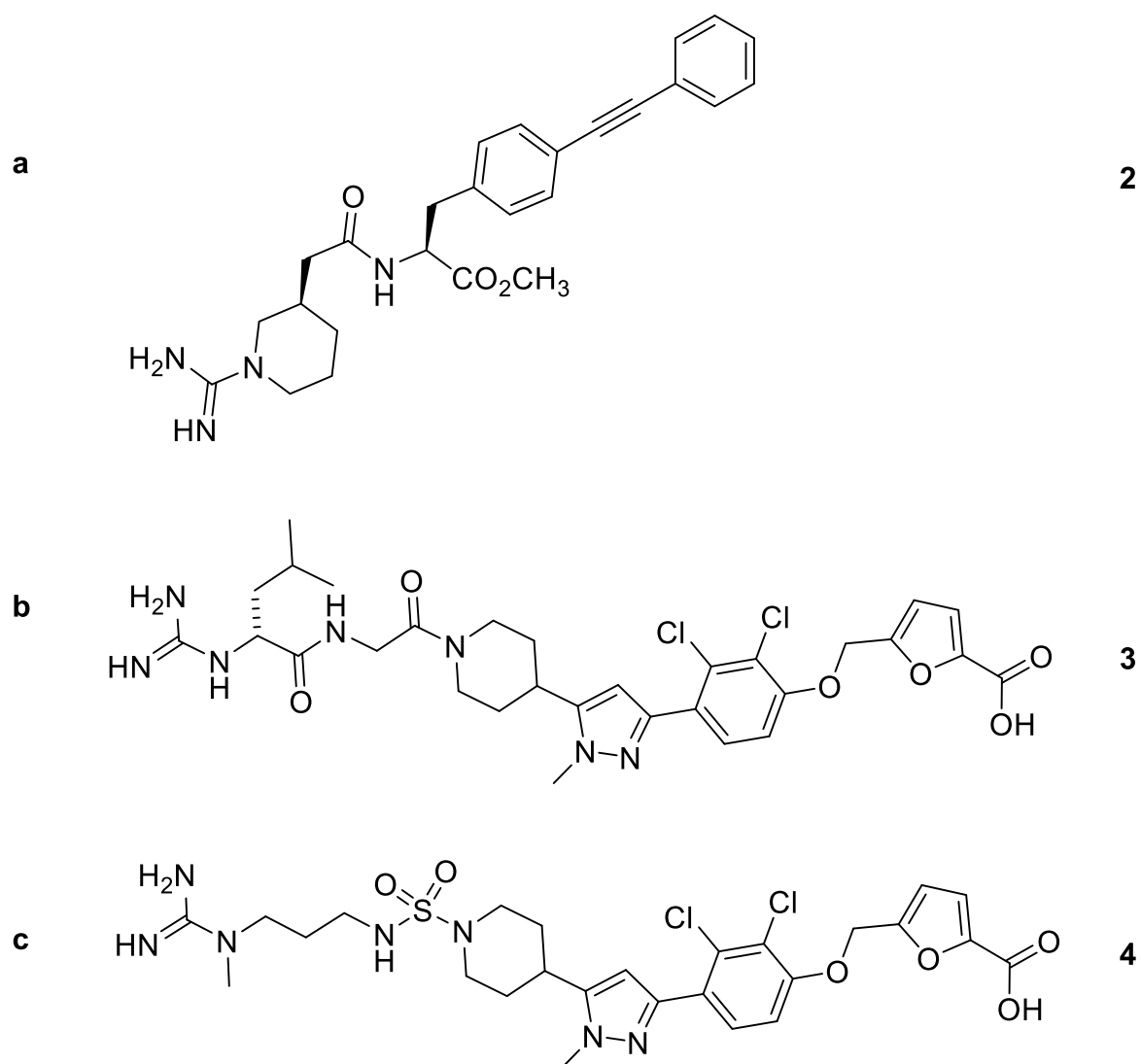
**Figure 12** – Figure to show small molecule inhibitors of the interaction between IL-2 and IL-2Rα. (**a**) acylphenylalanine based compound[16] (**b-c**) chemically modified derivatives of compound **a**.

The unearthing of these molecules is a revolution within this area of research, with further examples to be expected to continue.[17, 18]

An important protein target is inducible nitric oxide synthase (iNOS). Nitric oxide is a molecule which is vital in signal transduction and it is generated by the dimeric enzyme, nitric oxide synthase. The inducible isoform of this enzyme, iNOS, has been associated with tissue damage in a range of autoimmune diseases. An inhibitor designed specifically to target iNOS could therefore have valuable therapeutic use. McMillan and co-workers developed an inhibitor of iNOS, **5**, by the use of combinatorial chemistry (**figure 13**). X-ray crystallography studies confirmed perturbation of the substrate binding site and dimerization

interface. The inhibitor acts by disrupting the formation of the dimer by an allosteric mechanism. In *vivo* studies, using a rat model, demonstrate that the inhibitor displayed activity with $ED_{50}$ values <2 mg/kg. These results show the therapeutic potential of inhibitors of this nature.[13, 19]
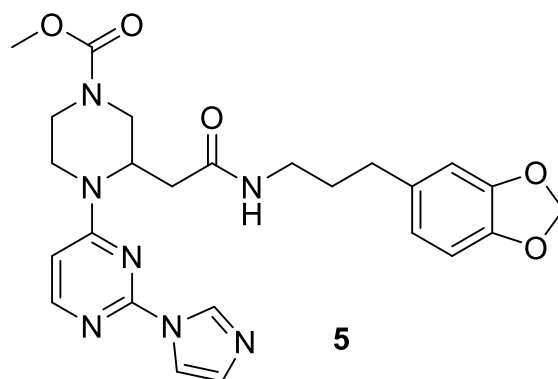


**Figure 13–** Figure to show the chemical structure of a small molecule inhibitor for inducible nitric oxide synthase (iNOS)[19]

Another important target is the tumour necrosis factor alpha (TNF-α). TNF-α is also a member of the cytokine family and is involved in systematic inflammation. There have been developments in the direct inhibition of TNF-α in the way of numerous inhibitory antibodies; such as Enbrel, Remicade and Humira. These have shown to be effective for treatment of rheumatoid arthritis.[13] Despite these advances; small molecule inhibitors are desirable due to advantages in cost and mode of administration. He *et al.*[20] developed the potent inhibitor of TNF-α (**6**) shown in **figure 14**. The inhibitor displaces a subunit of the biologically active trimer, resulting in the formation of the inactive dimer.
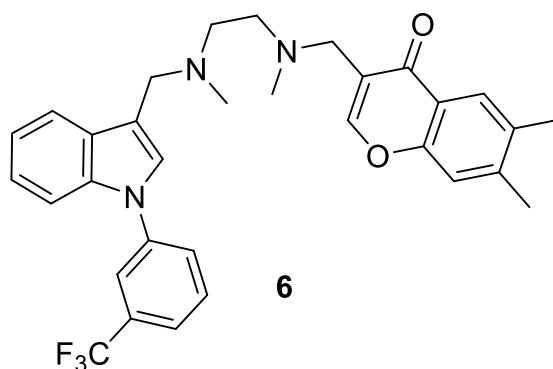


**Figure 14–** Figure to show the chemical structure of a small molecule inhibitor of tumour necrosis factor-α (TNF-α) developed by He *et al.*[20]

### 2.2.2 α-Helix Mimetics

A breakthrough within this field was the discovery of the important role helical segments play in a range of protein-protein interactions. Therefore, the synthesis of helical mimics gives rise to potential therapeutic development.[21] It has been deduced that approximately 15% of the protein data bank (August 2009) is made up of protein-protein complexes. Furthermore, 62% of these complexes possess a helix at the interface. This data therefore highlights the importance of α-helices in protein-protein interactions.[22] In 2008, work by Per Restorp and Julius Rebek Jr. described the synthesis of a series of heterocyclic piperazine based scaffolds **7** to **10** (**figure 15**), which are able to mimic the i, i+4, i+8 and i+11 side chains of an α- helix. The general synthetic procedure reported can be used in the synthesis of α-helix mimics, tailored to a specific interaction. These compounds were specifically designed to mimic the amphiphilicity of α-helices. This was accomplished by having a hydrophilic surface for hydrogen bonding and a hydrophobic surface which could interact with the protein.[23]



7: R = $^i$Pr, R' = $^i$Pr
8: R = $^i$Pr, R = Bn
9: R = Bn, R' = Bn
10: R = Bn, R' = $^i$Pr
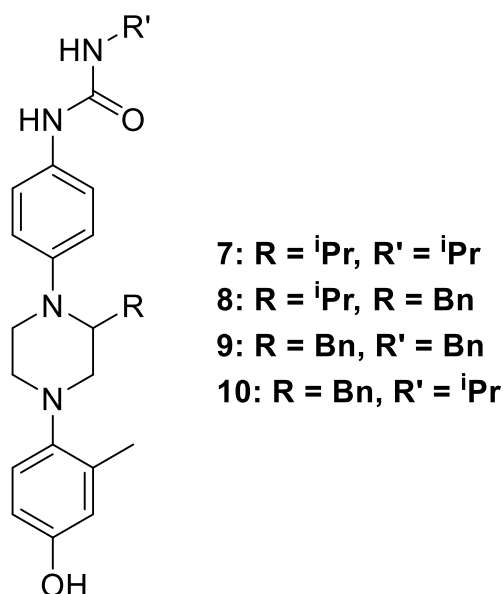
**Figure 15**– Figure to show the chemical structure for the skeleton for a series of heterocyclic piperazine based scaffolds (compounds **7** to **10**) developed by Per Restorp and Julius Rebek Jr.[23]

The importance of inhibition of protein-protein interactions for cancer therapy is of vital importance. The tumour suppressor protein, P53, is a potent transcription factor which protects cells from harmful transformations. *H*DM2 is responsible for regulation of level and

activity of p53 and overexpression of *h*DM2 will subsequently result in the impairment of the protein's function.[24] The interaction between p53 and *h*DM2 involves three hydrophobic residues from the tumour suppressor protein coordinating in a helical conformation to a hydrophobic cleft present on *h*DM2. The key hydrophobic residues are Phe19, Trp23 and Leu26.[25] Therefore, the inhibition of the interaction between *h*DM2 and p53 could stabilise the protein, providing a novel therapeutic approach to cancer therapy. Vassilev and co-workers[24] have developed a small molecule inhibitor which coordinates *h*DM2 within the binding pocket of p53, thus activating its pathway in cancer cells. Studies in nude mice have shown results of cell arrest, apoptosis and growth inhibition of human tumour xenografts. X-ray crystallography studies have shown that *h*DM2 has a deep cavity filled with side chains from the helical region of the peptide. The small molecule antagonists were a series of cis-imadazoline analogues referred to as Nutlins. After chemical optimisation, Nutlin-3 was developed (**figure 16**) and demonstrated inhibition of *h*DM2-p53 complexes with an $IC_{50}$ of 90nM. In addition, this small molecule antagonist displayed activity against xenografts in *vivo*.
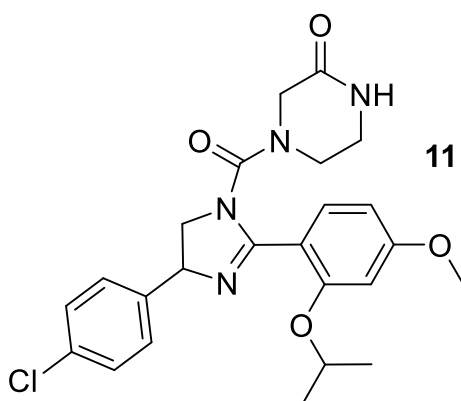


**Figure 16**– Figure to show the chemical structure of Nutlin-3, a cis-imadazoline based inhibitor developed by Vassilev and co-workers.[24]

Research concerning the disruption of this particular interaction has continued as a result of the therapeutic potential regarding cancer therapy. In 2009, Plante *et al.*[25] developed a series of oligobenzamide proteomimetic inhibitors. As stated previously, the three key residues present at the hDM2-p53 complex interface are Phe19, Trp23 and Leu26. An important strategy in the scaffold design of a helical mimic is that the scaffold is able to mimic the residues at i, i+4 and i+7 of the p53 helix. One of the compounds developed, the oligobenzamide (**figure 17**), was superimposed on the face of the p53 helix. It is apparent

that the O-alkyl substituents of the amino terminated tri-benzamide all lie on the same face and also mimic the orientation in space of the i, i+4 and i+7 residues of the α-helix. These results therefore demonstrate the ability to fabricate an effective mimic.
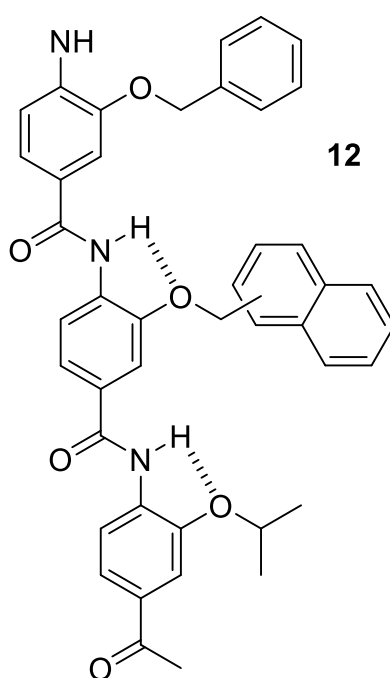


**Figure 17–** Figure to show the chemical structure of an oligobenzamide proteomimetic inhibitor developed by Plante and co-workers.[25]

As stipulated beforehand, there has been a large amount of interest in the creation of non-peptidic small molecule α-helical mimics as inhibitors for protein-protein interactions. In 2011, Lee *et al.*[26] reported the synthesis of a novel pyrrolopyrimadine based receptor **13** (**figure 18**). The ability of this scaffold to interrupt the p53-MDMX interaction was monitored, so as to determine its ability as an α-helical mimic. Initially, the scaffold was screened against a library of 900 compounds and primary amines which contained hydrophobic groups were selected. The hydrophobic groups were essential in mimicking the side chains of the three amino acids found in p53. This particular scaffold exhibits conformational rigidity, good aqueous solubility and cell permeability. Moreover, the synthetic route is relatively easy and as a result, the synthetic procedure will comply with the

construction of large libraries and high throughput screening. Consequently, this scaffold could be useful in the discovery of a range of inhibitors of this nature.
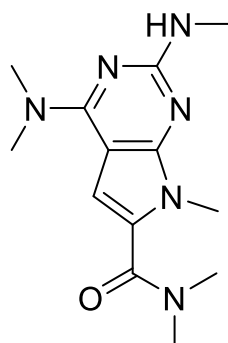


**13**

**Figure 18 –** The pyrrolopyramidine based α-helix mimic developed by Lee *et al.*[26]

This section is not an exhaustive account; therefore, for more information regarding disruption of protein-protein interactions with non-peptidic small molecule α-helix mimetics, the reader is directed to the following review by Hamilton and Cummings.[27]

### 2.2.3 Porphyrin and calixarene based receptors

Due to the difficulty in the design of small molecule inhibitors, large scaffold molecules have also been investigated as potential protein binding agents. As previously stated, the design of synthetic agents to bind to an active site has been investigated extensively. However, an alternative approach to the disruption of protein-protein association is by binding to the surface of a protein in the proximity of, but not directly within, the protein active site.[8] The peripheral surface is distinctive and characteristic to each individual protein and comprises of hydrophobic, hydrophilic and charged regions. In addition to electrostatic interactions, hydrogen bonding and π- π stacking interactions also feature at the interface between two connecting proteins.[12]

The greater part of molecules investigated disrupt interactions by binding inside active cavities on proteins; meaning synthetic molecules which intervene the function of a protein through binding to the outer surface, are comparatively uncharted. Not only could this expose

new drug candidates, but it will assist in the comprehension of the periphery of proteins and the understanding of surface recognition.[28]

In 1985, Fischer *et al.* provided evidence that a tetracarboxyphenyl porphyrin (**figure 19**) proved to be a corresponding topographical mimic for cytochrome-c binding with a $K_d$ of 5µM.[29] Cytochrome-c is an electron transport protein found in horse heart and is questionably one of the most studied proteins. It is considered an attractive target as it plays an important role in both electron transfer and aptosis. The surface of the heme edge is bordered by a series of arrangements of cationic lysine residues and hydrophobic domains, signifying a strong dependence, in particular, on electrostatic interactions.[12]
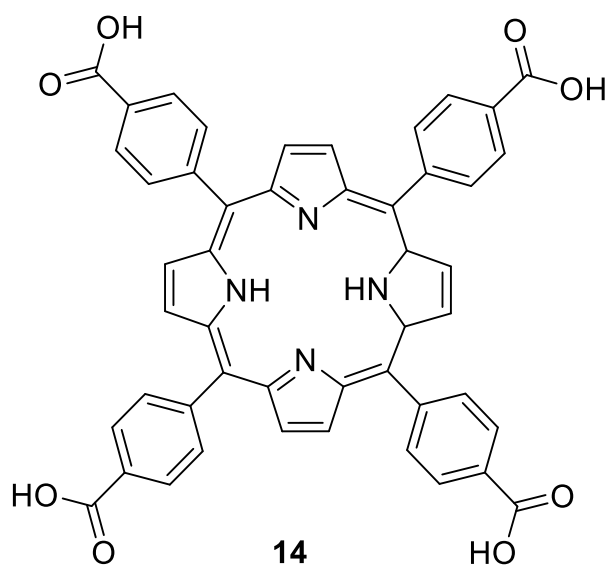


**Figure 19**- Figure to show the chemical structure of tetracarboxyphenyl porphyrin.

Hamilton *et al.* continued work in this area investigating both tetraphenyl porphyrin scaffolds[28,30-32] and calix[4]arene scaffolds[33,34] using a range of techniques, including fluorescence spectroscopy. In 1997, Hamilton *et al.*[33] developed the strategy of using a macrocyclic scaffold, to which peptide loops could be covalently attached. Subsequently, an antibody mimic, based upon calix[4]arene linked to four constrained peptide loops, was fabricated (**figure 20**)[35]. Calix[4]arene was selected as it is not only easily obtainable but it can be locked into a cone conformation, which results in para substituents being propelled onto the same edge of the ring, thereby forming a binding domain.[33]

**15**
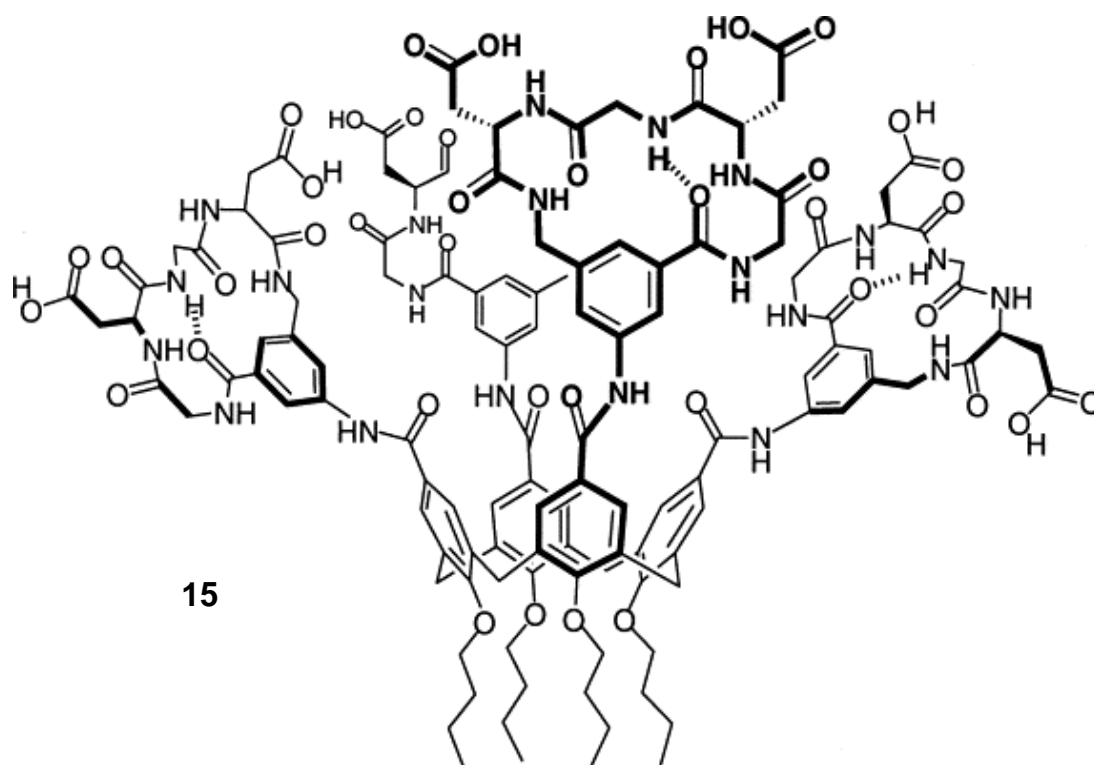
**Figure 20** – Figure to show the chemical structure for an antibody mimics based upon a calix[4]arene scaffold and covalently attached to four peptide loops of the sequence (Gly-Asp-Gly-Asp). This mimic was used for the surface recognition of cytochrome-c and designed by Hamilton and co-workers.[i] Reprinted with permission from [**Lin, Q.; Hamilton, A. D. C. R. Chim.** 2002**, 5, 441-450**]. Copyright [2002] Elsevier Masson SAS. All rights reserved

The initial target protein used was cytochtome-c. It is both well studied and well characterised and is known to have a positively charged surface. The peptide loops are comprised of negatively charged (Gly-Asp-Gly-Asp) sequence. Negatively charged peptide loops are required in order to complement the positively charged surface of the target protein. Subsequent X-ray studies showed that four peptide loops could interact with four lysine residues present, thereby meaning that the synthetic receptor will cover a large area of the surface of the protein. The receptor was shown to disrupt cytochrome c/cytochrome c peroxidase complex formation, consistent with the X-ray studies.[35] Further work by this research group demonstrated that an antibody mimic of this nature was also able to interact with the surface of chymotrypsin, disrupting serine protease-proteinaceous inhibitor interactions.[36] Calixarene receptors proved disadvantageous as a result of the arduous synthetic procedures involved, and the low yields obtained. For further information on

supramolecular scaffold based receptors, similar to those mentioned above, the reader is directed to the following literature.[37-39]

In 2000, this research group demonstrated that the surface of cytochrome-c could be recognised by receptors based on a tetraphenyl porphyrin scaffold with a variety of amino acid and peptide derivatives around the outside edge (**figure 21**).[28] The results showed that the relative affinity of a receptor to the protein surface was dependent upon the amount of hydrophobic and anionic groups present. These receptors bound with a high affinity in an aqueous medium with receptor **19** showing the highest affinity for the surface of cytochrome-c exhibiting a $K_d$ of 20 nM. In addition to protein surface recognition, these results have unearthed a potential medicinal property for receptor **19**. Previous reports have confirmed that cytochrome-c can interact with the apoptopic protease activating factor, APAF1.[40] This interaction can result in the activation of aptosis. Therefore, receptors of this nature could prove useful in the disruption of this particular protein-protein interaction.[28]

**16** R= -COOH

**17** R=

**18** R=

**19** R=
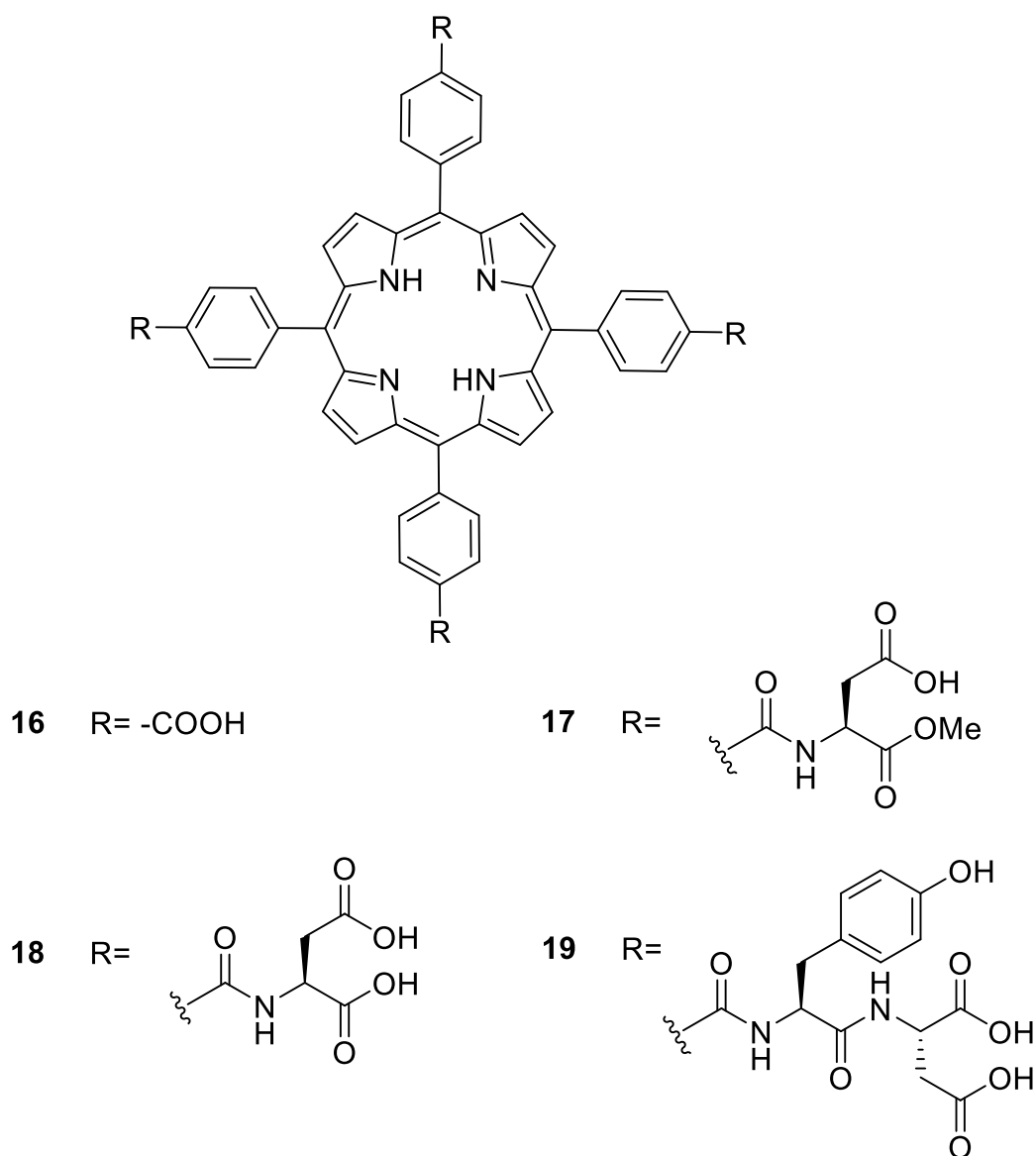
**Figure 21**- Figure to show the chemical structures for a series of tetraphenyl Porphyrin scaffolds for the recognition of the peripheral surface of Cytochrome-C designed by Hamilton and co-workers.[28]

As previously mentioned, the peripheral surface of a protein is crucial in mediating protein-protein binding in numerous biological processes, such as cell proliferation and cell growth. Therefore, synthetic molecules which complement the structural features of the protein periphery are expected to bind, thereby disrupting surface, as opposed to the enzyme active site. In 2003, Hamilton *et al.*[37] reported a series of tetrabiphenyl porphyrin-based receptors, one of which, **20** (**figure 22**), shows a particularly high affinity towards the surface of cyt-c ($K_d$ = 0.6 nM). Circular dichroism was employed to investigate the effect of coordination of this receptor on the protein. In the absence of the receptor, the melting temperature of cytochrome-c was 85 °C. However, in the presence of the porphyrin receptor, the melting

temperature was reduced to 35ºC. These results provide a platform for the subsequent development of other porphyrin-based receptors for protein surface recognition and protein denaturation. In relation to this work, Hamilton and co-workers have also developed various metalloporphyrin dimers which have resulted in accelerated proteolysis of cytochrome-c.[38, 39]



**20**
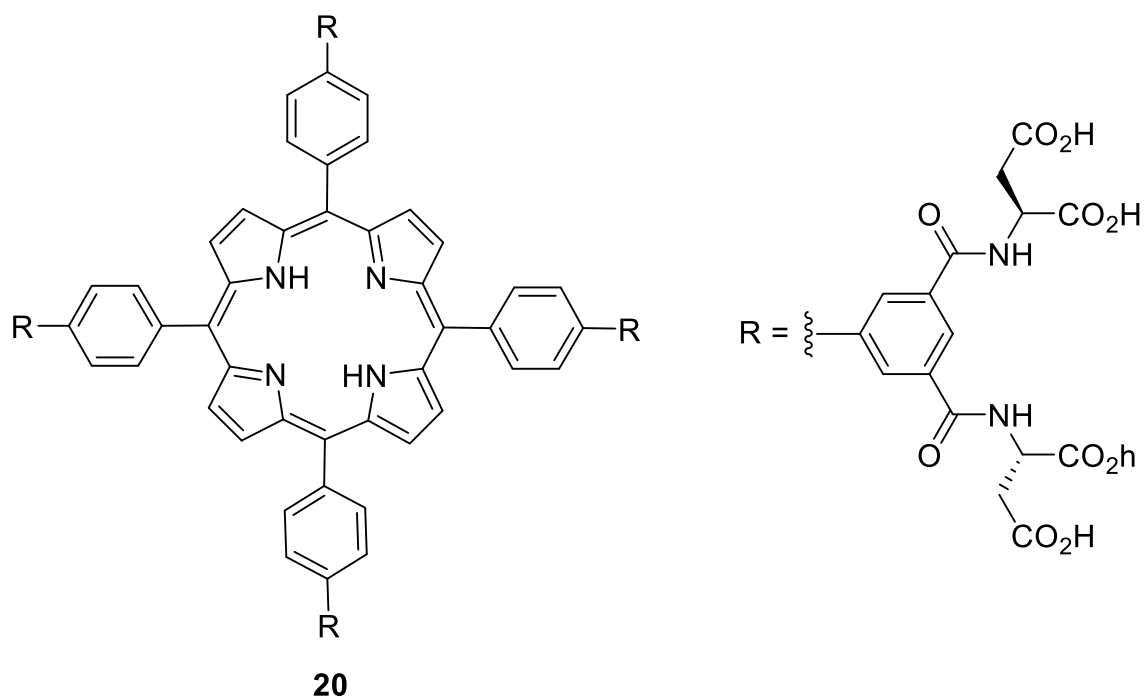
**Figure 22**– Figure to show the chemical structure of a tetrabiphenyl porphyrin-based receptor for the surface recognition and enhanced unfolding of cytochrome-c.[37]

In 2003, Trauner *et al.*[41] developed a class of porphyrin based ligands for surface recognition of potassium channels. The four-fold symmetrical molecules act as mimics of peptide toxins, and subsequently bind to the four subunits of the channel. These ligands bind to the $K_v1x$ class of potassium channels, partially obstructing conductance. Potassium channels regulate membrane potential and play a part in a range of cellular processes. As a result, they have become a target for drug design. Synthetic inhibitors could provide therapeutic solutions to numerous conditions, such as various autoimmune disorders and cardiac related illnesses.[42] The series of porphyrin ligands were used for competitive binding assays with ^{125}I-hongo-toxin1-A19Y/Y37Ff. This toxin coordinates to the outer vestibule of $K_v1.3$ channels. This particular voltage-gated potassium channel is crucial in human T-lymphocyte activation. Results have shown that the cationic ligands **21**, **22** and **23** (**figure 23**) displayed the strongest interaction with the $K_v1.3$ channel. The cationic side chains could form salt bridges to aspartate residues, explaining the high affinity shown. The geometry of ligands **21**, **22** and **23**

was also correct for sufficient binding. Ultimately, the development of this class of compounds could unearth novel therapeutic agents for a wide range of ailments.[41]



**21**:  R = HN-(CH$_2$)$_2$-NH$_2$
**22**:  R = HN-(CH$_2$)$_4$-NH$_2$
**23**: R = HN-Lys-HN-(CH$_2$)$_3$-NH$_2$
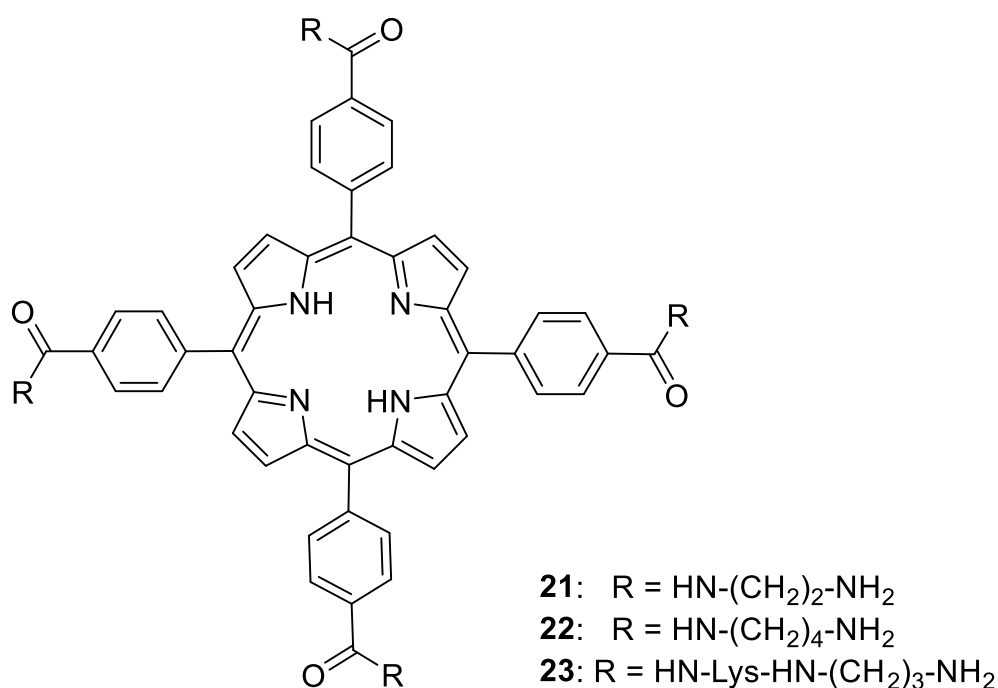
**Figure 23–** Figure to show the chemical structures for a series of cationic porphyrin-based ligands for the surface recognition of potassium channels developed by Trauner *et al.*[41]

Notwithstanding these intimidating challenges, there have been many advances in this area of research and there are numerous examples of synthetic low molecular weight ligands able to inhibit two protein partners. For more information on this area of research, the reader is directed to the following literature reviews.[12-14, 44-48]

## 2.3 Aims and Objectives

As discussed earlier, protein-protein associations play a fundamental role in numerous biological processes. Furthermore, unwanted interactions can also occur, leading to numerous diseases such as sickle cell anaemia.[49] Therefore, being able to understand the manner by which proteins interact with each other is crucial for the development of potential novel inhibitors and drug molecules.[50] Due to the large interfacial areas proteins possess, discovering small drug like molecules as inhibitors has been difficult.[2] As can be seen from the introduction and highlighted literature, there have been some intriguing developments which show that small molecule inhibitors are becoming closer to realistic use in this area of research. There have been numerous successful reports of small molecules interfering with protein-protein interactions, and thus behaving as competent inhibitors to binding.[14] In nature, proteins bind large molecules, such as other proteins. **Figure 24** is a plot of known protein-protein complexes found in the literature.[9] The number of complexes with similar binding areas are grouped together and then these groups are plotted (i.e. number of protein-protein complexes with a particular interfacial area vs. the size of the interfacial area).
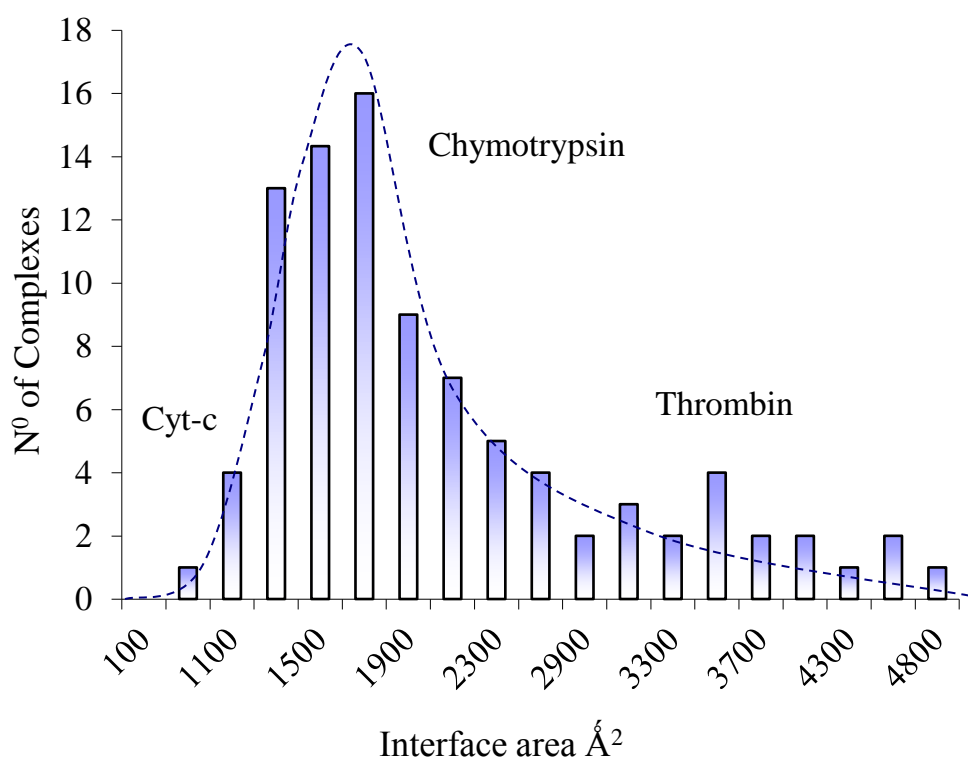


**Figure 24**- A graph to represent the distribution of interfacial areas from common protein-protein complexes.[9]

This plot shows that protein complexes cover a wide range of areas, which has triggered interest in the research of higher molecular weight molecules as potential synthetic inhibitors to protein-protein binding. Owing to the large interfacial area of proteins, the ability to synthesise a succession of macromolecular structures able to interact over a range of areas is an important target. As identified earlier, size is not the only factor to consider. The mechanism for protein-protein interactions also involves the three dimensional shape, functionality and the specific location of this functionality within the interacting area. Therefore, the aim of this research is to synthesise a succession of macromolecular structures which fit these fundamental criteria.

There are several large molecules to consider, the first being linear polymers. There have been numerous studies involving the interaction between linear polymers and proteins. Bruening *et al.*[51] demonstrated the high capacity binding of proteins by poly (acrylic acid) brushes; whereby thick polymer brushes were developed to immobilise multiple monolayers of proteins. The PAA brushes were derivatised with a nitro triacetate/copper complex ((NTA)-$Cu^{2+}$) and exhibited the ability to bind a wide variety of proteins. The capability of the interaction of proteins with a surface could prove irrefutably valuable in the area of protein purification. Another example can be seen in the work by Wowk *et al.* It was shown that the inhibition of bacterial ice nucleation could be achieved using simple linear polymers; namely polyglycerol and polyvinyl alcohol. It was shown to bind, and thus inhibit the ice nucleating activity of proteins from Pseudomonas syringae (an ice nucleating bacterium). This bacterium can be located on the surface of certain bacteria. Both polyglycerol and polyvinyl alcohol were investigated, with polyglycerol proving to be the more potent and specific inhibitor of the two, however, the combination of the two linear polymers exhibited more efficacy than either agent individually.[52]

For the purpose of this research specificity is crucial; therefore, linear polymers are far too dynamic and flexible. The interaction between proteins and linear polymers arises because of polyvalent effects. That is to say, the more charges present, the stronger the binding. As a result, there is no size specificity, as a linear polymer can freely change its shape to maximise binding. As a result, their interactions with proteins is predominantly referred to as 'non-specific'.[53]

The next class of molecule we took into consideration were dendritic polymers; namely hyperbranched polymers and dendrimers. As previously mentioned in chapter 1 of this report, dendritic polymers differ from conventionally branched polymers, due to the potential for branching at each and every monomer repeat unit, thereby resulting in a large quantity of functionalised terminal groups. Due to the surface of proteins possessing regions of high charge, dendritic polymers seem a viable option for this research.

Hyperbranched polymers have imperfectly branched irregular architectures in comparison to dendrimers, meaning they display a higher level of flexibility. Although not as flexible as linear polymers, we felt they may still be too flexible; as a result, they may not execute the desired level of specificity for the main target of this work. Dendrimers consist of a series of regular branching throughout their globular like structure surrounding a core. They are symmetrical and monodisperse, and exhibit an elevated degree of molecular uniformity and an element of rigidity compared to linear and hyperbranched polymers. Dendrimers have regular structures and exhibit a quantised size effect. Consequently, their maximum addressable area is quantifiable and is equal to their diameter squared. The peripheral surface of a dendrimer can also be easily functionalised. This is beneficial as the mechanism of protein-protein binding involves matching size, shape, terminal functionality and the position of this functionality. These specific qualities therefore make dendrimers an attractive option for application as large molecule inhibitors for protein-protein binding.

Other work within the Twyman group has demonstrated the presence of a size effect of dendrimers, which can be developed towards a size selective binding mechanism for the inhibition of protein-protein interactions. That is to say, for a particular protein, the dendrimer which binds the best is effectively the one whose addressable area is closest in size to the interfacial area of the target protein. When a large ligand interacts with the active site of an enzyme, it is effectively blocked-up, thereby hindering the function of the enzyme. Therefore, the dendrimer which binds the best will also be the most potent inhibitor.[50, 54] The dendrimers used were a series of PAMAM dendrimers, which are illustrated schematically overleaf in **figure 25**.
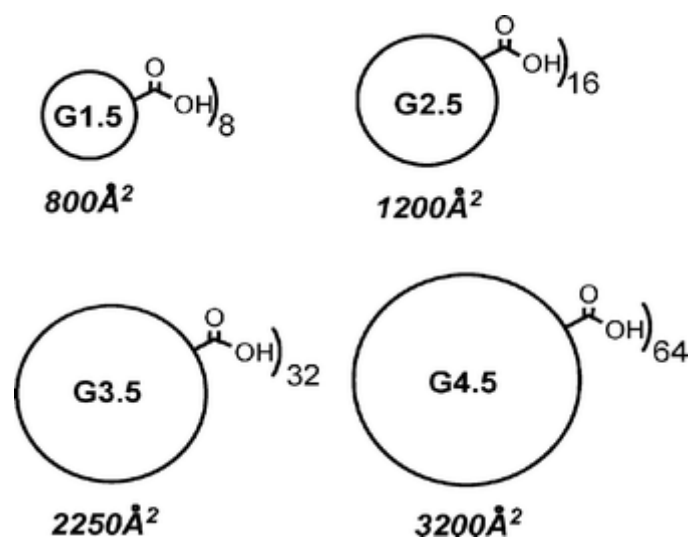
**F**i**gure 25 –** Figure to show a series of PAMAM dendrimers (and their corresponding addressable areas), which were investigated as size selective inhibitors for protein-protein binding. Reprinted with permission from [Chiba, F.; Hu, T.-C.; Twyman, L. J.; Wagstaff, M. *Chem. Commun. (Cambridge, U. K.)* **2008**, 4351]. Copyright [2010]  WILEY-VCH Verlag GmbH & Co. KGaA, Weinheim.

Although previous work has demonstrated this principle, the location for dendrimer interaction remains unknown, be it at the active site entrance or another location. For instance, it is possible that the dendrimer is binding to another location on the protein surface. This would cause a conformational change to the structure of the protein, rendering it denatured, which would result in the same inhibition data ascertained. In order to determine the effect that interaction with a dendrimer has upon the structure and stability of a protein, the technique of circular dichroism will be employed, due to its sensitivity towards protein secondary structure. Therefore, the principal aims of this aspect of the project are (i) to establish that binding is possible and (ii) to determine whether the protein is denatured upon interaction with a dendrimer.

## 2.4 Results and discussion

### 2.4.1 Dendritic macromolecules as inhibitors to protein-protein binding interactions

In order to carry out the aims outlined beforehand, the initial step was the synthesis of a range of different generation PAMAM dendrimers. The physical and chemical properties of this family of macromolecules are well known and the synthetic procedures behind them are recognised, [55, 56] making them a viable option for these studies. **Figure 26** represents a series of acid terminated PAMAM dendrimers to be synthesised and their corresponding addressable areas calculated from their diameter squared. The synthetic procedure of half and whole generation PAMAM dendrimers consists of two iterative steps; Michael addition and amidation. The addition process is required to generate half generation dendrimers with ester terminal groups and the amidation step gives rise to whole generation dendrimers with amine terminal groups.
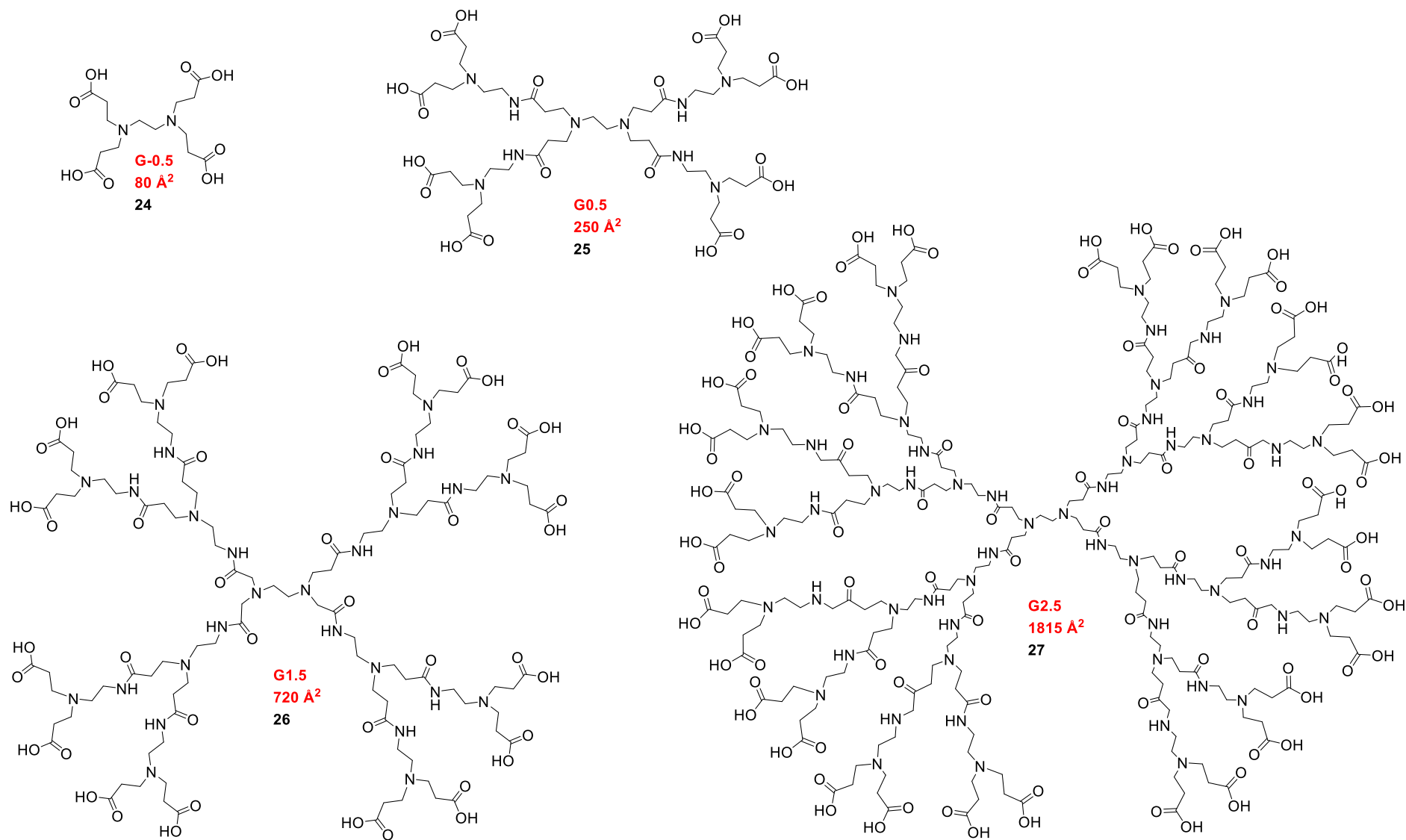
**Figure 26** – Series of acid terminated PAMAM dendrimers and their corresponding maximum addressable areas.

In general, Michael addition (**scheme 4**) involves alpha-beta unsaturated carbonyl compounds. The carbonyl substituent has an electron withdrawing effect, generating a delta positive charge on the alpha carbon. Due to resonance stabilisation, the beta carbon is rendered electropositive and is therefore susceptible to nucleophilic attack. In this reaction, the alpha beta unsaturated carbonyl system is methyl acrylate and the $NH_2$ groups on ethylene diamine acts as a difunctionalised nucleophile.
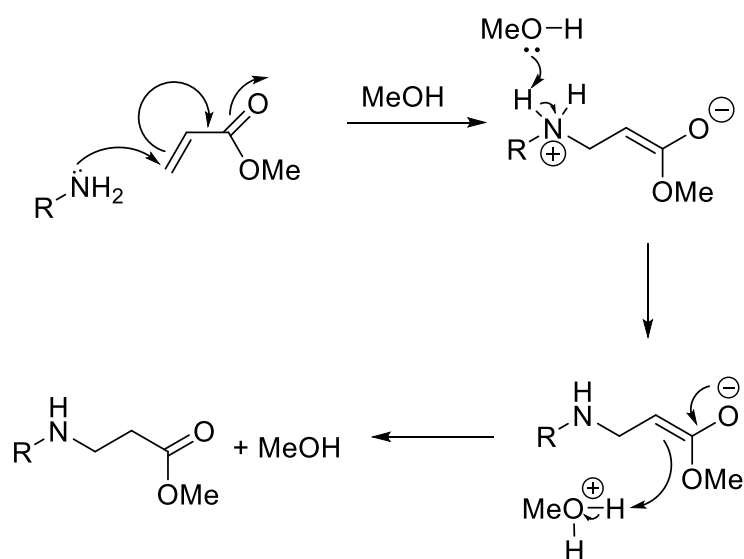


**Scheme 4** – Reaction mechanism for the Michael addition step in PAMAM dendrimer synthesis.

In the amidation step (**scheme 5**), the nucleophilic nitrogen from ethylene diamine attacks the electropositive carbonyl carbon of the methoxy group.
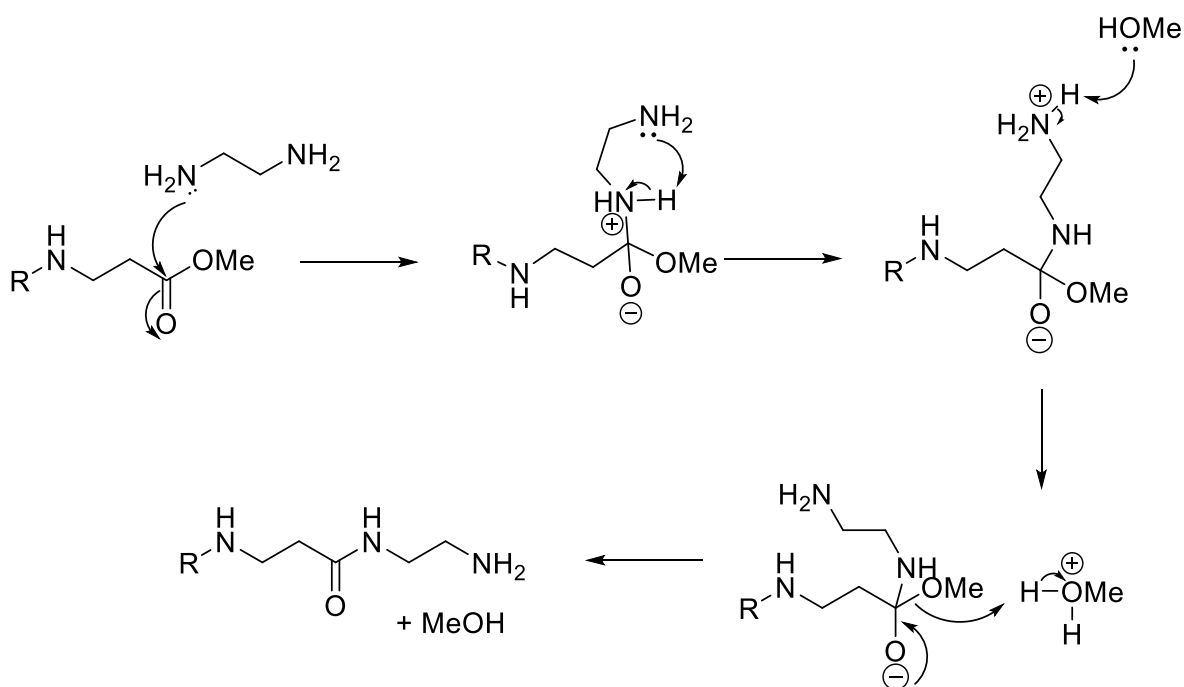
**Scheme 5** –Reaction mechanism for the amidation step of PAMAM dendrimer synthesis.

## 2.4.2 Synthesis of PAMAM dendrimers

### 2.4.2.1 Synthesis of PAMAM dendrimers with ether terminal functionality

In order to synthesise half generation dendrimers possessing ester terminal substituents, ethylene diamine was dissolved in methanol and an excess of methyl acrylate was added drop wise. For instance, with generation -0.5 (PAMAM dendrimer possessing four terminal ester groups) five molar equivalents of methyl acrylate was added to ethylene diamine and left to react at room temperature over a period of 24 hours to ensure the reaction reached completion. Excess methyl acrylate was removed via rotary evaporation and, to ensure complete eradication, the product was monitored by ^{1}HNMR. The solution altered from a colourless solution to viscous yellow oil after purification and isolation. As the generation of dendrimer increases, the viscosity of the product also increases.

### 2.4.2.2 Synthesis of PAMAM dendrimers with amine terminal functionality

With the amidation stage, a large excess of ethylene diamine is required. If the amine in question is not added in excess, defects will arise within the structure of the dendrimer. This will then result in the loss of molecular uniformity and monodispersity of the dendrimer. With the case of generation 0 (4 terminal amine groups), 0.017 moles of the ester terminated G-0.5 PAMAM dendrimer was reacted with 0.82 moles of ethylene diamine, which equated to 48 molar equivalents. The reaction time required for the amidation step varied with respect

to dendrimer generation. Longer reaction times were required for larger dendrimers due to the increase in terminal groups. G0 required a reaction of time of 5 days to reach completion while G1 and G2 required a reaction time of 7 days.

### 2.4.2.3 Characterisation

To ensure purity of product, a variety of characterisation techniques were implemented. The techniques employed were ^{1}HNMR and ^{13}CNMR spectroscopy, mass spectrometry and IR spectroscopy. **Figure 27** represents the proton NMR spectrum of G-0.5. It shows the methoxy peak at 3.68 (a signal characteristic to each ester terminated dendrimer). As the generation increases, the integral of this signal increases accordingly, due to the augmentation in methoxy groups. There are two triplets which can be seen at 2.48ppm and 2.78ppm, which correspond to the two methylene proton environments present. The methylene protons neighbouring the ester functional group will be more shielded in comparison to their neighbours, accounting for the difference in chemical shift. Finally, the singlet at 2.54ppm is indicative of the core protons of ethylene diamine. The ^{1}HNMR spectrum of G-0.5 is relatively clear-cut giving sharp signals. However, as the generation increases, many proton environments become comparable. This leads to considerable overlap, not to mention broadened triplets and multiplets. Although the spectra produced for larger generations is not quite as straight forward in comparison to smaller generations, classification can still be achieved with a sufficient level of accuracy.

Owing to their molecular uniformity and monodispersity, dendrimers have exact molar masses, meaning that mass spectrometry is an invaluable tool in dendrimer characterisation. From the results acquired, each whole and half generation displayed a molecular ion peak in the position corresponding to the exact molecular weight predetermined from ideal structures, consequently providing confidence in the synthetic procedure employed. IR data provided additional information, confirming correct functional groups inherent to both whole and half generation dendrimers. Although not an appropriate tool alone for characterisation, it is useful when combined with other techniques.
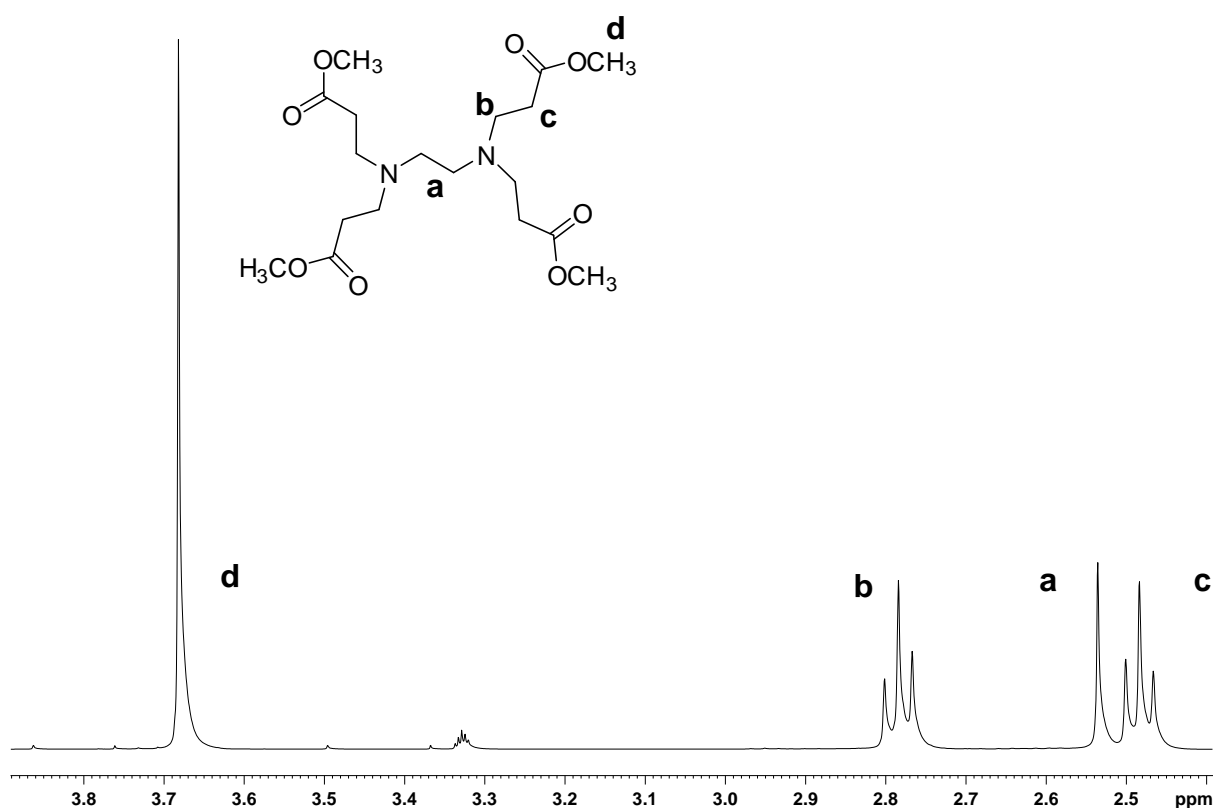
**Figure 27** – Figure to show the ^{1}HNMR spectrum of a G-0.5 PAMAM dendrimer with an ethylene diamine core.

## 2.4.2.4 Purification

The purification of each generation is a crucial stage in the synthetic procedure. If purification is not thorough, the outcome will be unwanted by-products and defects within the dendrimer architecture. Excess methyl acrylate in each Michael addition was easy to remove, owing to the high volatility of the compound. As a result, rotary evaporation was sufficient in the eradication of excess methyl acrylate present, meaning that each half generation PAMAM dendrimer could be purified without complications. Purification is essential after each amidation step as major problems arise if ethylene diamine is not totally removed. Excess ethylene diamine can behave as a new initiator centre, meaning a new dendrimer will also be synthesised. In addition, structural flaws and undesired by-products can also occur. Ethylene diamine is difficult to remove as it is able to form strong hydrogen bonds between the internal amide of the dendrimer and the peripheral amine groups. Both ^{1}HNMR and ^{13}CNMR can be utilised to verify the efficacy of purification. If ethylene diamine is present, a signal will be seen at 45 ppm in the ^{13}CNMR spectrum and 2.65 ppm in the [1]1HNMR spectrum, indicating purification is incomplete.

61

In order to completely eliminate ethylene diamine, the product must be washed repeatedly with an azeotropic mixture of toluene and methanol in a 9:1 ratio. The solvent is then removed by rotary evaporation. Due to the strong hydrogen bonds formed between ethylene diamine and the dendrimer, something must be incorporated which competes for the hydrogen bonding sites. Methanol is able to compete; however, it has a lower boiling point than EDA. Therefore, upon evaporation, the concentration will diminish, meaning ethylene diamine will occupy the newly available sites. By using an azeotropic mixture of toluene and methanol, the overall boiling point increases, thereby facilitating the removal of ethylene diamine.

An alternative method to the use of an azeotropic mixture of methanol and toluene is by washing with butanol. This method is more appropriate for higher whole generation dendrimers, owing to its ability to compete for hydrogen bonding sites. A hindrance to this is the difficulty in the removal of butanol from the product, as it has a very high boiling point of 116-118°C. As a result, it is extremely difficult to fully remove.

### 2.4.3 Hydrolysis of half generation PAMAM dendrimers
### 2.4.3.1 Hydrolysis of half generation PAMAM dendrimers in water

In order to bind to a protein which has positively charged areas around the periphery, each half generation dendrimer requires hydrolysing. Hydrolysis allows the conversion of ester groups to negatively charged carboxylic acid groups. An ester, when exposed to excess water, can hydrolyse without the formation of any unwanted side products. This reaction is extremely slow and rarely used for small aliphatic and aromatic compounds. Within the group, we have noticed that ester terminated dendrimers are not stable over time and appear to hydrolyse very quickly. It can be postulated that a different hydrolysis mechanism may be observed for dendrimers compared to aliphatic and aromatic compounds. We thought that dendrimer hydrolysis may occur by an autocatalytic reaction, where the rate of hydrolysis appeared to be faster for larger dendrimers (due to tighter more dense structures). It is probably no accident that ester terminated dendrimers are not commercially available. Therefore, adding ester terminated dendrimers to water may be the simplest way of obtaining the desired carboxylic acid terminated dendrimers, without any by-products (after freeze-drying). To test this theory, a series of ester terminated dendrimers (G-0.5 to G3.5) were dissolved in deuterium oxide in an NMR tube. The ^{1}HNMR spectrum for each generation was recorded at time intervals, and the depletion of the methoxy signal was recorded. **Figure**

**28** provides a graphical representation of the hydrolysis of G3.5 PAMAM dendrimer. As this is the largest dendrimer involved in the study, it was predicted to hydrolyse the fastest. The graph below shows that after 156 hours the dendrimer is only 28% hydrolysed. The time required for hydrolysis to reach completion is extensive and thus inappropriate for synthetic use. As a result, a different synthetic approach is utilised for successful hydrolysis of ester terminated dendrimers.
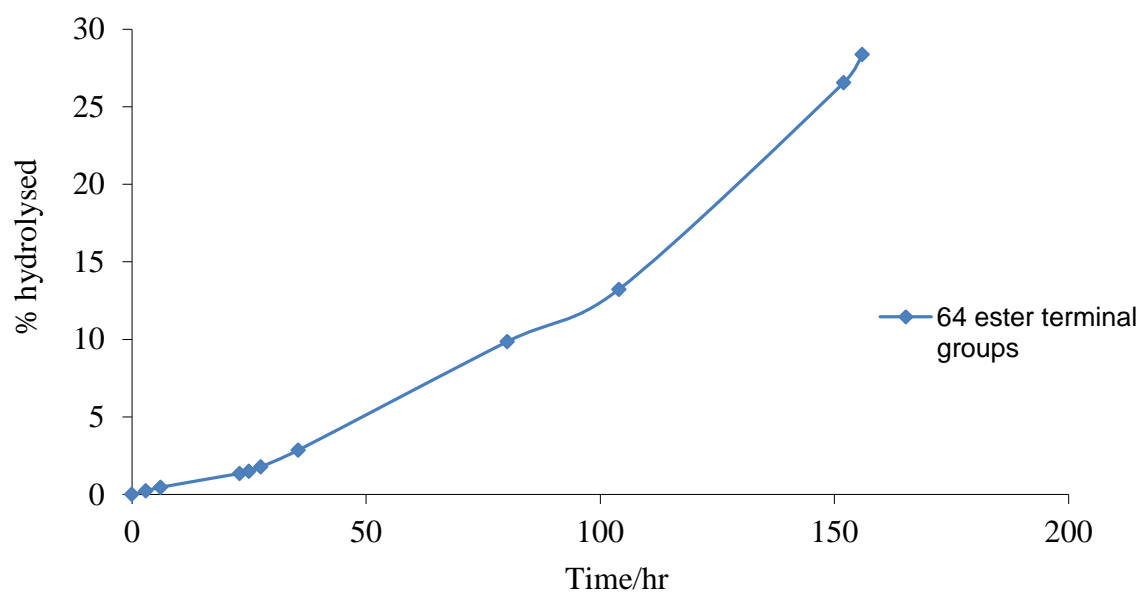


**Figure 28** – Graphical representation of hydrolysis of G3.5 PAMAM dendrimer, possessing 64 terminal ester groups, in deuterium oxide. The data shows that hydrolysis is 28% complete after 156 hours.

### 2.4.3.2 Hydrolysis of half generation PAMAM dendrimers using sodium hydroxide and ammonium chloride

Each ester terminated PAMAM dendrimer was hydrolysed (**scheme 6**) in a basic solution followed by neutralisation with ammonium chloride. Hydrolysis was achieved by adding two equivalents of sodium hydroxide to a solution of each half generation dendrimer in a solution of methanol and water in the ratio 4:1. Ammonium chloride is able to react with sodium hydroxide, generating ammonia, sodium chloride and water. Ammonia gas is expelled in the process and the other by-products do not interfere, meaning no further purification is required.
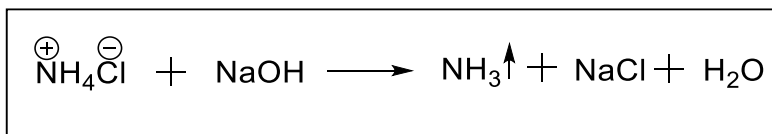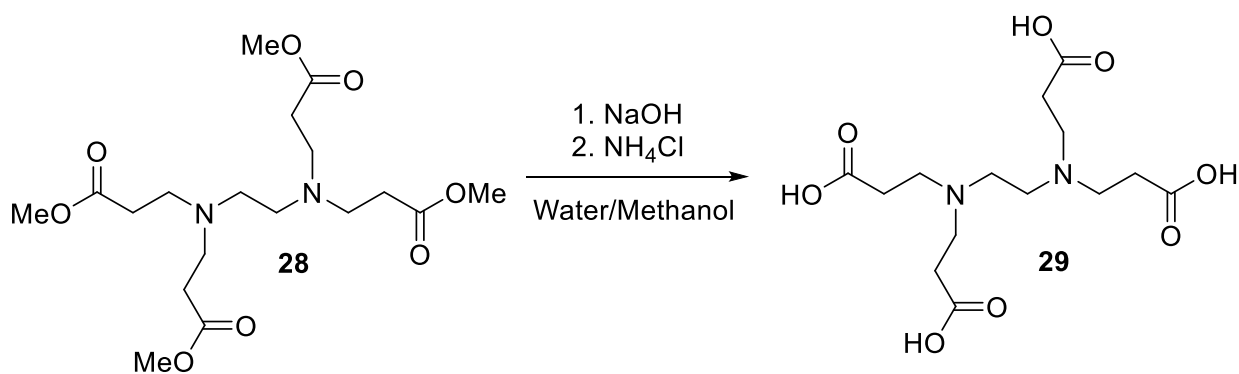
**Scheme 6**- Hydrolysis of a G-0.5 PAMAM dendrimer and equation, showing the role of ammonium chloride.

### 2.4.4 Assay of the binding activity of PAMAM dendrimers to Proteins

### 2.4.4.1 Chymotrypsin and Cytochrome-c

In this project, the two proteins studied were cytochrome c and chymotrypsin. Both proteins have been well documented and the chemistry of each, along with both the chemical and physical properties, has been reported in the literature.[34,57-68]

Cytochrome-c (**figure 29**) is a small heme protein involved in the mitochondrial transportation of electrons of the respiratory system, with an interfacial area of approximately $1100\text{Å}^2$. It transports electrons in an assortment of electron transport chains in eukaryotes and prokaryotes via collision reliant processes.[63] The heme moiety is linked covalently to the protein via thioether groups and the iron present functions as either an electron donor or an electron acceptor by interchanging between the ferrous and ferric oxidation states ($Fe^{2+}$ and $Fe^{3+}$). The changeability between these two states is facilitated by coupling between the heme iron electronic orbital and the porphyrin $\pi$ system.[66] The heme edge, which is exposed, is bordered by lysine, arginine and numerous other hydrophobic residues, creating an overall positively charged domain. This surface is regarded as the site for electron transfer to and from the heme moiety, meaning it is the area which interacts with a complementary protein partner. The corresponding protein partner will therefore possess anionic domains, allowing interaction to take place.[65]

64
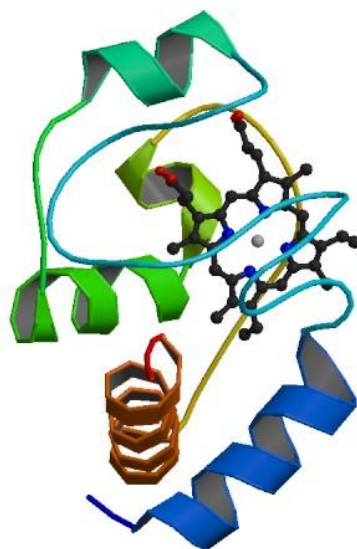
**Figure 29** – Figure to show the ribbon structure of human cytochrome-c with heme moiety (PDB ID: 3NWV).

Chymotrypsin (**figure 30**) is arguably one of the most studied and characterised proteins and has an interfacial area of approximately 2400Å. The entrance to the active site of the protein lies within this area. It is a member of the serine protease protein family, which collectively play crucial roles in medicinal chemistry, deeming them an appealing target for protein surface recognition. Not to mention, there is also a large family of natural protein inhibitors which have been known to bind to the peripheral regions and the active sites of a variety of serine proteases. The peripheral surface of α-Chymotrypsin possesses both lysine and arginine residues and is therefore essentially cationic, meaning that a complementary binding partner would contain anionic residues.[34, 57] Chymotrypsin is an important biological catalyst; it is a digestive enzyme which carries out proteolysis (the digestion of proteins).[67] Chymotrypsin comprises of a polypeptide chain of 245 amino acids. The biological role of chymotrypsin is to catalyse the hydrolysis of peptide bonds in proteins and polypeptides. Chymotrypsin has a high specificity; the carboxylic side of an amino acid, bearing aromatic side groups such as tyrosine, tryptophan and phenylalanine, are primarily targeted. The common feature of the aromatic ring in the side chain accounts for the substrate specificity.[69]
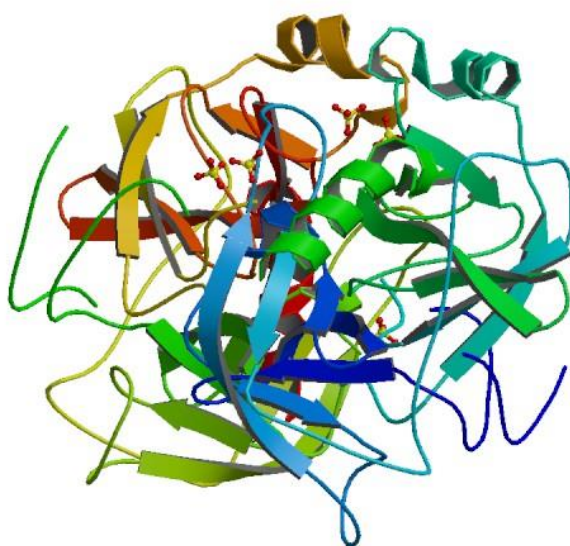
**Figure 30** – Figure to show the ribbon structure of native bovine α-chymotrypsin (PDB ID: 1YPH)

## 2.4.4.2 Assay of the use of PAMAM dendrimers as potential inhibitors of α-Chymotrypsin by UV spectroscopy

Other members of the group have obtained initial results based on the size selectivity of these dendritic systems. However, work cannot progress until it has been established that when a dendrimer interacts, it binds to the active site entrance and does not denature the protein. Firstly, an investigation into the inhibition of chymotrypsin by a PAMAM dendrimer of comparable addressable area will be carried out. It is important to establish that they bind and that the concentration employed allows sufficient interaction between protein and dendrimer. This will ensure that the concentration is correct for subsequent CD studies.

As previously mentioned, α-Chymotrypsin is a member of the serine protease family and its role is to catalyse hydrolysis of peptide bonds. It also exhibits a preference for large hydrophobic side chains belonging to aromatic amino acids, with cleavage predominantly occurring at the carboxyl end of the aromatic side group. In this section of the project, the catalytic efficacy of α-chymotrypsin can be kinetically examined by the hydrolysis of N-benzoyltyrosine-p-nitroanilide (BTNA), as the resulting product of hydrolysis is a UV active species (**scheme 7**). There is a colour change associated with this reaction. Upon generation of *p*-nitroaniline, the initial colourless solution becomes yellow in colour. Therefore, this reaction can be used to demonstrate whether or not PAMAM dendrimers are able to inhibit

the rate of hydrolysis catalysed by Chymotrypsin. The dendrimer which binds best to the protein in question will therefore be the superlative inhibitor for that particular protein, meaning that relative binding and efficacy of inhibition can be directly linked to one another.
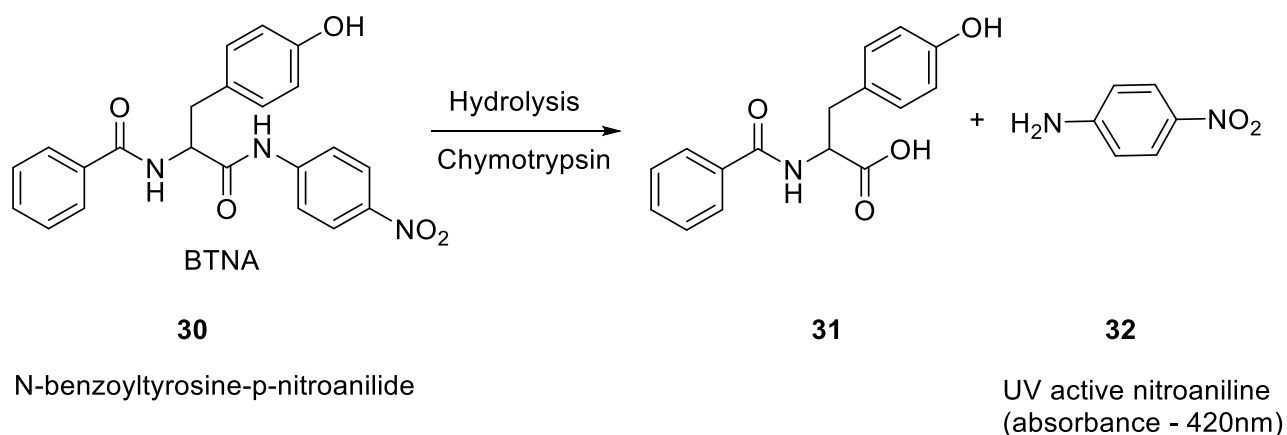


**Scheme 7**– Hydrolysis of N-benzoyltyrosine-p-nitroanilide (BTNA) by α-Chymotrypsin, generating UV active p-nitroaniline.

Prior to these studies, it is important to ensure that a reduced rate in hydrolysis is brought about by protein inhibition, and not interaction between the dendrimer and BTNA substrate (**30**). Therefore, a control reaction in the absence of chymotrypsin is required. If the dendrimer can coordinate to BTNA, a slower rate of hydrolysis would be observed. This would be due to a lower concentration of BTNA available for digestion by chymotrypsin, meaning a lower concentration of *p*-nitroaniline would be generated. To verify whether this interaction occurs, a UV cuvette was charged with dendrimer/buffer solution and BTNA substrate (in methanol), and identical conditions to protein catalysed hydrolysis, mentioned beforehand, were used. After 20 minutes the cuvette was removed and a colourless solution with a white precipitate was observed. The precipitate formed resulted in scatter within the spectrum. The precipitate formed is, in fact, BTNA precipitating out of solution, due to its insolubility in water. The result of this control reaction confirms that the dendrimer does not interact with the substrate, meaning inhibition observed is a result of interaction between the protein and the dendrimer.

The hydrolysis reaction can be monitored by UV spectroscopy by measuring the rate of production of the UV active species *p*-nitroaniline. Firstly, a control experiment was

performed (**figure 31**), by which a solution of the BTNA substrate in methanol was added to an aqueous solution of α-chymotrypsin (final concentrations were $1\times10^{-4}$M and $1\times10^{-6}$M respectively) at room temperature. From this experiment, it was possible to visualise when the hydrolysis reaction terminated and no further production of *p*-nitroaniline occurred.
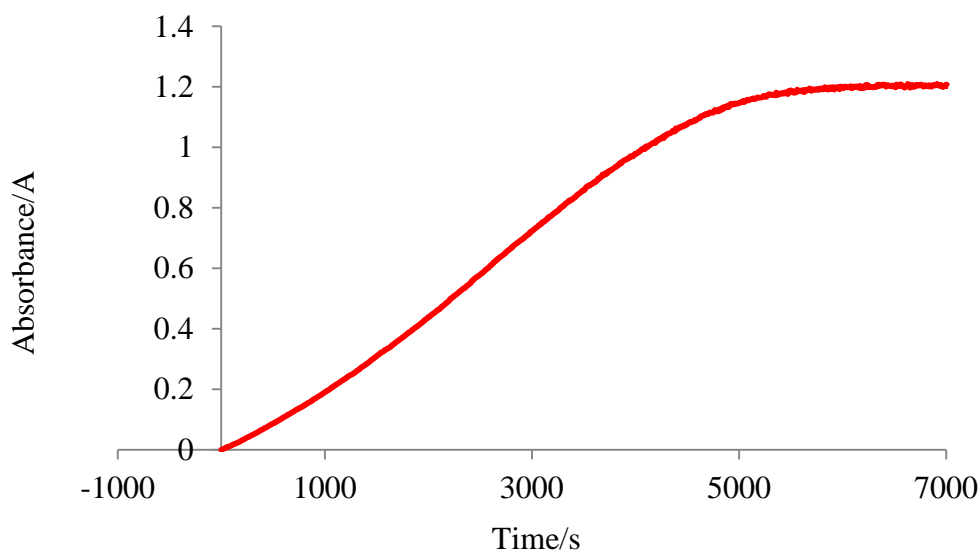


**Figure 31** - A graph to show the hydrolysis of N-benzoyltyrosine-p-nitroanilide catalysed by α-Chymotrypsin producing UV active p-nitroaniline.

Previous work within the group has demonstrated that there is a size selective based mechanism involved in the inhibition of protein-protein binding.[50,70] Results showed that G2.5 bound the best as it has a comparable interfacial area to α-chymotrypsin. Therefore, G2.5 PAMAM dendrimer baring 32 terminal carboxylic acid groups was used. A time scan experiment was set up to record the UV absorption at 410 nm (the UV absorption wavelength for *p*-nitroaniline) at 10 second intervals for a period of 600 seconds after the addition of BTNA, α-chymotrypsin and one equivalent of G2.5 PAMAM dendrimer (**figure 32**). The experiment was carried out in a neutral phosphate buffer solution of concentration 0.1M and pH 7.4. The pH of the mixture was checked and exhibited no change after each run. Therefore, this ensures that any change in enzyme activity was not a conformational change induced by an alteration in pH. As previously stated, chymotrypsin displays a preference for large hydrophobic aromatic side chains. As a PAMAM dendrimer does not possess these, it will not compete for the protein active site entrance, meaning that the inhibition mechanism could possibly arise from hydrogen bonds or electrostatic interactions between the negatively charged peripheral carboxylic acid groups and the cationic residues present on the exterior surface of the enzyme. This mechanism would impede the BTNA substrate reaching the

active site, or potentially alter the conformation of chymotrypsin, which would also inhibit catalysis.
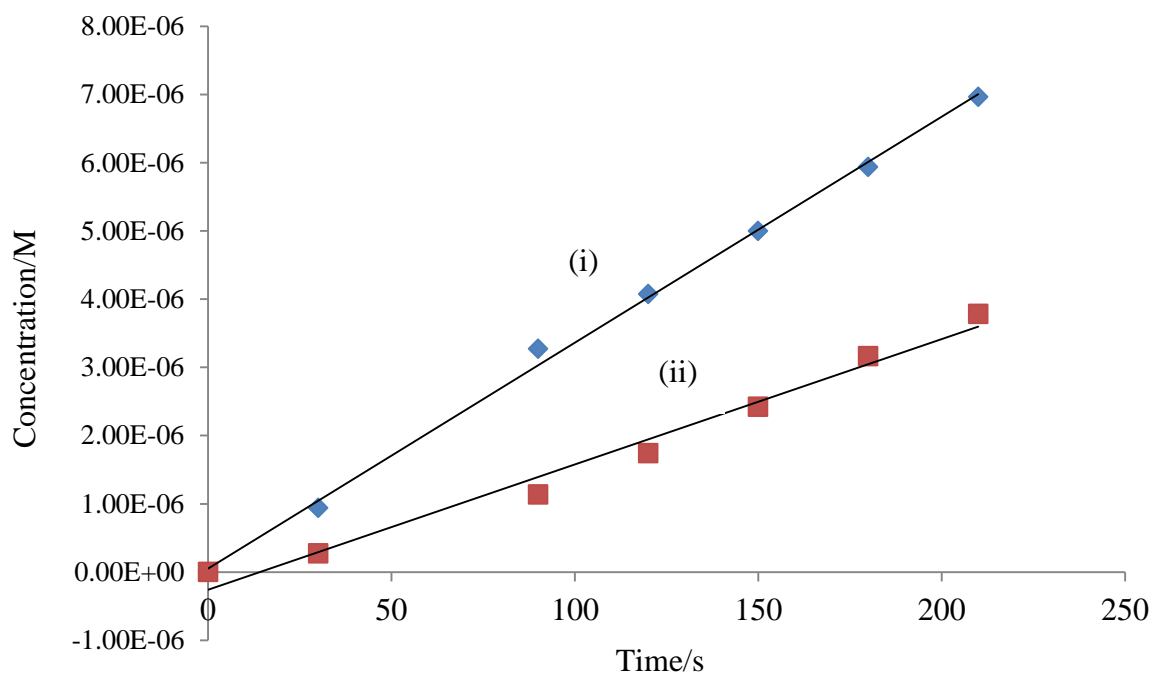


**Figure 32** – A graph to show the relationship between the intensity of UV absorption concentration of the catalysed hydrolysis of BTNA by α-Chymotrypsin in the (i) absence and (ii) presence of a G2.5PAMAM dendrimer.

For the control reaction, where no dendrimer is present during hydrolysis, a conventional reaction profile was noted and an initial reaction rate of $3.23 \times 10^{-8} Ms^{-1}$ was observed. The reaction was then repeated in the presence of an equimolar amount of G2.5 PAMAM dendrimer and chymotrypsin. From observing the reaction profiles of both experiments, the initial rate was lower when compared to the control reaction, giving a result of $9.46 \times 10^{-9} Ms^{-1}$. The results obtained indicate that, at $1 \times 10^{-6}$ M, 70% is bound. If at this concentration 70% binding takes place, then at $5 \times 10^{-6}$ M 100% interaction would be expected. As G2.5 PAMAM dendrimer has a comparable interfacial area to chymotrypsin (2250 Å and 2400 Å respectively), it can be assumed that this dendrimer can fit the interfacial area of the protein, thereby exposing all of the anionic carboxylic acid peripheral groups to the cationic exterior of the enzyme, and bind effectively. These results confirm that dendrimers can function as potent inhibitors; however, it has not been ascertained whether or not the dendrimer is

interacting with the protein, and subsequently altering the structure, which would render the target protein denatured.

## 2.4.5 Effect of binding upon protein structure and stability

There are numerous theories which could explain the outcome of the previous results. Firstly, the ideal situation could occur and the dendrimer could bind to the hotspot region of the protein. This would block the active site, but retain the structure of the protein. There is also the possibility that binding causes the enzyme to change shape, so as to maximise binding. As a result, the protein would denature, thereby losing its function. Finally, the dendrimer could bind to an alternative site on the protein surface. The occurrence of this could result in a protein altering its shape to accommodate the dendritic ligand. Change in shape could cause denaturation. Each one of these options is a plausible mechanism for the inhibition of enzyme activity reported in the earlier section. **Figure 33** is a schematic representation of these contrasting binding mechanisms.
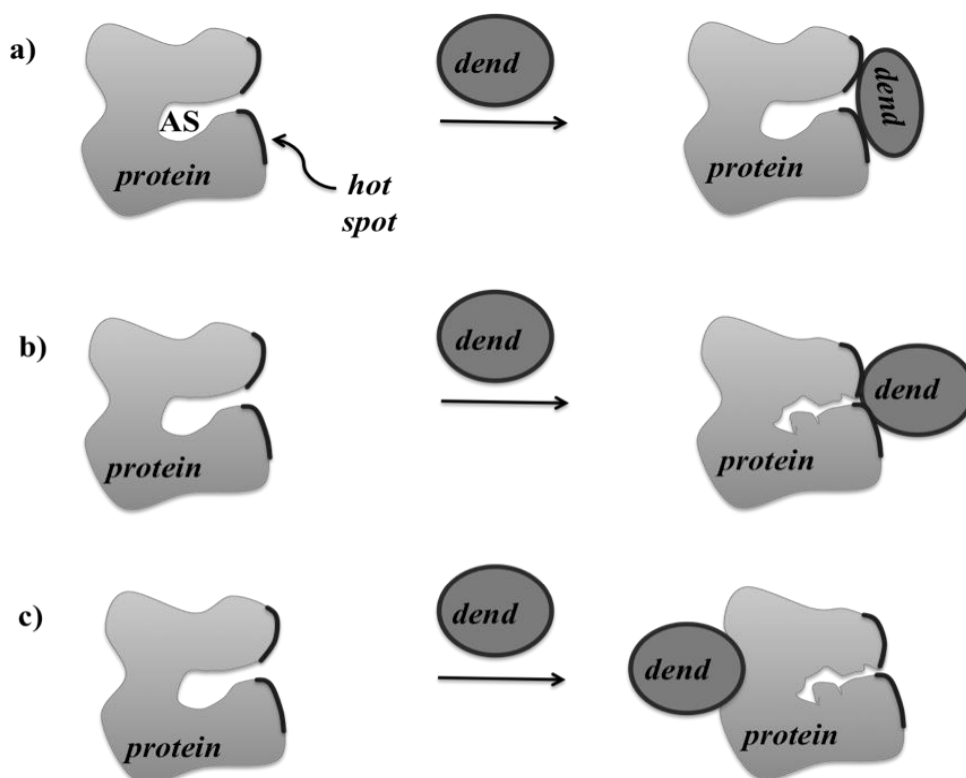


**Figure 33** - Schematic representation of the probable binding mechanisms which could account for inhibition of enzyme function: a) a hotspot mechanism where the dendrimer interacts with the enzyme hotspot, blocking the active site whilst retaining the enzyme structure b) a hotspot mechanism where the enzyme distorts in structure to maximise interaction, thereby, causing denaturation c) an interaction mechanism where the dendrimer binds to an alternative site on the enzyme triggering a structural change which renders the enzyme inactive.[1]

### 2.4.5.1 Circular Dichroism (CD) spectroscopy

In order to carry out the next part of this research an analytical technique known as circular dichroism (CD) spectroscopy will be employed. The area of structural biology has evolved enormously from as early as the late 1980's; with the protein data bank increasing in volume with more than 2000 high resolution protein structures being added annually. A tool with the ability to investigate protein structures and to measure the rate of alterations to protein structure would be of vital importance. Subsequently, CD spectroscopy has become a reliable and valued technique for examination and analysis of protein secondary structure. It can be viewed as a version of light absorption spectroscopy which involves plane polarised light. Circularly plane polarised light can be seen as being composed of two polarised components, each of matching magnitude; and circular dichroism is the disparity in absorption between these two components. The phenomenon of CD is highly sensitive to polypeptide and protein secondary structure. Therefore, it is important to take special care in experimental design and instrument calibration, due to the sensitivity of this technique.[71] For additional information about the intricacies of this technique and its involvement in protein structural determination the reader is directed to the literature.

### 2.4.5.2 Effect of binding upon protein structure

In order to calculate the probability or degree of denaturation, circular dichroism spectroscopy was utilised. By comparing the structure of the protein/dendrimer complex with that of the native protein it will be possible to ascertain any structural changes. CD spectra of each protein, in the presence and absence of a variety of different generation of dendrimers (G0.5, 1.5, 2.5 and 3.5), was carried out. The studies were performed initially by using $1x10^{-6}$M of dendrimer for both cytochrome-c and chymotrypsin. Solutions of both proteins were made up with each generation of dendrimer in order that the final concentrations were initially $1x10^{-6}$ M of protein and $1x10^{-6}$ M of each dendrimer. As a control and base line experiment, solutions of cytochrome-c and chymotrypsin were made up with pH7.4 phosphate buffer of final concentration $1x10^{-6}$M and a CD spectrum for each protein was generated. All experiments were carried out in phosphate buffer (concentration 0.1 M, pH7.4) at 37 °C (physiological temperature). **Figure 34** displays the spectra of both chymotrypsin and cytochrome-c and the spectra corresponding to the protein/dendrimer complexes. The experiments were repeated where the dendrimer concentration was $5x10^{-6}$ M and the results produced were identical for each dendrimer. Future work will involve the calculation of the

percentage inhibition for the other generations of dendrimer to determine whether sufficient binding will occur at the given concentration $1 \times 10^{-6}$ M.

(a)
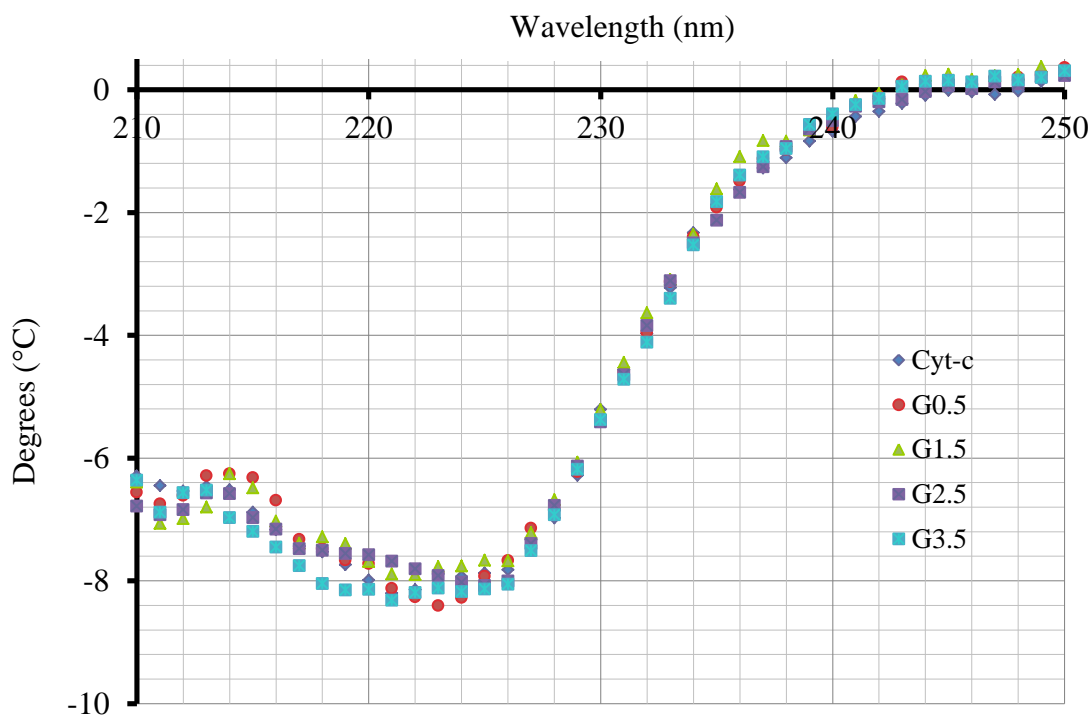


(b)
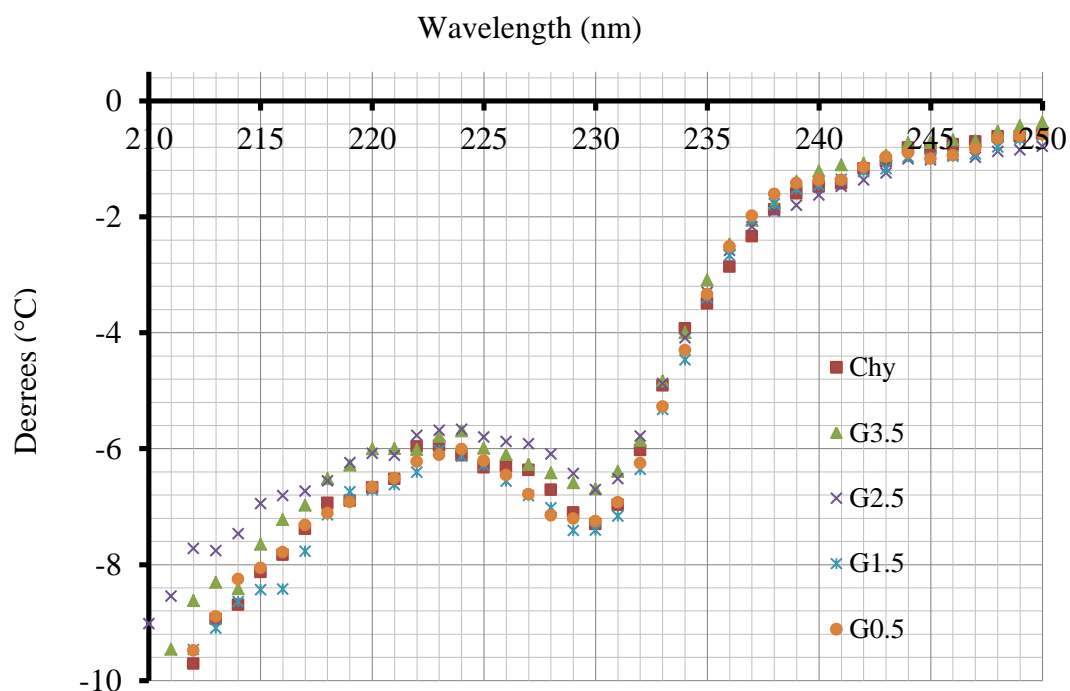


**Figure 34** – Figure to show the CD Spectra of native (a) Cytochrome-c and (b) Chymotrypsin and when bound to different generations of PAMAM dendrimers of concentration $1 \times 10^{-6}$M (results at $5 \times 10^{-6}$M produced results which were superimposable).

The spectra are the same before and after complexation with a dendrimer, confirming that binding does not result in conformational change to the native protein. If there was a variation in the structure of the proteins upon complexation then, as a result of the high sensitivity of this analytical technique, the spectra obtained would have displayed a notable change. From the results, there is little or no change in the protein structure when bound to the dendrimer compared to its native state, suggesting that there is slight or no change in conformation upon binding and inhibition. This could possibly be a result of the sufficient flexibility exhibited by the macromolecule. When a protein binds, it changes shape to maximise binding where the loss of structure is compensated by energy gain. The flexibility of the dendritic ligand means that it can change its shape with minimal loss in energy, meaning diminutive to no conformational change to the protein is required to maximise interaction. This can be referred to as the induced fit mechanism. Therefore, this provides confidence in the fact that, upon complexation, the proteins studied do not denature.

## 2.4.6 Effect of binding upon protein stability

A protein usually denatures under high temperatures or in the presence of a high concentration of a denaturant. Hamilton and co-workers focussed much of their research on molecules which are able to interact with protein peripheries by electrostatic or hydrophobic interactions over a large area of the protein in question. Some of their work involved the interaction of tetraphenyl porphyrin derivatives with the surface of Cytochrome-C which demonstrated strong binding.[38] This group of substituted porphyrin derivatives were not only found to bind effectively to the surface of Cytochrome-C, but were also discovered to induce unfolding of Cytochrome-C under conditions bordering physiological (pH of 7.4 and 50mM NaCl).[39] Hamilton *et al.* also carried out thermal denaturation research which established that Cytochrome-C, in the presence of two equivalents of a metalloporphyrin dimer that contained Cu(II), was nearly completely denatured over the entire temperature range.[38] Work within the Hamilton group has therefore illustrated a selection of macromolecules which are able to promote denaturation. The results obtained from CD spectroscopy mentioned previously showed that different generation PAMAM dendrimers had no effect upon the structure of either cytochrome-c or chymotrypsin under physiological conditions, thus suggesting that denaturation did not occur upon interaction.

Continuing on from this research, the thermal stability of both cytochrome-c and chymotrypsin, upon complexation to a dendrimer, was investigated at raised temperatures. A

control experiment for both cytochrome-c and chymotrypsin was essential, where each protein was dissolved in a neutral phosphate buffer solution with a final concentration of $1x10^{-6}$ M and heated by 1°C a minute from an initial temperature of 37 °C. A CD spectrum for each was subsequently generated so that the point at which both proteins fully unfold could be visualised. This process was repeated for each dendrimer (G0.5, 1.5, 2.5 and 3.5) to identify whether or not complexation to a dendrimer had an effect on the stability of the protein. Each protein/dendrimer complex was made up to identical concentrations as used for the previous CD studies. Two solutions for each protein/dendrimer complex were required; the first solution comprised of equimolar quantities of both dendrimer and protein (each at $10^{-6}$M), and the second comprised of $10^{-6}$ M of protein and $5x10^{-6}$ M of dendrimer. The dendrimer/protein complexes were subsequently heated up from 37°C by 1°C a minute and a CD spectrum was generated for each, examining the intensity of the peak at 230 nm and 224 nm for cytochrome-c and chymotrypsin respectively. **Figure 35** is a plot depicting the percentage of unfolding of chymotrypsin when in its native state and when bound to G2.5 PAMAM dendrimer.
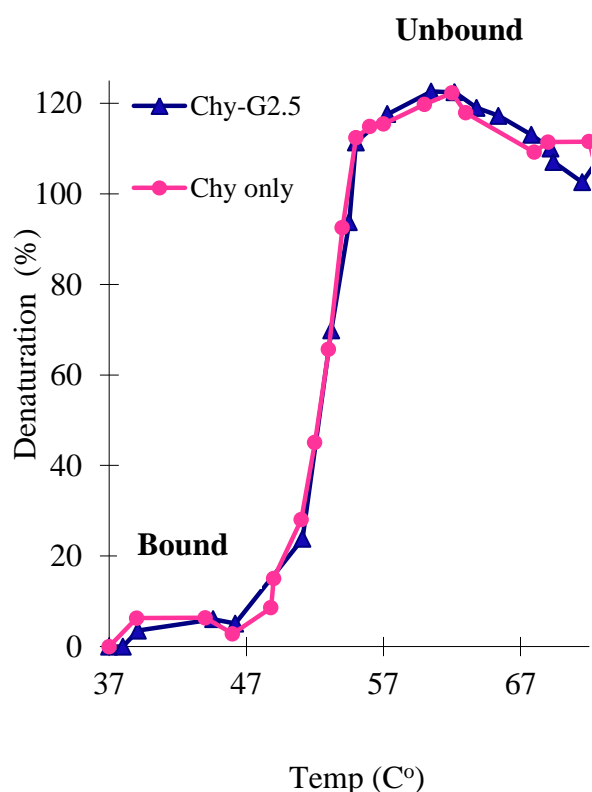


**Figure 35** –Figure to show the CD spectra of the percentage unfolding in relation to temperature of chymotrypsin when in its native state and when bound to a G2.5PAMAM dendrimer.

As can be seen from the results shown above, the plots for chymotrypsin in the presence and absence of a G2.5 PAMAM dendrimer are identical. The results obtained for the other generations of dendrimer bound to chymotrypsin were also comparable to the plot of the native protein. In the case of cytochrome-c, the results also indicate that denaturation is neither induced nor prolonged upon interaction with a dendritic polymer.

There are two possible explanations for the results obtained. Firstly, coordination to a dendrimer does not induce or prolong unfolding of the protein, meaning thermal stability is unaffected by complexation to a macromolecule of this nature. An alternative explanation of the results obtained is that the strength of interaction could potentially be dependent upon temperature. This presumption signifies that, above a specific temperature, the dendrimer may fully dissociate from the peripheral surface of the protein. This would effectively result in the temperature of denaturation remaining the same, thereby generating indistinguishable CD spectra. In order to verify which explanation is correct, additional studies are required. To determine the temperature which binding stops, future work will involve repeating hydrolysis of BTNA substrate by chymotrypsin, complexed to a dendrimer, over a temperature range of 35 ℃ to 45 ℃. This analysis would result in the identification of the point at which binding is no longer possible. It is hypothesised that, as the temperature is raised, the difference in rate of hydrolysis between the control reaction (in the absence of a dendrimer) and hydrolysis in the presence of a dendrimer will decrease as the temperature is raised. The point at which unfolding commences will result in the inability of chymotrypsin to digest the substrate. In conclusion, the results obtained from circular dichroism spectroscopy provide confidence that dendrimer/protein association, under physiological conditions, does not bring about any structural changes for cytochrome-c or chymotrypsin. That is to say, neither protein was denatured upon complexation. However, the effect upon thermal stability remains unclear and further research is required. Further work would include using a much stronger concentration of dendrimer to check for weak binding. For instance, at $10^{-4}$ M, the higher concentration of dendrimer would mean more would be bound and it might be possible to detect induced denaturation with an increase in temperature.

## 2.4.7 Direct binding assay of chymotrypsin with fluorescent labelled PAMAM dendrons

Whilst other members of the group were investigating the use of dendrimers as size selective inhibitors to protein-protein interactions, we continued to investigate binding. Specifically, we wanted to measure direct binding. This was done using fluorescence spectroscopy in

collaboration with Professor Neil Mckeown of Cardiff University. Direct binding between cytochrome-c and fluorescent labelled PAMAM dendrons, of varying generation, was assessed using the technique of fluorescence titrations. G1.5 and G2.5 fluorescent labelled dendrons were provided by Cardiff University and the chemical structure of both dendrons are found overleaf in **figure 36**.
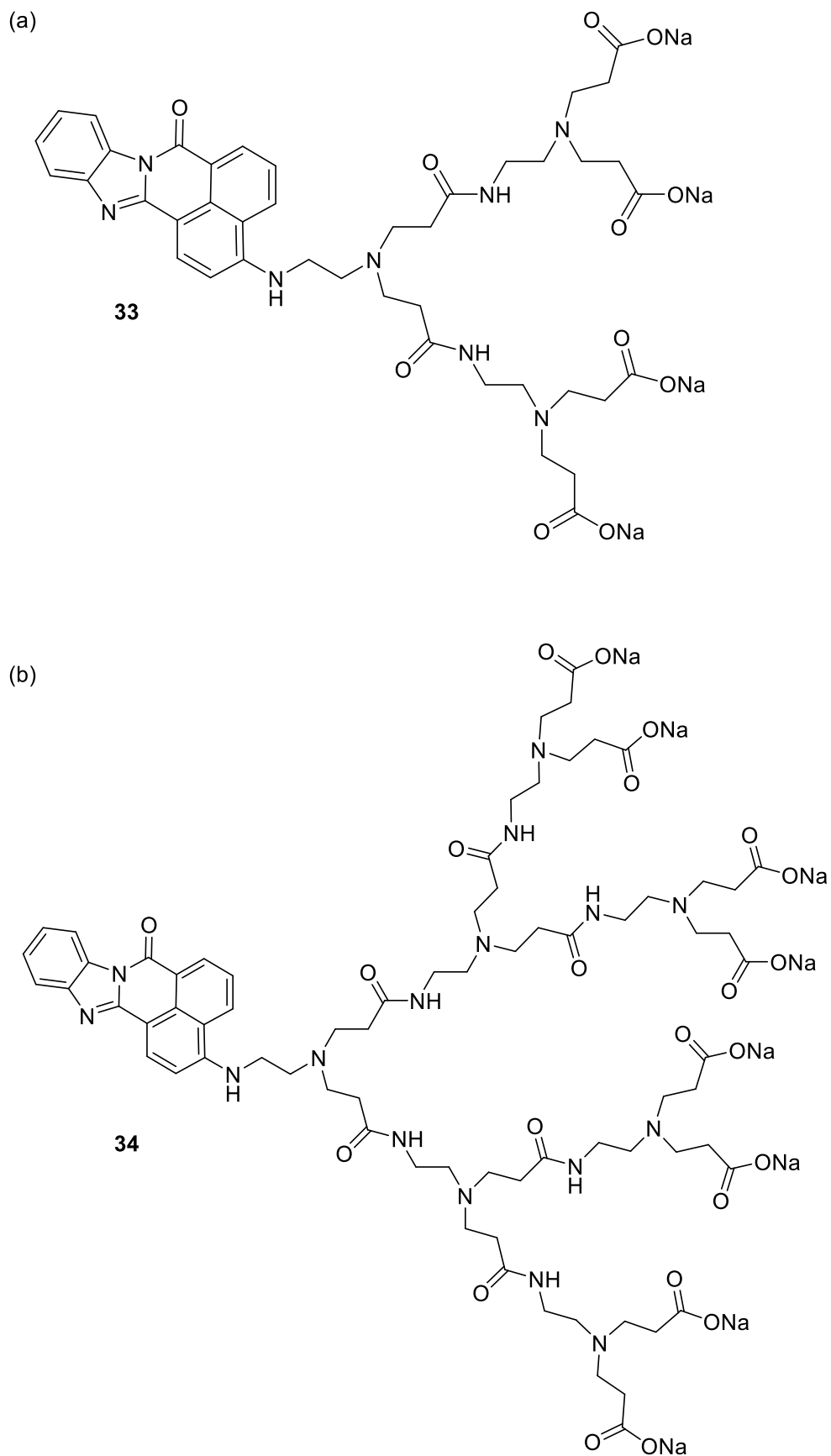
**Figure 36** – Figure to show the chemical structure of (a) G1.5 and (b) G2.5 fluorescent labelled PAMAM dendrons.

**2.4.7.1 Fluorescence titration assay**

Fluorescence results were obtained using a HORIBA Scientific Fluoromax-4 spectrofluorometer using its attached software (FluorEssence V3). In order to perform the titration experiments, the appropriate concentration of each dendron needed to be established. This was achieved by measuring the emission spectrum, of both dendrons, at a variety of different concentrations. A concentration of $10^{-6}$ M, for each dendron, was found to give the clearest emission spectrum. G1.5 and G2.5 were each titrated against cytochrome-c (from equine heart) and the quenching of the emission spectrum was recorded. Each $10^{-6}$ M solution of the fluorescence labelled dendrimers was prepared using ultra-pure water. A solution containing a large excess ($5\times10^{-3}$ M) of the guest, cytochrome-c, was then prepared using the corresponding dendrimer solution to ensure constant concentration of dendrimer throughout the titration. The dendrimer solution was accurately measured (3 mL) into a quartz cuvette and aliquots of ligand solution (between 10 µL and 50 µL) were added. Fluorescence emission scans were taken after each addition, monitoring the quenching of the emission spectrum of the labelled dendrimer (508 nm for each generation). Solutions were made up fresh and used immediately after preparation to ensure no damage to the protein. Repeats of each titration were performed to ensure accuracy of results. The titration data for each run can be found in **appendix A** of chapter 6.

As mentioned previously, the active site of cytochrome-c contains a porphyrin moiety and this is able to quench any appropriate chromophore. Therefore, upon addition of cytochrome-c, the emission spectrum for each labelled dendron is quenched. Quenching is therefore a result of direct interaction. This effect can be visualised in **figure 37**.
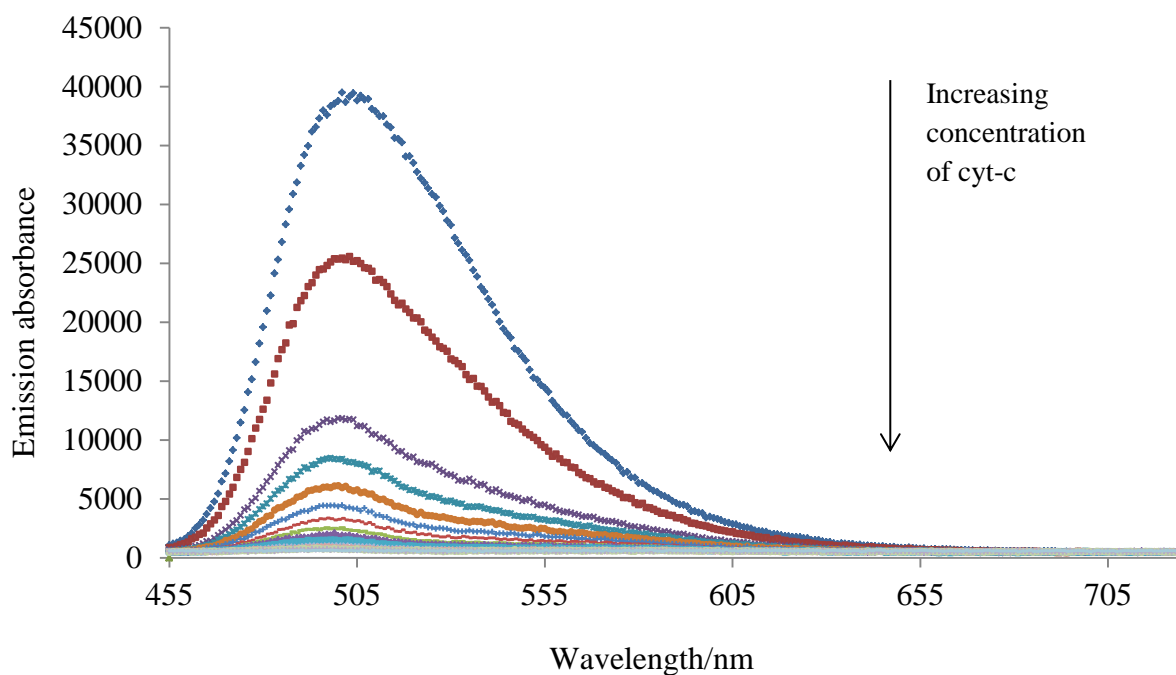
**Figure 37** – A representative graph to show the titration of fluorescent labelled G1.5 ($1\times10^{-6}$M) titrated against cytochrome-c ($0.5\times10^{-2}$M).

Binding software 14AllMaster, developed by Professor Chris Hunter from the University of Sheffield, was used to deduce the binding constant associated for cytochrome-c and each generation of dendron analysed. G1.5 and G2.5 both showed strong interaction, giving association constants of $4.2\times10^{4}$ ($\pm2.5\%$) and $3.2\times10^{4}$ ($\pm2\%$) respectively. The binding software assumes a 1:1 fit and binding can be presumed to be specific. The software gave a good fit, which can be seen from the low percentage errors calculated. Results show the smaller dendron to bind the strongest, which is not in accordance with initial predictions regarding size selectivity. This could be a result of the number of terminal groups able to interact with the protein surface. The smaller dendron may be able to use all terminal groups in binding, whereas the larger dendron is unable to use all terminal groups. Fewer terminal groups able to interact would result in fewer interactions per dendron, giving a lower association constant. The binding curves can be seen overleaf in **figure 38**.
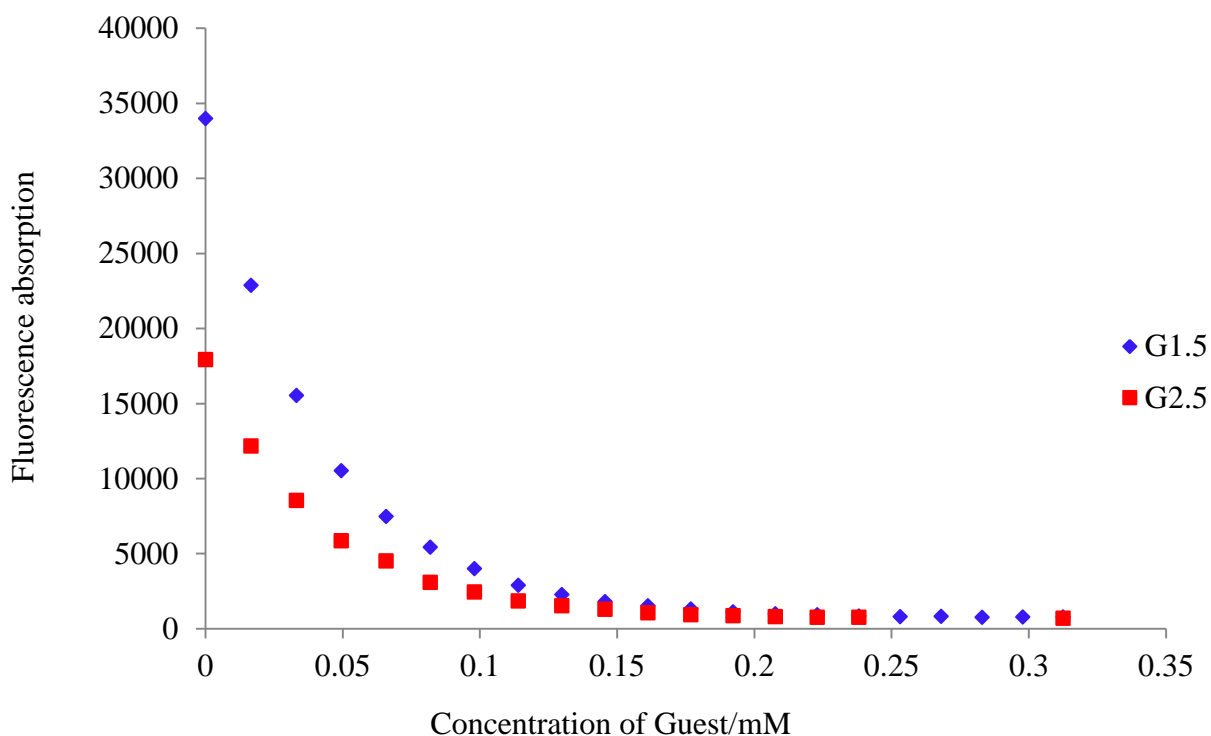
**Figure 38** – A graph to show the binding curves for G1.5 and G2.5 fluorescent labelled dendrons, when quenched with cytochrome-c.

In addition to an estimate of an association constant, the software program also generates a Job plot from the input data. The Job plots obtained from the software program are not in accordance with a 1:1 binding stoichiometry as they show a high stoichiometry for each dendron, where multiple dendrimers coordinate to a protein. A representative Job plot for G1.5 can be seen overleaf in **figure 39**. It could be that the stoichiometry is high, or the software is not providing an accurate representation of binding. The results obtained lead us to believe that binding is non-specific. However, future work would include a separate Job plot analysis in order to determine whether direct binding is specific or non-specific.
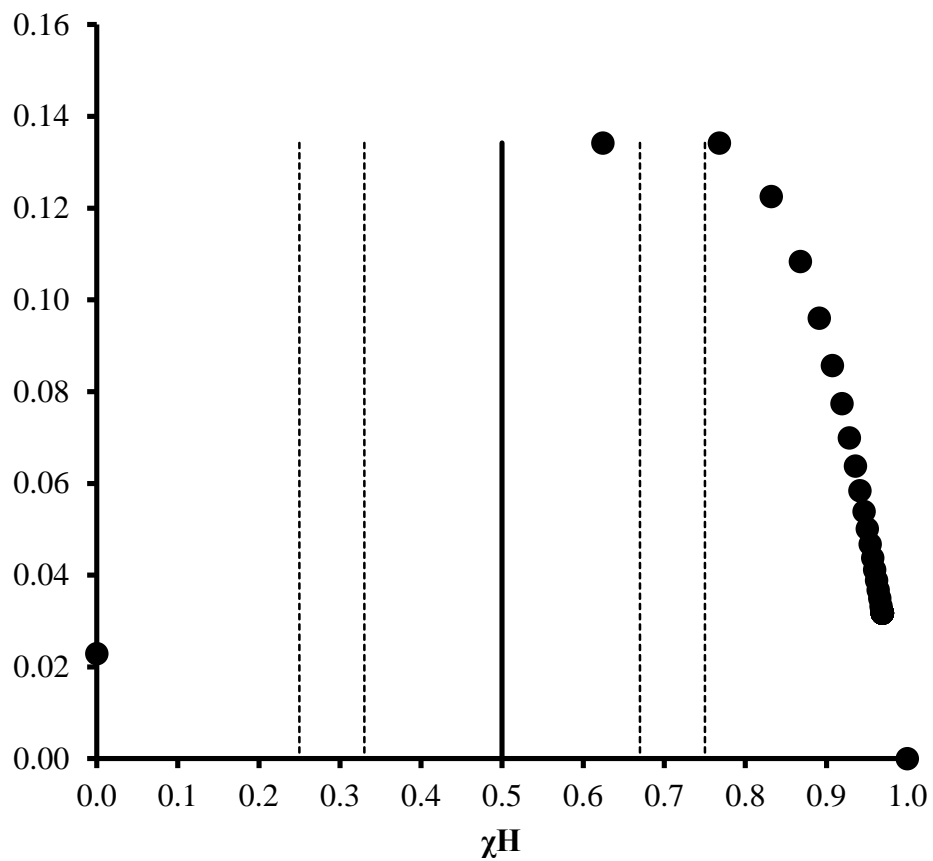
**Figure 39** – Figure to show the Job plot, generated using 14AllMaster binding software, for the titration of G1.5 fluorescent labelled dendron against cytochrome-c.

## 2.5 Future Work

The next phase of this research will involve the construction of a biological column for chromatographic use, where the column resin is doped with the target protein (**figure 40**), such as Chymotrypsin. A mix of a smaller generation dendrimer (i.e. G0.5) and a larger generation dendrimer with a comparable addressable area to the interfacial area of the target protein (i.e. G3.5 for Chymotrypsin), will be loaded onto the column. A GPC trace of the first and final fraction will be ascertained and, theoretically, the lower generation dendrimer will be eluted first. As binding to the protein will not be as strong compared to the larger generation dendrimer, the smaller dendrimer will not stick as well to the bio-column. Therefore, in the case of Chymotrypsin, the first fraction should solely contain G0.5 PAMAM dendrimer and the final fraction should solely contain G3.5 PAMAM dendrimer. This will continue on from work involving the demonstration of a size selective binding mechanism for protein-protein binding inhibition.
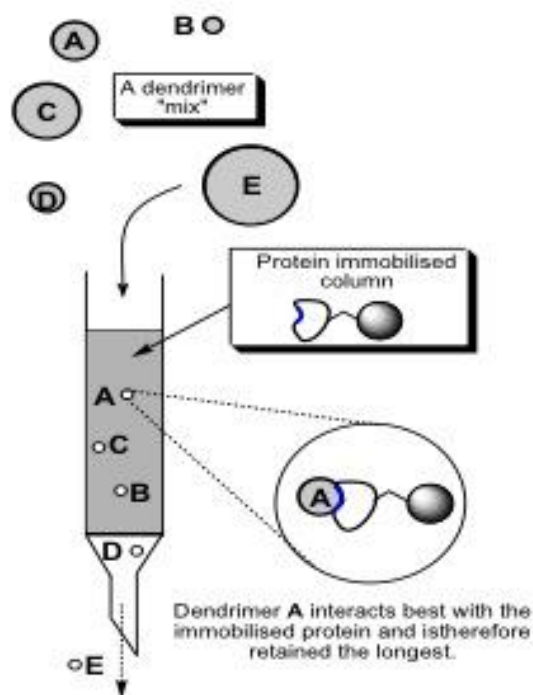


**Figure 40** – Figure to illustrate the doping of the column resin with the target protein.

As mentioned previously, Bogan and Thorn looked into amino acid preferences within the hot spot region. Results showed that hot spots are enriched with three amino acids with a frequency higher than 10% (tryptophan, tyrosine and arginine).[5] These amino acids can be considered 'good' amino acids as they show a high affinity towards the hot spot area. Those

which do not contribute productively to binding can be regarded as 'bad' amino acids. Therefore, another use for the bio-column is to load it with a series of dendrimers functionalised with different amino acids; some possessing a high affinity towards the hot spot region and others which do not. In theory, the dendrimer functionalised with 'good' amino acids will elute last as it will be expected to interact more powerfully with the protein, meaning dendrimers functionalised with 'bad' amino acids will elute first.

## 2.6 References

(1)     Chiba, F.; Mann, G.; Twyman, L. J. *Org. Biomol. Chem.* **2010**, *8*, 5056.

(2)     Toogood, P. L. *J. Med. Chem.* **2002**, *45*, 1543.

(3)     Gehmlich, K.; Pinotsis, N.; Hayess, K.; van, d. V. P. F. M.; Milting, H.; El, B. A.; Koerfer, R.; Wilmanns, M.; Ehler, E.; Fuerst, D. O. *J. Mol. Biol.* **2007**, *369*, 665.

(4)     Reichmann, D.; Rahat, O.; Cohen, M.; Neuvirth, H.; Schreiber, G. *Curr. Opin. Struct. Biol.* **2007**, *17*, 67.

(5)     Bogan, A. A.; Thorn, K. S. *J Mol Biol* **1998**, *280*, 1.

(6)     Fletcher, S.; Hamilton, A. D. *J. R. Soc. Interface* **2006**, *3*, 215.

(7)     Stites, W. E. *Chem. Rev. (Washington, D. C.)* **1997**, *97*, 1233.

(8)     Peczuh, M. W.; Hamilton, A. D. *Chem. Rev. (Washington, D. C.)* **2000**, *100*, 2479.

(9)     Lo, C. L.; Chothia, C.; Janin, J. *J. Mol. Biol.* **1999**, *285*, 2177.

(10)    Goh, C.-S.; Milburn, D.; Gerstein, M. *Curr. Opin. Struct. Biol.* **2004**, *14*, 104.

(11)    Clackson T.; Wells J. A.; *Science* **1995**, 267, 383-386.

(12)    Yin, H.; Hamilton, A. D. *Angew. Chem., Int. Ed.* **2005**, *44*, 4130.

(13)    Fry, D. C. *Biopolymers* **2006**, *84*, 535.

(14)    Cochran, A. G. *Chem. Biol.* **2000**, *7*, R85.

(15)    Qureshi, S. A.; Kim, R. M.; Konteatis, Z.; Biazzo, D. E.; Motamedi, H.; Rodrigues, R.; Boice, J. A.; Calaycay, J. R.; Bednarek, M. A.; Griffin, P.; Gao, Y.-D.; Chapman, K.; Mark, D. F. *Proc. Natl. Acad. Sci. U. S. A.* **1999**, *96*, 12156.

(16)    Tilley, J. W.; Chen, L.; Fry, D. C.; Emerson, S. D.; Powers, G. D.; Biondi, D.; Varnell, T.; Trilles, R.; Guthrie, R.; Mennona, F.; Kaplan, G.; LeMahieu, R. A.; Carson, M.; Han, R.-J.; Liu, C. M.; Palermo, R.; Ju, G. *J. Am. Chem. Soc.* **1997**, *119*, 7589.

(17)    Braisted, A. C.; Oslob, J. D.; Delano, W. L.; Hyde, J.; McDowell, R. S.; Waal, N.; Yu, C.; Arkin, M. R.; Raimundo, B. C. *J. Am. Chem. Soc.* **2003**, *125*, 3714.

(18)    Waal, N. D.; Yang, W.; Oslob, J. D.; Arkin, M. R.; Hyde, J.; Lu, W.; McDowell, R. S.; Yu, C. H.; Raimundo, B. C. *Bioorg. Med. Chem. Lett.* **2005**, *15*, 983.

(19)    McMillan, K.; Adler, M.; Auld, D. S.; Baldwin, J. J.; Blasko, E.; Browne, L. J.; Chelsky, D.; Davey, D.; Dolle, R. E.; Eagen, K. A.; Erickson, S.; Feldman, R. I.; Glaser, C. B.; Mallari, C.; Morrissey, M. M.; Ohlmeyer, M. H. J.; Pan, G.; Parkinson, J. F.; Phillips, G. B.; Polokoff, M. A.; Sigal, N. H.; Vergona, R.; Whitlow, M.; Young, T. A.; Devlin, J. J. *Proc. Natl. Acad. Sci. U. S. A.* **2000**, *97*, 1506.

(20)    He, M. M.; Smith, A. S.; Oslob, J. D.; Flanagan, W. M.; Braisted, A. C.; Whitty, A.; Cancilla, M. T.; Wang, J.; Lugovskoy, A. A.; Yoburn, J. C.; Fung, A. D.; Farrington, G.; Eldredge, J. K.; Day, E. S.; Cruz, L. A.; Cachero, T. G.; Miller, S. K.; Friedman, J. E.; Choong, I. C.; Cunningham, B. C. *Science (Washington, DC, U. S.)* **2005**, *310*, 1022.

(21)    Fletcher, S.; Hamilton, A. D. *Curr. Opin. Chem. Biol.* **2005**, *9*, 632.

(22)    Bullock, B. N.; Jochim, A. L.; Arora, P. S. *J. Am. Chem. Soc.* **2011**, *133*, 14220.

(23)    Restorp, P.; Rebek, J. *Bioorg. Med. Chem. Lett.* **2008**, *18*, 5909.

(24)    Vassilev, L. T.; Vu, B. T.; Graves, B.; Carvajal, D.; Podlaski, F.; Filipovic, Z.; Kong, N.; Kammlott, U.; Lukacs, C.; Klein, C.; Fotouhi, N.; Liu, E. A. *Science (Washington, DC, U. S.)* **2004**, *303*, 844.

(25)    Plante, J. P.; Burnley, T.; Malkova, B.; Webb, M. E.; Warriner, S. L.; Edwards, T. A.; Wilson, A. J. *Chem. Commun. (Cambridge, U. K.)* **2009**, 5091.

(26)    Lee, J. H.; Zhang, Q.; Jo, S.; Chai, S. C.; Oh, M.; Im, W.; Lu, H.; Lim, H.-S. *J. Am. Chem. Soc.* **2011**, *133*, 676.

(27)    Cummings, C. G.; Hamilton, A. D. *Curr. Opin. Chem. Biol.* **2010**, *14*, 341.

(28)    Jain, R. K.; Hamilton, A. D. *Org. Lett.* **2000**, *2*, 1721.

(29)    Clark-Ferris, K. K.; Fisher, J. *J. Am. Chem. Soc.* **1985**, *107*, 5007.

(30)    Jain, R. K.; Hamilton, A. D. *Angew. Chem., Int. Ed.* **2002**, *41*, 641.

(31)    Tsou, L. K.; Jain, R. K.; Hamilton, A. D. *J. Porphyrins Phthalocyanines* **2004**, *8*, 141.

(32)    Baldini, L.; Wilson, A. J.; Hong, J.; Hamilton, A. D. *J. Am. Chem. Soc.* **2004**, *126*, 5656.

(33)    Hamuro, Y.; Calama, M. C.; Park, H. S.; Hamilton, A. D. *Angew. Chem., Int. Ed. Engl.* **1997**, *36*, 2680.

(34)    Park, H. S.; Lin, Q.; Hamilton, A. D. *J. Am. Chem. Soc.* **1999**, *121*, 8.

(35)    Lin, Q.; Hamilton, A. D. *C. R. Chim.* **2002**, *5*, 441.

(36)    Park, H. S.; Lin, Q.; Hamilton, A. D. *Proc. Natl. Acad. Sci. U. S. A.* **2002**, *99*, 5105.

(37)    Aya, T.; Hamilton, A. D. *Bioorg. Med. Chem. Lett.* **2003**, *13*, 2651.

(38)    Wilson, A. J.; Groves, K.; Jain, R. K.; Park, H. S.; Hamilton, A. D. *J. Am. Chem. Soc.* **2003**, *125*, 4420.

(39)    Groves, K.; Wilson, A. J.; Hamilton, A. D. *J. Am. Chem. Soc.* **2004**, *126*, 12833.

(40)    Green, D. R.; Reed, J. C. *Science* **1998**, *281*, 1309.

(41)    Gradl, S. N.; Felix, J. P.; Isacoff, E. Y.; Garcia, M. L.; Trauner, D. *J. Am. Chem. Soc.* **2003**, *125*, 12668.

(42)

(43)    Coghlan, M. J.; Carroll, W. A.; Gopalakrishnan, M. *J. Med. Chem.* **2001**, *44*, 1627.

(44)    Boger, D. L.; Desharnais, J.; Capps, K. *Angew. Chem., Int. Ed.* **2003**, *42*, 4138.

(45)    Boger, D. L. *Bioorg. Med. Chem.* **2003**, *11*, 1607.

(46)    Berg, T. *Angew. Chem., Int. Ed.* **2003**, *42*, 2462.

(47)    Arkin, M. R.; Randal, M.; DeLano, W. L.; Hyde, J.; Luong, T. N.; Oslob, J. D.; Raphael, D. R.; Taylor, L.; Wang, J.; McDowell, R. S.; Wells, J. A.; Braisted, A. C. *Proc. Natl. Acad. Sci. U. S. A.* **2003**, *100*, 1603.

(48)    Arkin, M. *Curr. Opin. Chem. Biol.* **2005**, *9*, 317.

(49)    Ingram, V. M. *Nature (London, U. K.)* **1957**, *180*, 326.

(50)    Chiba, F.; Hu, T. C.; Twyman, L. J.; Wagstaff, M. *Macromol. Symp.*, *287*, 37.

(51)    Dai, J.; Bao, Z.; Sun, L.; Hong, S. U.; Baker, G. L.; Bruening, M. L. *Langmuir* **2006**, *22*, 4274.

(52)    Wowk, B.; Fahy, G. M. *Cryobiology* **2002**, *44*, 14.

(53)    Munro, P. D.; Jackson, C. M.; Winzor, D. J. *J. Theor. Biol.* **2000**, *203*, 407.

(54)    Chiba, F.; Hu, T.-C.; Twyman, L. J.; Wagstaff, M. *Chem. Commun. (Cambridge, U. K.)* **2008**, 4351.

(55)    Tomalia, D. A.; Baker, H.; Dewald, J.; Hall, M.; Kallos, G.; Martin, S.; Roeck, J.; Ryder, J.; Smith, P. *Polym. J. (Tokyo)* **1985**, *17*, 117.

(56)    Esfand, R.; Tomalia, D. A. *Drug Discovery Today* **2001**, *6*, 427.

(57)    Capasso, C.; Rizzi, M.; Menegatti, E.; Ascenzi, P.; Bolognesi, M. *J. Mol. Recognit.* **1997**, *10*, 26.

(58)    Theorell, H.; Akesson, A. *J. Am. Chem. Soc.* **1941**, *63*, 1804.

(59)    Theorell, H.; Akesson, A. *J. Am. Chem. Soc.* **1941**, *63*, 1812.

(60)    Theorell, H.; Akesson, A. *J. Am. Chem. Soc.* **1941**, *63*, 1818.

(61)    Theorell, H. *J. Am. Chem. Soc.* **1941**, *63*, 1820.

(62)    Koppenol, W. H.; Margoliash, E. *J. Biol. Chem.* **1982**, *257*, 4426.

(63)    Battistuzzi, G.; Loschi, L.; Borsari, M.; Sola, M. *JBIC, J. Biol. Inorg. Chem.* **1999**, *4*, 601.

(64)    Palmer, G. *J. Bioenerg. Biomembr.* **1993**, *25*, 145.

(65)    Zhou, J. S.; Kostic, N. M. *Biochemistry* **1993**, *32*, 4539.

(66)    Allhorn, M.; Klapyta, A.; Akerstroem, B. *Free Radical Biol. Med.* **2005**, *38*, 557.

(67)    Wilcox, P. E. *Methods Enzymol.* **1970**, *19*, 64.

(68)    Zhang, B.; Xing, Y.; Li, Z.; Zhou, H.; Mu, Q.; Yan, B. *Nano Lett.* **2009**, *9*, 2280.

(69)    Appel, W. *Clin. Biochem. (Ottawa)* **1986**, *19*, 317.

(70)    Chiba, F.; Hu, T. C.; Twyman, L. J.; Wagstaff, M. *Macromol. Symp.* **2010**, *287*, 37.

(71)    Kelly, S. M.; Jess, T. J.; Price, N. C. *Biochim. Biophys. Acta, Proteins Proteomics* **2005**, *1751*, 119.

# Chapter 3

## Anion Receptor Chemistry

# Chapter 3 – Anion Receptor Chemistry

## 3.1 Introduction to anion receptor chemistry

Anion coordination is a relatively new area in comparison to cation coordination. Nevertheless, anion recognition is an area which continues to grow.[1-5] The first synthetic receptor was established by Park and Simmons in 1968. A macrobicyclic receptor, which showed an affinity towards halide ions, was developed. This receptor utilised both electrostatic and hydrogen bond interactions, retaining a halide ion within the hydrocarbon cavity in an aqueous media.[6] Despite early pioneering work, anion receptor chemistry was essentially not investigated in depth until the mid-1970's.[7]

The rationale behind the newfound and widespread interest in this particular area is largely due to the important roles anions play. Anions are ubiquitous in numerous biological systems, as a huge majority of enzymes, co-factors and substrates are anionic in nature. Adenosine triophosphate (ATP) is a tetra ion, Deoxyribonucleic acid (DNA) is an important polyanion and another good example is Carboxypeptidase A. The function of Carboxypeptidase A is the hydrolysis of the C-terminal amino acids from polypeptide substrates. This enzyme displays a preference for substrates having large hydrophobic terminal side chains, such as phenylalanine. The mechanism of Carboxypeptidase A is a proteolytic mechanism involving the generation of an arginine-aspartate salt bridge.[8] Binding, involving a salt bridge, can also be seen in Ribonucleic acid (RNA) stem-loop structure- protein interactions[9] and zinc finger /DNA complexes.[10] An example of the crucial role anions play is apparent in maintaining the phosphorylation state of proteins, which is critical for a broad range of cellular processes. The two families of enzymes responsible are kinases and phosphatases. Alkaline Phosphatase (AP), a member of the Phosphatase group, possesses a shallow cationic active site. This positive charge enables the binding of anionic phosphate moieties which, in turn, leads to activation of the substrate for nucleophilic attack from serine residue.[11]

These are but a few examples portraying the crucial role anions play in numerous diverse biological systems. Although the previous examples outline some positive roles which anions play, it is also important to note that anions can also have deleterious effects. Anions can take a negative role in some diseases. Epilepsy, Myotonia and Cystic fibrosis are all examples of diseases that arise from the misregulation of chloride ion flux.[12-15] Anions can also be

potentially threatening to the environment; for instance, nitrate anions, present in fertilisers, run off the land and pollute the water supplies which brings about excessive algae production, thereby damaging aquatic life.[16] Therefore, the successful and specific coordination of anions has both therapeutic and environmental importance.

The properties of anions produce many challenges when designing a suitable receptor. The main attribute of an anion is its negative charge, meaning electrostatic forces can be considered when designing a suitable host. Anions are also considerably larger than their isoelectronic cations, resulting in a lower charge to radius ratio. As a result, electrostatic interactions are considerably less efficient when compared to smaller cations.[1] In addition to this; a receptor must possess a cavity of adequate size for sufficient encapsulation. The sensitivity of anions to pH should also be considered; this is due to the fact that anions are easily protonated at low pH levels, resulting in the loss of the negative charge. All these factors contribute to the rate of solvation of anions, thereby stressing their importance. Solvents can also affect the potency and selectivity of binding. For instance, polar protic solvents can form hydrogen bonds with an anionic species, thus meaning that there is added competition for the synthetic receptor to overcome. Anions can also display an assortment of geometries, presenting yet another challenge in receptor design as the cavity must correspond to the geometric structure of the anion. The variety of geometries which anions can adopt, along with numerous examples, can be visualised overleaf in **figure 41**.
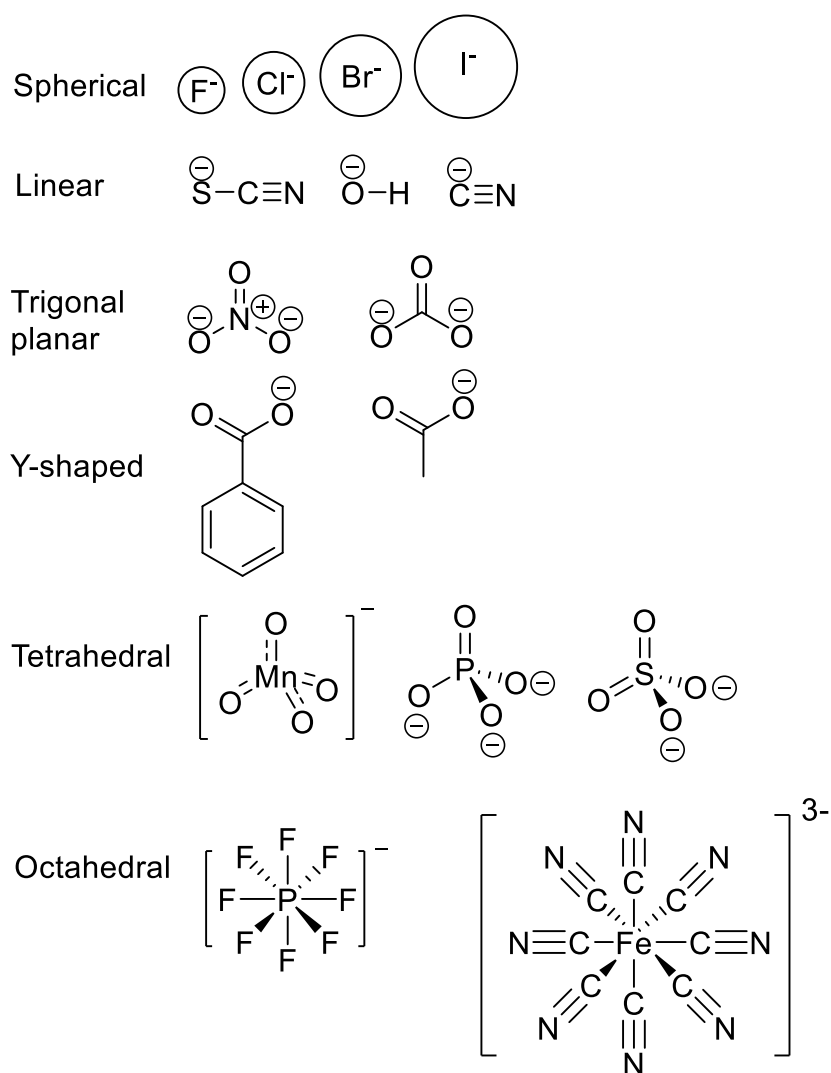
**Figure 41**– Figure to illustrate the variety of geometries which anions can adopt.

The area of anion receptor chemistry has generated a large level of interest within the field of supramolecular chemistry, which is attributable to the potential applications in the fields of medicine[17-19], the environment[20] and numerous chemical processes. This has led to the the fabrication of a wide array of synthetic receptors. There is a range of non-covalent interactions which can be utilised when designing a host. Firstly, given the nature of the charge of an anion, electrostatic interactions can be employed. These attractive forces can be in the form of ion pairing, ion-dipoles or dipole-dipoles. Any anion can be considered as an electron pair donor meaning interaction with an electron pair acceptor is a certainty. The most basic existing electron pair acceptor is an electropositive hydrogen atom which results in the formation of a hydrogen bond upon interaction with an electron pair donor. Hydrogen bonding is widely used in a variety of organic frameworks. They are naturally occurring in numerous biological systems, such as DNA base pairs and a wide variety of proteins. Despite

being weaker than electrostatic forces, they are directional, which is one reason they feature in a large number of synthetic receptors. In addition to these forces, hydrophobicity, π-π stacking interactions and Van der Waals forces can also be utilised to maximise affinity towards a guest molecule.

### 3.1.1 Ammonium and Guanidinium based receptors

As stated beforehand, electrostatic interactions are high in strength, making them an attractive option for synthetic supramolecular systems. The elementary synthetic methods by Park and Simmons, for the development of anion receptors, utilised the ammonium motif.[6] Protonated amines possess both electrostatic interactions and hydrogen bonds, which is the main rationale for the use of this group in synthetic receptors. Lehn *et al*. focussed initial research on the ammonium group and reported the fabrication of cryptand receptor systems which incorporated this motif. Upon protonation, complex formation with halide ions was accomplished, with a particularly high affinity towards chloride.[21] Lehn *et al*. then went on to synthesise a protonated cryptand which, unlike previous studies, was shape selective and demonstrated a high affinity towards the linear azide ion in aqueous media. The linear triatomic anion is retained within the cavity by two pyramidal arrangements of three '$^{+}N$-$H^{..}N^{-}$' hydrogen bonds, holding the terminal nitrogen sites in place.[22] Based on the early studies which demonstrate the ability of the ammonium group to coordinate anionic species, research has continued to grow with regards to this binding motif.

Felix *et al*.[23] have focussed research on polyammonium macrocyclic receptors. In 2007, the synthesis of a receptor system, **35**, which includes two phenanthroline units, was reported.[24] This macrocyclic structure is illustrated overleaf in **figure 42**.

**35**
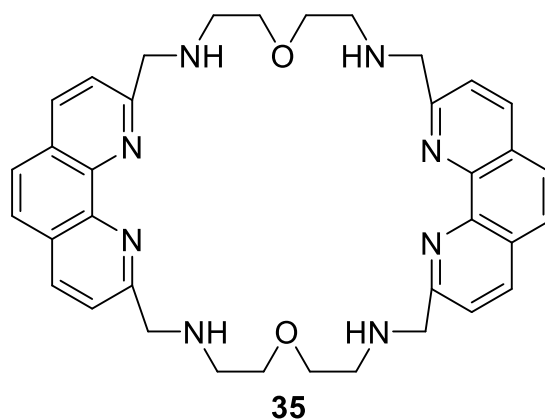
**Figure 42–** Figure to show a macrocyclic receptor which incorporates two phenanthroline units.[24] This Macrocyclic system selectively bound 1,3,5 benzene tricarboxylate (the anionic form of trimesic acid) and pyrene carboxylate. These anionic species were bound from a mixture containing a wide array of different carboxylate substrates.

More recently, Burns *et al*. have developed a family of bis-ammonium receptors to function as potential cationic peptide mimics. These receptor systems have been based on a scaffold, comprising of two bis linked phenol rings. Studies have demonstrated that a receptor, which contains preorganised ammonium groups, can coordinate to both dihydrogen phosphate and phosphatidyglycerol (PG). The synthetic procedure for the initial receptor salts fabricated can be seen overleaf in **scheme 8**.[25] This research illustrates the potential of receptors of this nature in the area of antimicrobial therapeutics.
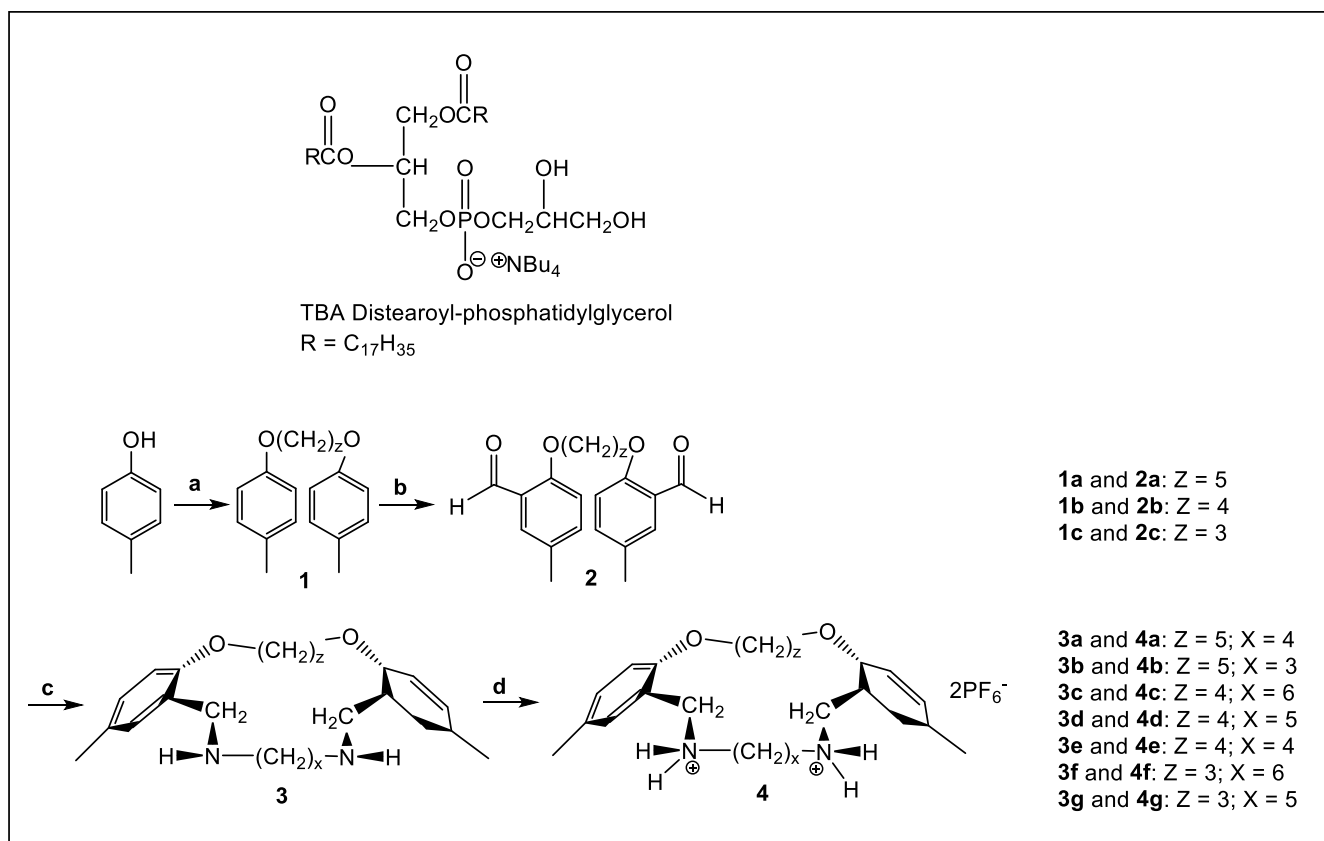
**Scheme 8** – Representation of the preparation of initial receptor salts: Reagents and conditions (a) $Br(CH_2)_zBr$, 18-crown-6, $K_2CO_3$, THF; (b) $(CH_2)_6N_4$, TFA, reflux; (c) (i) $H_2N(CH_2)_xNH_2$, EtOH, reflux, (ii) triethylsilane, Pd-C, MeOH; (d) HCL/MeOH then $NH_4PF_6$, $CH_2Cl_2$, $H_2O$. Adapted with permission from [Koralegedara, M. B.; Aw, H. W.; Burns, D. H. *J. Org. Chem.* **2011**, *76*, 1930]. Copyright 2011 American Chemical Society.

Another cationic motif that has received a great deal of attention is the guanidinium ion. This binding motif plays an important role in nature; namely in the identification of anionic substrates by enzymes and anti-bodies.[26] The guanidinium cation is the conjugate acid of guanidine and has a pKa of 13.5[26], meaning it remains protonated over a larger pH range than the ammonium motif.[3] In addition, It is also capable of forming several zwitterionic hydrogen bonds.[26] It is the combination of these characteristics which deem the guanidinium cation a suitable site for anion recognition. Preliminary work with this cationic species was carried out by Lehn *et al*.[26] Studies showed the development of a series of guanidinium based macrocycles **36** to **38** (**figure 43**). These receptor systems illustrated the promise of this binding motif, showing selectivity of complexation for phosphate, dihydrogen phosphate and triphosphate.

**36**         **37**         **38**
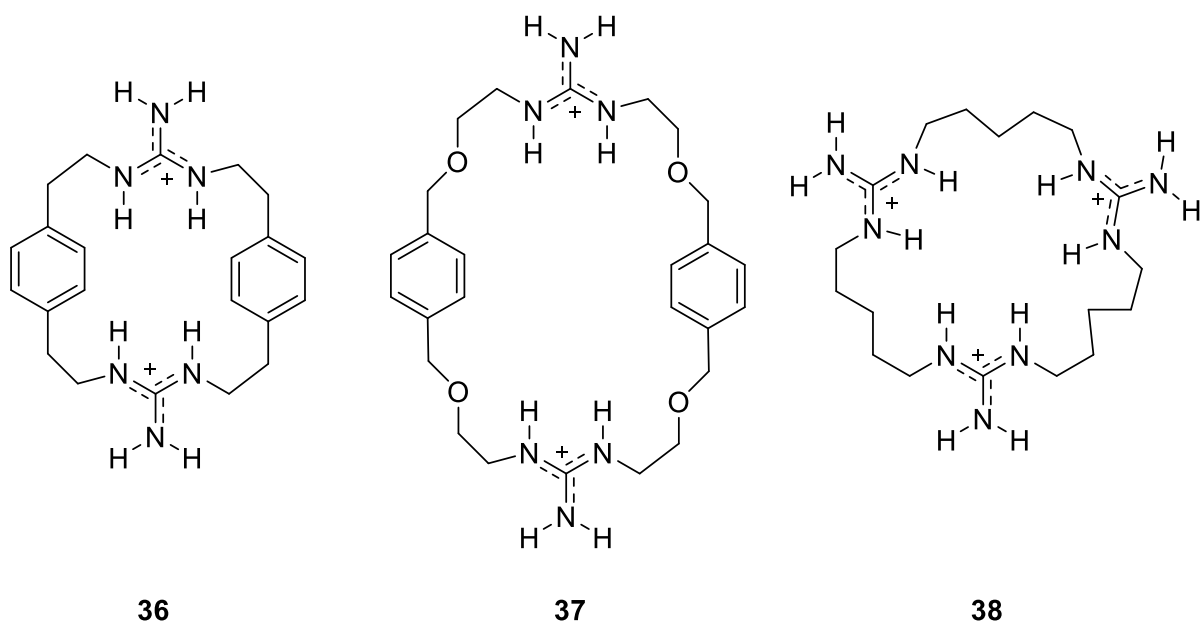
**Figure 43** – Figure to show the chemical structures for a series of cationic guanidinium macrocycles developed by Lehn *et al.*[26]

One function of the guanidinium moiety has been the coordination of oxo-anions. Pioneering work by Schmuck *et al.* has involved the development of guanidinicarbonylpyrroles, based upon the role of the guanidinium cation in nature. For instance, specific non-covalent binding can be seen with lactate digestion by lactate dehydrogenase and base pairing within nucleic acids. Guanidinicarbonylpyrrole receptors showed a significant improvement on the binding affinity of the guanidinium cation itself as it contains additional hydrogen bond donors within the binding site.[27] Schmuck and co-workers continued work in this particular area and developed novel receptors (**39** to **43**), which comprise of an ammonium cation connected to a guanidinicarbonylpyrrole motif by linkers of differing length.[28] Receptors **39** to **43** are illustrated overleaf in **figure 44**.
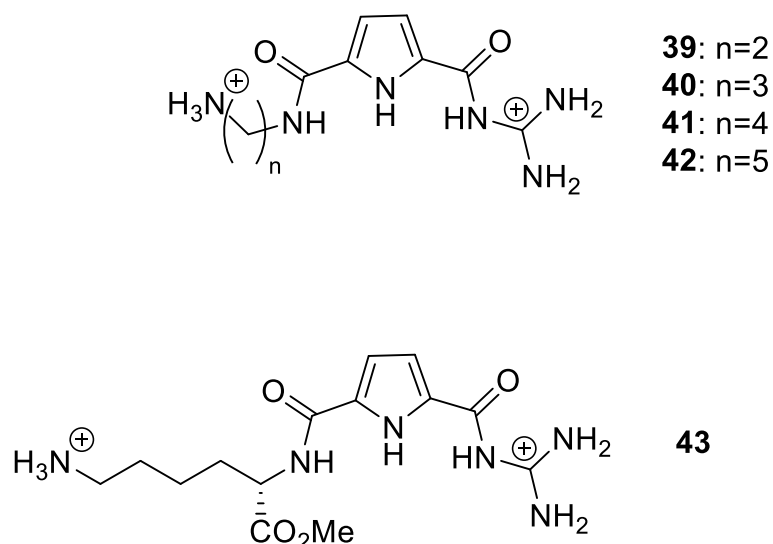
**Figure 44** – Figure to show the chemical structures of anionic receptors that comprise of an ammonium cation connected to a guanidinicarbonylpyrrole motif by linkers of differing length.[28]

For more information, regarding recent studies involving guanidinium based anion receptors, the reader is directed to the following literature by Schmuck *et al.*[29] This work examines nucleotide recognition in water using guanidinium based receptors. As this section reveals, cationic moieties, incorporated within both acyclic and Macrocyclic receptors, has shown promising results and utilised both electrostatic and hydrogen bonding, accounting for strong affinities in binding. In addition to ammonium and guanidinium based receptors; pyridinium[30-33], imidazole[34, 35] and triazole[12,36-38] based receptors have also utilised both hydrogen bonds and electrostatic interactions which have recently been explored. However, it is important to note that the pH dependence of charged receptors can restrict their use; therefore, neutral anionic receptors, which utilise hydrogen bonding, $\pi$-$\pi$ stacking interactions and Van der Waals forces, have received a great deal of interest.

### 3.1.2 Neutral anion receptor systems

Owing to the drawbacks of charged host molecules, neutral molecules have featured heavily in anion receptor chemistry. A large majority of synthetic hosts incorporate a functional group which can coordinate an anionic guest using hydrogen bonds. Some examples of functional groups which feature in a vast majority of neutral receptors can be seen in **figure 45**. Multiple hydrogen bond motifs can be included within a supramolecular receptor system, which is one advantage to this type of interaction. Furthermore, a hydrogen bond is directional, which results in the feasibility of designing shape specific anion receptors. Shape

specificity allows the distinction between anions of contrasting geometry and certain hydrogen bonding conditions in a non-polar solvent.[1] Therefore; it is evident why hydrogen bonding is a dominant non-covalent interaction within the area of anion recognition.
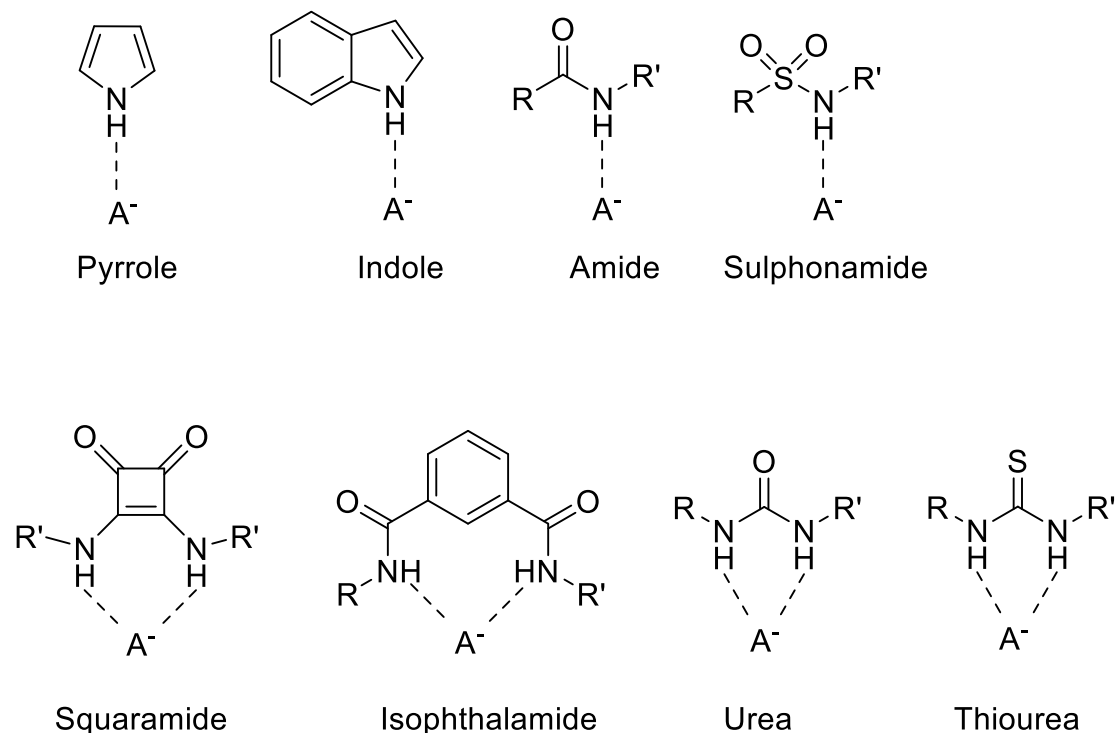


**Figure 45** – Figure to illustrate the common hydrogen bond donor groups and their anion binding motif that are frequently used in synthetic neutral anion receptors.

The main objective of this chapter is to supply the reader with the necessary information required to grasp the subjects' specific concepts, which will be employed in this area of research. This chapter will look at selected hydrogen bond donor groups that can be found in synthetic neutral anion receptors. Therefore, it is not an extensive account and, for this, the reader is directed to a number of recommended reviews in the literature.[3-5]

### 3.1.2.1 Amide based receptors

Amide NH groups have been utilised as hydrogen bond donor groups to generate a wide array of anion binding receptors. One of the first synthetic amide anion binding receptors was discovered by Pascal *et al.*[39] X-ray data of the sulphate binding protein salmonella typhimurium shows that sulphate is held via seven hydrogen bonds, five of which involve amide NH protons from the polypeptide backbone. This led to the synthesis of a synthetic organic macrocycle possessing seven inwardly-facing amide protons to encapsulate an

inorganic anionic species sufficiently. The macrocycle synthesised, **44**, was given the name 2, 15, 28-trioxo-3, 16, 29-triaza-6, 19, 32-trithial [7.7.7] (1, 3, 5- cyclophane) (**figure 46**).
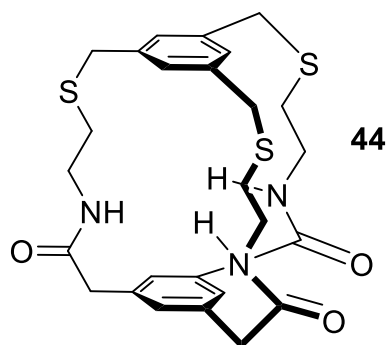


**Figure 46** - Figure to show the chemical structure of 2, 15, 28-trioxo-3, 16, 29-triaza-6, 19, 32-trithial [7.7.7] (1, 3, 5- cyclophane)[39]

In 2007, Lin *et al*.[40] reported the synthesis of a tetraamide Macrocyclic receptor **45** (**figure 47**). UV/Vis and ^{1}HNMR titration studies showed a high selectivity towards fluoride from a mixture of fluoride, chloride, bromide, acetate and dihydrogen phosphate ions. The affinity towards fluoride is thought to be a result of size complementarity between the guest and the cavity. In addition, upon interaction between the receptor and fluoride, a visible colour change was observed, attributable to hydrogen bond formation. This could result in the potential use of said macrocycle as a colourimetric sensor.



**45**
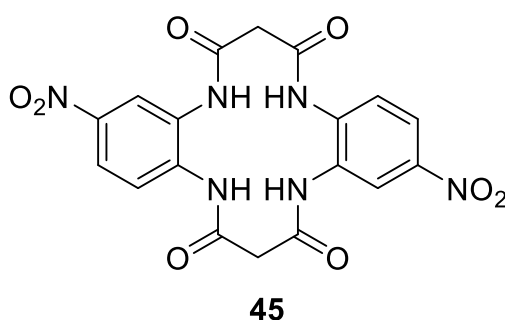
**Figure 47** – Figure to show the chemical structure of the Macrocyclic tetraamide (3'-nitrobenzo)[2,3-d]-(3''-nitrobenzo)[9,10-d]-1,4,8,11-tetraazacyclotetradecane-5,7,12,14-tetraone.[40]

The use of amide bonds within a furyl-cyclopeptide receptor has been demonstrated by Robina and co-workers.[41] From a combination of ESI-MS and ^{1}HNMR titration studies, the cyclopeptide receptor fabricated (**figure 48**) formed 1:1 complexes with chloride, acetate and

cyanide anions, with a particularly high binding affinity towards chloride. Kubick *et al.*[42] have also researched the anion recognition properties of cyclopeptide based cage receptors.



**46**
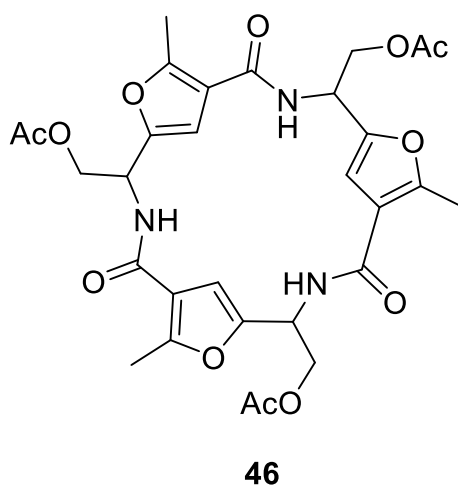
**Figure 48** – Figure to show the chemical structure of C$_3$-symmetric furyl-cyclopeptide receptor developed by Robina *et al.*[41]

### 3.1.2.2 Isophthalamide based receptors

As illustrated in **figure 45**, the isophthalamide unit can be used to coordinate an anionic guest. It has two amide NH groups which can assemble in a '*cleft-like*' structure, thus creating a cavity to coordinate an anionic species. In 1996, the initial use of this particular functional group was reported by Kim *et al*. An anion templated macrocycle (**scheme 9**), incorporating isophthalamide groups, was documented.[43]

47                          48                                          49
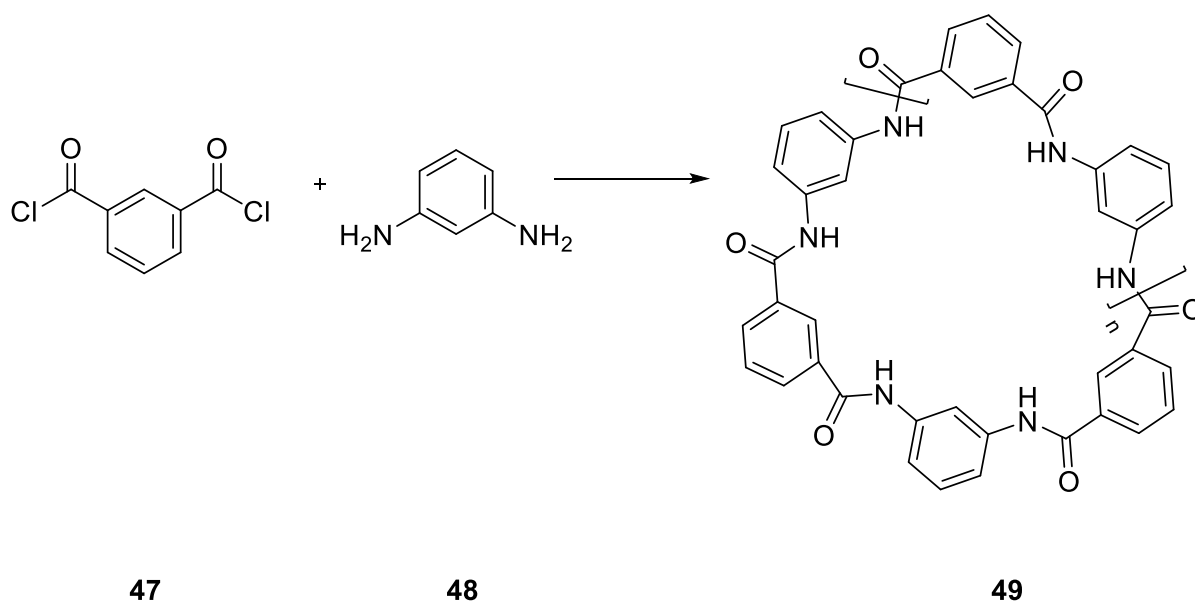
**Scheme 9** – Synthetic procedure of an anion templated macrocycle developed by Kim *et al.* Adapted with permission from [Kim, Y. H.; Calabrese, J.; McEwen, C. *J. Am. Chem. Soc.* 1996, *118*, 1545]. Copyright 1996 American Chemical Society.

Following this, numerous research was carried out involving this hydrogen bonding moiety.[44-46] The simplicity of synthesis in conjunction with a high affinity towards anionic species has triggered interest regarding this particular functional group.

In 2007, Gale *et al.* synthesised a range of receptors which incorporate the isophthalamide skeleton (**figure 49**). With receptor **51**, the inclusion of hydroxyl functional groups result in the formation of intramolecular hydrogen bonds, thus stabilising the syn-syn confirmation. The intramolecular hydrogen bonds not only make this receptor effective at anion coordination, but also competent in transportation of chloride.[19] However, Receptor **52** did not bind significantly to anionic guests.

**50**
*syn-anti*

**51**
*syn-syn*

**52**
*anti-anti*
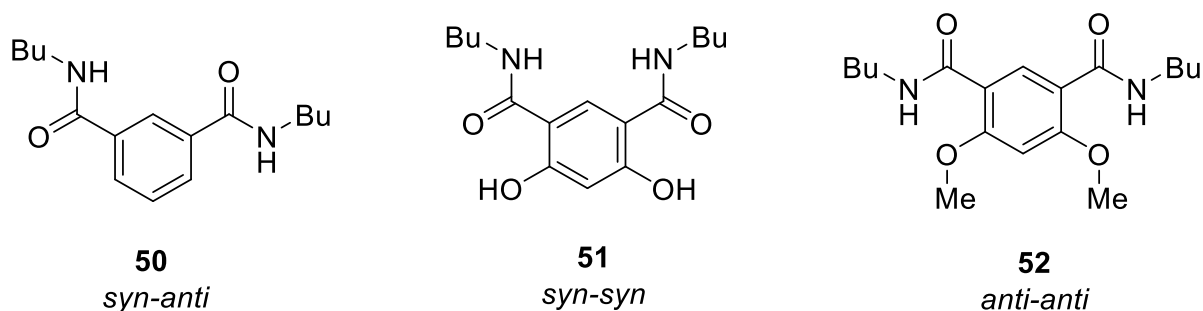
**Figure 49** – Figure to show a series of isophthalamide based anion receptors for transmembrane chloride transport.[19]

In 2009, Bernier and co-workers[47] reported the synthesis of a Macrobicyclic anion receptor **53** that comprised of a tetraoxadiaza macrocycle, accommodating both a dibenzofuran spacer and an isophthalamide head unit. The chemical structure can be seen below in **figure 50**.



**53**
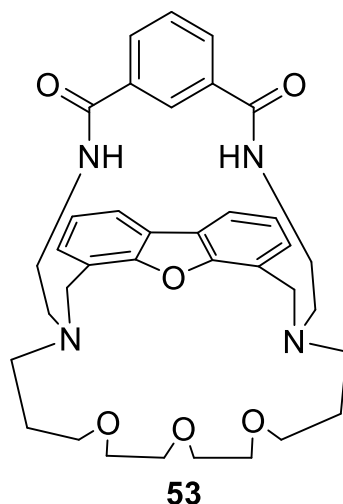
**Figure 50**– Figure to show the macrobicyclic anion receptor developed by Bernier *et al.* based on an isophthalamide head unit and tetraoxadiaza macrocycle.[47]

The macrocycle was able to remove halide salts from aqueous solutions in organic media. The capability to bind halides was monitored by ^{1}HNMR titrations in deuterated chloroform, deuterated dimethyl sulphoxide and acidified deuterium oxide. The highest association constant was observed for chloride with the protonated macrocycle. The results from these studies show the potential of receptors of this nature in the area of chloride transport.

The isophthalamide group has continued to receive a high level of interest in the area of supramolecular chemistry, not just in the area of anion coordination but also in the area of ion-pair recognition. Beer *et al.*[48] have developed a heteroditopic calix[4]diquinone triazole

receptor, which contains an isophthalamide cavity (**figure 51**). From analysis by UV/Vis and ^{1}HNMR, a monovalent cation-anion pair cooperatively binds in a polar solvent mixture of 2% water/acetonitrile. Studies have shown that cation interaction by the triazole nitrogen donor groups and the calix [4] diquinone oxygen donor groups improves the strength in coordination of the halide anion at the isophthalamide cavity.
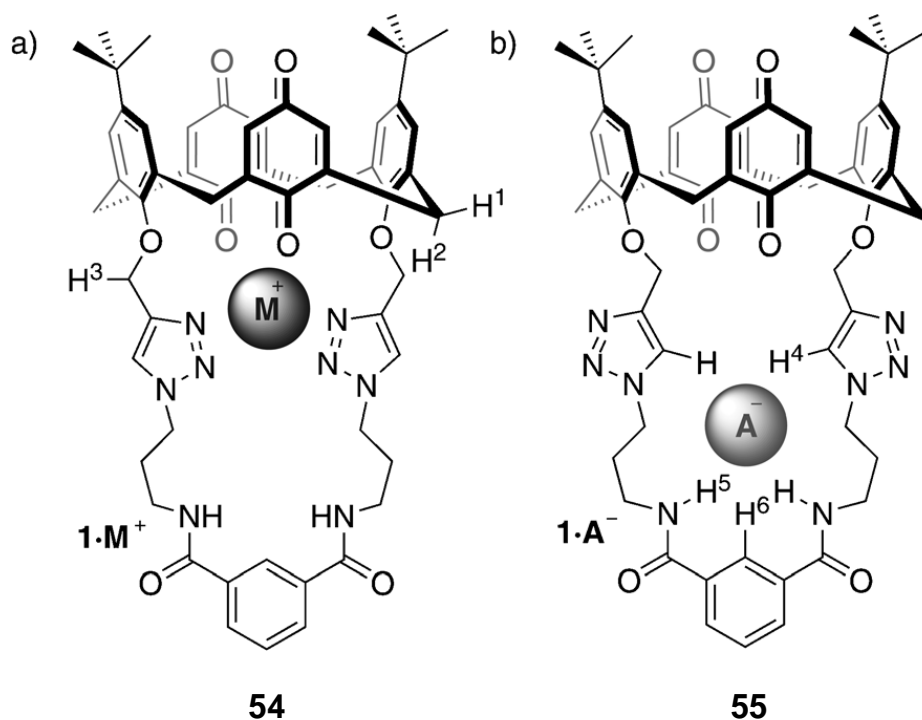


**Figure 51** – Figure to show the heteroditopic ion-pair receptor **1**. The triazole groups act as (a) Lewis bases for coordination of a metal cation and (b) hydrogen bond donors for anion coordination. Reprinted with permission from [Picot, S. C.; Mullaney, B. R.; Beer, P. D. *Chem.--Eur. J.* **2012**, *18*, 6230]. Copyright 2012 WILEY-VCH Verlag GmbH & Co. KGaA, Weinheim.

### 3.1.2.3 Pyrrole and Indole based receptors

An important feature of pyrrole and indole is that they can only behave as a hydrogen bond donor. This eliminates the possibility of intramolecular hydrogen bonding, which could hinder anion recognition. With receptors possessing hydrogen bond donor and acceptor groups, there is added internal competition for a hydrogen bond donor. This is a key issue that requires forethought when designing a receptor of this nature.[49] Pyrroles are relatively uncomplicated to functionalise and can be included within both acyclic and cyclic structures. As a result, pyrrole has been researched in great depth for use in a wide variety of synthetic receptors. The incorporation of pyrrole within anionic receptors was first pioneered by

Sessler *et al*. In 1992, the fabrication of a pentapyrrolic sapphyrin structure was documented. This macrocyclic structure, when protonated, formed a 1:1 complex with halide anions, with a particularly high affinity towards fluoride. Selectivity towards fluoride was around $>10^3$ stronger than both chloride and bromide.[50] Sessler *et al*. expanded this work by developing protonated sapphyrins, which behave as effective phosphate receptors.[51] In 2007, Sessler *et al*. reported the fabrication of a series of acyclic pyrrole anion receptors. The receptors synthesised contain a central pyridine ring connected to pyrrole units via 2-aminopyrrole-derived amide bonds (**56** and **57**). The central pyridine ring was also replaced by a phenyl ring giving receptor **58**. Furthermore, the amide linkages were reversed, generating the acyclic receptor **59** (**figure 52**). Results show that, by having a central pyridine ring, anion coordination is stabilised. In addition, reversing the configuration of amide bonds alters the selectivity of the receptor. Receptor **56** is selective towards benzoate and **57** towards acetate, whereas **59** is selective towards chloride.[52]
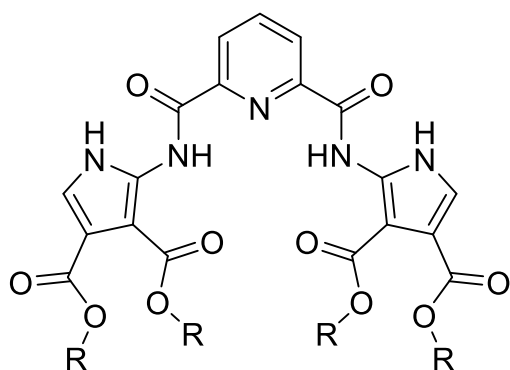
**56**: R = CH$_2$CH3

**57**: R = CH2CH2C(CH3)3
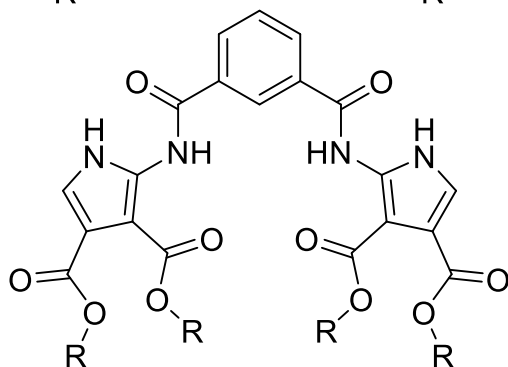
**58**: R = CH$_2$CH$_3$
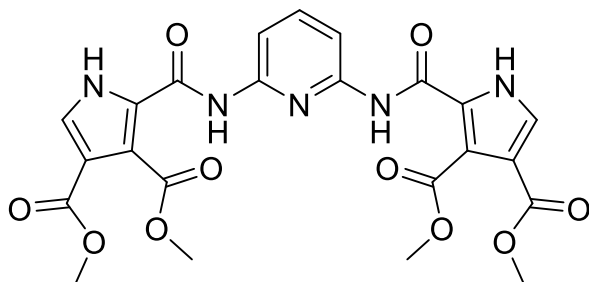
**59**

**Figure 52**– Figure to show the chemical structure of a series of acyclic Pyrrole based receptors developed by Sessler and co-workers.[52]

There have not only been advances in acyclic pyrrole based receptors; Mani and co-workers have developed pyrrolic macrocycles which incorporate amine linkages by using the Mannich reaction (**figure 53**). The larger macrocyclic receptor displayed a considerable affinity to halide coordination.[53]

**60**            **61**
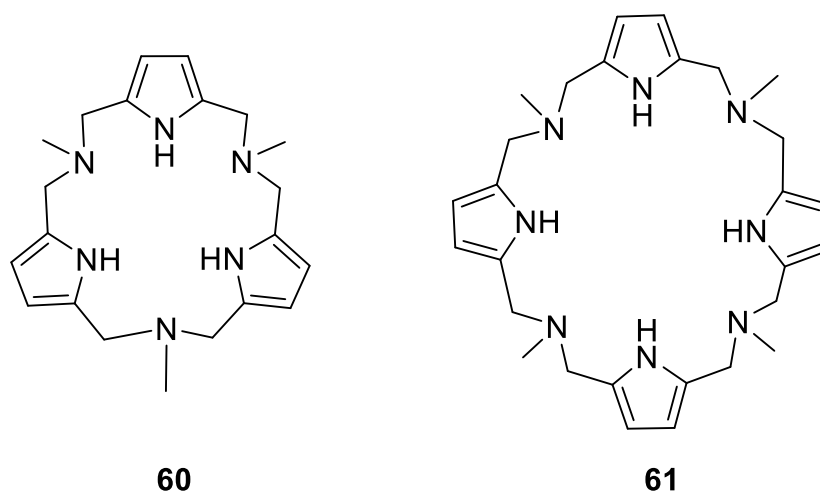
**Figure 53**– Figure to show the chemical structures of both an azatripyrrolic and an azatetrapyrrolic macrocycle, synthesised via the mannich reaction.[53]

Indole is an aromatic heterocyclic organic compound which contains a pyrrole ring fused to a benzene ring and, like pyrrole, contains a single hydrogen bond donor. Indole is also more acidic in comparison to pyrrole as a result of supplementary inductive and resonance effects from the adjacent benzene ring. The small rise in acidity means that indole is able to form stronger hydrogen bonds with an anionic guest when compared to the pyrrole unit.[54]

While pyrrole has received a great deal of attention in the area of anion receptor chemistry, indole has been relatively unexplored. In 2005, Beer *et al*. generated indolocarbazole receptors **62** to **65** (**figure 54**) by modifying the Fischer indolisation reaction with 1, 2 cyclohexanedione and a suitable aryl functionalised hydrazine. Each receptor showed the highest affinity towards benzoate after analysis by UV/Vis spectroscopy. The simplicity of functionalisation of the indolocarbazole skeleton and the efficiency in anion coordination deems preorganised receptors of this nature highly useful in anion supramolecular chemistry.[55]
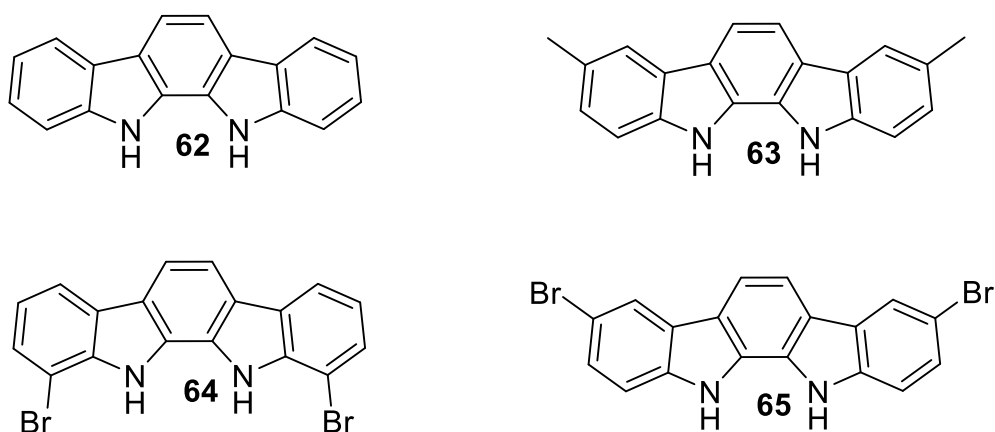
**Figure 54** – Figure to show the chemical structures of a series of indolocarbazole receptors developed by Beer *et al.*[55]

Jeong *et al.* have looked at both acyclic[56] and macrocyclic[57,58] indole receptors. In 2007[58], the synthesis of two indocarbozole macrocycles was reported (**figure 55**). The macrocyclic receptors have anion binding cavities of differing size and are both rigid in structure, thus limiting conformational flexibility.
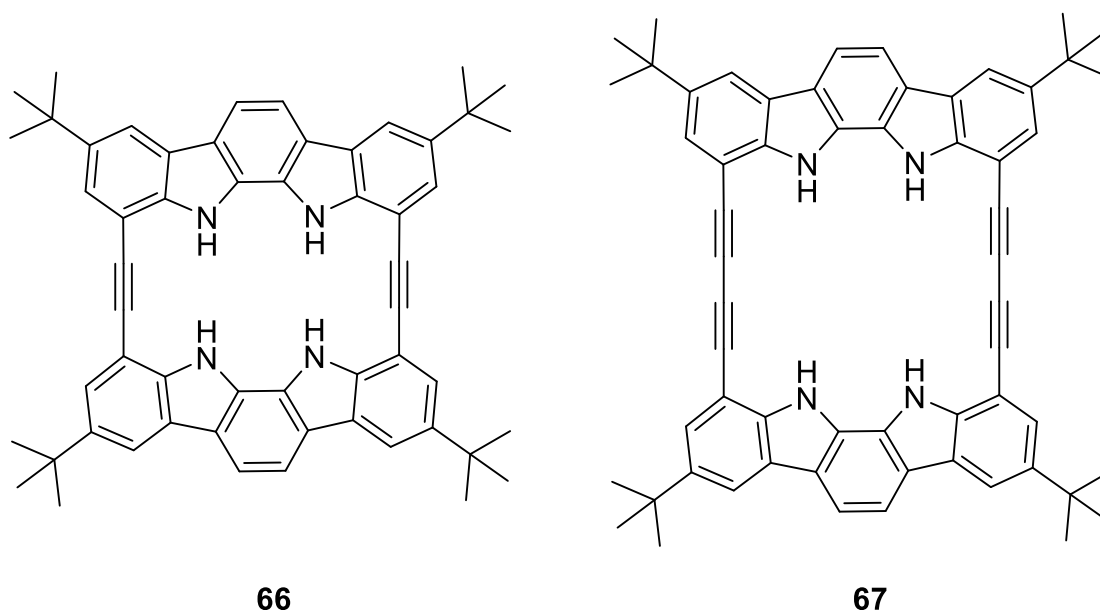


**Figure 55** – Figure to show the chemical structures for two macrocyclic indole based receptors, which have been developed by Jeong *et al.*[58]

In the case of the smaller macrocycle, azide coordinated in an *'end-on'* fashion with the NH groups forming hydrogen bonds to a terminal nitrogen atom in the azide ion. For the larger cavity, a more stable mode is adopted. Each indolocarbozole unit forms a hydrogen bond to the azide terminal nitrogen atoms in an *'end-to-end'* fashion. Coordination properties with

other anions were investigated with interesting results. With the halides, in the smaller macrocycle, the relative order of binding is Cl⁻ > Br⁻ > I⁻, which is in accordance with the hydrogen bond accessibility of halide anions. With the larger macrocycle, iodide is coordinated with the highest affinity showing that the size of the cavity is the deciding factor in coordination; the iodide ion and cavity are equivalent in size.[58]

In 2010, Gale and co-workers[59] developed a range of diindolyurea receptors (**figure 56**) and analysed the relative binding affinities of each receptor towards a range of oxo-anions. Receptors **68** and **69** formed 1:1 complexes with sulphate ions; however, upon addition of added equivalents of sulphate, the result was the generation of higher order complexes. Regardless of possessing fewer hydrogen bond donor groups, receptor **70** still binds sulphate strongly. Furthermore, upon complexation of dihydrogen phosphate and bicarbonate anions to the receptors containing 8 hydrogen bond donors (**68** and **69**), the pKa of the bound species are altered to the extent that they are deprotonated by free anions in solution.
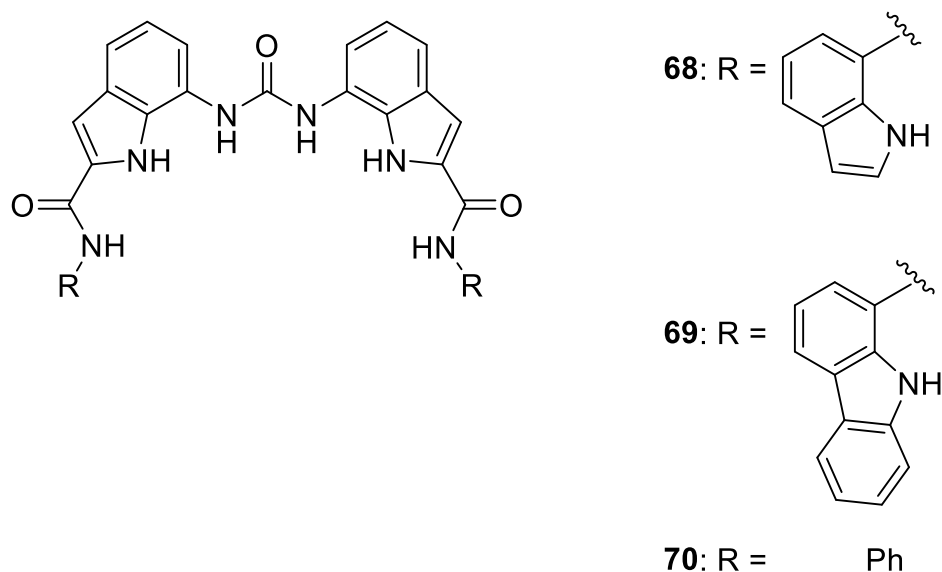


**Figure 56** – Figure to show the chemical structures for a series of diindolurea receptors developed by Gale *et al.*[59]

### 3.1.2.4 Urea and thiourea based receptors

Urea and thiourea receptors were first established by Wilcox[60] and Hamilton.[61] These particular functional groups have since received a high level of interest for their potential in anion coordination. Urea and thiourea based receptors provide a good environment for '*y-shaped*' anions, such as oxo-anions (carboxylate, benzoate and acetate).[62] Urea and thiourea

groups have two –NH donor groups; they can either coordinate a singular spherical anionic species by creating a 6-membered ring, or neighbouring oxygen atoms on an oxo-anion to create an 8-membered ring (**figure 57**).[63]



**Figure 57** – Figure to show the two distinct ways in which (thio)urea based receptors coordinate to an anionic guest: (a) Both NH donor groups coordinate to a spherical anion, producing a 6-membered ring (b) each NH donor group coordinates to two adjacent oxygen atoms present in an oxo-anion, producing an 8-membered ring.

Work by Pfeffer et al.[64] has demonstrated the inclusion of both urea and thiourea groups in combination with amide groups in a variety of indole based receptors (**figure 58**). A flexible carbon linker of varying length was used to connect the indole group to a thiourea/urea group, allowing some level of flexibility. By the inclusion of a spacer, the groups can cooperate when coordinating an anionic guest. From utilisation of $^1$HNMR titration techniques, each receptor was shown to coordinate a series of anionic guests. With dihydrogen phosphate, it was apparent that every NH donor present was involved in coordination.



**71**　　　　　　　**72**　　　　　　　**73**

**Figure 58** – Figure to show the chemical structure for a series of indole based receptors by Pfeffer and co-workers, which contain thiourea and urea groups.[64]

In 2009, Gale and co-workers developed a series of urea based receptors (**figure 59**). Studies demonstrated that the higher the number of NH donor groups within the receptor, the larger the shift of the urea NH protons. In order to achieve successful coordination with an alkylcarbamate anion, the receptor must compete with the ammonium cation that forms upon complexation. Previous results indicate that the higher the number of donor groups, the more likely it is that stabilisation of the alkylcarbamate will occur. Therefore, diindolyurea and carbazolyl urea should display the greatest strength of interaction with carbamate anions.[65]
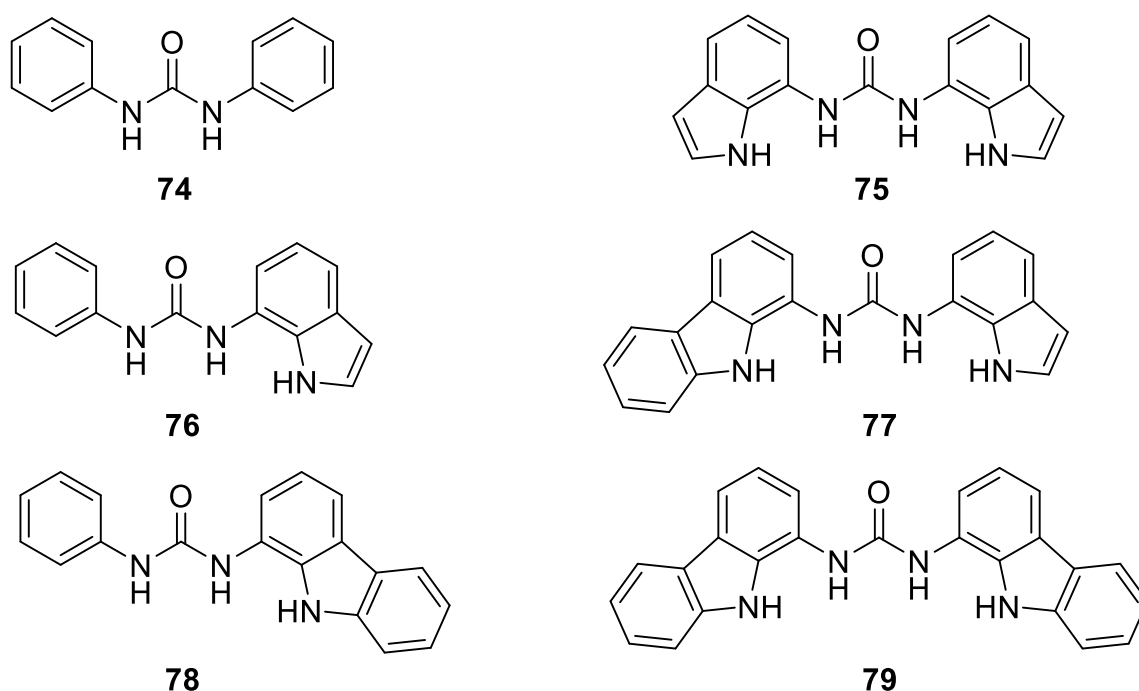


**Figure 59** – Figure to show the chemical structures for a series of urea based receptors developed by Gale *et al.*[205]

This research group then went on to demonstrate that the alkyl ammonium cation could itself be stabilised by a crown ether structure, which is illustrated in **figure 60** overleaf. Stabilisation of the cation by a crown ether resulted in an enrichment in the hydrogen bonding interaction between the receptor and the alkylcarbamate anion.[65]

**80**
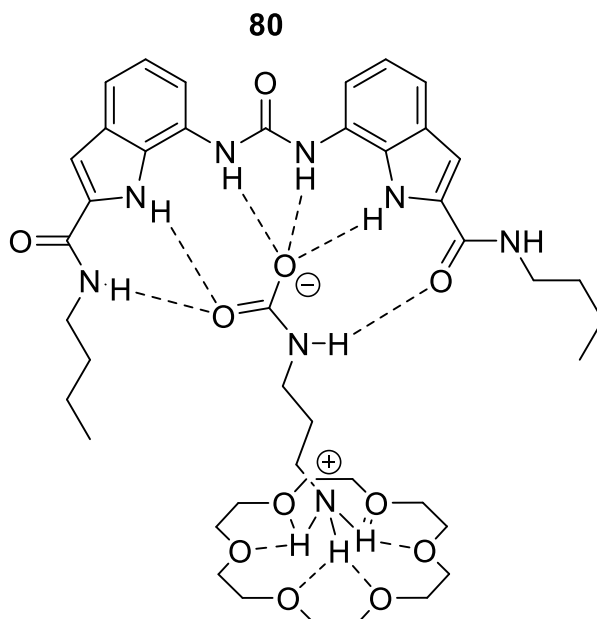


**Figure 60** – Figure to represent the interaction between an alkylammonium-alkylcarbamate salt (formed from 1, 3-diaminopropane and carbon dioxide) with a urea based receptor and 18-crown-6.[66]

An area of chemistry, which urea and thiourea based receptors can feature, is the area of colourimetric sensing. In 2011, work by Bhardwaj *et al.*[67] showed the development of a series of neutral tripodal and bipodal receptors which contain thiourea/urea groups for coordination and a *p*-nitrobenzene unit for signalling. These receptors have been reported to behave as selective colourimetric sensors. The chemical structures of the neutral receptors are shown overleaf in **figure 61**.
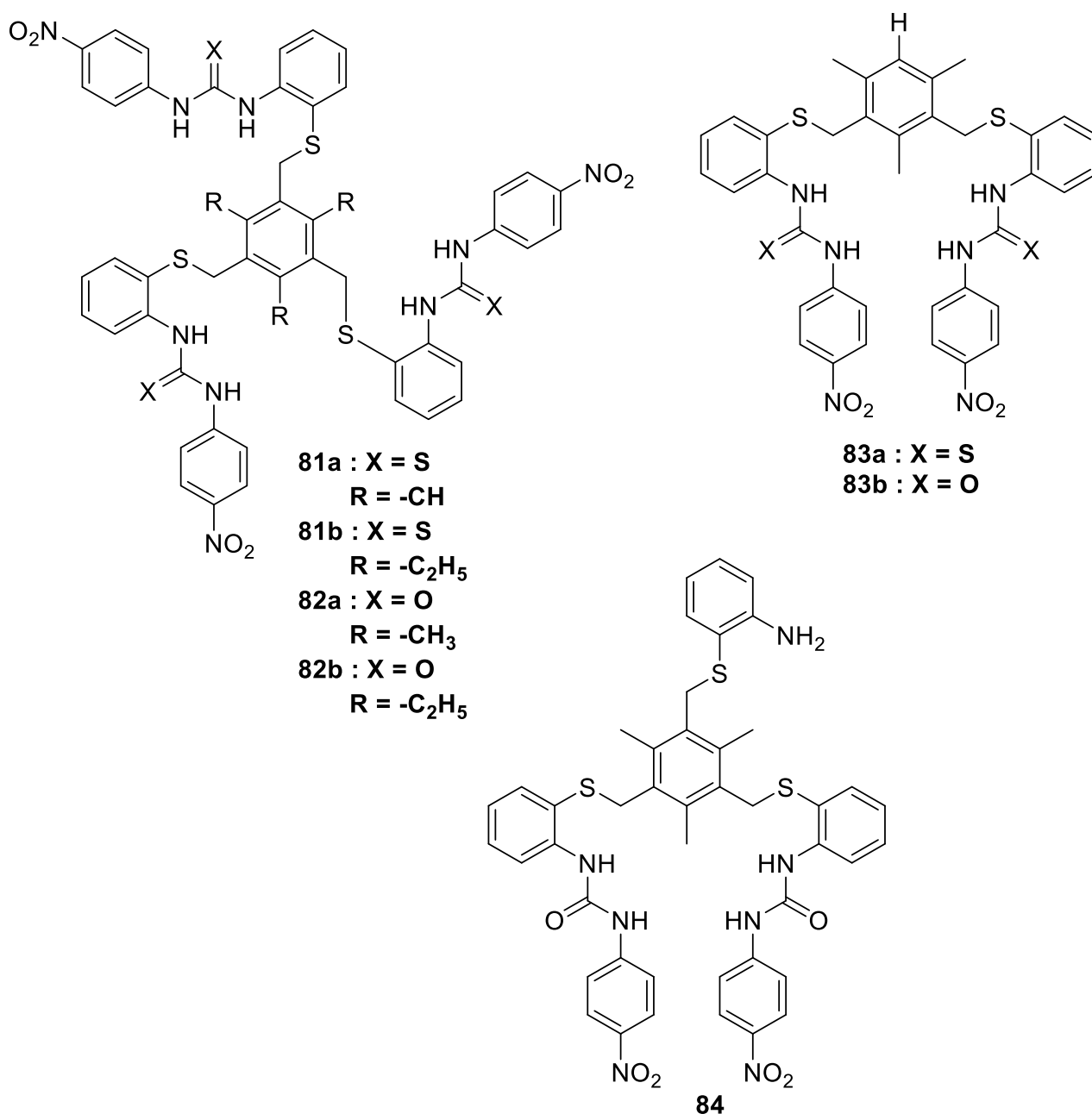
**Figure 61** – Figure to show the chemical structures for a series of neutral tripodal and bipodal thiourea/urea based receptors developed by Bhardwaj *et al.*[67]

Results show that the thiourea derivatives are highly selective towards fluoride. With the urea derivatives, complexation is dependent upon the reversible acid-base reaction which takes place between the acidic urea NH donor groups and the basic fluoride anion. Despite being selective towards fluoride, urea derivatives only show low sensitivity in comparison to their thiourea counterparts. As a result, sensing only takes place at high fluoride concentrations. The difference in the activity of the urea and thiourea receptors is attributable to the intrinsic acidity. Thiourea displays a higher intrinsic acidity in comparison to urea, meaning it is

capable of forming stronger hydrogen bonds. Work by Yatsimirsky and co-workers[68] compared the strength of binding of thiacalix[4]arenes functionalised with both urea and thiourea moieties. Studies showed stronger binding for the urea based receptors in comparison to thiourea analogues, despite the elevated intrinsic acidity.

It is evident that there have been numerous advances with respect to neutral anion receptors, which incorporate a variety of hydrogen bond donor groups. However, this research will focus on the isophthalamide moiety and this particular group will be explored in more detail at a later point in this chapter.

## 3.2 Aims and Objectives

### 3.2.1 The importance of anion receptor chemistry in nature

The chemistry of anion coordination is continuing to attract attention within the area of supramolecular chemistry. Anions play crucial roles in numerous areas, such as biology, medicine and the environment.[16, 69-71] Therefore, being able to design synthetic receptors has been at the forefront of numerous research within this area. There have been numerous contrasting designs for synthetic receptors, the majority of which showing a preference for harder anions, such as fluoride, over bulkier softer anions, such as carboxylate. Therefore, the ability to bind hydrophobic anions in aqueous media still remains a challenge synthetically.

Anion receptors within nature overcome all synthetic obstacles, as the binding site is tailored to a specific anionic substrate in aqueous media, regardless of the nature of the anion. As previously mentioned in the introductory section to this chapter, an example of the crucial role anions play is evident in sustaining the phosphorylation state of proteins, which is significant for a wide variety of cellular processes. Both kinases and phosphatases are the collective groups of protein responsible for this procedure. Alkaline Phosphatase (AP), a member of the Phosphatase family, is an example of an anion receptor found in nature. As stated earlier, it possesses a shallow active site containing an arginine residue, a magnesium ion and two zinc ions, rendering it positively charged (**figure 62**). This positive charge is responsible for the binding of anionic phosphate moieties and, due to the shallow nature of the active site, only the phosphate moiety of the substrate will interact with the enzyme.[11] Numerous studies have taken place on examining the structure of protein anion binding sites. More enzymes are known to contain arginine in comparison to other amino acids, which is due to the fact that arginine operates as an anion binding site, showing a preference for hydrophobic substrates in particular.[72] Amino acids tend to be non-polar in nature, meaning that alkaline phosphatase is a water soluble protein that has a hydrophobic cavity, therefore, it is a notable example of how nature can preferentially bind soft hydrophobic anions in an aqueous medium. Therefore, it can be seen from the literature that, in nature, hydrophobic receptors can be located within a water soluble environment. Therefore, nature uses the principle of encapsulation to coordinate a hydrophobic anion within a water soluble environment. The main aim of this part of the project is to mimic this principle and design an anion receptor which is encapsulated within a water soluble environment.
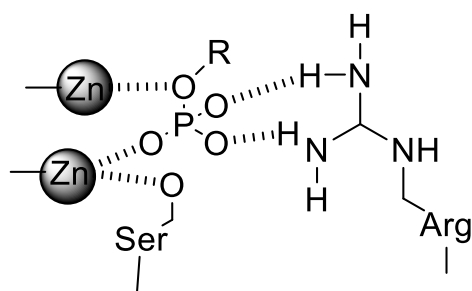
**Figure 62**- Figure to show a phosphate monoester binding to the active site of Alkaline Phosphatase (AP).[11]


### 3.2.2 Approach and consideration

In order to design a water soluble molecule comparable to nature it is important to consider the various components required. Firstly, an appropriate anion receptor site which is able to favour binding of hydrophobic anion substrates is required. Secondly, an appropriate water soluble molecule is required to encapsulate the receptor within a hydrophilic environment.


### 3.2.2.1 Design principles of the anion binding receptor

As mentioned beforehand, the most palpable method for anion binding is by utilising electrostatic interactions, for instance, using a positive charge will generate a strong ionic bond. A potential hindrance to a cationic receptor is the presence of a counter ion which could potentially compete with the anionic substrate in question. As discussed in the introductory section of this chapter, another intermolecular force that could be used for anion recognition is the hydrogen bond. An anion can alternatively be considered as an electron pair donor, meaning interaction with an electropositive H atom (electron pair acceptor) will result in a strong interaction. More electron pair acceptor groups present within the receptor will enhance binding strength due to cooperative effects. However, the alignment of hydrogen bonds must be convergent as it is essentially a dipole, thereby unearthing a potential obstacle for design. Finally, when engineering a binding site to show a preference towards hydrophobic anions, the site must itself be hydrophobic and organic in nature. This will lead to hydrophobic effects being utilised in retaining the anion within the cavity. The addition of aromatic rings could also encourage cooperative π-π stacking interactions. A hydrophobic binding site would enhance specificity to the desired anionic substrates so the site must itself be non-polar.

**3.2.2.2 Encapsulation of the binding site within a water soluble environment**

The next step in the design process is to decide upon a molecule by which to encapsulate the binding site within, so that it is encased within a hydrophilic environment. Linear polymers were initially considered but were considered too dynamic and flexible for this purpose, therefore, dendritic polymers were also explored. Dendrimers are an innovative type of macromolecule. They are monodisperse and both their molecular uniformity and structurally perfect architectures has made them desirable for a variety of diverse applications. There have been numerous studies involving the utilisation of dendrimers for encapsulation, employing both a non-covalent and covalent approach. Due to the perfectly branched nature of these polymeric molecules, they are able to trap organic molecules inside. This non covalent approach makes use of intermolecular interactions and hydrophobic effects to retain the target molecule. The Twyman group reported a modified PAMAM synthesis generating a water soluble dendrimer which is able to solubilise small hydrophobic molecules within the interior as illustrated in **figure 63**.[73] Another example is the dendritic box reported by Meijer *et al.*, which demonstrates a dendrimers ability to exhibit non-covalent encapsulation. The dendritic box allows the possibility for molecules to be held in place by chemically closing off the periphery, and thus blocking an escape pathway. This allows enveloped guest molecules to be selectively ejected, depending on their size/volume, by modifying the nature of the peripheral surface.[74, 75] The possibility for non-covalent encapsulation of small molecules within  a dendritic structure allows potential for the use of these macromolecules in drug delivery and catalysis.[76]
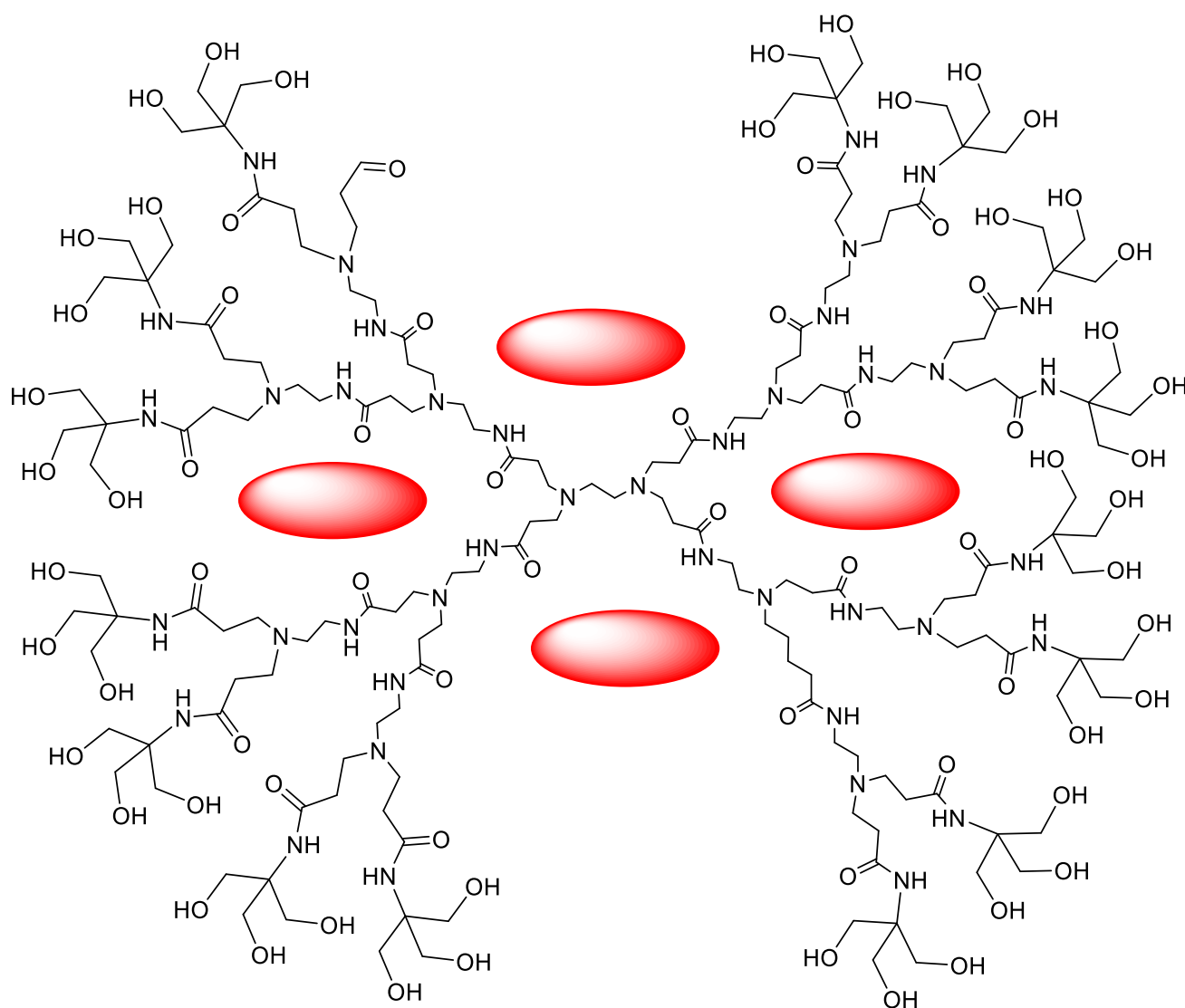
**Figure 63**- Figure to show a water soluble PAMAM dendrimer solubilising hydrophobic organic molecules within the interior of the architecture.[73]

With dendrimers, there is an exponential growth in molecular weight for a numerical enlargement in volume. This has pointed towards a theory, by which there will be a critical molecular weight where the core is effectively encapsulated by the sterically hindered and densely packed dendritic architecture.[76] The dendrimer core is a unique environment and can sometimes be described as a microenvironment.[75] Functionalisation of the core will mean the dendritic structure will be able to control the microenvironment around an active site. An example of this can be seen in the work by Diederich *et al.,* involving the generation of porphyrin cored dendrimers to function as synthetic models for globular proteins. To achieve this, a dendrimer was constructed around a porphyrin core using a divergent method (**figure**

**64**). Electrochemical studies have uncovered that the redox potential of the metalloporphyrin core was not influenced by the exterior solvent, but was controlled by the nature of the dendritic generation and branching, thus revealing, that as generation increased, the more electron rich the environment around the core became. Essentially, the dendrimer acts as a solvent as it shelters the core from the surrounding chemical environment.[77]
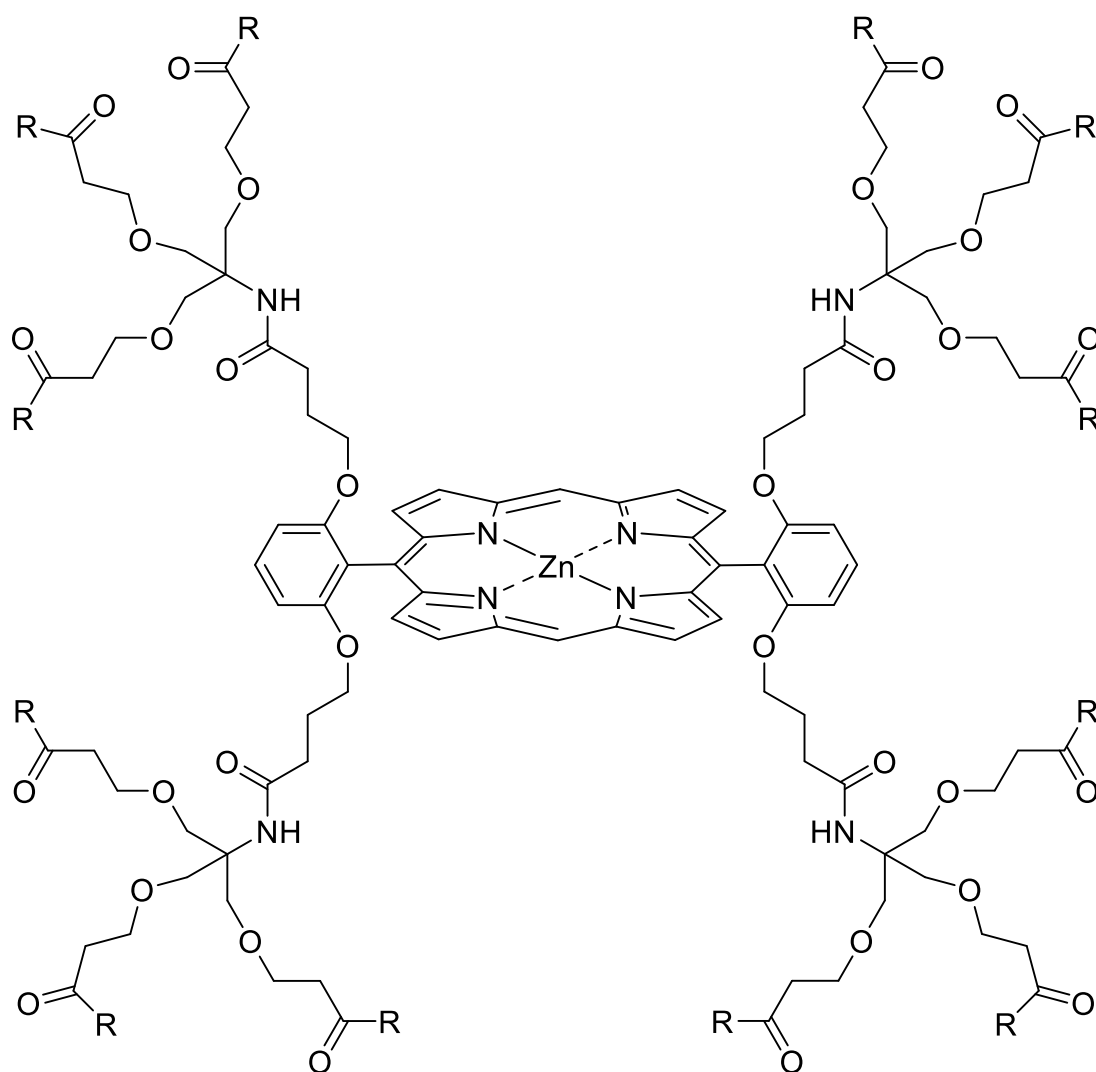
**Figure 64** – Figure to show the chemical structure of the skeleton of a metalloporphyrin cored dendrimer as a synthetic model for globular heme proteins.[77]

There is an important drawback to consider when contemplating utilising dendrimers for a specific application. The multistep synthetic procedure that is required is exhaustive, complex and is expensive to accomplish, not to mention the difficulty in purification. Therefore, hyperbranched polymers were considered as a potential substitute. Hyperbranched polymers, with nearly indistinguishable properties to dendrimers, can be easily synthesised in a one-step

synthesis, thereby showing potential as materials for large scale industrial use.[78] Despite their structural defects when compared to dendrimers, they can still uphold a three dimensional globular configuration which is comparable to that of a dendrimer. Therefore, covalent and non-covalent encapsulation is a potential application for these macromolecules. Frey *et al*. exploited the properties of these macromolecules to demonstrate non-covalent encapsulation of hydrophilic pincer-platinum (II) complexes by synthesising amphiphilic hyperbranched polyglycerol nanocapsules. **Figure 65** represents a sulfonate functionalised pincer platinum (II) complex **85**, which was successfully encapsulated. These nano reactors showed potential in homogenous catalysis, as they enabled double Michael addition reactions to take place. The synthetic procedure for a molecular hyperbranched nanocapsule is illustrated in **scheme 10**. The synthesis involves the incomplete esterification of hyperbranched polyglycerols. Encapsulation was carried out by shaking solutions of the nano capsules in dichloromethane with aqueous solutions of the hydrophobic square planar platinum (II) complexes and monitored using UV-Vis spectroscopy. The encapsulated platinum (II) complexes exhibit catalytic activity regarding double Michael addition. Conversely, this occurred to a lesser extent than when compared to the free platinum (II) complexes. Nevertheless, it is a successful example for the generation of a hyperbranched polymer microenvironment for a homogenous catalyst, via a non-covalent approach.[78, 79]
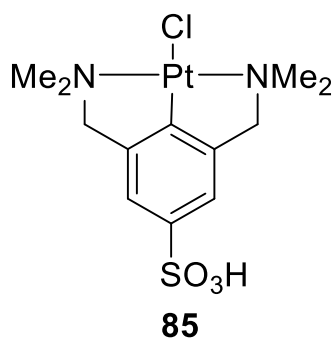


**Figure 65** – Figure to show the chemical structure of a sulfonate pincer platinum (II) complex. This complex was used by Frey and co-workers to exploit the properties of hyperbranched polyglycerols and was encapsulated successfully via non-covalent interactions.[78, 79]
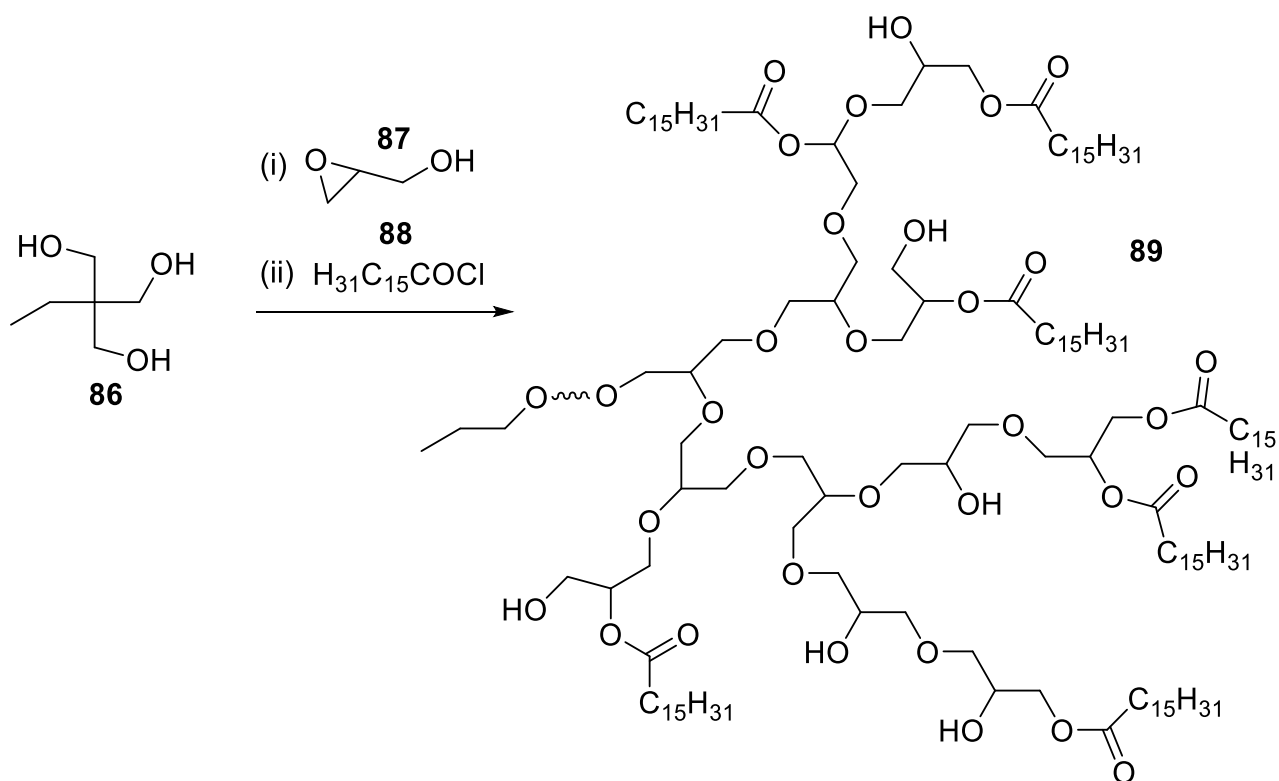
**Scheme 10**- Synthesis of a molecular hyperbranched nanocapsule involving incomplete esterification of hyperbranched polyglycerols.[79]

### 3.2.2.3 Design of an anion receptor based on a hyperbranched polymer

Due to the expensive preparative method and protracted procedures involved in dendrimer synthesis, hyperbranched polymers were considered. Even though they are relatively unexplored in comparison, they appear to be a viable option for this research. Both covalent and non-covalent encapsulation methods have been well established. However, the covalent approach was selected as it ensures site selectivity of the binding site, so this will be the approach selected. A final consideration which is imperative to the covalent incorporation of the anion receptor is the compatibility with the polymerisation method selected, in order to achieve successful incorporation. The principal aim of this work is to covalently incorporate an organic soluble anion receptor within a water soluble hyperbranched polymer environment and compare the relative binding affinity of various hard and soft anions between the covalently encapsulated receptor and free receptor. **Scheme 11** is a simplified schematic representation of this aim.

$A^- = F^-, Cl^-, Br^-, I^-, C_6H_6CO_2^-, CH_3CO_2^-, H_2PO_4^-$
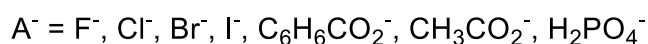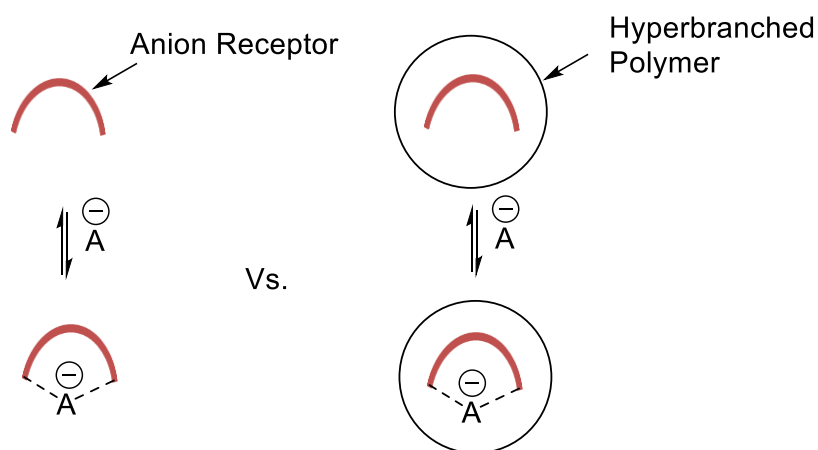
**Scheme 11** - Schematic representation of the principal aim of this research project.

### 3.2.2.4 Encapsulation of a receptor within an organic soluble environment

Despite the overall aim being the encapsulation of an anion receptor within a water-soluble environment, it is important to determine if there is any effect of covalent encapsulation within a polymeric environment upon anion coordination and relative binding trends. Therefore, prior to encapsulation within a water-soluble environment, covalent incorporation within an organic soluble polymer system must be attempted as a proof of principle. Due to the synthetic obstacles of encapsulation within a water soluble system, an organic soluble system provides an easier synthetic approach, in addition to allowing a proof of principle of the effect of encapsulation of an anion binding core within a polymeric structure. The addition of a new electronic environment surrounding a receptor could result in two potential outcomes. Firstly, the trend in which anions would ordinarily interact to the native receptor could be modified as the new surrounding environment could provide an optimum environment for a specific anion, thus resulting in a difference in selectivity. It is also possible that there are no changes in relative binding trends (compared to the native receptor). Furthermore, as a result of the new steric barrier in place, there could potentially be a reduction in the binding affinity of an anionic guest. Therefore, the determination of the effect of covalent incorporation inside an organic polymer is the initial task of this project.

## 3.3 Results and Discussion

### 3.3.1 Core functionalisation polymerisation – synthetic considerations

As previously mentioned in the aims and objectives section of this chapter, the covalent approach was initially chosen due to the site selectivity it ensures. Consequently, the initial stage of this research was the selection of an appropriate polymer and anion receptor core.

### 3.3.1.1 Selection of the polymer for organic soluble core Functionalisation

As described beforehand, the ultimate goal for this research is to produce an anion receptor incorporated within a water soluble polymer. However, it was initially decided that the covalent incorporation of a binding core within an organic soluble polymer would be investigated. As discussed earlier, the motive behind this was for proof of principle that an anion binding site can be covalently incorporated within a hyperbranched polymer. An organic soluble system would be synthetically simpler, generating a more robust system compared to covalent incorporation within a water soluble polymer. The generation of an organic soluble system will also provide information upon the effect upon anion coordination, compared to the receptor in its native state. There is currently an effective polymer system in-house within the group. The Twyman group has demonstrated complete core incorporation for nitrophenyl acetate and the simple AB$_2$ monomer 3, 5-diacetoxybenzoic acid. The synthesis involved a reversible esterification mechanism[80] and will be discussed further in section **3.3.5**. Therefore, it was hypothesised, that this process could be exercised to synthesise an anion receptor system possessing a binding site with high levels of core incorporation. The chemistry of this monomer is not only well known within the Twyman research group, but has also been the focus of research outside,[81] making it an appropriate choice for this work. The monomer 3, 5-diacetoxybenzoic acid has an aromatic ring. It is therefore hypothesised that benzoate would bind more favourably within the polymeric anion receptor, due to cooperative π-π stacking effects.

### 3.3.1.2 Synthesis of 3, 5 diacetoxybenzoic acid

The monomer 3, 5 diacetoxybenzoic acid was produced using a single step reaction between 3, 5 dihydroxybenzoic acid and acetic anhydride (**scheme 12**). This synthetic procedure was based upon a methodology outlined in the work by Turner *et al.*[82]
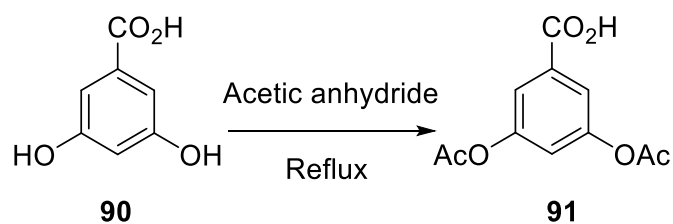
**Scheme 12** – Synthesis of 3, 5 diacetoxybenzoic acid.

The monomer was refluxed with excess acetic anhydride, generating a yellow solution. The acetic anhydride was then subsequently removed via vacuum distillation. Care was required not to exceed a temperature of 80°C to avoid self-polymerisation from occurring. After dissolution in refluxing chloroform the product was filtered hot and upon addition of petroleum ether 40:60, a white solid precipitated out of solution. After filtration, the product was dried thoroughly and characterised. The $^1$HNMR data obtained was in accordance with the literature displaying a broad singlet at 10.32 ppm, indicative of the carboxylate proton. A doublet and triplet at 7.75 and 7.20ppm respectively were observed for the aromatic ortho and para protons and, finally, a singlet was observed at 2.32ppm which was characteristic of the methyl protons present on the acetate groups. The mass spectra showed an ion peak at 237 Daltons, indicative of the MH$^-$ peak and the melting point determined was in accordance with the literature. Elemental analysis gave results within 0.5% of the expected values giving confidence in the purity of the sample. Infra-red spectroscopy and X-ray crystallography (**appendix B**) were also employed to provide additional analytical information, confirming the synthetic procedure was successful.

### 3.3.1.3 Design of the anion receptor

When contemplating a suitable anion binding receptor there are certain necessary requirements to consider. The requirements are, firstly, that the core is stable under the conditions required for polymerization. Furthermore, it is crucial that the core is compatible with the mechanism involved. Finally, the third requirement is that the core is analytically visible in the final product. Therefore, the nature and the functionality of the receptor are important. There are two types of receptor to deliberate, a cyclic receptor and a cleft receptor. A cyclic receptor is a pre-organised system where the anion receptor site is fixed both in the bound and unbound state; however, it is synthetically challenging. On the other hand, a cleft receptor is not preorganised as free rotation is allowed about the bonds, it only becomes fixed when the anion is held in place by interactions; however, this type of receptor is less of a

challenge to prepare. Furthermore, by synthesising a receptor which exhibits little preorganisation, allows the manufacture of receptors which are not only efficient, but can be fabricated on a multi gram scale from commercially available and economically priced starting materials.[45] As a result, the cleft seemed an appropriate choice of receptor to begin with.

When considering the structure of the cleft it was decided that a difunctionalised symmetrical molecule would be appropriate. This type of molecule would allow simultaneous polymerisation to both ends so the cleft will be efficiently encapsulated within the hyperbranched polymer. The terminal functionality is extremely important and is solely dependent upon the monomer in question and the mechanism of polymerisation. The monomer in question is an $AB_2$ monomer; this means that it is a requirement for the core unit chosen to contain B functionality. When a B group of a core unit interacts with the A group of a monomer unit, additional B groups will propagate as a result. As no interaction can occur between like functional groups, the only feasible reactions are propagation and termination. A schematic representation of this idea can be seen in **scheme 13**.
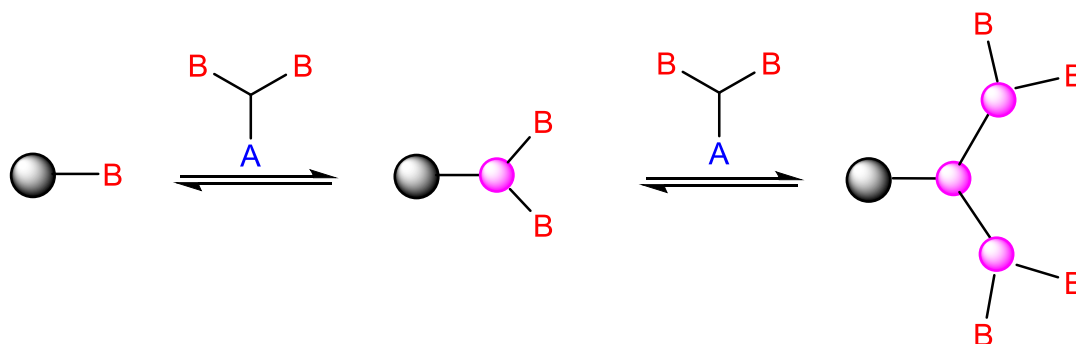


**Scheme 13** – Schematic representation of the interaction of a core unit and an $AB_2$ monomer unit.

For the organic soluble 3, 5-diacetoxybenzoic acid monomer and resulting polymer, an acetoxy group is imperative in the correct place, in order to propagate the polymer by coupling to the acid functional group present on the monomer.

As mentioned in the introductory section of this chapter, there has been a great deal of interest regarding anion receptors which possess an isophthalamide moiety (**figure 66**).

Receptors of this nature have been reported to be effective H bond donors; therefore, a decision was made to incorporate this functional group, due to past success.
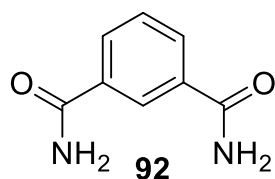


**Figure 66** – Figure to show the chemical structure of isophthalamide.

### 3.3.2 Synthesis of $N^1$, $N^3$-bis (4-hydroxyphenyl) isophthalamide

A di-functional, symmetrical, isophthalamide based receptor was designed. The receptor requires two acetoxy functional groups to propagate the polymer; the chemical structure for the desired final product can be seen in **figure 67**.
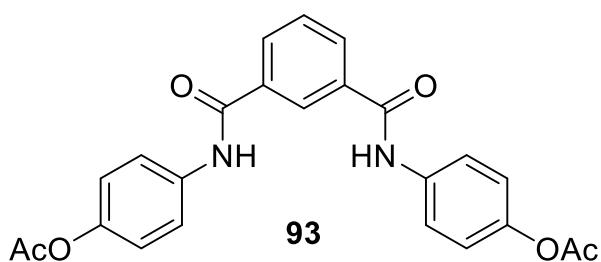


**Figure 67**– Chemical structure of N, N – bis (4-acetoxyphenyl) isophthalamide.

With the design in place the next step was to determine the synthetic route to attain said structure. From retrosynthetic analysis it was deduced that the simplest route to the desired product was the synthesis of N, N – bis (4-hydroxyphenyl) isophthalamide, followed by the acetylation of the terminal hydroxyl groups (**scheme 14**).
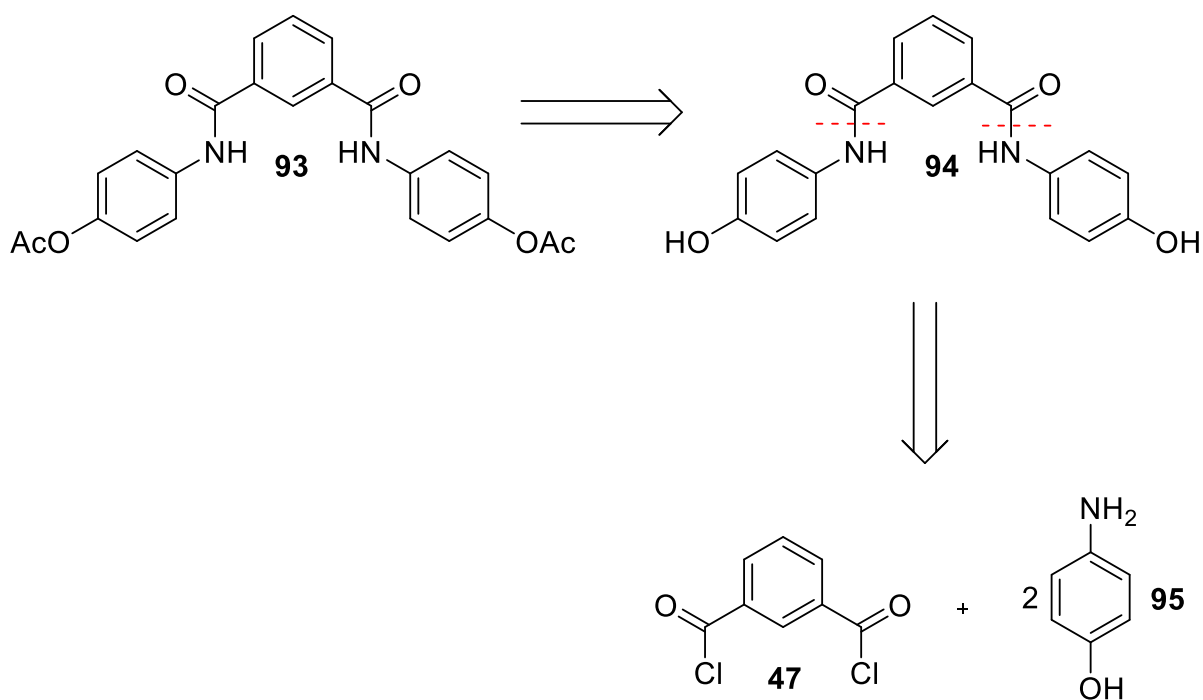
**Scheme 14** – Retrosynthetic analysis of N, N – bis (4-acetoxyphenyl) isophthalamide. The red dotted lines indicate the points of disconnection where bonds could be broken into the corresponding synthons.

As seen in **scheme 14**, the synthons used to generate the amide bond are an amine and an acid chloride. In the literature, a preparative method for a para substituted structure **96** (**figure 68**) similar to the designed receptor was reported.[83] Amide synthesis was achieved by acylation and the Schotten-Baumann reaction was employed. This type of acylation reaction involves the use of a base, which can drive the equilibrium to generate an amide.
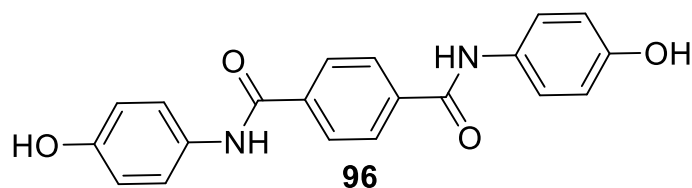


**Figure 68** – Figure to show the chemical structure of N1,N4-bis(4-hydroxyphenyl) terephthalamide.[83]

A reaction flask containing 4-aminophenol was degassed and triethylamine (distilled in the presence of a drying agent) and anhydrous 1-methyl-2-pyrrolidinone (NMP) were added via a syringe. The reaction mixture was heated to 60ºC and a solution of isophthaloyl chloride (in NMP) was added drop wise and stirring was continued for a period of 30 minutes. The

temperature was then raised to 80 °C and stirring was continued for an additional 20 minutes. The salt by-product, triethylammonium chloride, was removed by vacuum filtration and the reaction mixture was concentrated by rotary evaporation yielding the dark purple crude product. The next obstacle of the synthetic procedure was purification of the crude material and recrystalisation was the technique selected. However, after solubility investigations involving an array of different solvents, upon addition of methanol, the purple/brown solid became white in colour. It appeared that methanol was dissolving the impurities responsible for the apparent discoloration of the product. In order to determine the effect of addition of methanol, the white solid obtained was filtered, dried thoroughly and characterised using a variety of analytical tools. From analysis of the ^{1}HNMR both the integration and coupling are indicative of the signals expected, as shown in **figure 69**. The peaks corresponding to the OH protons and NH protons can also be visualised as two singlets, both with an integral of two protons at 10.20 ppm and 9.34 ppm respectively.
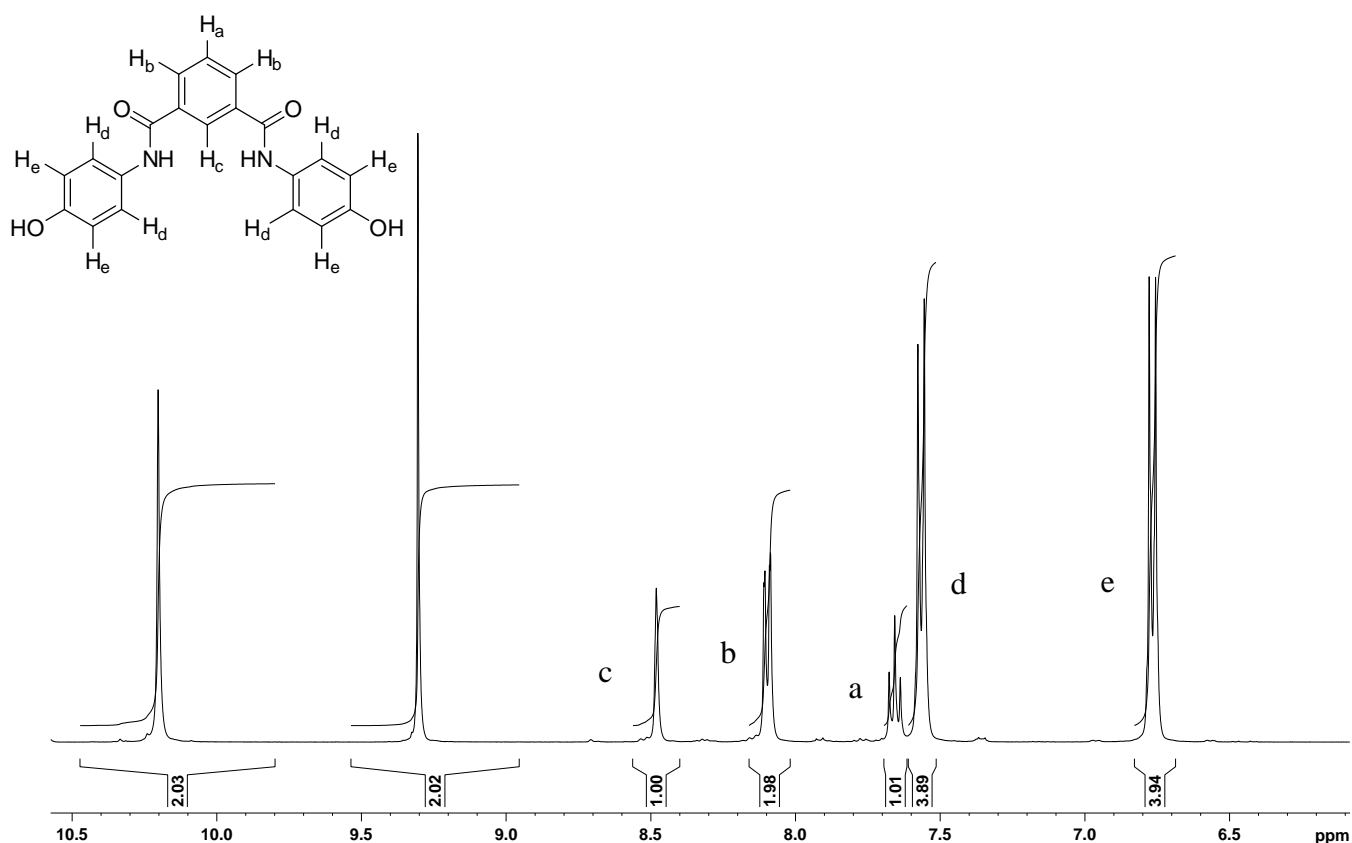


**Figure 69** – Figure to show the ^{1}HNMR spectrum for N, N-bis (4-acetoxyphenyl) isophthalamide.

124

The mass spectrum showed a signal at 349 which is indicative of the MH$^+$ ion peak. Infra-red spectroscopy and $^{13}$C NMR were also used to confirm the chemical structure of the product and ensure that synthesis and purification were successful.

### 3.3.3 Synthesis of N, N-bis (4-acetoxybenzaldehyde)

The next stage of the synthetic procedure is the acetylation of the hydroxyl terminal groups. An oven dried flask was charged with N, N – bis (4-hydroxyphenyl) isophthalamide and anhydrous pyridine before being degassed with a vacuum and argon gas. Acetyl chloride was added drop wise and the reaction mixture was left to stir at room temperature for a period of 4 hours. Pyridine was removed via rotary evaporation and the crude product was purified by column chromatography, eluted with ethyl acetate. Acetylation of a hydroxyl group is frequently carried out in the presence of an organic base. In this case, the organic base utilised is pyridine. Pyridine not only functions as the solvent in this reaction, but also has numerous other important roles in this reaction. The first of these is to neutralise acidic protons which are generated, ensuring that a high acid concentration does not develop. The second role is that of a nucleophilic catalyst, whereby it has direct involvement in the reaction.[85]

A variety of analytical tools were used to determine the success of the experimental procedure. From analysis of the proton NMR spectrum it was apparent that acetylation was successful as the –OH signal, present in the spectrum for N, N – bis (4-hydroxyphenyl) isophthalamide, was no longer present. A signal at 2.28 ppm could now be visualised, which is specific to the methyl protons of the acetate groups now present. The mass spectrum gave a signal at 433, indicative of the MH$^+$ ion. Furthermore, elemental analysis also showed results within 0.5% of the theoretical values expected. Infra-red spectroscopy and $^{13}$CNMR were tools also used in the determination of the chemical structure of N, N – bis (4-acetoxyphenyl) isophthalamide. The combination of all the analytical techniques used provides confidence in the purity of the final product, thereby meaning it was of sufficient quality for core incorporation within a hyperbranched polymer.

### 3.3.4 Polymerisation of 3, 5 diacetoxybenzoic acid

Initially, the polymerisation was executed in the absence of a core as a control reaction to use as a reference. The polymer was synthesised in a solution phase where diphenyl ether was the acting solvent. The reaction mixture was added to a round bottom flask which was fitted with

a one-piece distillation kit. Care was taken to ensure the reaction was carried out in the absence of air, meaning the reaction mixture needed to be repeatedly evacuated and flushed with nitrogen to ensure the maintenance of the appropriate reaction conditions. The reaction was executed using a two-stage procedure involving two different temperatures. Firstly, the reaction was heated to 225 °C for a period of 45 minutes, ensuring complete dissolution of the monomer. The temperature was then lowered to 180 °C and the system was placed under low vacuum for a period of 4 hours, so as to initiate equilibrium. This allowed removal of acetic acid by-product generated, thus steering the reaction to completion (**scheme 15**). After the vacuum was removed, the polymer was dissolved in hot THF and precipitated into cold methanol. The product was then isolated, washed with methanol and dried thoroughly prior to analysis.
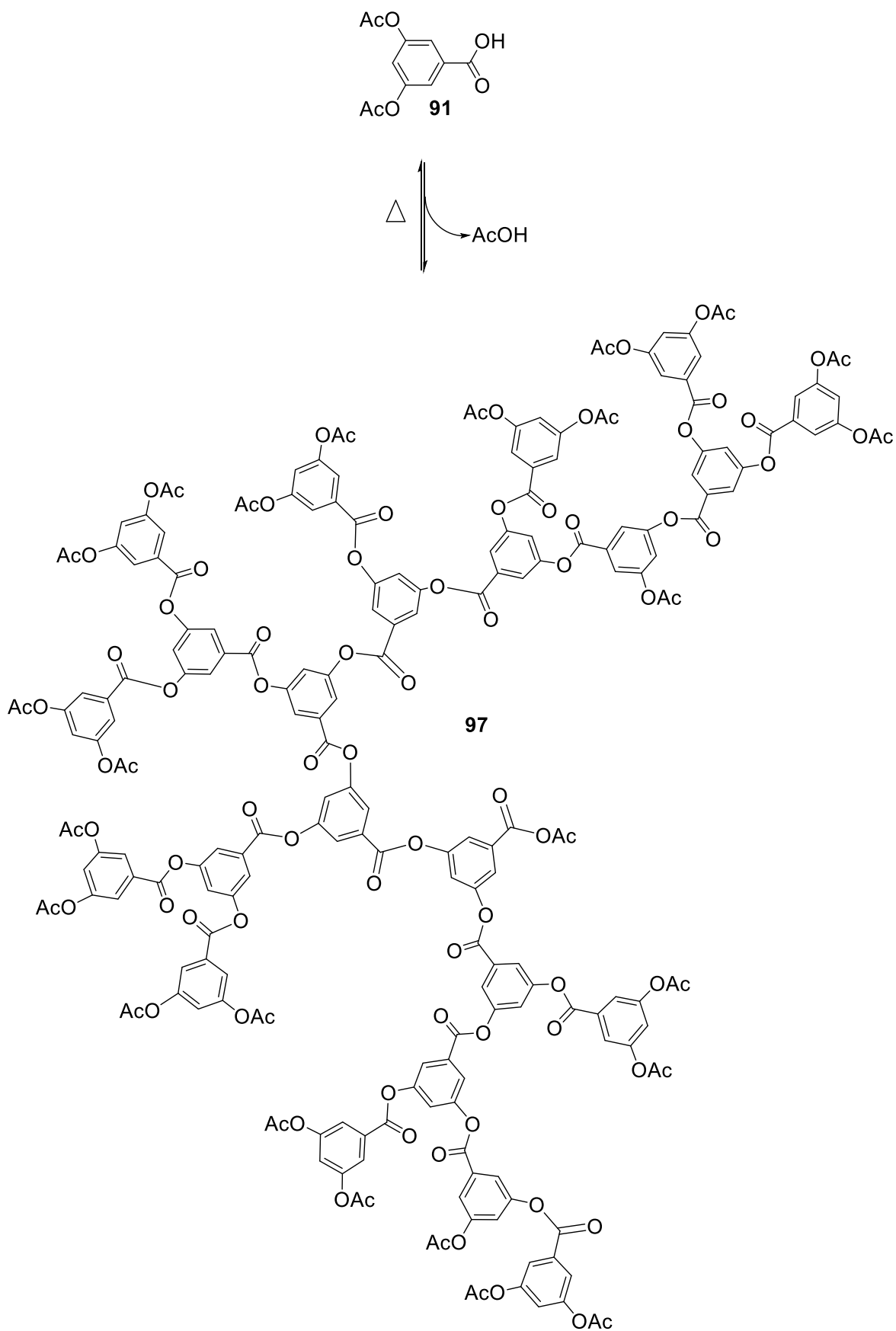
**Scheme 15** – Representation for the polymerisation of 3, 5 Diacetoxybenzoic acid.

Confirmation that the reaction had taken place was ascertained using ^{1}HNMR spectroscopy. It confirmed the absence of the carboxylic acid proton at 10.32 ppm, which was present in the spectrum for the monomer. Further confirmation can be seen in the diminution of the intensity of the peak at 2.32 ppm, corresponding to the methyl protons. With each propagation step of the polymerisation reaction, an acetoxy functional group is used up and, subsequently, two are added to the developing polymer. Therefore, as the polymer increases in size, the ratio of the terminal acetoxy groups to the level of internal groups decreases; this results in a decline in the integral size corresponding to the methyl protons.

### 3.3.5 Total core incorporation

As mentioned earlier, this monomer has received a great deal of attention within the group, therefore, the chemistry of polymerisation is well known. As discussed earlier, Twyman *et al.*[80] exploited this polymerisation and reported total core incorporation for a hyperbranched polymeric system. The polymerisation occurs through a reversible transesterification reaction mechanism, which is directed by thermodynamics. The reversible nature of the reaction ensures that core units will be evenly distributed and incorporated during the course of polymerisation. The polymerisation involved a one-step synthetic procedure with *p*-Nitrophenyl acetate as the core molecule. Provided that the core unit is more reactive than the monomer, the core will continually be involved. This will ensure that there will be an even distribution across the complete molecular weight range. Another advantage to a reversible polymerisation is the ability for the system to self-correct until equilibrium is attained, thus giving rise to a statistical distribution of core units.

### 3.3.5.1 Core incorporation of N, N – bis (4-acetoxyphenyl) isophthalamide

The synthesis was modified to include N, N – bis (4-acetoxyphenyl) isophthalamide as a core molecule. The core/monomer mixture (1:20 mole ratio) was heated with an equal weight of diphenyl ether and a method equivalent to that followed for unmodified poly 3, 5-diacetoxybenzoic acid was employed. After removal of the vacuum, the next step was the isolation and purification of the polymer. The product formed was a thick brown, glass-like solid which, unlike the unmodified polymer, was only partially soluble in THF. The slight amount which dissolved was precipitated in excess methanol, and the white solid which emerged was washed thoroughly with ice cold methanol and dried thoroughly prior to analysis. From the proton NMR spectrum, small broad signals could be observed at 8.52 and 8.89 ppm, which indicate core incorporation. However, the integrals of these values are

extremely low in comparison to the acetoxy proton signal, suggesting minimal core incorporation. Only a small amount of polymer was obtained, and subsequently used up in characterisation, therefore the procedure was repeated. When reattempting the synthetic procedure with this core molecule, the brown, glass-like solid produced was insoluble in refluxing THF. Poly 3, 5 diacetoxybenzoic acid is soluble in THF, regardless of what core has been incorporated; therefore, the insolubility of the polymer produced indicates another process is taking place, which differs from the process expected. It has been postulated that trans-etherification could be taking place, as opposed to desired trans-esterification mechanism. This could lead to cross linking, which could explain the difficulty in dissolution. However, how this occurs exactly still remains unknown to us. In order to confirm that this undesired effect is a result of the chemistry and not the chemist, it is important to verify that the method for core incorporation is viable and the monomer synthesised is suitable. In order to show this, a known successful reaction, which involves *p*-nitrophenyl acetate as a core unit, was attempted.

### 3.3.5.2 Polymerisation of 3, 5 diacetoxybenzoic acid with 4-Nitrophenyl acetate core

The synthesis was modified to include 4-nitrophenyl acetate as a core unit. The core/monomer mix (1:20 mole ratio) was heated with an equal weight of diphenyl ether using the same procedure mentioned prior. After the period under low vacuum was complete, the polymer was dissolved in refluxing THF and precipitated in excess methanol. There were no issues experienced with the dissolution of the product with use of this particular core unit. The polymer was washed repeatedly with ice cold methanol so that any trace amounts of unreacted 4-nitrophenyl acetate could be eradicated. The product was subsequently isolated by vacuum filtration. By using ^{1}HNMR, it was possible to verify the presence of the core molecule. A signal can be seen at 8.39 ppm, which is absent in unmodified poly 3, 5-diacetoxybenzoic acid (**figure 70**). This additional peak is indicative of the aromatic beta protons from the 4-nitrophenyl ester. To validate physical incorporation of the core within the polymeric structure, 4-nitrophenyl acetate was added to the NMR sample. A peak corresponding to free 4-nitrophenyl acetate was observed at a lower chemical shift of 8.31ppm, thus confirming core incorporation (**figure 70 c**)

a)



b)

Incorporated
4-Nitrophenol



c)

Free 4-
Nitrophenol

Incorporated
4-Nitrophenol



Incorporated
4-Nitrophenol
Incorporated
4-Nitrophenol
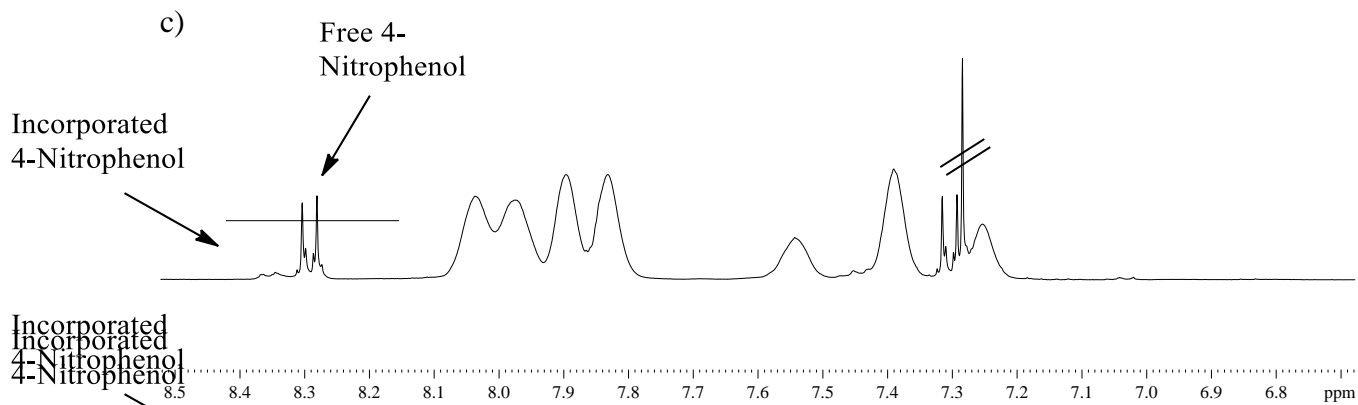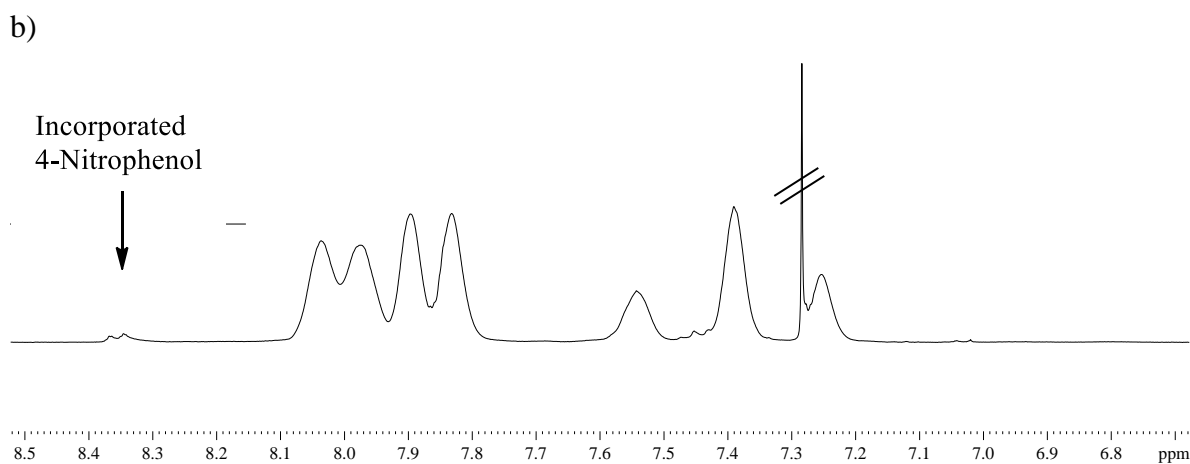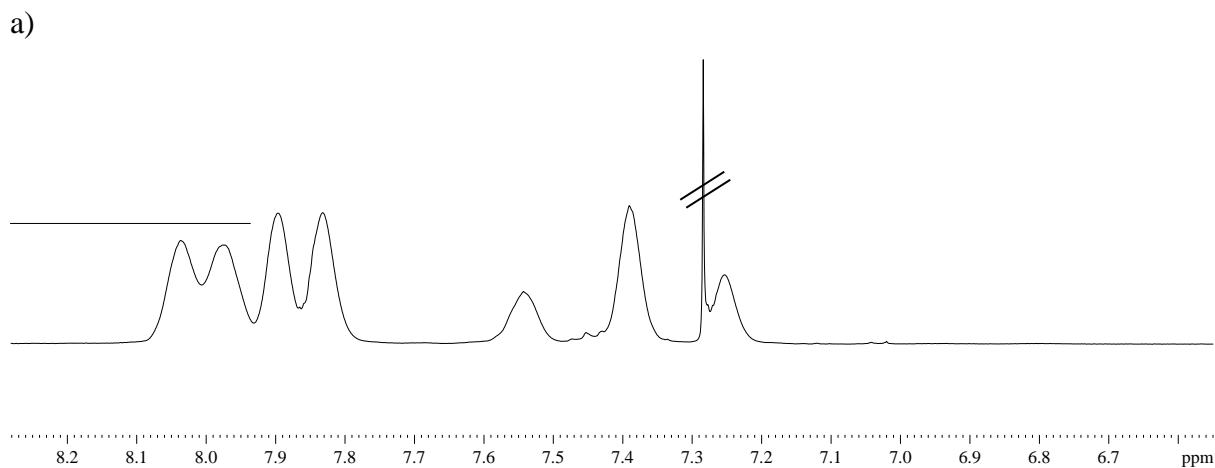
**Figure 70** – Figure to show the ^{1}HNMR spectrum of a) unmodified poly 3, 5 diacetoxybenzoic acid  b)  poly 3, 5 diacetoxybenzoic acid with 4-nitrophenyl acetate core and c) poly 3, 5 diacetoxybenzoic acid with 4-nitrophenyl acetate core that has been doped with 4-nitrophenyl acetate. The marked signals are representative of resolved chloroform in deuterated chloroform.

### 3.3.5.3 Purification of N, N – bis (4-acetoxyphenyl) isophthalamide

As core incorporation was successful with 4-nitrophenyl acetate, the synthetic procedure can be deemed suitable. Therefore, the cross linking must involve the core molecule alone. Although analytical data showed the core to be of high purity, it is important to acknowledge

130

that there could still potentially be slight impurities present, which are interfering with the reaction. It was therefore postulated that rigorous purification of N, N – bis (4-acetoxyphenyl) isophthalamide was the next course of action. The core underwent a hot filtration by dissolution in methanol and the brown solid turned grey in colour. The grey solid generated was dried meticulously prior to analysis. From examining the ^{1}HNMR, it was apparent that the core hydrolysed during the hot filtration process, generating isophthalic acid (**figure 71**). This would usually be difficult due to resonance effects.
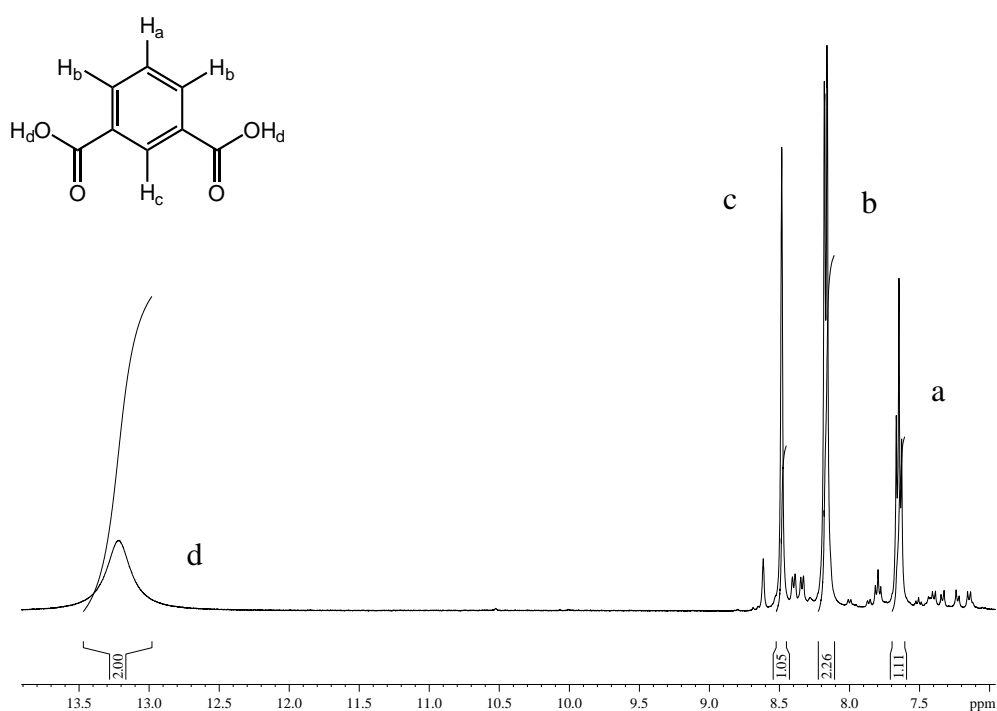


**Figure 71** – Figure to show the ^{1}HNMR spectrum for isophthalic acid.

The resonance of an amide bond usually proceeds by movement of the lone pair on the Nitrogen atom, thus generating a C-O⁻ moiety (**scheme a**). However, from analysis of the ^{1}HNMR spectrum, there appears to be an alternative resonance mechanism involved. It has been hypothesised that this involves the movement of the lone pair in the opposite direction to that predicted, thereby triggering the collapse of the molecule. In the predicted mechanism (**scheme 16 a**) the carbonyl carbon is not susceptible to nucleophilic attack. The mechanism proposed in **scheme 16 b** involves the role of the electron withdrawing acetate group para to the amide group, rendering the carbonyl carbon electrophilic. As a result, the carbonyl group is now susceptible to nucleophilic attack. As a result, the amide bond can now be broken, explaining the formation of isophthalic acid.

(a)
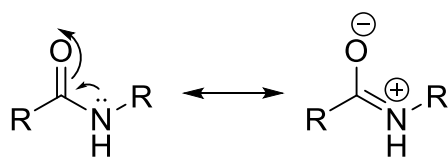


(b)
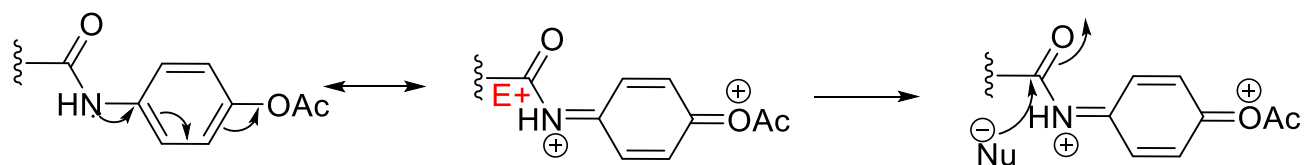


**Scheme 16** - Representation of the (a) resonance within an amide bond (b) resonance mechanism for the collapse of (isophthaloylbis (azanediyl) bis (4, 1-phenylene) diacetate to isophthalic acid.

Analysis from attempted purification demonstrates that the core is unstable to elevated temperatures, resulting in the formation of isophthalic acid. As the temperature required for polymerisation is considerably higher than the temperature reached during hot filtration, the core is evidently too unstable for covalent incorporation. The collapse of N, N – bis (4-acetoxyphenyl) isophthalamide to the di-acid therefore explains the cross-linking observed in the original attempt at core incorporation. The synthesis of poly 3, 5 diacetoxybenzoic acid with an N, N – bis (4-acetoxyphenyl) isophthalamide core can be visualised in **scheme 17**. Consequently, this specific receptor is incompatible for incorporation. The acetate group is located in the para position, leads to movement of electrons between the 1 and 4 positions. If the position of the acetate groups were changed to the meta position, this movement of electrons would no longer be possible. Restricting this movement could result in the generation of a receptor which could withstand the polymerisation conditions and potentially solve this problem. It was postulated to make this necessary change, thus fabricating N, N – bis (3-acetoxyphenyl) isophthalamide.
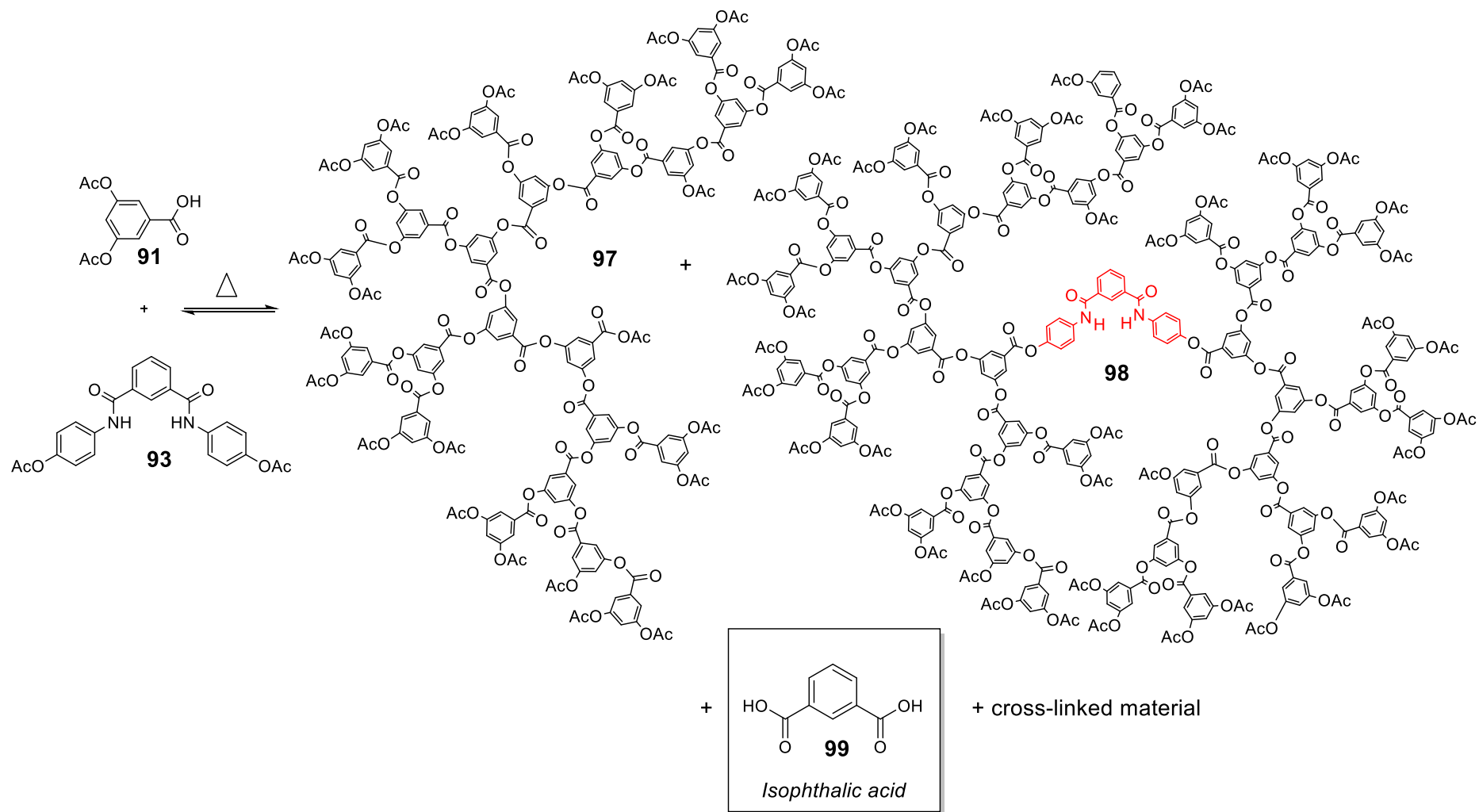
**Scheme 17** - Synthesis of poly 3, 5 diacetoxybenzoic acid with N, N – bis (4-acetoxyphenyl) isophthalamide core

133

### 3.3.6 Synthesis of N, N – bis (3-hydroxyphenyl) isophthalamide

The retrosynthetic analysis for N, N – bis (3-acetoxyphenyl) isophthalamide followed a similar route to that of N, N – bis – (4-acetoxyphenyl) isophthalamide, whereby the hydroxyl terminated receptor was synthesised first, followed by acetylation of the terminal hydroxyl groups (**scheme 18**).
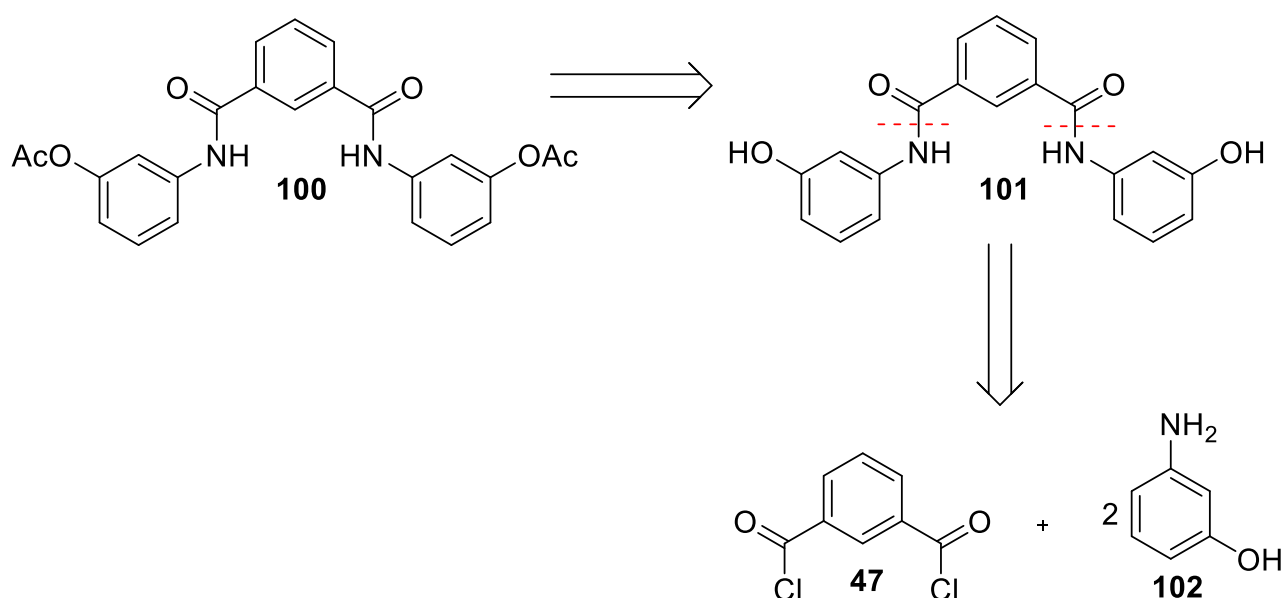


**Scheme 18**- Retrosynthetic analysis of N, N – bis (4-acetoxyphenyl) isophthalamide. The red dotted lines indicate the points of disconnection where bonds could be broken into the corresponding synthons.

A reaction flask was charged with 3-aminophenol and anhydrous N, N'-Dimethylacetamide and then degassed and flushed with argon. The reaction flask was subsequently cooled to 0ºC and then isophthaloyl chloride was added drop-wise by a syringe. The reaction flask was then stirred for a period of 6 hours and allowed to return to room temperature. After completion, the reaction mixture was then poured into 1L of ice cold distilled water and the white solid obtained was isolated by filtration. The crude product was purified by dissolution in refluxing ethanol followed by a hot filtration, the filtrate was then poured into excess distilled water and the precipitate was isolated by vacuum filtration. The experimental procedure was adapted from the literature[85], with the addition of an alternative purification process.

A variety of analytical tools were implemented to determine the chemical structure. From analysis of the ^{1}HNMR both the integration and coupling is representative of the signals

expected, as shown in **figure 72**. The peaks corresponding to the OH protons and NH protons can also be visualised as two singlets, both with an integral of two protons at 10.31ppm and 9.47ppm respectively.
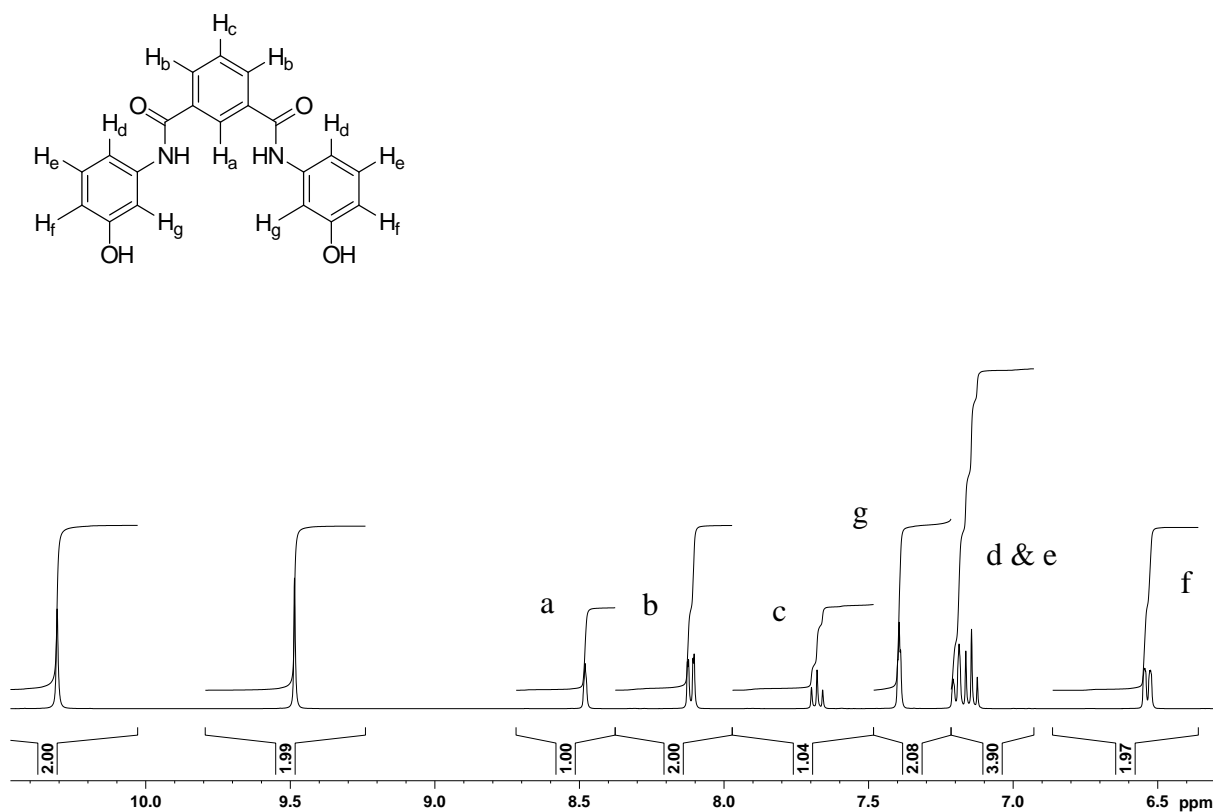


**Figure 72** – Figure to show the ^{1}HNMR spectrum for N, N – bis (3-hydroxyphenyl) isophthalamide.

Elemental analysis gave results within 0.5% of the theoretical values deduced and the mass spectrum showed a signal at 349, indicative of the $MH^+$ ion. X-ray crystallography (**appendix B**), ^{13}CNMR and Infra-red spectroscopy were also tools used. The combination of this array of analytical techniques demonstrated that the synthetic procedure and purification was a success. As a result, N, N – bis (3-hydroxyphenyl) isophthalamide obtained, was of sufficient purity to be carried forward to the next stage of synthesis.

### 3.3.7 Synthesis of N, N – bis (3-acetoxyphenyl) isophthalamide

The next stage of the synthetic procedure was to acetylate the hydroxyl terminal groups. A similar procedure to the acetylation of N, N – bis (4-hydroxyphenyl) isophthalamide was adopted. An oven dried flask was charged with N, N – bis (3-hydroxyphenyl) isophthalamide and anhydrous pyridine before being degassed with vacuum and argon gas. Acetyl chloride

was added drop wise and the reaction mixture was left to stir at room temperature for a period of 4 hours. After removal of pyridine via vacuum distillation, the crude product was dissolved in dichloromethane and washed with saturated sodium hydrogen carbonate solution and distilled water three times each to ensure any acid present is removed. The organic layer was collected and reduced down and dissolved in chloroform. The cream precipitate formed was filtered by gravity filtration and purified by recrystalisation. The crude material was dissolved in a minimum of hot dichloromethane and petroleum ether (40:60) was added drop wise until the solution remained cloudy. The crystals were isolated by gravity filtration after slow evaporation. From analysis of the proton NMR spectrum it was apparent that acetylation was successful as the –OH signal, present in the spectrum for N, N – bis (4-hydroxyphenyl) isophthalamide, was no longer present. A signal at 2.30 could now be visualised, which is specific to the methyl protons of the acetate groups now present. An accurate mass spectrum gave a signal at 433.1406, indicative of the MH$^+$ ion and also confirming the chemical formula. Furthermore, $^{13}$CNMR and Infra-red spectroscopy were also employed to provide additional analytical information, confirming the synthetic procedure was successful.

The crystals generated from recrystalisation were allowed to evaporate slowly so as to ensure adequate crystals for X-ray crystallography were obtained. As mentioned previously, cleft-like receptors are freely rotating in solution and not fixed in binding confirmation; a variety of different confirmations can thus be adopted (**figure 73**)[45], with only syn-syn allowing for binding.
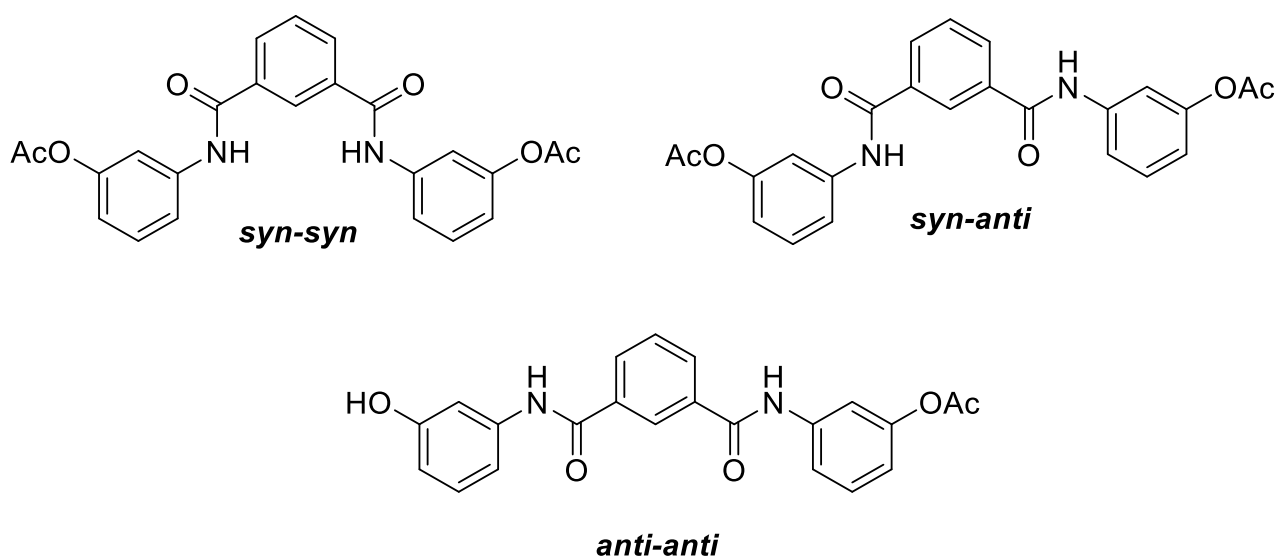


**Figure 73** – Figure to show the different conformations of N, N – bis (3-acetoxyphenyl) isophthalamide.[45]

When the crystals were analysed it was apparent that they crystallised in the binding confirmation. It is pleasing to note that the crystals obtained are in the correct conformation for coordination. However, in solution, there is rapid rotation about bonds in the absence of a guest resulting in equilibrium between numerous potential confirmations as seen in **figure 73**. The crystal structure obtained can be visualised in **figure 74**. In the work by Kavallieratos *et al.*[45] it has been demonstrated that, in the absence of an anionic guest, isophthalamide based receptors show syn-anti or anti-anti confirmations, as opposed to the syn-syn confirmation, which is optimal for anion interaction. The syn-syn confirmation is usually adopted when an anionic guest is introduced; the two linear hydrogen bonds formed drive this confirmation. It was therefore unexpected that X-ray crystallography showed crystals adopting the syn-syn confirmation.
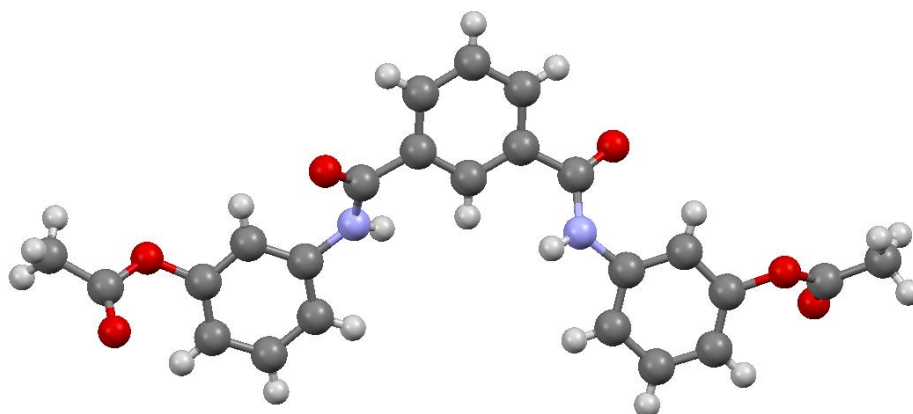
**Figure 74** – Figure to show the X-ray crystal structure of N, N – bis (4-hydroxyphenyl) isophthalamide.

## 3.4 Determination of the optimum molecular weight for anionic interaction

Previous work by Dr. Adam Ellis[86, 87] of the Twyman group† has involved the effect of molecular weight of a zinc porphyrin cored hyperbranched poly 3, 5 diacetoxybenzoic acid system upon interaction with a variety of pyridyl ligands (pyridine, 3, 5 – lutidine and 3-phenyl pyridine). The purpose of this work was to probe the concept of dense packing. The two main forces which direct an interaction can be categorised as electronic and steric effects. A core unit will possess a different electronic environment to that of the bulk solvent and can provide an optimum environment for a guest species. Steric effects also play a crucial role in binding. If there is a steric barrier present between the core unit and the ligand, binding will be hindered. In the work carried out by Dr Ellis, the HOMO-LUMO interaction is optimum

when the pyridyl ligand in question is coordinated perpendicular to the plane of the zinc porphyrin, thus permitting maximal orbital overlap. Therefore, if sterics play a part in the disturbance of optimal orbital overlap, then the association constant, $K_a$, would diminish. The predictions were that, as molecular weight increased, dense packing will undoubtedly occur. At the molecular weight that the onset of dense packing occurs, the ligand will no longer be able to access the core unit. As a result, there will be a large drop in the association constant observed. Results have shown that, as the size increases the value of $K_a$ also increases as a result of positive electronic effects provided by the polymeric structure. This increase occurred up to a point (~6000-8000 for each ligand), and for molecular weights beyond this value, there was a sharp decrease in the association constant. These results suggest that steric effects have overcome any positive electronic effects and the onset of dense packing occurs around this molecular weight, thwarting access of ligand to core. The graphical data for pyridine, showing this effect, is reported below in **figure 75**.
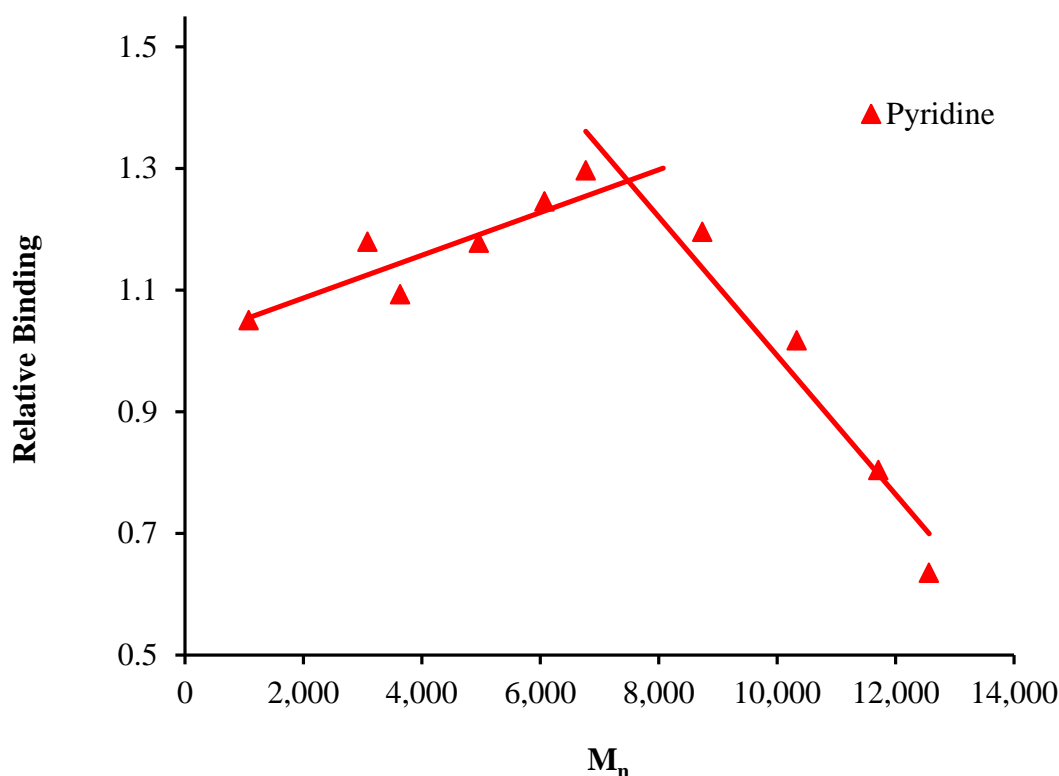


**Figure 75** – A graph to show the binding data for interaction of zinc porphyrin cored hyperbranched poly 3, 5-diacetoxybenzoic acid, of varying molecular weight, with a pyridine ligand.

†For previous work in the Twyman group regarding dense packing and dendritic systems, the reader is directed to the following literature.[88-90]

From analysis of the experimental data obtained for poly 3, 5 diacetoxybenzoic acid with a Nitrophenyl acetate core, using a 1:20 core to monomer ratio afforded a polymer of approximately 9000 molecular weight. Taking into account past studies, it was hypothesised that, this molecular weight would be beyond the point of dense packing; the core would be too sterically hindered from an anionic guest species. Therefore, a smaller core to monomer ratio will be employed to, hopefully, generate an anion receptor polymer of adequate size for optimal binding. An ideal size would range between 4000-5000 molecular weights to optimise electronic effects.

### 3.4.1 Polymerisation of 3, 5-diacetoxybenzoic acid with N, N'- Bis-(3-acetoxy-phenyl)-isophthalamide core using a 1:5 ratio

In the reaction flask, N, N'- Bis-(3-acetoxy-phenyl)-isophthalamide and monomer were introduced (1:5) along with diphenyl ether solvent. The general procedure for polymerisation of 3, 5 diacetoxybenzoic acid, as discussed in section **3.3.4**, was subsequently followed. Contradictory to N, N'- Bis-(4-acetoxy-phenyl)-isophthalamide, the crude mixture dissolved readily in refluxing THF. The polymer solution was then precipitated into excess ice cold methanol and left in a freezer overnight, so as to maximise precipitation. The product was then isolated, washed with methanol and dried thoroughly prior to analysis. The most crucial tool in determining whether core incorporation is successful is proton NMR spectroscopy. From analysis of the ^{1}HNMR spectrum (**figure 76**), broad signals from the core can be seen to both the right and left of the polymer signals. The broadness of the signals generated provides confidence that they represent incorporated core as opposed to free unreacted core. A broad multiplet can be seen at 8.55-8.67 ppm which is indicative of the NH signal which is the most deshielded. There is also a broad multiplet at 8.20-8.33 ppm. This signal arises from the two equivalent protons on the central aromatic ring and the proton (on the same ring) which does not neighbour another proton. There is a considerable amount of overlap between the polymer signals and remaining core signals due to the similarity in chemical shift and complicated coupling patterns formed. Therefore, direct assignment of these particular signals is extremely difficult. To the right of the dominant polymer signals, there is a broad multiplet at 6.72-6.90 ppm. This is representative of the protons para to the –CNH group, which are the most shielded core protons present.
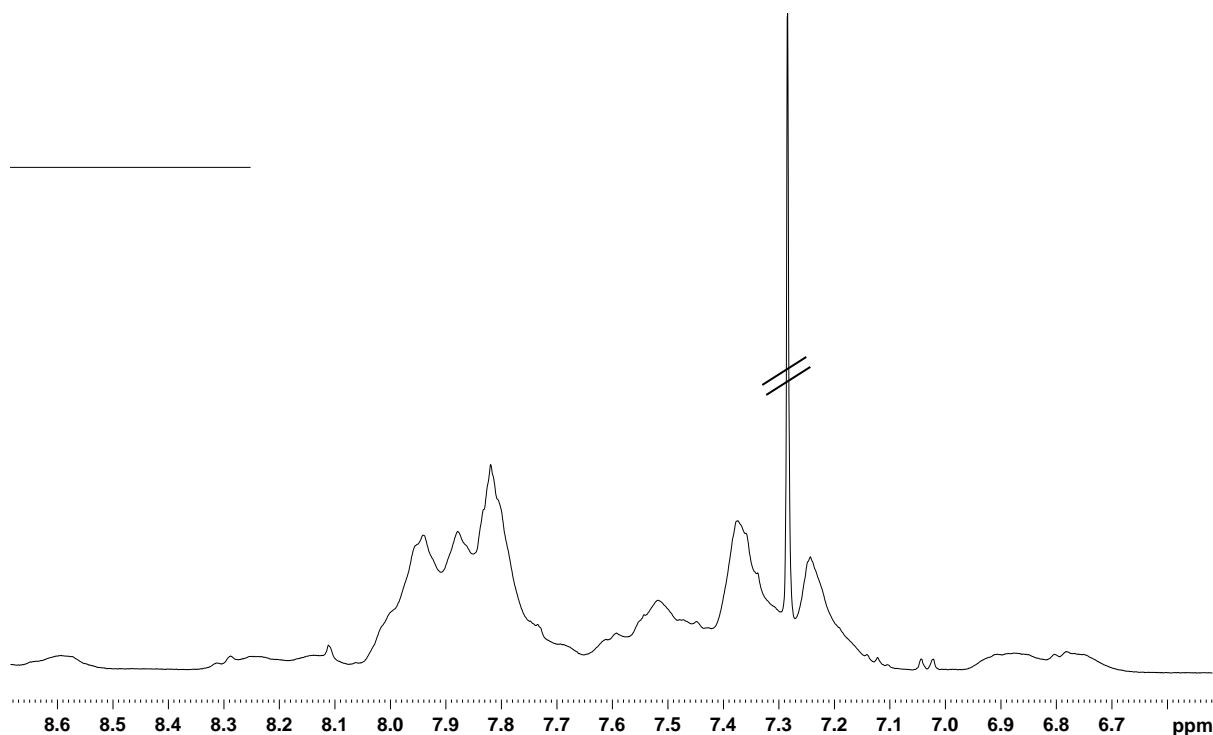
**Figure 76** – Figure to show the ^{1}HNMR expansion (6.5 ppm to 8.7 ppm) of poly 3, 5 diacetoxybenzoic acid with N, N'- Bis-(3-acetoxy-phenyl)-isophthalamide core (1:5). The marked signal is resolved chloroform in deuterated chloroform.

Two techniques are used in molecular weight determination, the first being GPC analysis. GPC illustrated a molecular weight of 4000. It is important to note that GPC provides an underestimation for the molecular weight of dendritic polymers as it is calibrated against linear polystyrene. This is a result of the branched architecture of a dendritic polymer; the nature of the structure means that they adopt a more compact arrangement in solution when compared with an equivalent linear polymer. The other technique used was [1]NMR estimation by analysis of the core signals. This is achieved through the comparison of the –NH core protons compared to the signal at 2.25 ppm (not shown) from the acetoxy terminal groups. The monomer, 3, 5-diacetoxybenzoic acid, is of type $AB_2$, meaning that the number of B functionalities (acetoxy) is equivalent to one less than the number of monomer units. Upon each addition of monomer, one B group is expended, but two are subsequently contributed. Molecular weight estimation from an HNMR spectrum is therefore an overestimation and presumes total core incorporation, not taking into account any polymeric impurities. The value obtained from proton NMR estimation was 4670; the discrepancy between the two techniques is slight, giving confidence that there is a high level of core incorporation. With a molecular weight of approximately 4000 molecular weight, it falls in the molecular weight region prior to dense packing, so it is an appropriate size to use for binding studies. The

proton spectrum can also be used to estimate the number of monomer units present, meaning an estimated structure can be devised. In the case of this particular ratio the number of monomer units was estimated as 20 (**figure 77**). IR analysis of the polymer also provided confidence in the reaction. Aromatic C-H stretches could be seen between 2009 and 2158 cm$^{-1}$, the ester carbonyl functionality gave a strong signal at 1741cm$^{-1}$ and a signal at 1286 cm$^{-1}$ was representative of an ester (OC (O) R) stretch.
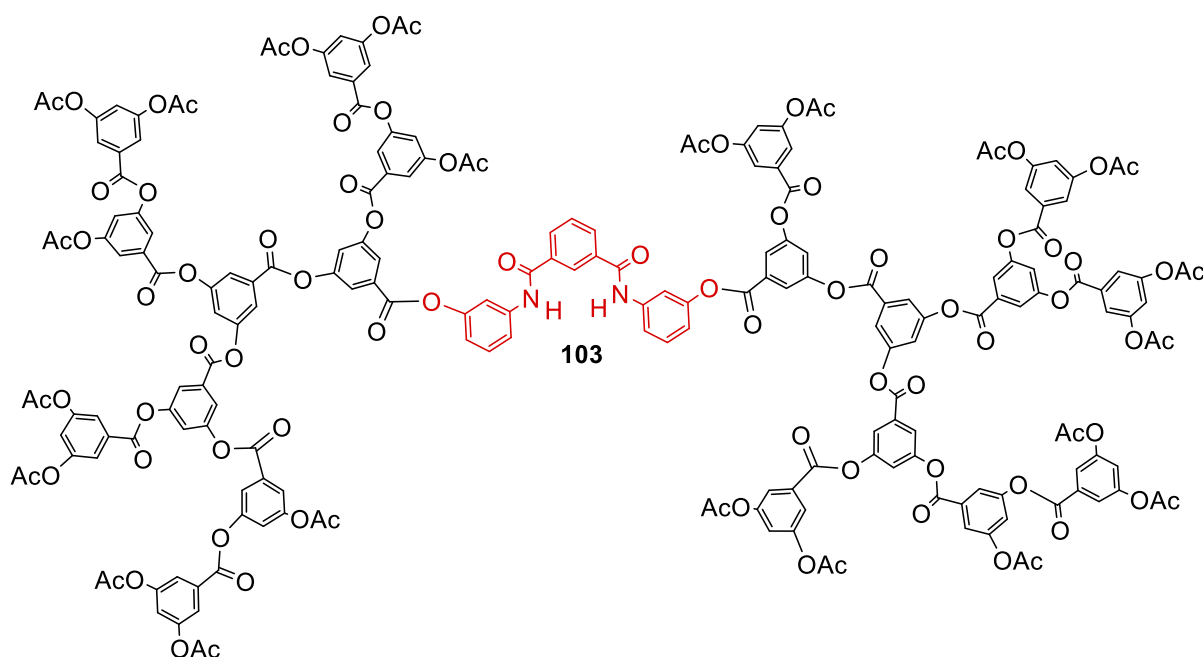


**Figure 77**– Figure to show the proposed chemical structure for poly 3, 5 diacetoxybenzoic acid with N, N'- Bis-(3-acetoxy-phenyl)-isophthalamide core (1:5).

## 3.4.2 Anion binding assay

With successful synthesis of an isophthalamide based anion receptor, and the subsequent effective incorporation of said core within a hyperbranched polymer, the next step was to analyse the binding efficacy of both. The majority of research in the area of anion receptor chemistry has utilised the technique of ^{1}HNMR titrations to analyse anion coordination to a hydrogen bond donor. Due to past success of this technique, it was the appropriate choice for analysis. As mentioned in the introductory section of this chapter, certain properties anions possess can hinder receptor design. Two important properties mentioned previously are the size and various geometric shapes that they can adopt. In the selection of anions to use for the binding assay, it was decided that a contrasting range would provide a more in-depth set of results. Benzoate, acetate and dihydrogen phosphate were selected as they are organic in

nature and possess geometric limitations, therefore, it will be interesting to see the effect of binding when access to the core is restricted by the polymer. The halides were also selected; unlike the previous anions stated, they are spherical in nature so the relative size of each should be a dominant factor in the efficacy of interaction to the host. As both the core and polymer are organic soluble, the NMR solvent required for the titration experiments is deuterated chloroform. The anions were therefore purchased from Sigma Aldrich as tetrabutylammonium salts.

### 3.4.2.1 ^{1}HNMR Titration analysis

Both N, N'- Bis-(3-acetoxy-phenyl)-isophthalamide and the core-functionalised hyperbranched polymer were each titrated against the various anionic guests. Each titration began with 0.7 mL of the host species at the correct concentration in deuterated chloroform in an NMR tube. The anionic guest, at the correct concentration in deuterated chloroform, was added in aliquots (10-25 µL) to the host. NMR scans (32) were run following each addition and the position of the NH chemical shift (ppm) was monitored (**figure 78**). Upon addition of anionic guest and the resultant coordination to the NH protons, a chemical shift downfield is observed. This shift downfield continues to the point at which the NMR solution becomes saturated with anionic guest, meaning to no further change in the chemical shift of the signal is observed.
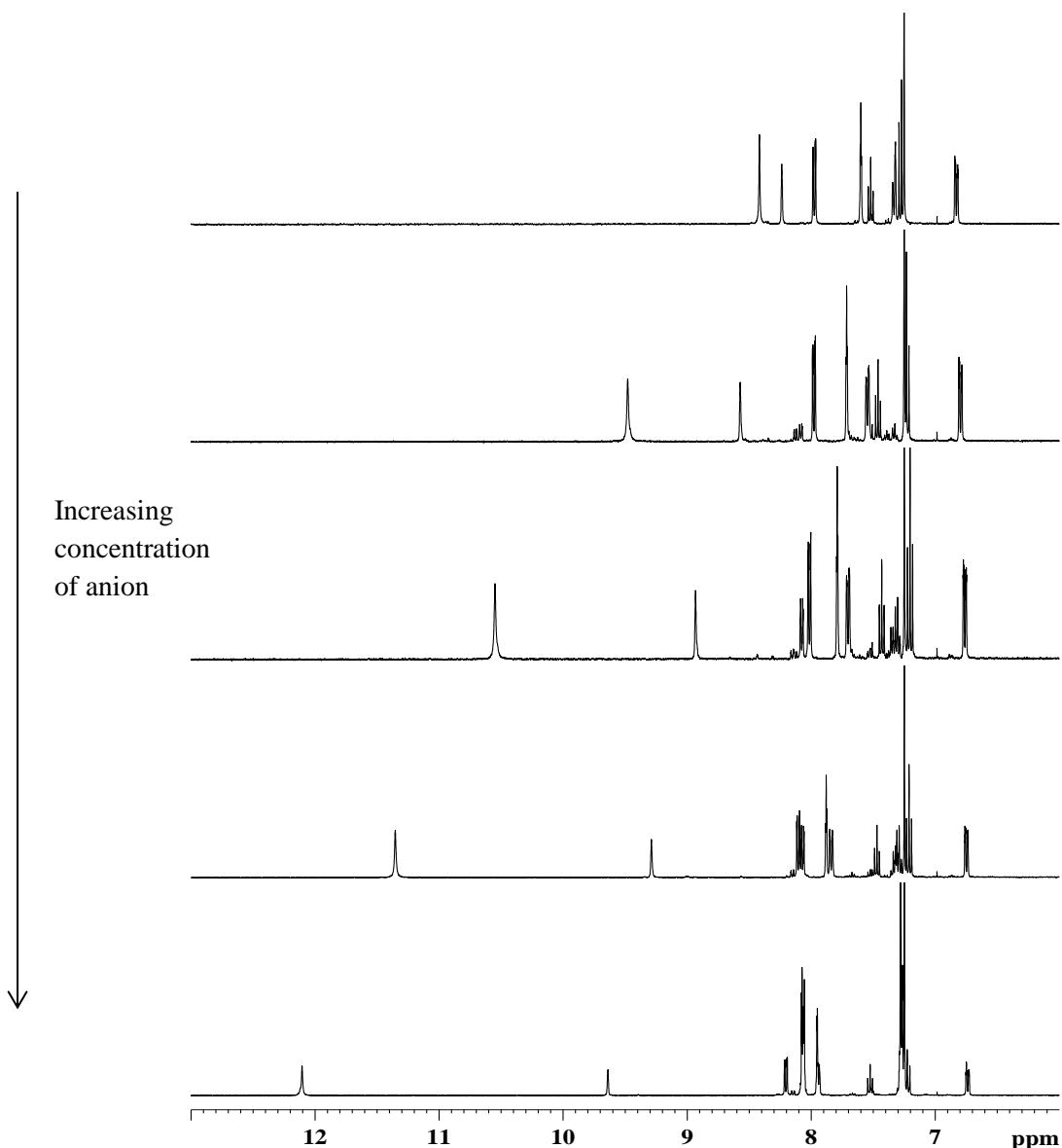
**Figure 78** – Figure to show ¹H NMR spectra depicting the change in NH resonances in compound **1** when titrated against tetrabutylammonium benzoate.

Solutions were made up fresh and used immediately after preparation. Topspin 2.6 software was used to process the spectra that was generated, and 14allMaster† was the software used to deduce the binding constant and obtain Job plots for each titration. Representative software images and the corresponding Job plot for the core receptor and tetrabutylammonium iodide can be seen in **figure 79** and **figure 80**. It is important to note that the binding software used is extremely sensitive to both the concentration of host and guest; therefore, numerous concentrations were tested in order to deduce an appropriate concentration of both species for the binding assay. This was complex as it involved striking a balance between minimal error of fit to the binding curve as well as an appropriate concentration for visualisation.
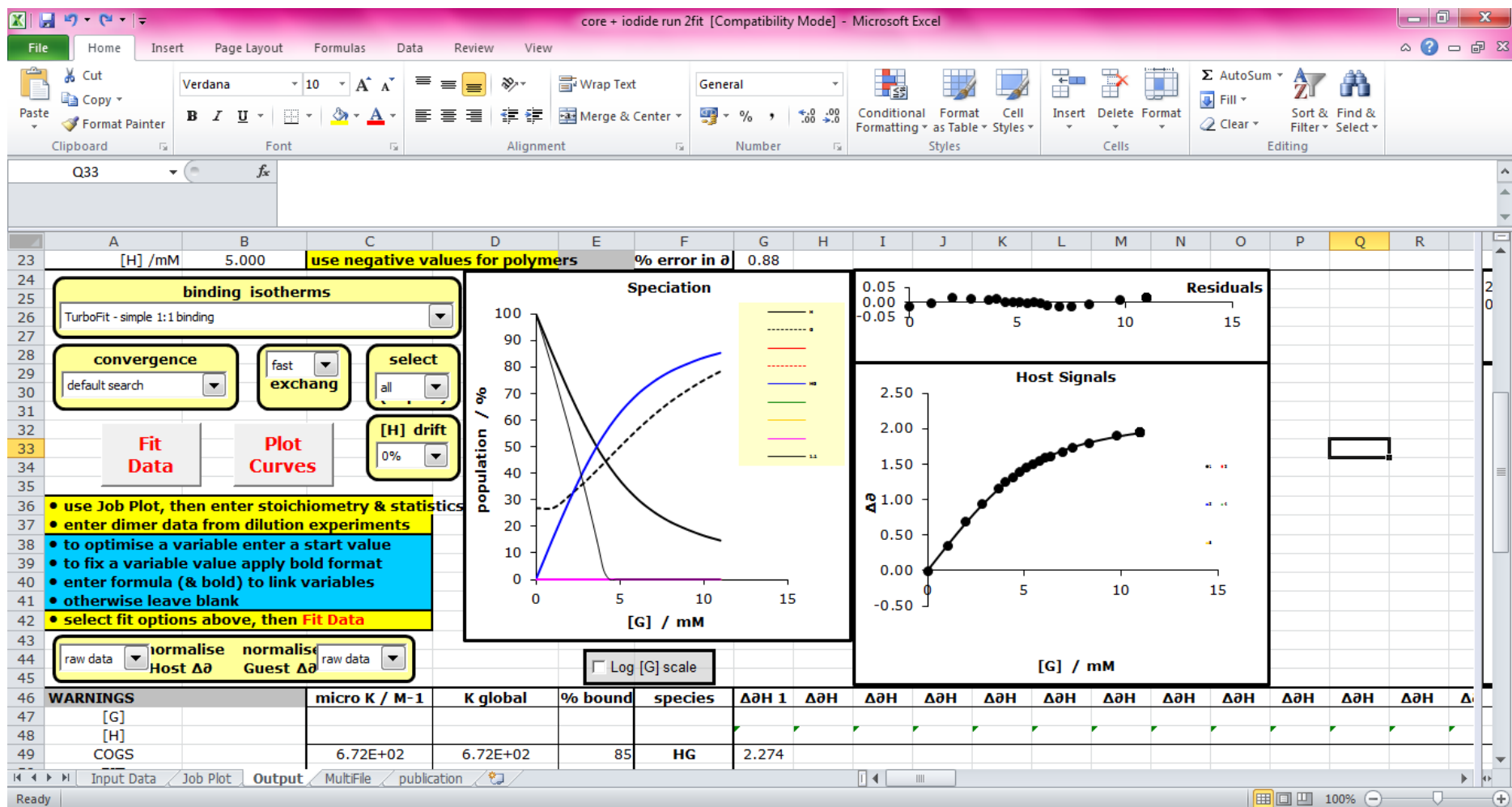
**Figure 79** – Figure to show the print screen of a 14allMaster NMR titration software output which illustrates the binding curve, association constant and associated error of fit for the anion core titrated against tetrabutylammonium iodide.
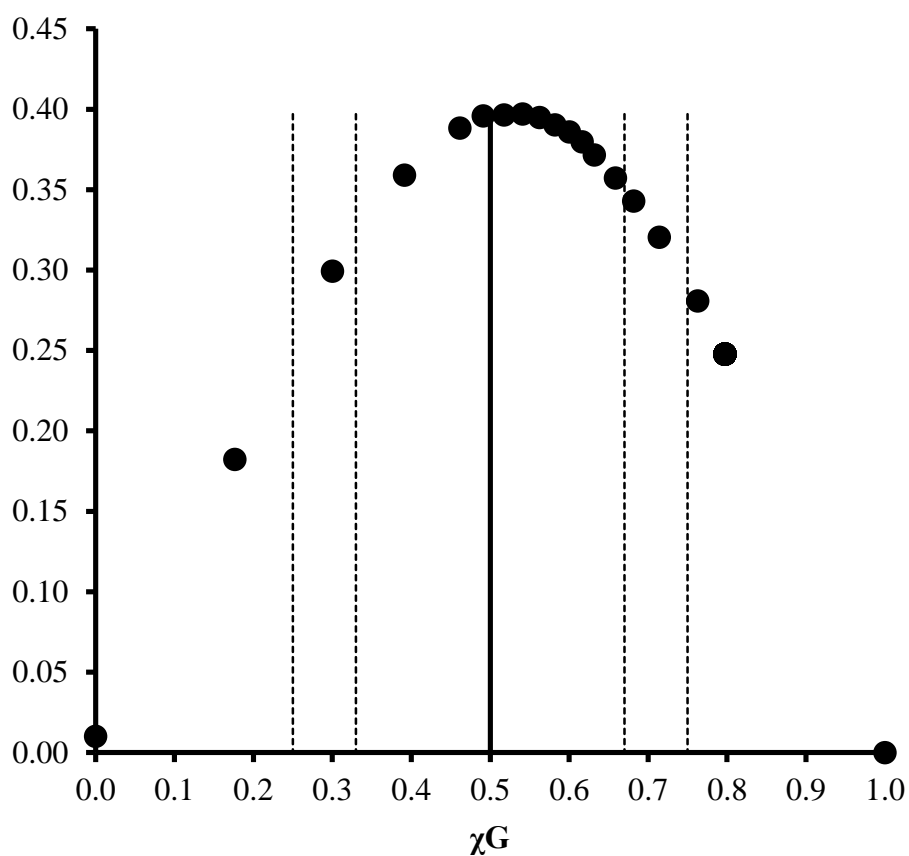
**Figure 80** – Figure to show the Job plot obtained from 14allMaster software for the anion core titrated against tetrabutylammonium.

From the Job plot shown in **figure 80**, it is apparent that binding is one to one; this binding motif was seen for both the core and polymer with each anionic guest. The binding constants obtained are tabulated overleaf in **table 1**.

146

|  | Core | 1:5 HBP ($M_n - 4000$) |
|---|---|---|
| $F^-$ | I) 9670 <br> II) 8130 <br> **8900 ± 1690** | I) 1800 <br> II) 1910 <br> **1855 ± 328** |
| $Cl^-$ | I) 66800 <br> II) 67100 <br> **66950 ± 20100** | I) 1783 <br> II) 1580 <br> **1682 ± 572** |
| $Br^-$ | I) 6250 <br> II) 5530 <br> **5890 ± 360** | I) 11000 <br> I) 9820 <br> **10410 ± 2600** |
| $I^-$ | I) 894 <br> II) 672 <br> **783 ± 111** | I) 3570 <br> II) 3740 <br> **3655 ± 391** |
| $C_6H_5CO_2^-$ | I) 6740 <br> II) 8620 <br> **7680 ± 940** | I) 7500 <br> II) 7240 <br> **7370 ± 884** |
| $CH_3CO_2^-$ | I) 4920 <br> II) 5530 <br> **5225 ± 605** | I) 6210 <br> II) 6550 <br> **6380 ± 702** |
| $H_2PO_4^-$ | I) 1120 <br> II) 1030 <br> **1075 ± 45** | I) 638 <br> II) 572 <br> **605 ± 33** |

**Table 1 –** Table to illustrate the binding constants and associated errors obtained for N, N'-Bis-(3-acetoxy-phenyl)-isophthalamide and the core-functionalised polymer (1:5). All data obtained from a 1:1 fit. All titrations were performed in deuterated chloroform at room temperature.

From initial analysis of the halides, it is evident that the polymer is having a negative effect upon interaction of chloride and fluoride whereas, for the larger, softer bromide and iodide ions, binding is significantly increased in the polymeric system. Dihydrogen phosphate displays weaker binding in the polymeric system, whereas, benzoate and acetate appear to show no significant change, meaning that, at this molecular weight, the steric effects and geometric restraints appear to not be having an adverse effect upon binding.

### 3.4.3 Effect of molecular weight upon anion binding

As mentioned previously in **3.4**, work within the group involved the examination of the effect of molecular weight upon binding affinities of pyridyl ligands with zinc porphyrin cored hyperbranched polymeric systems. The trend realised for each ligand was that as molecular weight increased, the binding constant increased due to positive electronic effects from the polymer system. This increase occurred up to a point in which there was a dramatic drop in association, this point was the threshold at which the onset of dense packing was realised and access to the core restricted. From comparison of binding to the anion receptor and to the hyperbranched polymeric system of 4000 molecular weight interesting results were obtained for the different anionic species. It appeared that the geometric constraints of the non-spherical anions were not problematic for a polymer this size. For the smaller halides, the polymer had an adverse effect upon binding, whereas, for the softer more diffuse bromide and iodide ions, the polymeric system was providing a better environment as a host. Therefore, the next stage of this project was to synthesise polymer systems, both higher and lower than 4000 molecular weight. The core to monomer ratio was altered to fabricate an oligormeric, open structure (1:1) and a larger polymeric system with a molecular weight higher than the point of onset of dense packing (1:20). This would provide insight into whether steric effects and geometric limitations play an important role in binding.

### 3.4.3.1 Polymerisation of 3, 5-diacetoxybenzoic acid with N, N'- Bis-(3-acetoxy-phenyl)-isophthalamide core using a 1:1 ratio to generate an oligormeric system

For the smaller system a molecular weight between 1000 and 2000 would be an ideal polymeric model for an expanded cleft structure. As a 1:5 core to monomer ratio gave a molecular weight of 4000, a 1:1 core to monomer ratio was attempted. In the reaction flask, N, N'- Bis-(3-acetoxy-phenyl)-isophthalamide and monomer were introduced (1:1) along with diphenyl ether solvent. The general procedure for polymerisation of 3, 5 diacetoxybenzoic acid, as detailed in section **3.3.4**, was consequently followed. As identified

beforehand, ^{1}HNMR is critical in the confirmation that the core has been covalently introduced. The ^{1}HNMR spectrum can be seen below in **figure 81**.
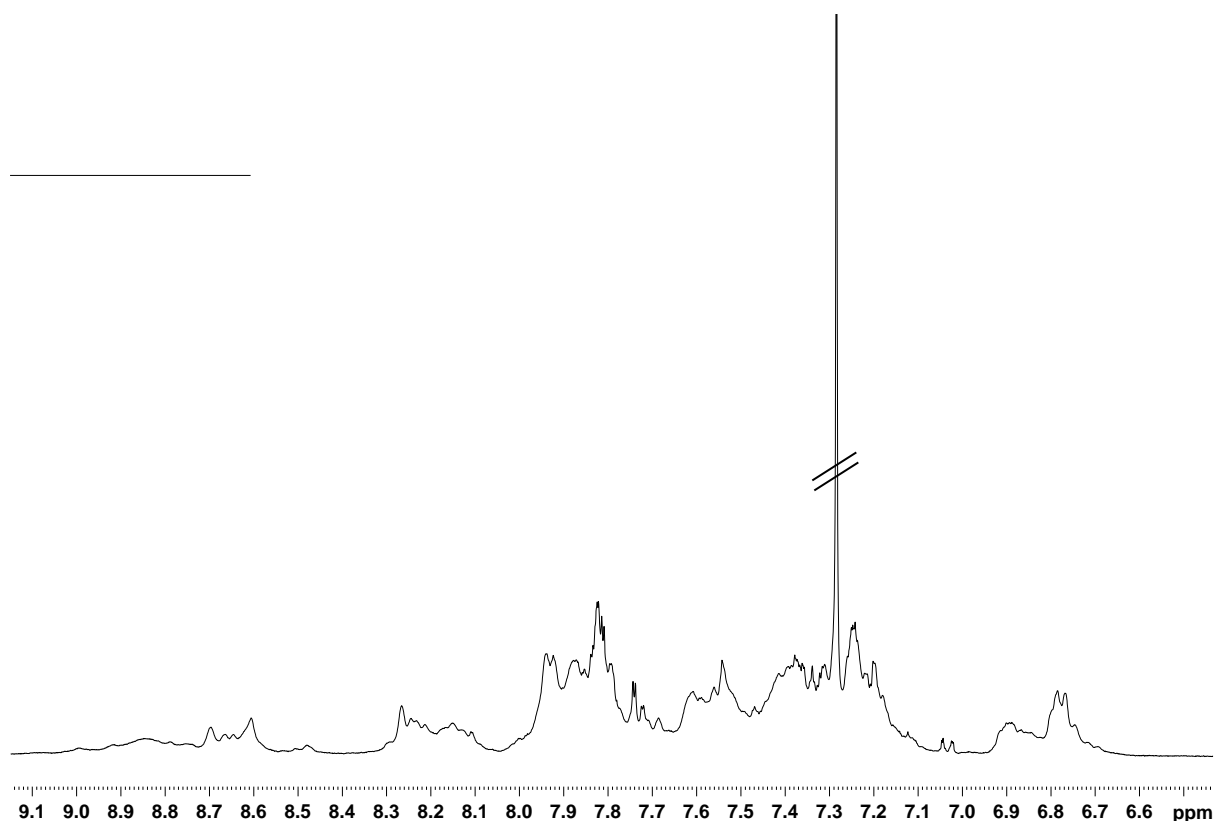


**Figure 81** – Figure to show the ^{1}HNMR expansion (6.4 ppm to 9.1 ppm) of poly 3, 5 diacetoxybenzoic acid with N, N'- Bis-(3-acetoxy-phenyl)-isophthalamide core (1:1). The marked signal is resolved chloroform in deuterated chloroform.

When the core to monomer ratio is reduced, the polymer peaks are not as dominant, resulting in a spectrum with more signal overlap in comparison to higher ratios. As a result of this, spectral assignment becomes problematic. A broad multiplet can be seen from 8.57 to 8.74 ppm which houses the NH protons. Infra-red also provided product validation by verifying functional groups present. GPC analysis gave a molecular weight of 1554 and the value obtained from NMR was 2034. The small margin between both estimations provides confidence in a high level of core incorporation. From the NMR spectrum it was calculated that approximately 7 monomer units surround a core unit. The estimated chemical structure is displayed in **figure 82**.
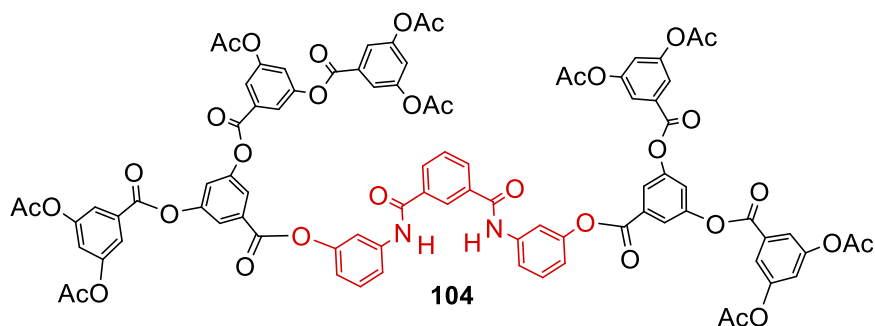
**Figure 82** – Figure to show the chemical structure of poly 3, 5 diacetoxybenzoic acid with N, N'- Bis-(3-acetoxy-phenyl)-isophthalamide core (1:1).

### 3.4.3.2 Polymerisation of 3, 5-diacetoxybenzoic acid with N, N'- Bis-(3-acetoxy-phenyl)-isophthalamide core using a 1:20 ratio to generate a large polymeric system

The general procedure for polymerisation was employed with the alteration to the monomer mass. For higher amounts of monomer, the polymer signals become more dominant, thereby reducing the sharpness of core signals observed. The $^1$HNMR spectrum (figure 83) gives a broad multiplet from 8.57 to 8.67 ppm, which is representative of the NH protons from the receptor incorporated. As is apparent from the spectra, the polymer signals predominate and, as a result, the core signals become thwarted. With a higher core to monomer ratio, concentration determination for titration analysis was crucial as the core signals are weaker and harder to distinguish; therefore, too low a concentration would lead to a high inaccuracy in spectral interpretation.
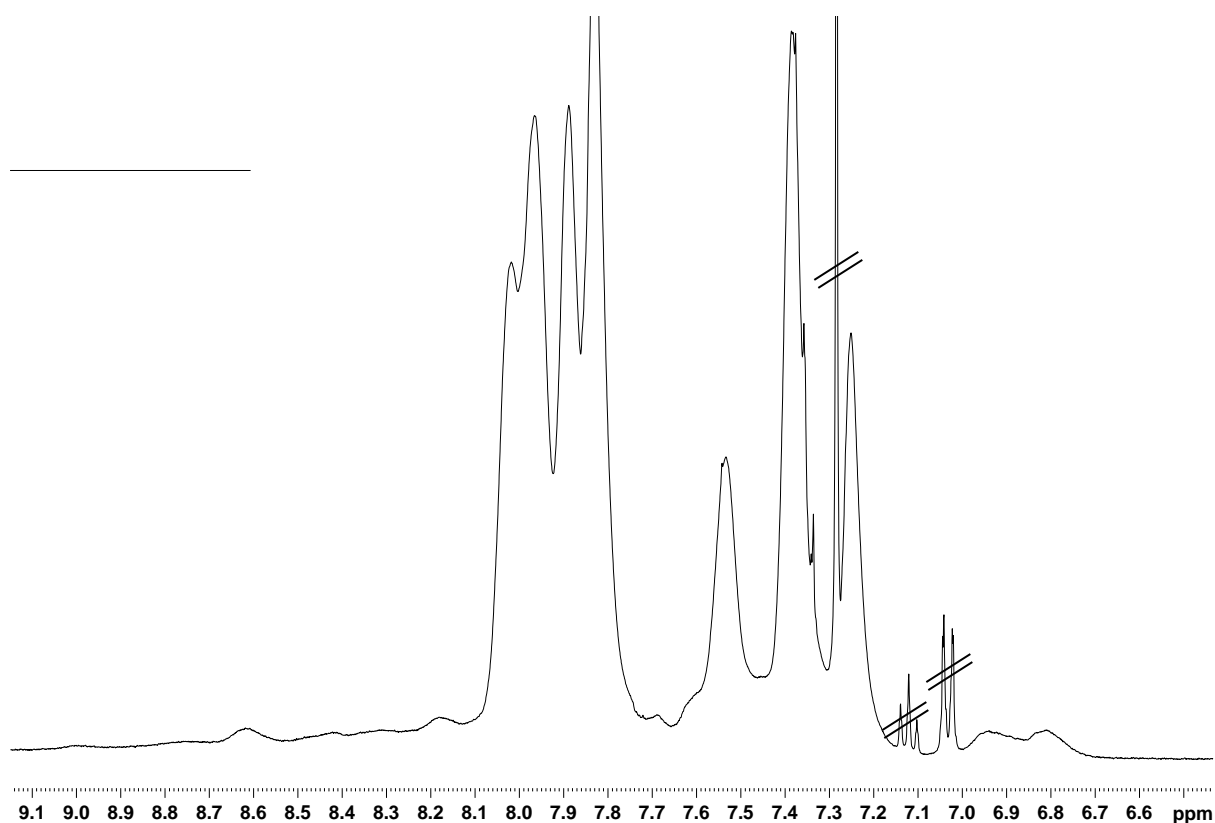
**Figure 83** - Figure to show the ^{1}HNMR analysis of poly 3, 5 diacetoxybenzoic acid with N, N'- Bis-(3-acetoxy-phenyl)-isophthalamide core (1:20). The marked signals are due to presence of resolved chloroform and residual diphenyl ether solvent in deuterated chloroform.

GPC analysis gave a molecular weight value of 10, 500 and NMR gave a value of 12, 229. The discrepancy between estimations is higher in this case than for polymers with a lower core to monomer ratio. In spite of this, the margin between the values is still relatively small, meaning that the core incorporation is relatively high. From the proton NMR spectrum it was estimated that there were approximately 40 monomer units surrounding the anion receptor, generating a more globular polymeric system (**figure 84**).
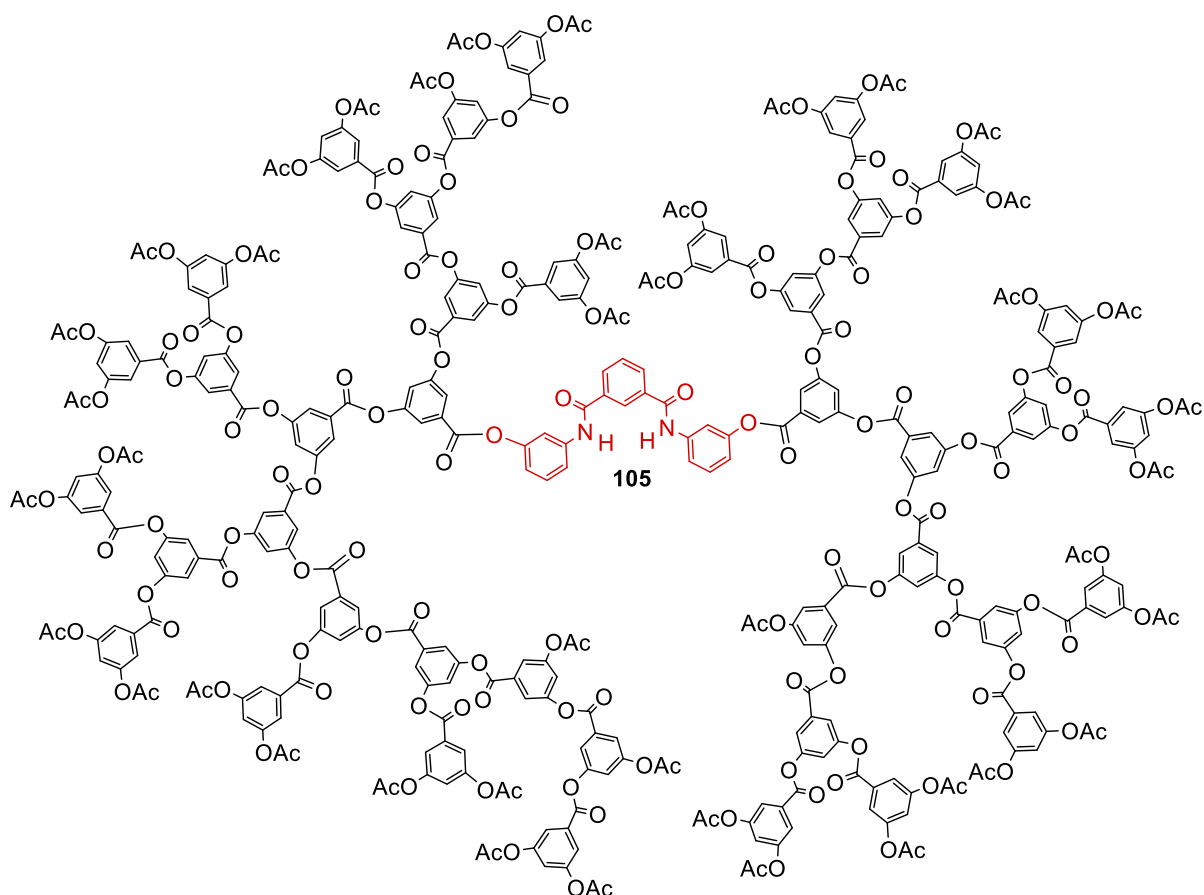
**Figure 84** – Figure to show the estimated chemical structure for of poly 3, 5 diacetoxybenzoic acid with N, N'- Bis-(3-acetoxy-phenyl)-isophthalamide core (1:20).

### 3.4.3.3 Effect of molecular weight upon interaction

With the fabrication of three polymers of contrasting molecular weights, the next stage was the investigation into binding of an oligormeric polymer system and a globular polymer system, where access to the core is more restricted. After deduction of appropriate concentrations, the procedure for analysis by NMR titrations, mentioned in **3.2.4.1**, was employed. The binding constants for the core and each polymeric system are tabulated overleaf in **table 2**. The data has also been normalised with respect to the core so as to focus solely on the effect of polymer size. The normalised data is also tabulated overleaf in **table 3** and also illustrated in a column chart in **figure 85.**

| | Core | 1:1 HBP ($M_n$ – 1600) | 1:5 HBP ($M_n$ – 4000) | 1:20 HBP ($M_n$ – 10500) |
|---|---|---|---|---|
| $F^-$ | I) 9670<br>II) 8130<br>**8900 ± 1690** | I) 1930<br>II) 2060<br>**1995 ± 379** | I) 1800<br>II) 1910<br>**1855 ± 328** | I) 2460<br>II) 2040<br>**2250 ± 210** |
| $Cl^-$ | I) 66800<br>II) 67100<br>**66950 ± 20100** | I) 1460<br>II) 1510<br>**1485 ± 178** | I) 1783<br>II) 1580<br>**1682 ± 572** | I) 1180<br>I) 1180<br>**1180 ± 212** |
| $Br^-$ | I) 6250<br>II) 5530<br>**5890 ± 360** | I) 12300<br>I) 13700<br>**13000 ± 1200** | I) 11000<br>I) 9820<br>**10410 ± 2600** | I) 10300<br>II) 11200<br>**10750 ± 1720** |
| $I^-$ | I) 894<br>II) 672<br>**783 ± 111** | I) 1220<br>II) 1030<br>**1125 ± 95** | I) 3570<br>II) 3740<br>**3655 ± 391** | I) 1410<br>II) 1290<br>III) 1340<br>**1347 ± 63** |
| $C_6H_5CO_2^-$ | I) 6740<br>II) 8620<br>**7680 ± 940** | I) 8690<br>II) 9440<br>**9065 ± 688** | I) 7500<br>II) 7240<br>**7370 ± 884** | I) 547<br>II) 464<br>**505 ± 41.5** |
| $CH_3CO_2^-$ | I) 4920<br>II) 5530<br>**5225 ± 605** | I) 5040<br>II) 5590<br>**5315±275** | I) 6210<br>II) 6550<br>**6380 ± 702** | I) 224<br>II) 241<br>**232.5 ± 8.5** |
| $H_2PO_4^-$ | I) 1120<br>II) 1030<br>**1075 ± 45** | I) 633<br>II) 616<br>**625 ± 21** | I) 638<br>II) 572<br>**605 ± 33** | I) 81.7<br>II) 82.8<br>**82.25 ±7** |

**Table 2** – Table of binding constants and relative errors associated with the binding fit for the anion binding core, N, N'- Bis-(3-acetoxy-phenyl)-isophthalamide, and core functionalised hyperbranched polymers of varying molecular weights when titrated against a range of anionic guests. All titrations were performed in deuterated chloroform at room temperature.

|  | Core | 1:1 HBP ($M_n$ – 1600) | 1:5 HBP ($M_n$ – 4000) | 1:20 HBP ($M_n$ – 10500) |
|---|---|---|---|---|
| $F^-$ | 100 | 22.4 ($\pm$4.3) | 18.6 ($\pm$3.3) | 25.3 ($\pm$2.4) |
| $Cl^-$ | 100 | 2.2 ($\pm$0.3) | 2.5 ($\pm$0.8) | 1.8 ($\pm$0.3) |
| $Br^-$ | 100 | 220.7 ($\pm$20.0) | 176.7 ($\pm$44.2) | 182.5 ($\pm$29.2) |
| $I^-$ | 100 | 143.7 ($\pm$12.1) | 466.8 ($\pm$49.9) | 172.0 ($\pm$8.1) |
| $C_6H_5CO_2^-$ | 100 | 118.0 ($\pm$10.6) | 96.0 ($\pm$11.5) | 6.6 ($\pm$0.6) |
| $CH_3CO_2^-$ | 100 | 101.7 ($\pm$5.3) | 122.1 ($\pm$13.4) | 4.4 ($\pm$0.2) |
| $H_2PO_4^-$ | 100 | 58.1 ($\pm$2.0) | 56.3 ($\pm$3.1) | 7.7 ($\pm$0.6) |

**Table 3** – Table to show the relative binding affinities for anions to each polymer. (Relative to the core which was normalised to 100%).

(a)



(b)
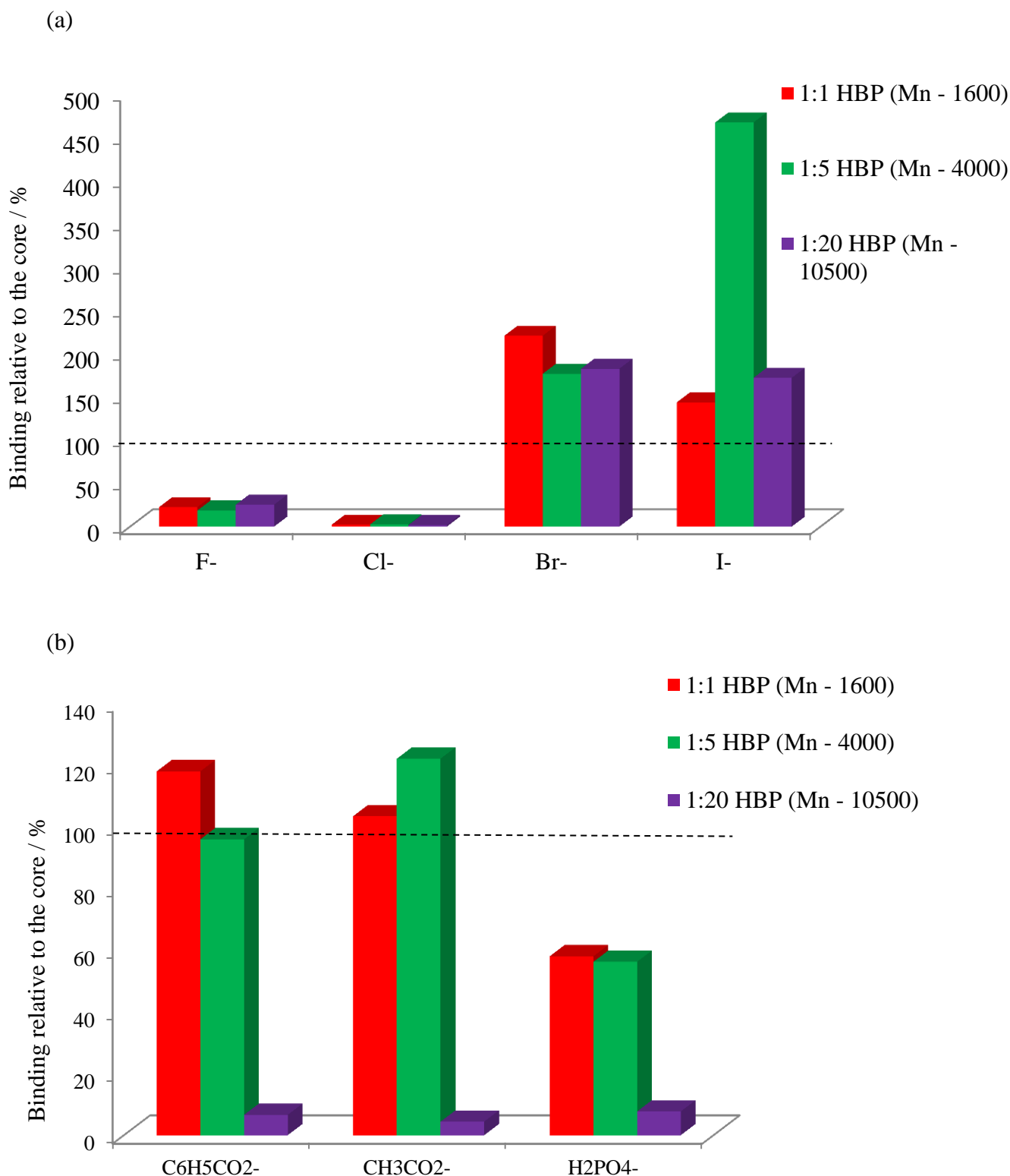


**Figure 85** – A column chart to show the binding effects for (a) halides to each polymer relative to the core (normalised to 100%) and (b) benzoate, acetate and dihydrogen phosphate to each polymer relative to the core (normalised to 100%). The dashed lines are representative of the core data; below the line indicates a negative effect upon binding and above the line indicates a positive effect upon binding. Individual column charts with error bars for each hyperbranched polymer system can be found in **appendix D**.

From analysis of the data concerning the non-spherical anions, similar trends are observed as seen with the zinc porphyrin cored system. Past the point of onset of dense packing, the added steric barrier results in a dramatic drop in association constant for the 1:20 hyperbranched polymer system. With the organic ions there is also the added obstacle of geometry. With restricted access to the core, the added complication of geometric restraints could therefore account for the poor association constants calculated with this monomer to core ratio. With acetate and benzoate, binding appears to be as effective in the 1:1 and 1:5 polymer when compared to association to the native receptor, whereas interaction of dihydrogen phosphate, strongest binding is observed for the core. From analysis of the data for the halide ions, a noticeable result is seen for iodide in the 1:5 hyperbranched polymer system. The polymer of 4000 molecular weight showed considerably stronger binding compared to the free core and other polymer systems. The result appeared irregular but, after several repetitions, the observation was confirmed. For bromide, the oligormeric polymer provided a more optimum environment compared to larger polymers. Nevertheless, it is still evident that bromide is more strongly bound when the receptor is covalently incorporated within poly 3, 5 diacetoxybenzoic acid as opposed to its native state. A different scenario is observed for the smaller halide anions. By covalent incorporation of the receptor, there is depletion in the association constants, effectively meaning both ions are deselected. In order to facilitate observation of these trends and see the effect of molecular weight upon each anionic guest individually, line graphs have been created for each anion and are found overleaf (**figure 86 to 92**).
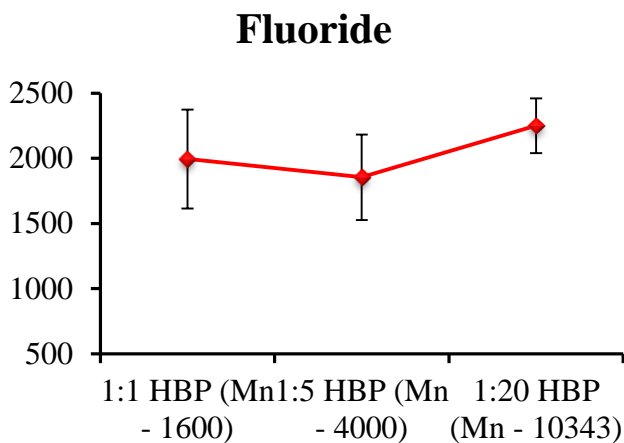
**Figure 86** – A Line graph to show the effect of molecular weight upon interaction with tetrabutylammonium fluoride.
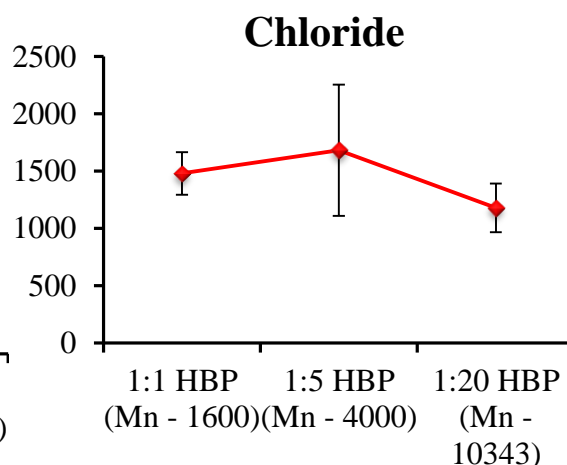


**Figure 87** – A Line graph to show the effect of molecular weight upon interaction with tetrabutylammonium chloride.
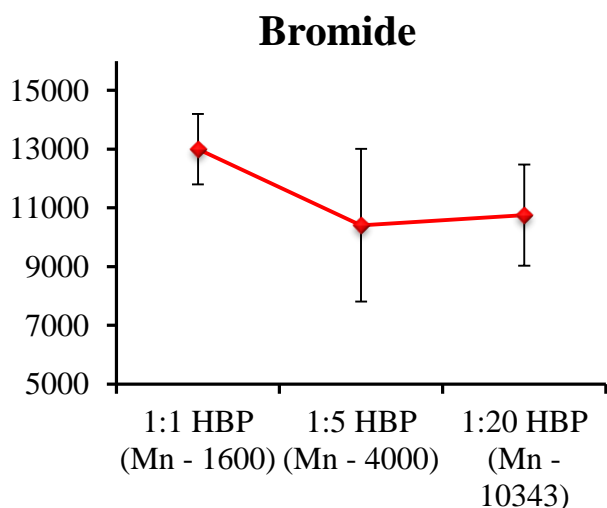


**Figure 89** – A Line graph to show the effect of molecular weight upon interaction with tetrabutylammonium bromide.
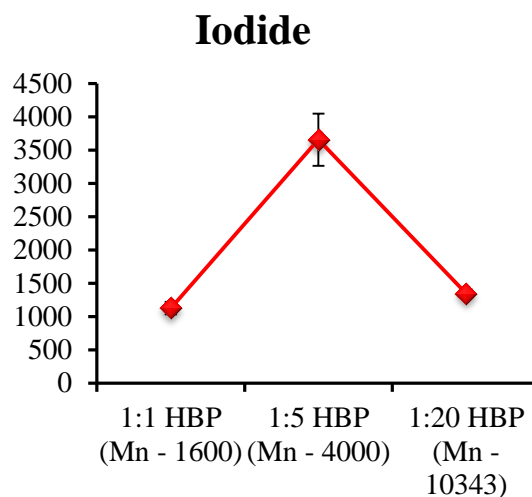


**Figure 88** – A Line graph to show the effect of molecular weight upon interaction with tetrabutylammonium iodide.
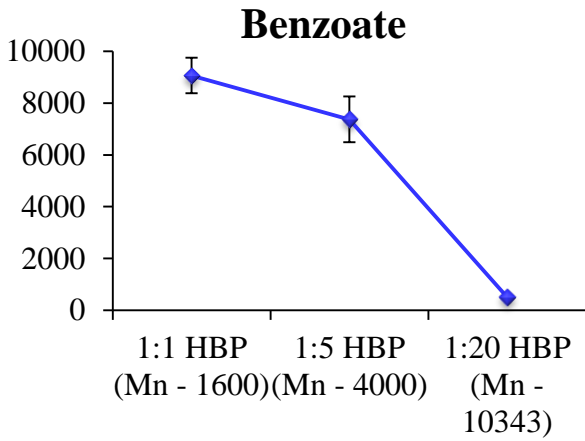
**Benzoate**

**Figure 91**– A Line graph to show the effect of molecular weight upon interaction with tetrabutylammonium benzoate.
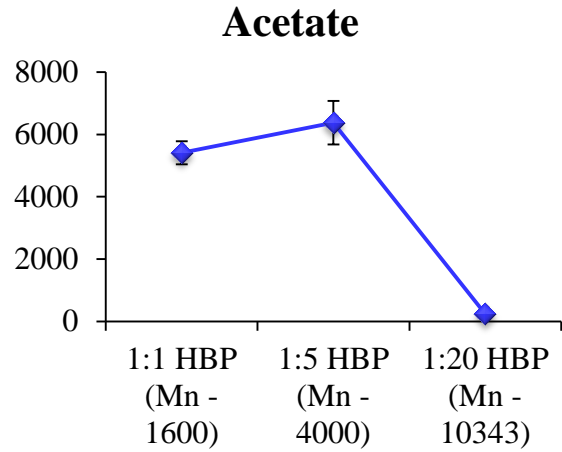


**Acetate**

**Figure 90** – A Line graph to show the effect of molecular weight upon interaction with tetrabutylammonium acetate.



**Dihydrogen Phosphate**
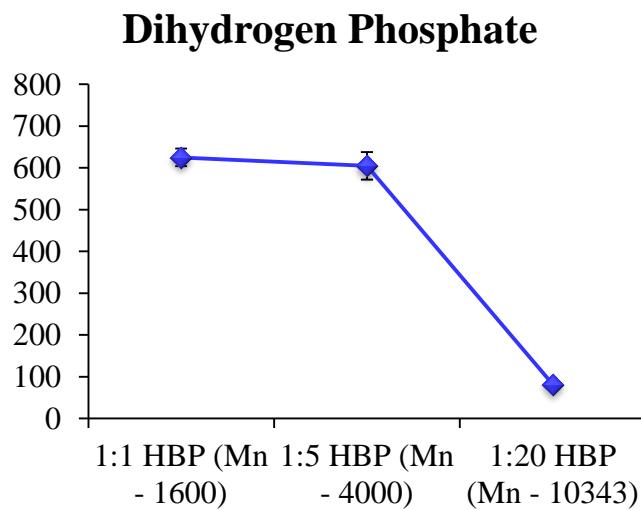
**Figure 92** – A Line graph to show the effect of molecular weight upon interaction with tetrabutylammonium phosphate monobasic.

From the data obtained, it appears that the incorporation of the isophthalamide based receptor within poly 3, 5 diacetoxybenzoic acid results in increased selectivity of larger, softer anions; namely bromide and iodide. Kavallieratos *et al.*[45] used a plot of Gibbs free energy versus the ionic radii for a selection of hard and soft anions in order to clarify any trends observed regarding selectivity. Therefore, it was postulated that the inclusion of a plot of this kind, relative to the data obtained, would help elucidate the trends experienced for the core and range of polymer receptors. In **table 4** one can see the data for the ionic radii of the ions selected (with the exception of benzoate), experimental hydration free enthalpies (scaled by $10^{-1}$)[91] and the corresponding $\Delta G$ values for the core and polymer systems. This data has also been presented as a scatter graph, and can be seen in **figure 93**. The hydration data of the ions provides confirmation that smaller, harder anions are more able acceptors of Hydrogen bonds compared to bulkier softer anions.[45]

| Anionic Guest | Ionic radius | $\Delta G$ (hydration) $(10^{-1}$ kJmol$^{-1})$ | $\Delta G$ (core) (kJmol$^{-1}$) | $\Delta G$ (1:1 HBP) (kJmol$^{-1}$) | $\Delta G$ (1:5 HBP) (kJmol$^{-1}$) | $\Delta G$ (1:20 HBP) (kJmol$^{-1}$) |
|---|---|---|---|---|---|---|
| $F^-$ | 0.133 | -46.5 | -22.53 | -18.83 | -18.65 | -19.12 |
| $Cl^-$ | 0.181 | -34 | -27.53 | -18.09 | -18.40 | -17.52 |
| $Br^-$ | 0.196 | -31.5 | -21.51 | -23.47 | -22.92 | -22.99 |
| $I^-$ | 0.22 | -27.5 | -16.51 | -17.41 | -20.33 | -17.85 |
| $CH_3CO_2^-$ | 0.162 | -36.5 | -21.21 | -21.30 | -21.71 | -13.50 |
| $H_2PO_4^-$ | 0.2 | -46.5 | -17.29 | -15.95 | -15.87 | -10.93 |

**Table 4** – Table to show the ionic radii of anionic guests and the corresponding experimental $\Delta G$ values for the core and polymer systems. Experimental hydration free enthalpies $(10^{-1})$ and the ionic radii data has been taken from the literature.[91]
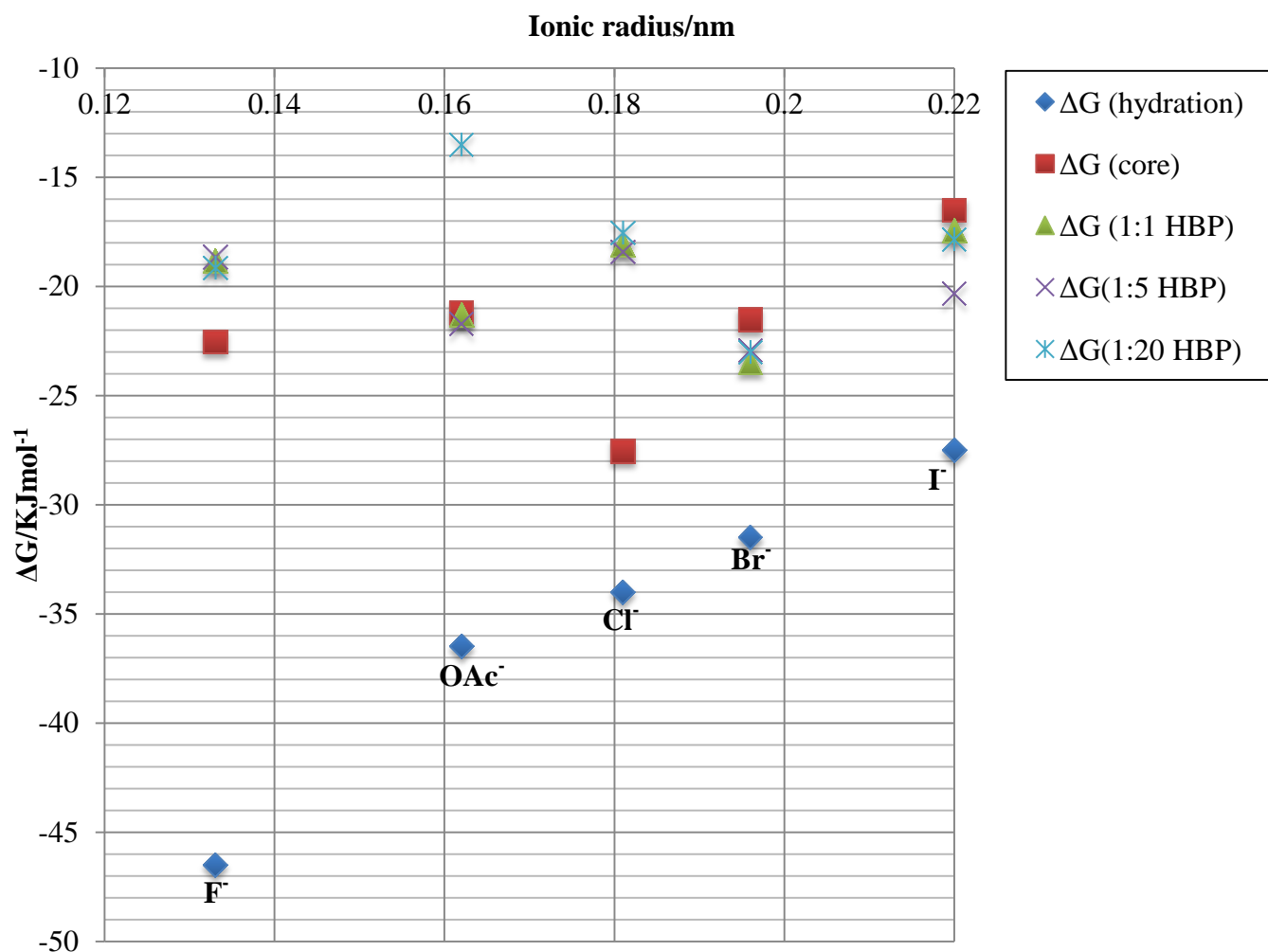
**Figure 93** – A plot to represent ΔG vs. ionic radius for fluoride, acetate, chloride, bromide and iodide.

The scatter graphs presented in **figure 93** show the relative selectivity for each polymer system and the native receptor. From comparison of the hydration data with the experimental data, it is apparent that the polymer systems deviate from expected binding results, whereby, larger softer anions appear to be selected over small hard anions. From analysis of the scatter graphs, the core appears most stable for chloride. Therefore, in geometrical terms, the native receptor provides the best geometry for chloride. The scatter graph for the native receptor also shows the same gradient as the hydration data for chloride, bromide and iodide. However, with the hyperbranched polymer systems, the trend differs. As the anion binding site is identical for all receptor systems, the hyperbranched polymer must be involved in binding, whereby the polymeric structure is perhaps providing additional stability. It has been shown in previous studies that fixed receptors and synthetic anion receptors on the whole

have a tendency to bind smaller anions more favourably, whereas selective receptors for bulky, softer anionic guests is synthetically more challenging. Therefore, the results observed for the hyperbranched polymer systems and their selectivity towards bromide and iodide are extremely promising.

Work by Kavallieratos *et al.*[45] showed the enhanced binding affinity towards smaller halides by the incorporation of a nitrogen atom in close proximity to the anion binding site (**scheme 19**). The lone pair is sterically more bulky when compared to an aromatic C-H bond and, as a result, the repulsion between the lone pair and negatively charged guest will reduce the binding strength. This adverse effect will be more notable for larger more diffuse ions (bromide and iodide), thus resulting in a higher selectivity for smaller harder ions (fluoride and chloride). Therefore, a possibility for future work could be to implement this synthetic approach in order to see whether the poor selectivity towards fluoride and chloride in the current isophthalamide polymeric systems could be improved.
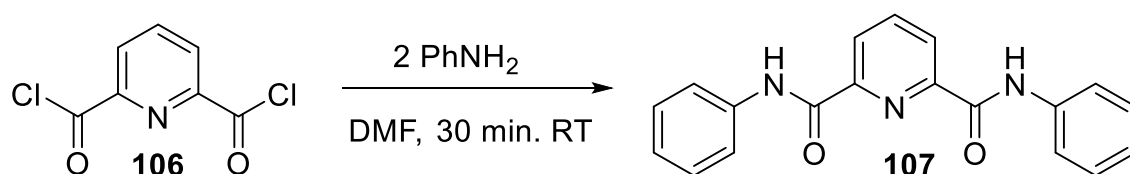


**Scheme 19** – The synthetic procedure, developed by Kavallieratos *et al.*, for an anion receptor which possesses a nitrogen atom in close proximity to the binding site, resulting in an improvement in affinity towards smaller harder anions.[45]

## 3.5 Fabrication of a water soluble hyperbranched polymeric anion receptor

As mentioned previously, developing an organic system was to serve as proofs of principle, demonstrating that an anion receptor can be covalently incorporated and still maintain the ability to bind anionic species. The ultimate goal, as stated beforehand, is to develop a core functionalised water soluble system. An effective organic binding system has been realised; therefore, the next stage was development of a core functionalised water soluble polymeric system.

### 3.5.1 Selection of the monomer for a water soluble polymeric system

Glycidol was decided as the monomer of choice when designing a water soluble dendritic polymer. Glycidol is an organic moiety containing both epoxide and alcohol functionality, which is able to polymerise to form a water soluble hyperbranched polymer. Polyglycidol has been explored in numerous areas of chemistry, including core encapsulation. Frey *et al.* demonstrated the complete incorporation of a photo-sensitiser core within hyperbranched poly ether polyols. They used ring opening multi-branching polymerisation (ROMP) of glycidol utilising slow addition of monomer, demonstrating the possibility to integrate a photoactive core within a hyperbranched polymer.[92] Kim *et al.* demonstrated the use of this monomer as a reducing and stabilising agent in the synthetic procedure for water soluble, multifunctional, metal nanoparticles. The conditions involved in this research were completely green in nature, meaning that this polymer exhibits promise for biomedical use.[93] Glycidol (**87**) has been studied extensively within the Twyman group, meaning the chemistry of this monomer is well understood. Glycidol is also particularly well established within literature, thereby deeming it an appropriate choice for this purpose.

As is the case with the polymerisation of 3, 5 diacetoxybenzoic acid, the terminal functionality of the core molecule is crucial for compatibility with the polymerisation reaction. For polymerisation with glycidol, a core should ideally possess at least one –OH terminal group. Upon addition of base, the hydroxyl group will be deprotonated, resulting in generation of a RO⁻ moiety. This species can now attack the epoxide, triggering polymerisation (**scheme 20**).
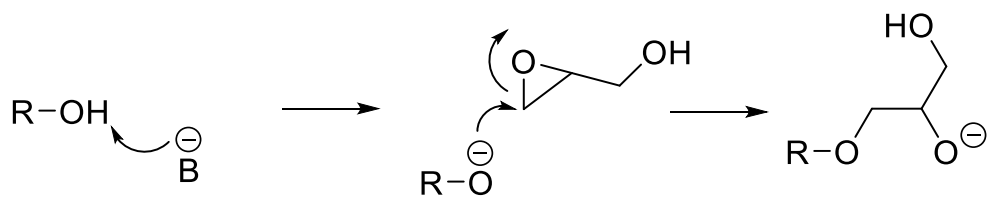
**Scheme 20** – Mechanism of the polymerisation of glycidol upon reaction with a hydroxyl terminated core.

N, N' – bis (3-acetoxyphenyl) isophthalamide proved to be a potent anion receptor for the organic soluble system and was compatible with polymerisation after repositioning of the terminal groups. As a result of this, it was postulated that N, N' – bis (3-hydroxyphenyl) isophthalamide was selected as the core for development of a water soluble polymeric system.

The polymerisation of 3, 5 diacetoxybenzoic acid is driven by thermodynamics, whereas, the polymerisation of glycidol is an irreversible kinetic reaction. A polymerisation driven by kinetics has numerous disadvantages in comparison to a reversible thermodynamic polymerisation reaction. It is not possible for core molecules to be distributed in a uniform manner within the polymer. The level of core incorporation is dependent upon the rates of individual reactions which occur throughout polymerisation. In theory, there are two routes possible, polymerisation via monomer propagation or polymerisation via core propagation (**scheme 21**). Another factor to be considered is the relative reactivity of the core in relation to the monomer. This will determine whether core incorporation is favoured towards either the high or low molecular weight range. A drawback to this method is the impossibility to achieve complete core incorporation, as a result, a high level of core is required experimentally.
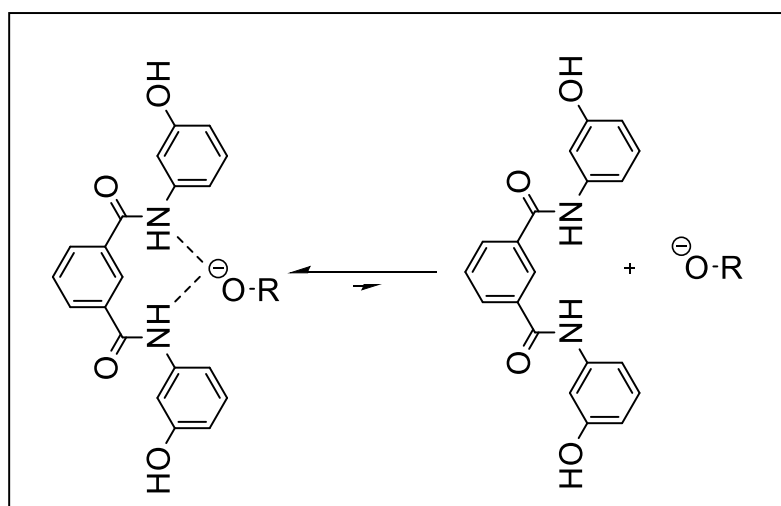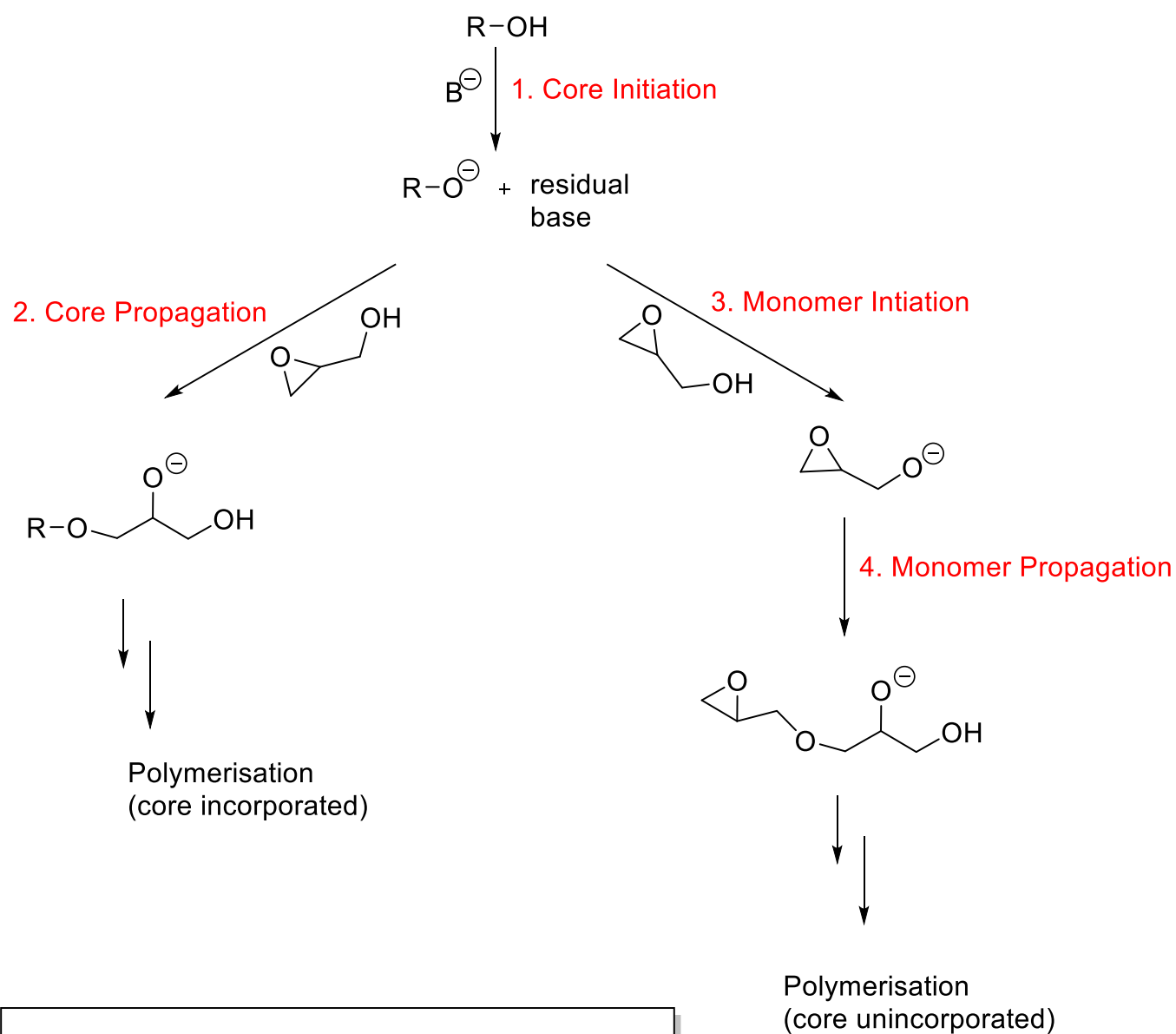
**Scheme 21**– Representation of the two potential routes in the polymerisation of glycidol in the presence of a core molecule. The insert shows a possible receptor interaction with anionic species generated during the polymerisation process.

### 3.5.2 Polymerisation of glycidol with a N, N' bis – (3-hydroxyphenyl) isophthalamide core (1:20)

The molar ratio of core to monomer implemented was 1:20 for this methodology. Firstly, N, N' – bis (3-hydroxyphenyl) isophthalamide was dissolved in diethylene glycol dimethyl ether solvent in a 3-neck round bottom flask. The solution was heated to 50°C and subsequently heated to 90°C, upon complete dissolution of the core. After a period of 20 minutes, half an equivalent of sodium hydride was added and it was at this point a colour change was observed. The colourless solution became pale yellow in colour, upon addition of the base. After 90 minutes glycidol was added to the solution slowly over a period of 12 hours via a syringe pump. The reaction was left to stir for a further 5 hours before cooling to room temperature. Polyglycidol, with or without core incorporation, is insoluble in diethylene glycol dimethyl ether, meaning the solvent can be disposed of and the polymer will form an adhesive oil film on the inner surface of the reaction flask. However, after disposal of the solvent, no polymer appeared to remain. As can be seen from **scheme 21**, there are numerous anionic species generated throughout this polymerisation process. The core is highly capable of coordinating anionic guests, thereby preventing monomer propagation. However, the initial deprotonation of the phenolic species gave a colour change, indicating free anion was present in solution. Unfortunately, the equilibrium must have been shifted extensively in favour of the complexed species (effectively meaning any propagating and initiating anions are completely bound and unavailable for further reaction). This can be seen in the insert of **scheme 21**.

### 3.5.3 Polymerisation of glycidol with a 4-Nitrophenol core (1:20)

In order to confirm that it is the chemistry and not the chemist, polymerisation of glycidol was performed using 4-Nitrophenol as a core molecule (**scheme 22**). This molecule is not capable of coordinating anionic guests and has also been well studied within the Twyman group.
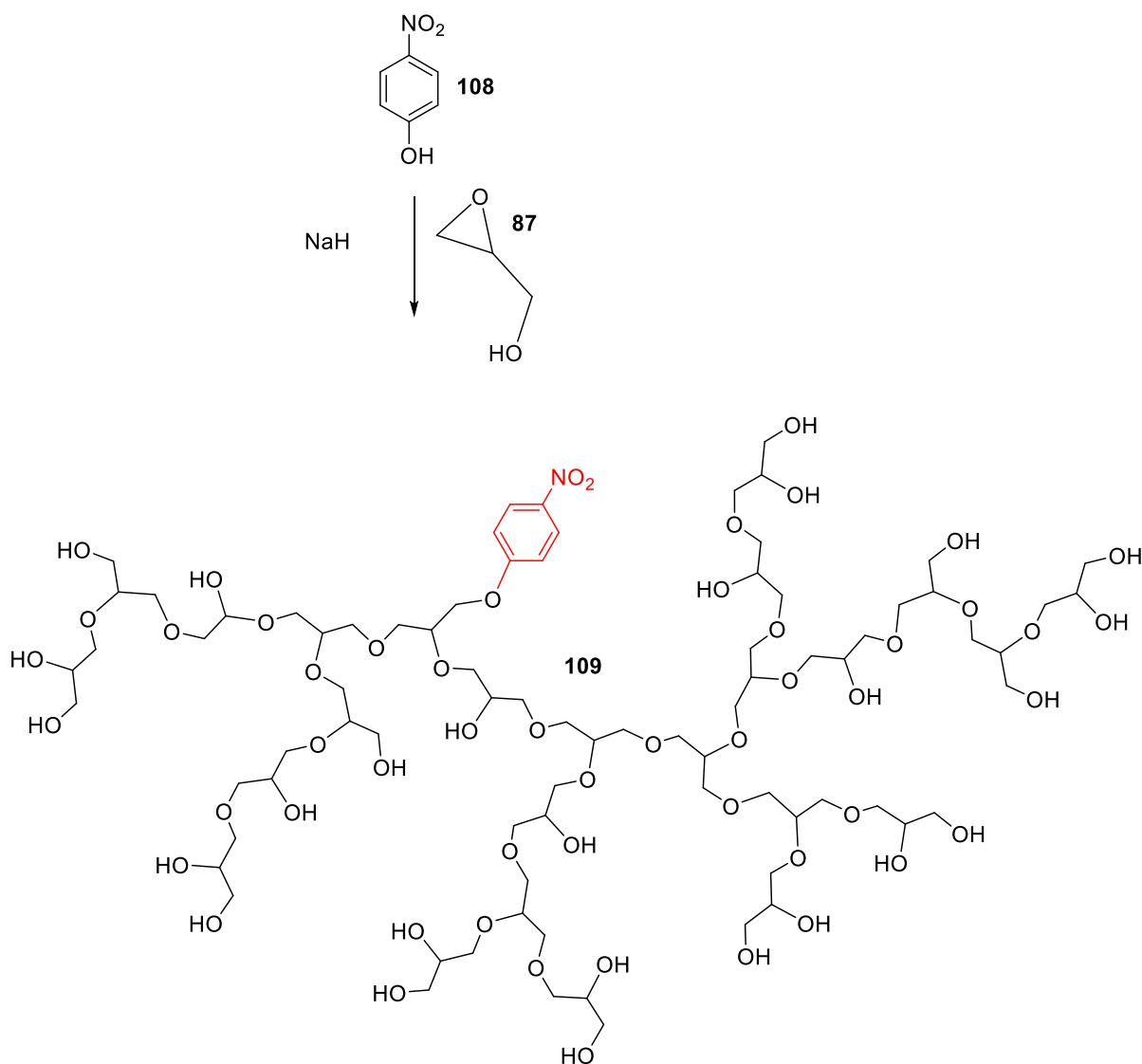
**Scheme 22** – Reaction scheme for the incorporation of 4-Nitrophenol in polyglycidol.

The general procedure discussed in section **3.5.2** was employed. However, upon removal of the solvent, a thin layer of adhesive oil could be seen lining the reaction flask, giving confidence that the polymerisation had been successfully achieved. After removal of solvent, the polymer was then dissolved in methanol before precipitation into excess acetone. The polymer was washed repeatedly with acetone and dried in a vacuum oven prior to analysis. As is the case for the determination of core incorporation within poly 3, 5 diacetoxybenzoic acid, proton NMR spectroscopy is also a crucial tool in establishing successful covalent incorporation of 4-Nitrophenol within polyglycidol. From implementation of ^{1}HNMR, the core can be visualised within the polymeric structure. There are two proton environments present for 4-nitrophenol; two aromatic protons ortho to the nitro functionality and two aromatic protons ortho to the hydroxyl functionality. The two protons ortho to the nitro group

166

can be seen at 8.15 ppm, and the two protons ortho to the hydroxyl group can be seen at 7.05 ppm. The nitro functionality is more electron withdrawing, in comparison to the hydroxyl group, thus explaining why the two protons ortho to the nitro group will be more deshielded. An expansion of the ^{1}HNMR of the core protons can be seen in **figure 94**. The final peak of interest in the proton NMR spectrum is a broad multiplet occurring between 3.2-4.0 ppm, which is representative of the multiple proton environments within the polymer. This multiplet corresponds to the methine, methylene and hydroxyl proton environments present within the polyglycidol architecture.
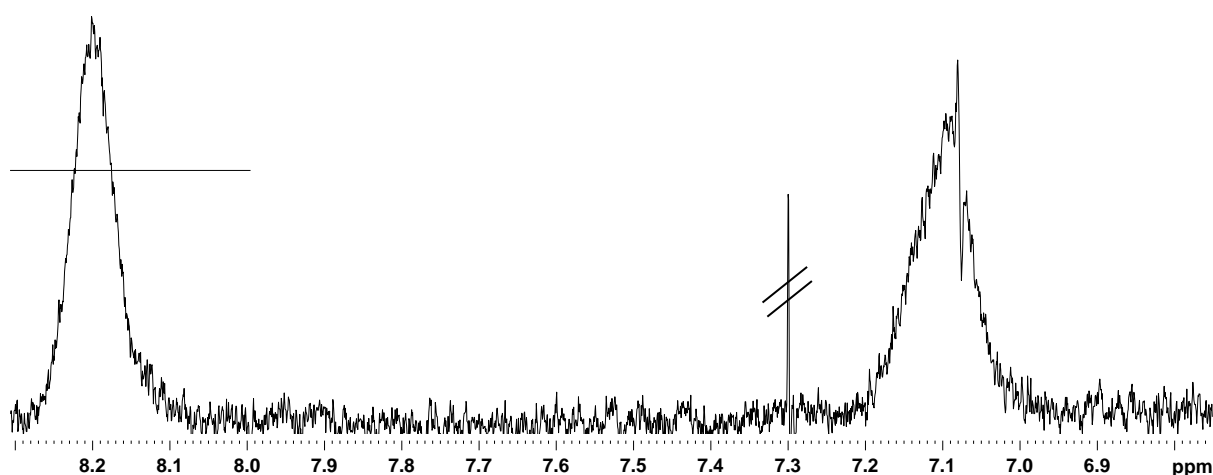


**Figure 94 –** Figure to show the ^{1}HNMR expansion of the aromatic protons present in 4-Nitrophenol. Marked signal is indicative of resolved chloroform in deuterated chloroform.

In order to verify that the core has been covalently incorporated, the NMR sample was doped with 4-nitrophenol. The spectrum generated possessed two additional doublets at 8.1 ppm and 6.8 ppm respectively, indicative of unincorporated 4-nitrophenol. An expansion of the doped spectrum can be seen in **figure 95**, the unincorporated4-Nitrophenol gives sharp doublets, whereas, core incorporated 4-Nitrophenol gives broader signals.
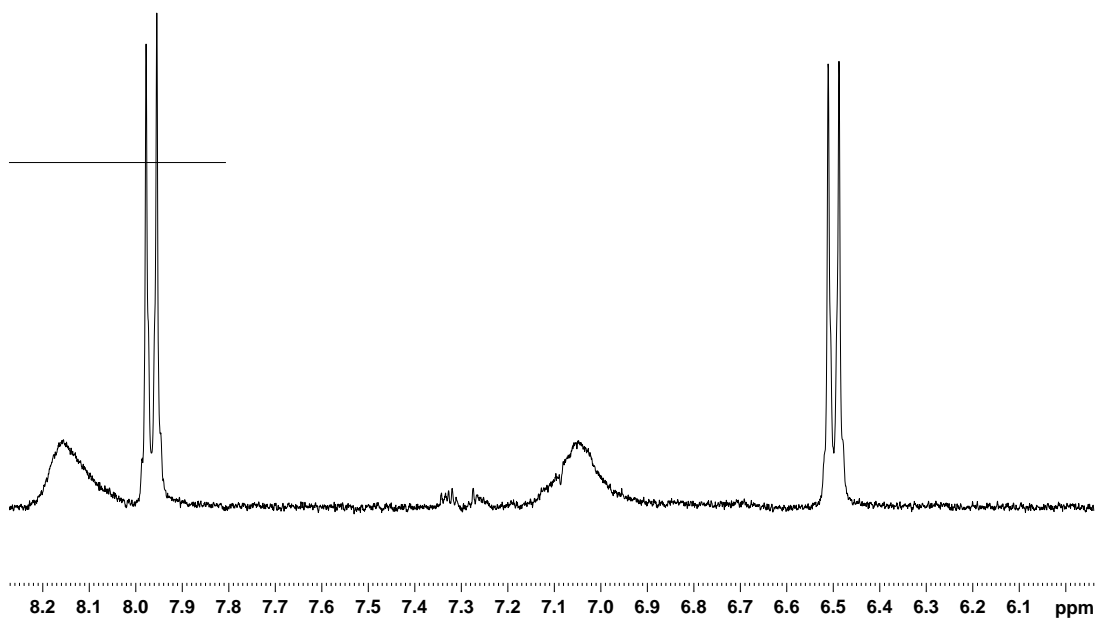
**Figure 95** –Figure to show the ^{1}HNMR expansion of core functionalised polyglycidol doped with 4-Nitrophenol.

## 3.6 Non-covalent encapsulation of an anion receptor

Unfortunately, due to the nature of the polymerisation, an anion receptor does not appear to be suitable for core incorporation within polyglycidol; therefore, an alternative approach must be employed so that a fully functioning water soluble anion receptor system can be fabricated. Conversion of the terminal groups of the organic soluble hyperbranched polymeric system would be synthetically challenging, meaning non-covalent encapsulation was considered as a potential solution. Dendritic polymers are not the only materials which could be used to create a water soluble anion receptor; another approach could involve the use of di-block polymer micelles. Polymeric micelles have been studied extensively and have shown potential for use in numerous applications such as nano-bioreactors, viral gene vectors and drug delivery agents.[94] The reasoning behind the growing fascination for block copolymers is their ability to self- assemble, both in bulk and solution. Amphiphilic block copolymers signify a large series of materials ranging from simple linear di-block structures containing a hydrophilic segment and a hydrophobic segment to much more complex multi-block systems. This type of polymer can spontaneously self-assemble to give a supramolecular nanoparticle possessing a hydrophobic core shielded by a hydrophilic periphery. As previously mentioned, these polymeric micelles have shown promise in the area of medicinal chemistry, namely drug delivery. The drug molecule can be encapsulated within the hydrophobic interior, protected from the hydrophilic region of the micelle and be transported and distributed where desired. There are numerous examples in the literature utilising these micelles for this specific application. Quaglia *et al.* developed and investigated micelles based on amphiphilic poly (ε-caprolactone) and poly (ethylene oxide) copolymers with both linear and star architectures. Results obtained showed that these polymeric micelles displayed low toxicity towards red blood cells, thus showing potential as drug delivery agents for lipophilic drug molecules.[95] Zhang *et al.* have developed a series of monomethoxy poly (ethylene glycol)- poly (lactide) (mPEG-PLA) di-block copolymers. These micelles were prepared and used to investigate the encapsulation of Cyclosporin, a highly lipophilic immunosuppressant drug used in post allogeneic organ transplant and severe cases of Ulcerative Colitis. Cyclosporin was encapsulated effectively and results demonstrated that the polymeric micelles maintained the release of the drug moiety. The intestinal absorption of cyclosporin was improved by these nanocarriers, thus showing promise for enhancing oral absorption of weakly absorbed drugs.[96] More recently, Wang *et* al. have reported the synthesis of PEG-PE micelles and demonstrated their compatibility with drug molecules;

namely doxorubicin hydrochloride and vinorelbine tartrate. The loaded micelles not only showed sustained release, but an elevated level of stability.[97] These are merely a few examples of the use of these polymeric materials in the area of drug delivery, for more information the reader is directed to the following literature.[98-100] Therefore, for the purpose of this research, a linear amphiphilic di-block polymer could be used to encapsulate an anion receptor.

In collaboration with Caroline Glover and Dr. Adam Ellis, the synthesis of polymeric micelles and the exploitation of encapsulation properties of these vehicles were realised. The block polymer chosen was the biocompatible poly (ethylene glycol) methyl ether − block − poly (ε-caprolactone) (mPEG-b-PCL$_n$). This particular di-block polymer has received a great deal of interest in recent years and featured in numerous pieces of literature for its potential in the area of therapeutic medicine. For further information regarding the therapeutic potential of mPEG-b-PCL micelles, the reader is directed to the following literature.[101-108]

### 3.6.1 Synthesis of mPEG-b-PCL$_n$ di-block copolymer

The synthesis of a range of di-block copolymers and polymeric micelles was performed, under supervision, by Caroline Glover, a master's student in the Twyman research group. A series of di-block copolymers, with varying composition of PCL/mPEG molar ratios, were prepared for comparison. The first stage of synthesis involved the addition of oven dried mPEG to a 2-neck round bottomed flask and stirred for 60 minutes at 130ºC under vacuum. The apparatus was refilled with nitrogen and ε-caprolactone was added (varying amounts) via a syringe. This was followed by the addition of 0.05% w/w tin (II) 2-ethyl hexanoate catalyst. The reaction mixture was then stirred for a period of 24 hours at 130ºC to yield a white solid at ambient temperature. The white solid obtained was dissolved in dichloromethane and precipitated into petroleum ether 40-60 to yield the di-block copolymer. This synthetic procedure proceeds via catalysed ring opening polymerisation of ε-caprolactone monomer, initiated by mPEG (**scheme 23**).

(i) n = 5
(ii) n = 10
(iii) n = 20
(iv) n = 60
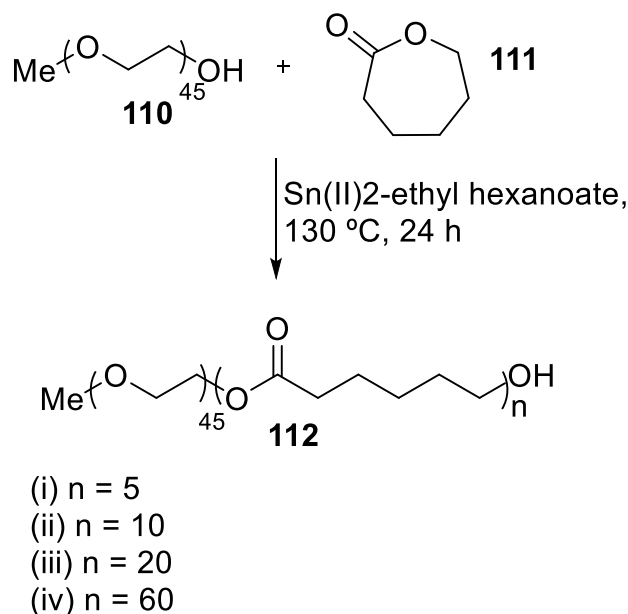
**Scheme 23–** Synthesis of mPEG$_{45}$-b-PCL$_n$ (where n = 5, 10, 20 and 60).

Analysis of the polymers was also carried out by Caroline Glover; the experimental data obtained from said analysis is recorded in the experimental chapter of this thesis. The $^1$HNMR spectra provided evidence of the structures. The methylene protons of poly ($\varepsilon$-caprolactone) in the product can be found at 2.32, 1.66, 1.39 and 4.07 ppm; these signals are indicative of $\alpha$, $\beta+\delta$, $\gamma$ and $\varepsilon$ positions to the ester carbonyl group respectively. There are also two singlets at 3.39 and 3.65 ppm which are characteristic of the mPEG section of the di-block copolymer. Infra-red spectroscopy also provides structural evidence as it confirms the presence of the ester carbonyl functional group with a signal at 1721 cm$^{-1}$. The presence of this stretch confirms the success of the ring opening polymerisation. The GPC and NMR molecular weight estimations, along with the PDI and the theoretical and experimental chain lengths of the poly ($\varepsilon$-caprolactone) segment, are tabulated overleaf in **table 5**.

| | n = 5 | n = 10 | n = 20 | n = 60 |
|---|---|---|---|---|
| **Molecular weight from GPC** | 1921 | 2506 | 4344 | 7772 |
| **Molecular weight from NMR** | 2399 | 3057 | 5893 | 10025 |
| **Theoretical length of poly (ε - caprolactone) chain** | 5 | 10 | 20 | 60 |
| **Experimental length of poly (ε - caprolactone) chain** | 4 | 10 | 23 | 68 |
| **PDI** | 1.20 | 1.18 | 1.23 | 1.34 |

**Table 5** – Table to show the molecular weight values obtained from GPC and NMR, the PDI and the theoretical and estimated chain lengths of poly (ε - caprolactone) segments in each of the di-block copolymers synthesised.

### 3.6.2 Exploiting the encapsulation properties of polymeric micelles

Previous results within the group have shown that micelles usually lie within the range of 20 to 40 nm in diameter, with a hydrophobic cavity of approximately between 10 and 15 nm. The size of the structure to be encapsulated can be approximated in angstroms and subsequently converted to nanometres, so as to deduce whether it is of adequate size to sit within the hydrophobic pocket. The polymer receptor (1:20) was estimated to be approximately 1nm is size, meaning each polymeric receptor system are well within range to fit comfortably within the internal hydrophobic cavity. To estimate the size in nanometres, the ^{1}HNMR spectrum was used to calculate the approximate number of monomer units present in the polymer. This calculation was then used to deduce a proposed chemical structure. The approximate distance between a C1 and C3 in a three carbon chain (propyl unit) is approximately 1.5 Å. A carbon chain can be broken down into propyl units and the maximum distance of any chain can be estimated by calculating the number of propyl units (or 3 atom chains) and multiplying by 1.5 Å. Therefore, using this information, the distance from one end of the estimated polymer structure to the other can be estimated in Angstroms. It is postulated that, when a species is encapsulated within a micelle structure, the micelle will subsequently swell, regardless of the nature of the encapsulated guest. As the anion receptor polymer system is not UV active it will be difficult to ascertain whether or not encapsulation within a polymeric micelle has occurred. Therefore, encapsulation of a porphyrin and porphyrin cored hyperbranched polymers of varying molecular weights were to be encapsulated first. This was necessary so as to confirm that the method of encapsulation

is sufficient and also show that encapsulation of a hyperbranched poly-3, 5 diacetoxybenzoic acid systems could be accomplished.

### 3.6.3 Synthesis of tetraphenyl porphyrin (TPP)

The poly 3, 5 diacetoxybenzoic acid anion receptor system does not possess a UV active core, meaning visualisation within the micelle is difficult. In order to first probe the encapsulation properties of micelle structures, aromatic porphyrin molecules were chosen. Porphyrin structures exhibit high absorption in the visible spectrum and, as the loaded compound must be detected in order to confirm encapsulation, a porphyrin seemed an appropriate choice. The first porphyrin synthesised is tetraphenyl porphyrin (TPP), which is shown in **scheme 24**. The first stage of synthesis involved the addition of pyrrole and 4-benzaldehyde to a reaction flask containing propionic acid. The flask was equipped with a reflux condenser and the solution was heated to reflux for a period of 30 minutes. The product was subsequently isolated by vacuum filtration.
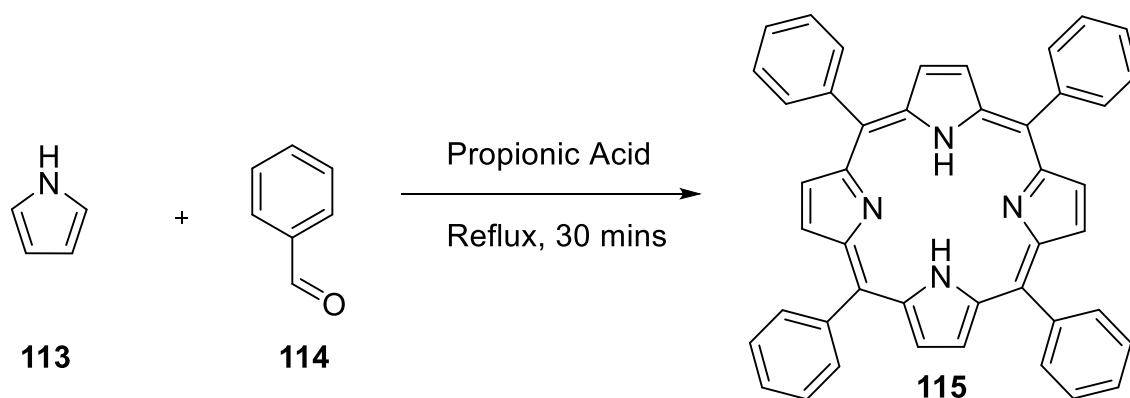


**Scheme 24** – Reaction scheme for the synthesis of TPP.

Validation of the desired product was reached by the use of a range of analytical techniques. An important tool used for the characterisation of the macrocycle was ¹HNMR spectroscopy. A singlet can be visualised at 8.90, integrating to 8 protons, which is indicative of the pyrrolic methine protons. There are also signals at 8.27 and 7.81 ppm, which correspond to the *ortho*, *meta* and *para* Phenylic protons. The porphyrin structure was confirmed by the presence of the NH singlet at -2.71 ppm. These protons are found up field as they are located within the shielding cone of the porphyrin. Further evidence was given from mass spectrometry; the ES-MS spectrum gave a signal at 615, which is indicative of the $MH^+$ ion. UV/Vis spectroscopy

showed the presence of the characteristic high absorption Soret band at 418.5 nm, along with four Q bands, which gave weaker absorption at 515.0, 550.0, 590.5 and 645.0 nm respectively. The Q bands are much weaker as they correspond to the pseudoparity forbidden S0 to S1 transition. The combination of these techniques with IR and $^{13}$CNMR gives confidence in the success of the synthetic procedure and the purity of the product obtained. Tetraphenyl porphyrin is simple to synthesise but has zero solubility in water, meaning that any improvement in water solubility is difficult to quantify. Furthermore, previous work within the group showed that TPP had a tendency to aggregate; meaning encapsulation was also challenging to quantify. To overcome these problems, it was decided that a porphyrin with higher solubility in water should also be studied.

### 3.6.4 Synthesis of 3, 5-dihydroxyphenyl porphyrin

The second porphyrin required for encapsulation studies is 3, 5-dihydroxyphenyl porphyrin. The synthetic procedure for this particular macrocycle involved multiple steps; the first stage involved the synthesis of 3, 5-dimethoxyphenyl porphyrin and the second stage involved the demethylation of said macrocycle, giving 3, 5-dihydroxyphenyl porphyrin.

### 3.6.4.1 Synthesis of 3, 5-dimethoxyphenyl porphyrin

The initial step involved the use of the Rothemund[109] and Adler-Longo[110, 111] method. This method will be discussed in further detail in Chapter 4 (**section 4.3.2.2**). Equal molar quantities of 3, 5-dimethoxybenzaldehyde and pyrrole were refluxed in propionic acid for a period of 30 minutes (**scheme 25**). The product was isolated via vacuum filtration and washed meticulously with methanol.
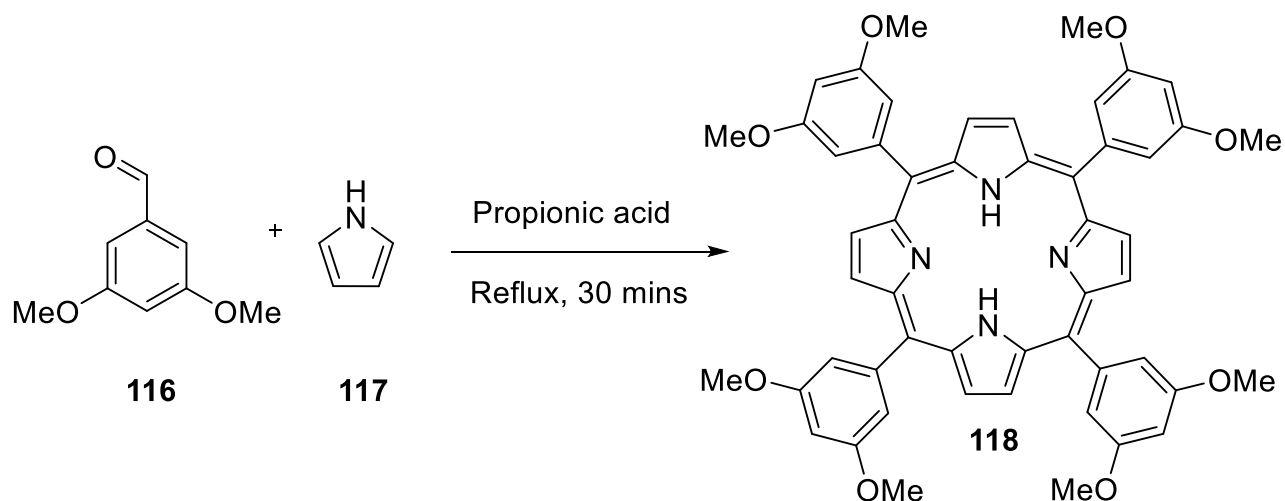
**Scheme 25–** Synthesis of 3, 5-dimethoxyphenyl porphyrin.

The UV/Vis absorption spectrum confirmed the existence of porphyrin by showing the presence of the high absorption Soret band at 421 nm and four weaker Q bands at 515, 550, 589 and 649.5 nm respectively. From analysis of the $^1$HNMR spectrum, there is a signal at 8.97 ppm, corresponding to the pyrrolic methine protons. There are two multiplets at 7.43 and 6.93 ppm, which are indicative of the *ortho* and *para* Phenylic protons. A singlet signal can be seen at 3.99 ppm integrating to 24 protons, corresponding to the methyl protons present on the methoxy functional groups. A singlet can also be seen at -2.80 ppm which relates to the highly shielded NH protons. ES-MS also displays a signal at 855 for the MH$^+$ ion, thereby providing additional structural evidence. The next stage of the synthetic procedure was the demethylation of the *octa*-methoxy functionalised porphyrin macrocycle.

### 3.6.4.2 Demethylation of 3, 5-dimethoxyphenyl porphyrin

Demethylation was performed by using boron tribromide as the demethylation agent. Boron tribromide is widely used in the de-alkylation of methyl aryl ethers.[112] The synthetic procedure is illustrated below in **scheme 26**.
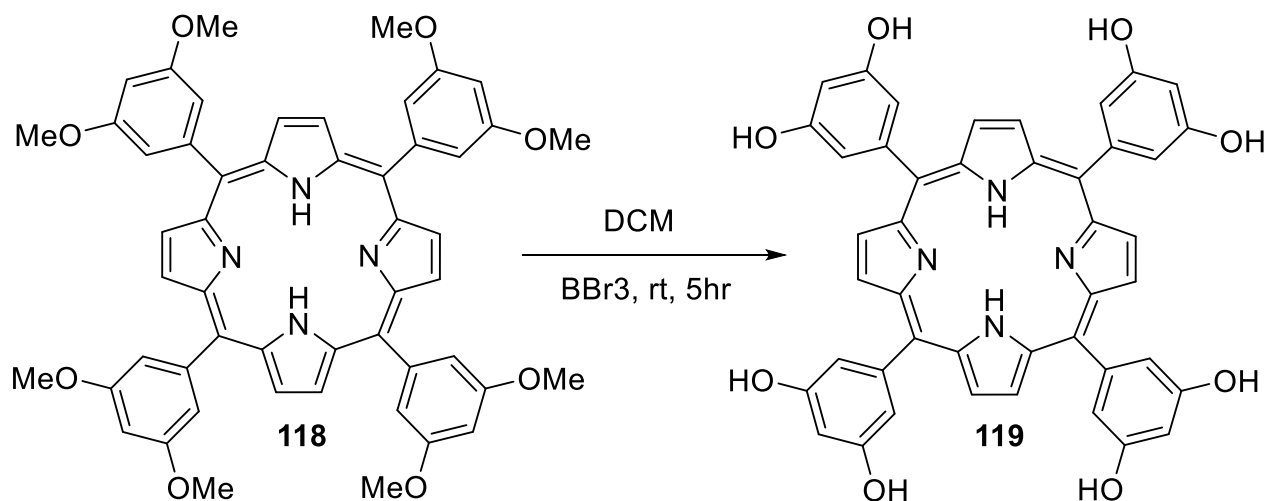
**Scheme 26** – Synthesis of 3, 5-dyhydroxyphenyl porphyrin.

A reaction flask was charged with 3, 5-dimethoxyphenyl porphyrin and anhydrous dichloromethane solvent and stirred under an atmosphere of nitrogen for a period of 10 minutes. Boron tribromide was added drop-wise to the reaction mixture via a syringe, inducing a green colour change. The Lewis acidic species interacts with oxygen, leading to the loss of a bromide ion. This then attacks the methyl group, successively ejecting methyl bromide. Hydrolysis subsequently takes place and replaces each bromide with a hydroxyl group, whilst boron leaves as boric acid.

The reaction took place at room temperature under nitrogen, followed by careful quenching with distilled water. Due to the violence of the interaction between surplus boron tribromide and water, stirring was continued for an additional 20 minutes to ensure any excess boron tribromide present is removed. Once quenching is complete, the reaction mixture was neutralised with sodium hydrogen carbonate in order to remove any acid present, followed by the extraction with ethyl acetate. Boric acid generated during the reaction results in the colour change. The green colour of the solution, prior to neutralisation, is due to protonated porphyrin. Upon neutralisation with sodium hydrogen carbonate, the organic phase becomes a more characteristic purple colour and the aqueous phase becomes colourless. Insoluble impurities which form at the solvent interface were removed via vacuum filtration. The solvent was removed by rotary evaporation, yielding the product. From analysis of the $^1$HNMR spectrum, the peak corresponding to the methyl protons was no longer present. In addition to this, the $^{13}$CNMR spectrum showed a loss of the signal at 55.3 ppm, which was

representative of the methoxy carbon. Additional evidence was provided by Infra-red spectroscopy, which showed a broad O-H stretch at 3025 cm$^{-1}$. Furthermore, the ES-MS spectrum showed a signal at 743, which was specific to the MH$^+$ ion. The Soret band and four Q bands were visualised in the UV/Vis absorption spectrum; therefore, the combination of each analytical tool used gives confidence in the successful demethylation of 3, 5-dimethoxyphenyl porphyrin.

### 3.6.5 Poly 3, 5 – diacetoxybenzoic acid with a 3, 5 diacetoxyphenyl porphyrin core

The polymer was provided by Adam Ellis and was synthesised from 3, 5-dihydroxyphenyl porphyrin. The first step involved the acetylation of 3, 5-dihydroxyphenyl porphyrin with acetic anhydride to generate 3, 5 diacetoxyphenyl porphyrin. The porphyrin was then reacted with the monomer, 3, 5-diacetoxybenzoic acid, to generate the polymer. The synthetic procedure and characterisation for both 3, 5-diacetoxyphenyl porphyrin and poly 3, 5 – diacetoxybenzoic acid with a 3, 5 diacetoxyphenyl porphyrin core can be found in the experimental chapter of the PhD thesis by Dr. Adam Ellis, pages 176 and 177 (compounds 12 and 13).[86]

### 3.6.7 Micelle Formation

Micelle samples of di-block copolymers were prepared, under supervision, by Caroline Glover using a direct dissolution method, in which an aqueous solution of polymer (at the appropriate concentration for micelle formation) was vigorously stirred for a period of 30 minutes using a shaker device.

### 3.6.7.1 Determination of the critical micelle concentration (CMC)

Prior to encapsulation studies, the appropriate concentration required for analysis needed to be determined. For micelles to form in solution, the concentration of polymer must be just above the critical micelle concentration (CMC). The determination of appropriate concentration is crucial as, if the concentration is too high, larger aggregated species will form instead of the desired micelle structure. Similarly, if the concentration is below the CMC, unimers will exist and no self-assembly will take place. In order to determine this concentration, Caroline Glover examined the changing hydrodynamic diameter with varying concentrations of mPEG-b-PCL$_n$ polymeric solutions. The data obtained for the PCL chain of 5 is illustrated in **figure 96**.
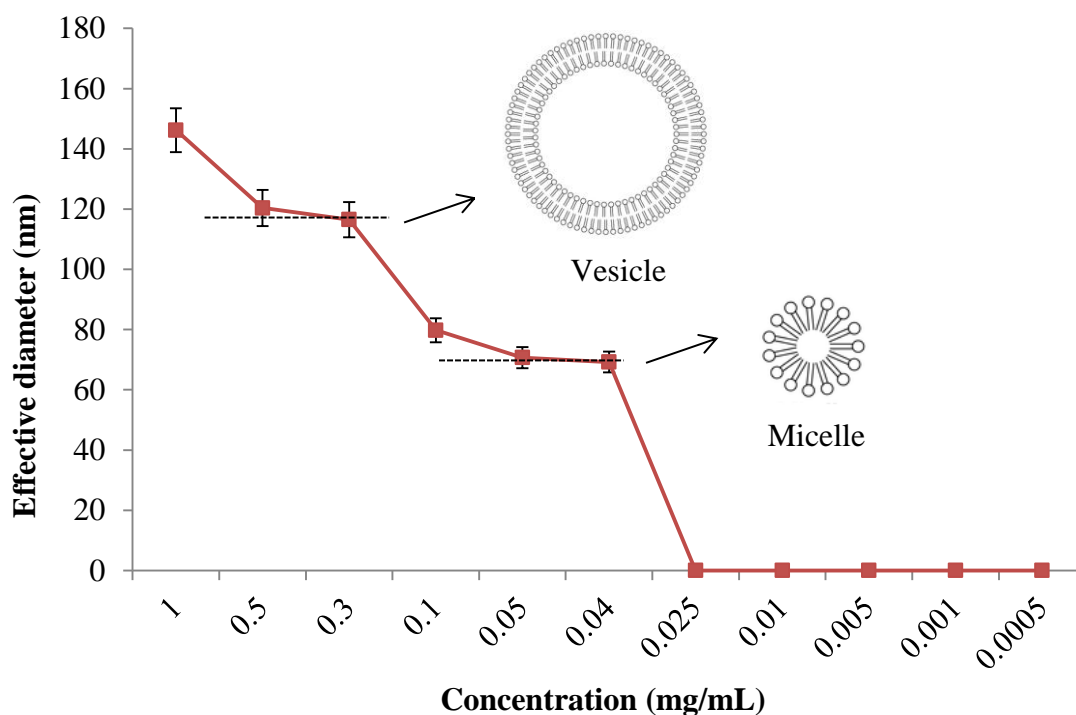
**Figure 96** - A graph to show the change in hydrodynamic diameter with a range of concentrations of mPEG-b-PCL$_5$ polymeric micelles.

The CMC data for chain lengths of 10 and 20 showed similar trends to the CMC line graph above. As can be seen from the data, the optimum concentration for micelle formation is 0.3 mg/mL. Succeeding micelle formation, the hydrodynamic diameter was measured using dynamic light scattering (DLS) and the analysis was based upon volume distribution. It is important to note that analysis by DLS utilises zeta potentials, thereby generating values that are considerably larger than a standard micelle. This is because it is not simply a measurement of particle size, but a measurement of the particle size and the associated solvent, which in this case is water.

### 3.6.7.2 Encapsulation studies

As specified beforehand, in addition to the two porphyrin macrocycles synthesised, two different molecular weight hyperbranched polymeric systems were used for encapsulation studies and were provided by Dr. Adam Ellis.[86] It was essential to use a hyperbranched poly 3, 5-diacetoxybenzoic acid system, as this is the polymer used for anion receptor design and will provide the necessary comparison. The polymers each contained a 3, 5 diacetoxyphenyl porphyrin core, which enables confirmation of encapsulation through UV/Vis spectroscopy. For the porphyrin macrocycles and core functionalised hyperbranched polymeric systems, an

absorption signal was observed between 417 and 423 nm, indicating successful encapsulation of each species. The hydrodynamic diameter was measured prior to encapsulation and then again after encapsulation of each of the compounds. The data obtained can be seen below in **figure 97**.
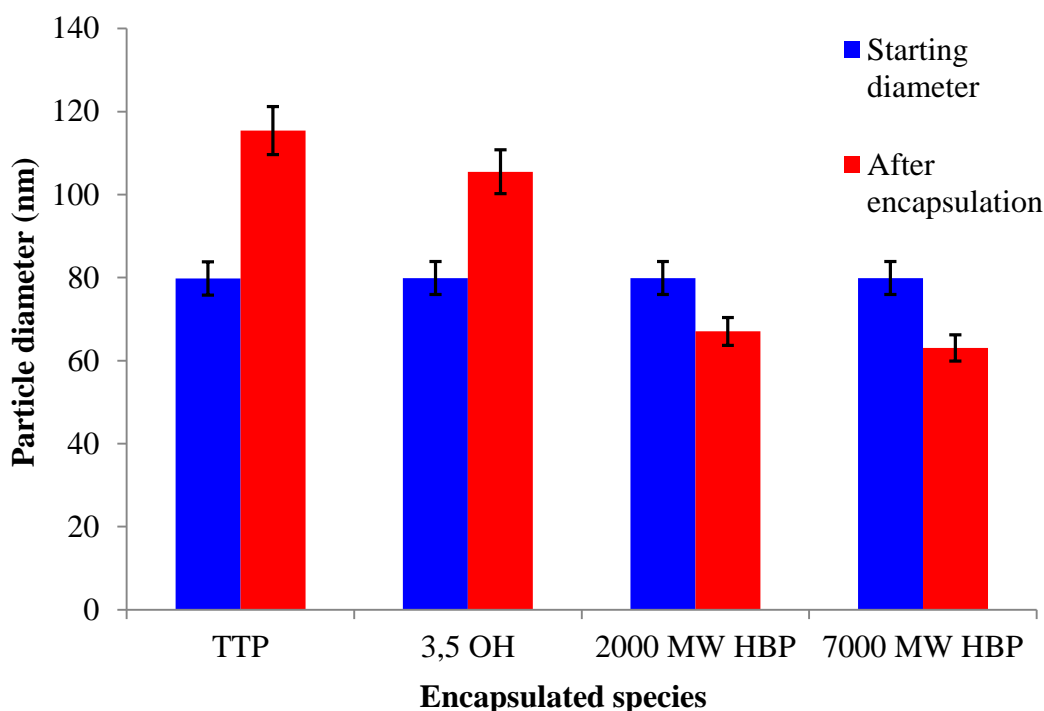


**Figure 97** – A graph to show the hydrodynamic diameter of loaded mPEG-b-PCL$_5$ at 0.3 mg/mL. The blue columns represent the initial diameter measured prior to encapsulation and the red columns show the change to the diameter after encapsulation of a variety of guests.

As can be seen from the column chart, when each porphyrin macrocycle is loaded into a polymeric micelle, there is a swelling of diameter observed. This is the postulated effect upon loading. However, this is not the case for the core functionalised hyperbranched polymer systems. Instead of a swelling observed, the micelle structure appears to shrink when the hyperbranched polymer is encapsulated. After repetition of these results, the same effect is observed. It can be postulated that the hydrophobic segments appear to be dipping into the encapsulated polymer, effectively meaning the hyperbranched polymer is dissolving the hydrophobic regions of the di-block copolymer. This could account for the shrinking of the micelle diameter after encapsulation. In spite of this, the molecule as a whole is still water soluble. In order to gain a better understanding of the chemistry involved, transmission electron microscopy (TEM) was used[†] for visualisation of the micelle structures both before and after encapsulation of various molecules (**figure 98**).

**(a)**
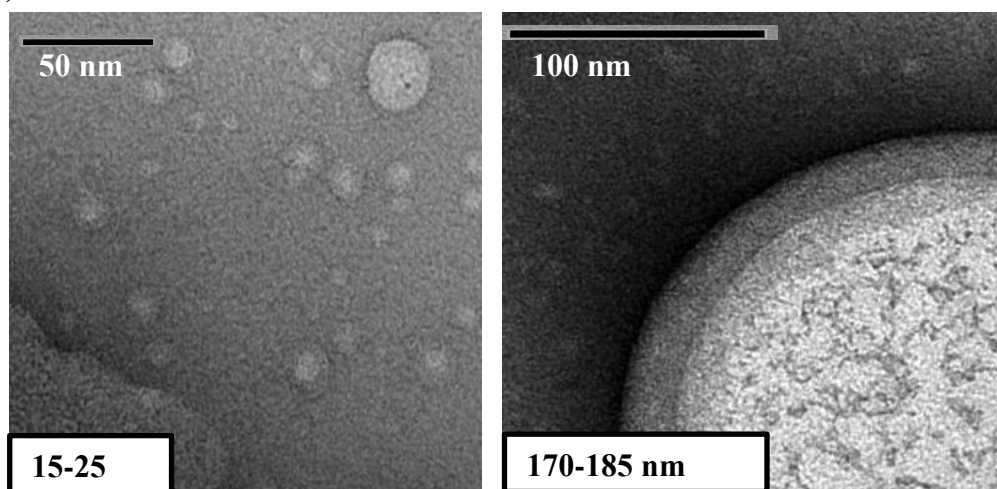


**(b)**
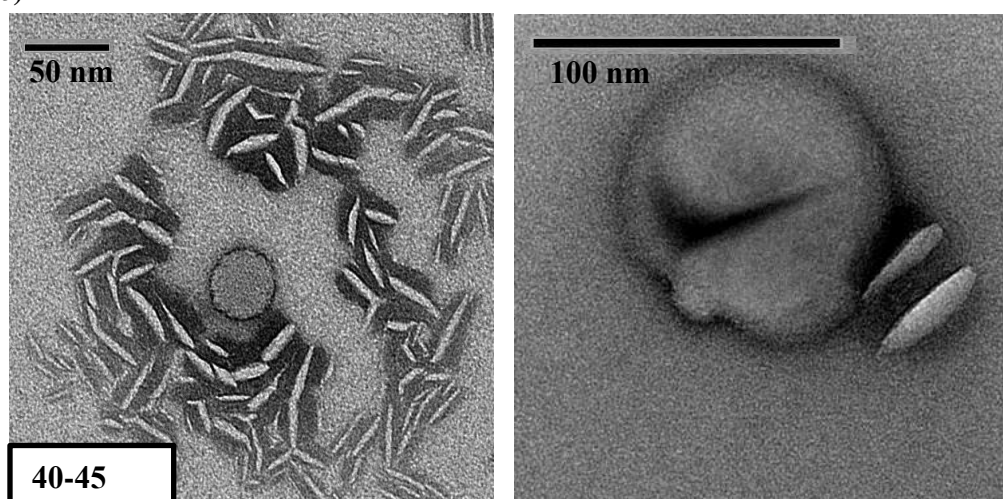


**(c)**
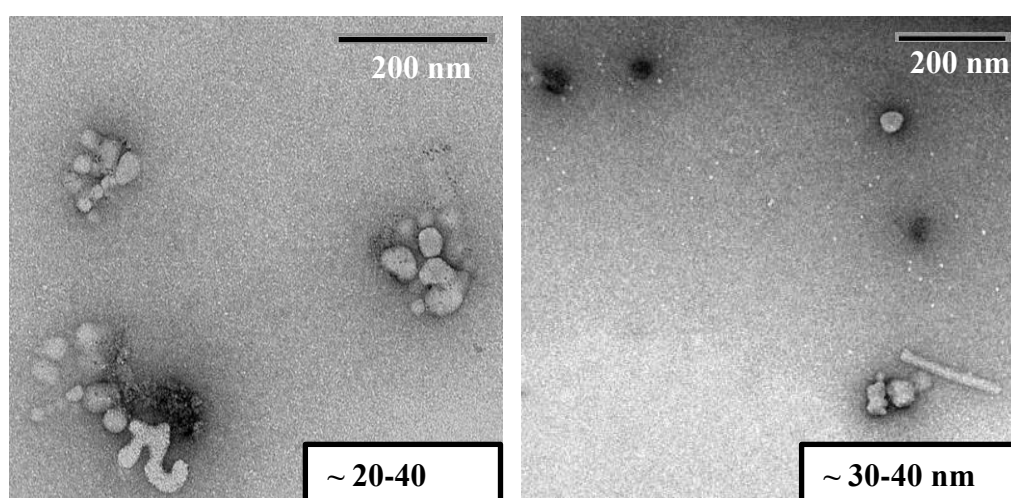


**Figure 98** – A figure to show the TEM images for (a) mPEG-*b*-PCL$_{10}$ at 0.3mg/mL (b) 3, 5 dihydroxyphenyl porphyrin macrocycle encapsulated within mPEG-*b*-PCL$_{10}$ at 0.3mg/mL and (c) 3, 5 dihydroxyorphyrin cored hyperbranched polymer encapsulated within mPEG-*b*-PCL$_{10}$ at 0.3 mg/mL.

From the TEM images of the di-block prior to encapsulation, it is evident that there are micelles present, ranging between 15 and 25 nm. There is also a larger vesicular structures present. This could account for the large particle sizing measurements obtained via DLS. The presence of a large vesicle would lead to a high amount of scattering and even the presence of only a few larger aggregates, in comparison to smaller micelle structures, would have a significant effect upon the particle size measured. This is a potential explanation for the large values obtained from DLS analysis.

From examination of the TEM images of the di-block micelle after encapsulation of a 3, 5 dihydroxyorphyrin macrocycle, the structures visualised are larger in size than the micelles obtained prior to encapsulation, explaining the observed swelling. It is also apparent that the morphology of the structures has changed after inclusion of a porphyrin macrocycle. The observed structures deviate slightly from spherical micelles and appear as ricicle type structures, this could be a result of the occurrence of π-π stacking. In addition, there is also the presence of larger aggregates such as vesicles.

The images shown for the micelles which contain a 3, 5 dihydroxyorphyrin cored hyperbranched polymer deviate from the DLS measurements obtained. As detailed before, the micelles appear to shrink in size from analysis of the particle measurements before and after encapsulation. However, the TEM images obtained show spherical micelles which are larger in size than those without an encapsulated guest. From analysis of the TEM there are no larger aggregated species present such as the vesicles shown in **figure 98** and **99**. As a result, there would be less scattering experienced, thus explaining the smaller value obtained from DLS spectroscopy. It can therefore be concluded that the polymer is not dissolving the hydrophobic regions of the di-block polymer. As originally hypothesised, the micelles are behaving as expected and swelling in size due to the presence of the guest.

Following these results, the hyperbranched polymeric anion receptor was encapsulated and the hydrodynamic diameter was subsequently recorded. A similar result was observed, whereby the micelle structure appeared to shrink in size after introduction of the hyperbranched polymeric receptor system. This is the same observation for the porphyrin cored hyperbranched polymer guest. For the porphyrin cored system, as mentioned above, the TEM images showed that swelling occurred, despite the apparent reduction in particle size,

from DLS analysis. Therefore, TEM images were obtained for the hyperbranched polymeric anion receptor (**figure 99**).

**(a)**



**(b)**
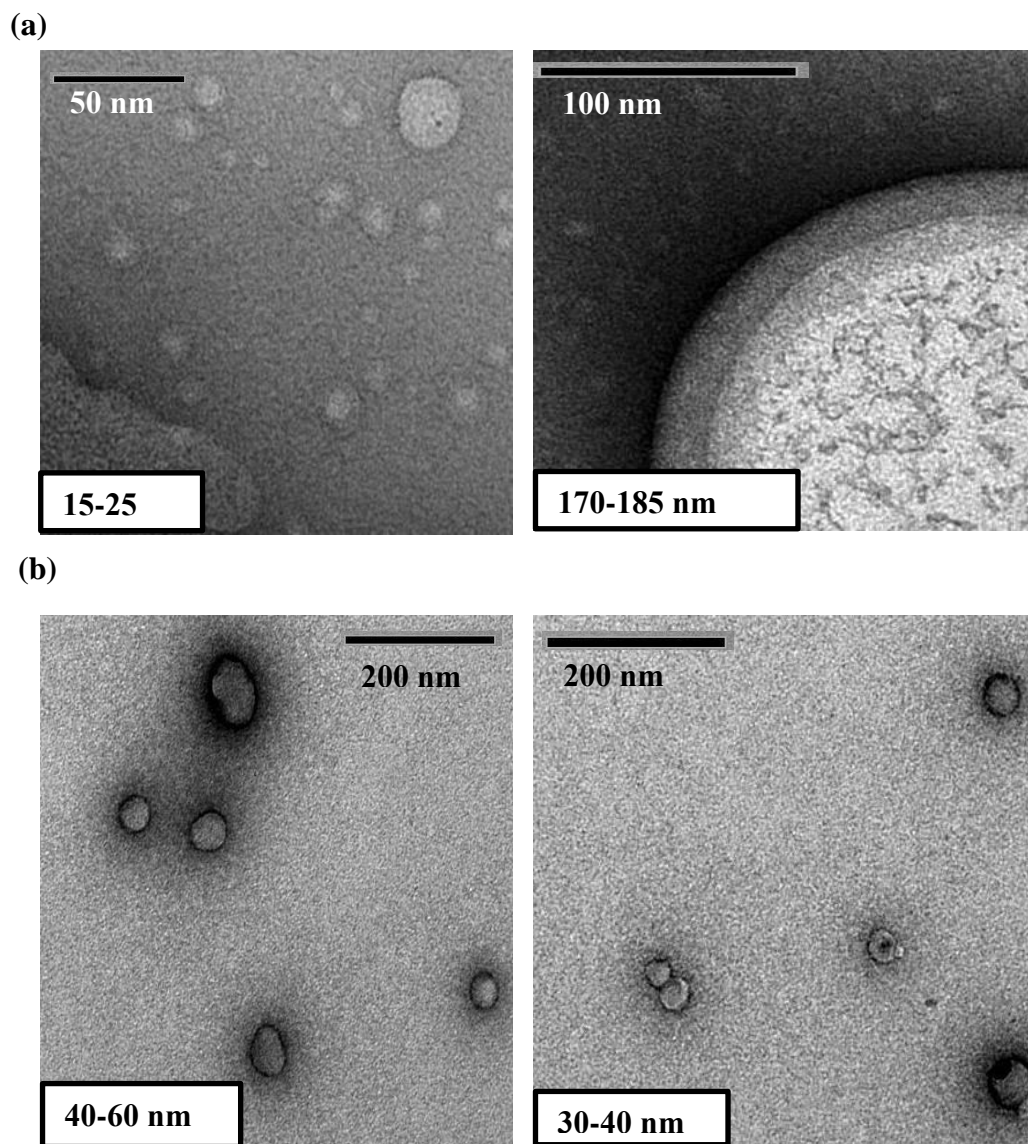


**Figure 99** – Figure to show the TEM images for (a) mPEG-*b*-PCL$_{10}$ at 0.3mg/mL and (b) hyperbranched polymeric anion receptor encapsulated within mPEG-*b*-PCL$_{10}$ at 0.3mg/mL.

From analysis of the TEM images of the micelles after encapsulation of poly-3, 5-diacetoxybenzoic acid with an anion receptor core, swelling of the micelles appears to take place. Although there is no conclusive evidence that it has been successfully encapsulated within the di-block copolymer micelle, similar results to the porphyrin cored hyperbranched

polymer are obtained. Therefore, it can be presumed that encapsulation of the anion receptor system has been successful.

## 3.7 Future work

A polymeric micelle can be used to successfully encapsulate an organic soluble species, deeming it a viable option for generating an anion receptor system. The drawback of the designed receptor is difficulty in verifying successful encapsulation within the micelle architecture. Work by Gale and Twyman[113] looked into the use of calix[4]pyrrole-4-nitrophenolate as a colourimetric anion sensor. The deep characteristic yellow colour of the 4-nitrophenolate ion (**figure 100**) ceases upon coordination with a receptor. As a result, this complex was used as a halide sensor in a displacement assay, by which the halide displaced the 4-nitrophenolate ion, regenerating the intense yellow colour to the solution.



**120**
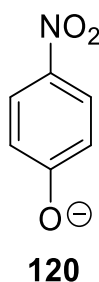
**Figure 100**– Figure to show the chemical structure of the 4-nitrophenolate anion.

It was therefore postulated that the anion receptor synthesised, pre-coordinated to 4-nitrophenolate, could be encapsulated within a polymeric micelle. Succeeding encapsulation, a similar displacement assay could be carried out, whereby an organic soluble halide anion could be introduced into the system to investigate the potential sensor capabilities of the water soluble anion receptor system. Furthermore, this would provide evidence of successful encapsulation of the receptor within the micelle. In addition to developing an effective water soluble system, the chemistry of the receptor itself can also be changed in order to develop different systems which could exhibit different selectivity. The hydrogen bonding donor group used in this research is the isophthalamide group. As discussed in the introductory section of this chapter, there are numerous different hydrogen bonding motifs which can be exploited. Therefore, structural changes to the receptor could lead to changes in anion selectivity. The results showed the hyperbranched anion receptor system (1:20) to show poor selectivity towards benzoate and acetate. It has been shown that both urea and thiourea based

receptors have been shown to provide an effective binding site for '*y-shaped*' anions such as these.[2] Therefore, this group could be utilised instead, as a way of developing a hyperbranched polymeric system which could be more selective towards benzoate and acetate over halide ions.

# 3.8 References

(1) Beer, P. D.; Gale, P. A. *Angew. Chem., Int. Ed.* **2001**, *40*, 486.

(2) Bates, G. W.; Gale, P. A. *Struct. Bonding (Berlin, Ger.)* **2008**, *129*, 1.

(3) Caltagirone, C.; Gale, P. A. *Chem. Soc. Rev.* **2009**, *38*, 520.

(4) Gale, P. A. *Chem. Soc. Rev.* **2010**, *39*, 3746.

(5) Wenzel, M.; Hiscock, J. R.; Gale, P. A. *Chem. Soc. Rev.* **2012**, *41*, 480.

(6) Park, C. H.; Simmons, H. E. *J. Amer. Chem. Soc.* **1968**, *90*, 2431.

(7) Llinares, J. M.; Powell, D.; Bowman-James, K. *Coord. Chem. Rev.* **2003**, *240*, 57.

(8) Christianson, D. W.; Lipscomb, W. N. *Accounts of Chemical Research* **1989**, *22*, 62.

(9) Puglisi, J. D.; Chen, L.; Frankel, A. D.; Williamson, J. R. *Proceedings of the National Academy of Sciences of the United States of America* **1993**, *90*, 3680.

(10) Berg, J. M. *Accounts of Chemical Research* **1995**, *28*, 14.

(11) Burlingham, B. T.; Widlanski, T. S. *J. Org. Chem.* **2001**, *66*, 7561.

(12) Haridas, V.; Sahu, S.; Praveen, K. P. P.; Sapala, A. R. *RSC Adv.* **2012**, *2*, 12594.

(13) Caputo, A.; Hinzpeter, A.; Caci, E.; Pedemonte, N.; Arous, N.; Di, D. M.; Zegarra-Moran, O.; Fanen, P.; Galietta, L. J. V. *J. Pharmacol. Exp. Ther.* **2009**, *330*, 783.

(14) Grasemann, H.; Ratjen, F. *Expert Opin. Emerging Drugs* **2010**, *15*, 653.

(15) Ito, M.; Tsuda, H.; Oguro, K.; Mutoh, K.; Shiraishi, H.; Shirasaka, Y.; Mikawa, H. *Neurochem Res* **1990**, *15*, 933.

(16) Moss, B. *Chemistry & Industry* **1996**, 407.

(17) Ojida, A.; Takashima, I.; Kohira, T.; Nonaka, H.; Hamachi, I. *J. Am. Chem. Soc.* **2008**, *130*, 12095.

(18) Davis, A. P.; Sheppard, D. N.; Smith, B. D. *Chem. Soc. Rev.* **2007**, *36*, 348.

(19) Santacroce, P. V.; Davis, J. T.; Light, M. E.; Gale, P. A.; Iglesias-Sanchez, J. C.; Prados, P.; Quesada, R. *J. Am. Chem. Soc.* **2007**, *129*, 1886.

(20) Kim, Y.; Gabbai, F. P. *J. Am. Chem. Soc.* **2009**, *131*, 3363.

(21) Graf, E.; Lehn, J. M. *J. Am. Chem. Soc.* **1975**, *97*, 5022.

(22) Lehn, J. M.; Sonveaux, E.; Willard, A. K. *J. Am. Chem. Soc.* **1978**, *100*, 4914.

(23) Carvalho, S.; Delgado, R.; Fonseca, N.; Felix, V. *New J. Chem.* **2006**, *30*, 247.

(24) Cruz, C.; Delgado, R.; Drew, M. G. B.; Felix, V. *J. Org. Chem.* **2007**, *72*, 4023.

(25) Koralegedara, M. B.; Aw, H. W.; Burns, D. H. *J. Org. Chem.* **2011**, *76*, 1930.

(26) Dietrich, B.; Fyles, T. M.; Lehn, J. M.; Pease, L. G.; Fyles, D. L. *J. Chem. Soc., Chem. Commun.* **1978**, 934.

(27) Schmuck, C. *Coord. Chem. Rev.* **2006**, *250*, 3053.

(28) Schmuck, C.; Bickert, V. *J. Org. Chem.* **2007**, *72*, 6832.

(29) Schmuck, C.; Kuchelmeister, H. Y.; *Chem. Eur. J.*: **2011**, 17, 5311

(30) Ghosh, K.; Sarkar, A. R.; Patra, A. *Tetrahedron Lett.* **2009**, *50*, 6557.

(31) Ryu, B. J.; Lee, A. L.; Lee, Y. J.; Nam, K. C. *Bull. Korean Chem. Soc.* **2009**, *30*, 3089.

(32) Bergamaschi, G.; Boiocchi, M.; Monzani, E.; Amendola, V. *Org. Biomol. Chem.* **2011**, *9*, 8276.

(33) Gong, W.-t.; Gao, B.; Bao, S.; Ye, J.-w.; Ning, G.-l. *J. Inclusion Phenom. Macrocyclic Chem.* **2012**, *72*, 481.

(34) Saha, S.; Ghosh, A.; Mahato, P.; Mishra, S.; Mishra, S. K.; Suresh, E.; Das, S.; Das, A. *Org. Lett.* **2010**, *12*, 3406.

(35) Molina, P.; Tarraga, A.; Oton, F. *Org. Biomol. Chem.* **2012**, *10*, 1711.

(36) Haridas, V.; Sahu, S.; Praveen, K. P. P. *Tetrahedron Lett.* **2011**, *52*, 6930.

(37) Haridas, V.; Sahu, S.; Venugopalan, P. *Tetrahedron* **2011**, *67*, 727.

(38) Yu, G.; Zhang, Z.; Han, C.; Xue, M.; Zhou, Q.; Huang, F. *Chem. Commun. (Cambridge, U. K.)* **2012**, *48*, 2958.

(39) Pascal, R. A.; Spergel, J.; Van, E. D. *Tetrahedron Lett.* **1986**, *27*, 4099.

(40) Shang, X.-F.; Xu, X.-F.; Lin, H.; Shao, J.; Lin, H.-K. *J. Mol. Recognit.* **2007**, *20*, 139.

(41)     Molina, L.; Moreno-Clavijo, E.; Moreno-Vargas, A. J.; Carmona, A. T.; Robina, I. *Eur. J. Org. Chem.* **2010**, 4049.

(42)     Fiehn, T.; Goddard, R.; Seidel, R. W.; Kubik, S. *Chem.--Eur. J.* **2010**, *16*, 7241.

(43)     Kim, Y. H.; Calabrese, J.; McEwen, C. *J. Am. Chem. Soc.* **1996**, *118*, 1545.

(44)     Kavallieratos, K.; de, G. S. R.; Austin, D. J.; Crabtree, R. H. *J. Am. Chem. Soc.* **1997**, *119*, 2325.

(45)     Kavallieratos, K.; Bertao, C. M.; Crabtree, R. H. *J. Org. Chem.* **1999**, *64*, 1675.

(46)     Hughes, M. P.; Smith, B. D. *J. Org. Chem.* **1997**, *62*, 4492.

(47)     Bernier, N.; Carvalho, S.; Li, F.; Delgado, R.; Felix, V. *J. Org. Chem.* **2009**, *74*, 4819.

(48)     Picot, S. C.; Mullaney, B. R.; Beer, P. D. *Chem.--Eur. J.* **2012**, *18*, 6230.

(49)     Gale, P. A. *Chem. Commun. (Cambridge, U. K.)* **2008**, 4525.

(50)     Shionoya, M.; Furuta, H.; Lynch, V.; Harriman, A.; Sessler, J. L. *J. Am. Chem. Soc.* **1992**, *114*, 5714.

(51)     Kral, V.; Furuta, H.; Shreder, K.; Lynch, V.; Sessler, J. L. *J. Am. Chem. Soc.* **1996**, *118*, 1595.

(52)     Sessler, J. L.; Barkey, N. M.; Pantos, G. D.; Lynch, V. M. *New J. Chem.* **2007**, *31*, 646.

(53)     Mani, G.; Jana, D.; Kumar, R.; Ghorai, D. *Org. Lett.* **2010**, *12*, 3212.

(54)     Bordwell, F. G.; Drucker, G. E.; Fried, H. E. *J. Org. Chem.* **1981**, *46*, 632.

(55)     Curiel, D.; Cowley, A.; Beer, P. D. *Chem. Commun. (Cambridge, U. K.)* **2005**, 236.

(56)     Lee, J.-Y.; Lee, M.-H.; Jeong, K.-S. *Supramol. Chem.* **2007**, *19*, 257.

(57)     Chang, K.-J.; Moon, D.; Lah, M. S.; Jeong, K.-S. *Angew. Chem., Int. Ed.* **2005**, *44*, 7926.

(58)     Kim, N.-K.; Chang, K.-J.; Moon, D.; Lah, M. S.; Jeong, K.-S. *Chem. Commun. (Cambridge, U. K.)* **2007**, 3401.

(59)     Gale, P. A.; Hiscock, J. R.; Jie, C. Z.; Hursthouse, M. B.; Light, M. E. *Chem. Sci.* **2010**, *1*, 215.

(60)     Smith, P. J.; Reddington, M. V.; Wilcox, C. S. *Tetrahedron Lett.* **1992**, *33*, 6085.

(61)     Fan, E.; Van, A. S. A.; Kincaid, S.; Hamilton, A. D. *J. Am. Chem. Soc.* **1993**, *115*, 369.

(62)     Li, A.-F.; Wang, J.-H.; Wang, F.; Jiang, Y.-B. *Chem Soc Rev* **2010**, *39*, 3729.

(63)     Amendola, V.; Fabbrizzi, L.; Mosca, L. *Chem. Soc. Rev.* **2010**, *39*, 3889.

(64)     Pfeffer, F. M.; Lim, K. F.; Sedgwick, K. J. *Org. Biomol. Chem.* **2007**, *5*, 1795.

(65)     Edwards, P. R.; Hiscock, J. R.; Gale, P. A. *Tetrahedron Lett.* **2009**, *50*, 4922.

(66)     Edwards, P. R.; Hiscock, J. R.; Gale, P. A.; Light, M. E. *Org Biomol Chem* **2010**, *8*, 100.

(67)     Bhardwaj, V. K.; Sharma, S.; Singh, N.; Hundal, M. S.; Hundal, G. *Supramol. Chem.* **2011**, *23*, 790.

(68)     Perez-Casas, C.; Hoepfl, H.; Yatsimirsky, A. K. *J. Inclusion Phenom. Macrocyclic Chem.* **2010**, *68*, 387.

(69)     Burkhard, P.; Tai, C. H.; Jansonius, J. N.; Cook, P. F. *J Mol Biol* **2000**, *303*, 279.

(70)     Holloway, J. M.; Dahlgren, R. A.; Hansen, B.; Casey, W. H. *Nature (London)* **1998**, *395*, 785.

(71)     Tai, C.-H.; Burkhard, P.; Gani, D.; Jenn, T.; Johnson, C.; Cook, P. F. *Biochemistry* **2001**, *40*, 7446.

(72)     Riordan, J. F. *Mol. Cell. Biochem.* **1979**, *26*, 71.

(73)     Twyman, L. J.; Beezer, A. E.; Esfand, R.; Hardy, M. J.; Mitchell, J. C. *Tetrahedron Lett.* **1999**, *40*, 1743.

(74)     Stiriba, S.-E.; Frey, H.; Haag, R. *Angew. Chem., Int. Ed.* **2002**, *41*, 1329.

(75)     Dykes, G. M. *Journal of Chemical Technology & Biotechnology* **2001**, *76*, 903.

(76)     Gorman, C. B.; Smith, J. C. *Acc. Chem. Res.* **2001**, *34*, 60.

(77)     Dandliker, P. J.; Diederich, F.; Zingg, A.; Gisselbrecht, J. P.; Gross, M.; Louati, A.; Sanford, E. *Helv. Chim. Acta* **1997**, *80*, 1773.

(78)     Irfan, M.; Seiler, M. *Ind. Eng. Chem. Res.*, **2011**, *49*, 1169.

(79)     Slagt, M. Q.; Stiriba, S.-E.; Klein, G. R. J. M.; Kautz, H.; Frey, H.; van, K. G. *Macromolecules* **2002**, *35*, 5734.

(80)     Gittins, P. J.; Alston, J.; Ge, Y.; Twyman, L. J. *Macromolecules* **2004**, *37*, 7428.

(81)     Kricheldorf, H. R.; Hobzova, R.; Schwarz, G.; Schultz, C.-L. *J. Polym. Sci., Part A: Polym. Chem.* **2004**, *42*, 3751.

(82)     Turner, S. R.; Voit, B. I.; Mourey, T. H. *Macromolecules* **1993**, *26*, 4617.

(83)     Kondo, S.; Miyata, H.; Tosoh Corp., Japan . 2006, p 6 pp.

(84)     Carey, F. A.; Sundberg, R. J.; Editors *Advanced Organic Chemistry, Part A: Structure and Mechanisms, Fourth Edition*; Kluwer Academic/Plenum Publishers, 2000.

(85)     Padmanaban, M.; Kakimoto, M.; Imai, Y. *Polym. J. (Tokyo)* **1990**, *22*, 587.

(86)     Ellis, A. PhD Thesis, University of Sheffield, 2011.

(87)     Ellis, A.; Twyman, L. J. *Macromolecules* **2013**, 46, 7055-7074

(88)     Zheng, X.; Oviedo, I. R.; Twyman, L. J. *Macromolecules (Washington, DC, U. S.)* **2008**, *41*, 7776.

(89)     Gittins, P. J.; Twyman, L. J. *J. Am. Chem. Soc.* **2005**, *127*, 1646.

(90)     Burnett, J.; King, A. S. H.; Twyman, L. J. *React. Funct. Polym.* **2006**, *66*, 187.

(91)     Marcus, Y. *J. Chem. Soc., Faraday Trans.* **1991**, *87*, 2995.

(92)     Pastor-Perez, L.; Barriau, E.; Berger-Nicoletti, E.; Kilbinger, A. F. M.; Perez-Prieto, J.; Frey, H.; Stiriba, S.-E. *Macromolecules (Washington, DC, U. S.)* **2008**, *41*, 1189.

(93)     Li, H.; Jo, J. K.; Zhang, L. D.; Ha, C.-S.; Suh, H.; Kim, I. *Langmuir* **2010**, *26*, 18442.

(94)     Lo, C.-L.; Lin, K.-M.; Huang, C.-K.; Hsiue, G.-H. *Adv. Funct. Mater.* **2006**, *16*, 2309.

(95)     Quaglia, F.; Ostacolo, L.; Nese, G.; Canciello, M.; De, R. G.; Ungaro, F.; Palumbo, R.; La, R. M. I.; Maglio, G. *J. Biomed. Mater. Res., Part A* **2008**, *87A*, 563.

(96)     Zhang, Y.; Li, X.; Zhou, Y.; Wang, X.; Fan, Y.; Huang, Y.; Liu, Y. *Nanoscale Res. Lett.* **2010**, *5*, 917.

(97)     Wang, J.; Wang, Y.; Liang, W. *J. Controlled Release* **2012**, *160*, 637.

(98)     Nam, Y. S.; Kang, H. S.; Park, J. Y.; Park, T. G.; Han, S.-H.; Chang, I.-S. *Biomaterials* **2003**, *24*, 2053.

(99)     Nishiyama, N.; Bae, Y.; Miyata, K.; Fukushima, S.; Kataoka, K. *Drug Discovery Today: Technol.* **2005**, *2*, 21.

(100)    Liu, G.-Y.; Lv, L.-P.; Chen, C.-J.; Hu, X.-F.; Ji, J. *Macromol. Chem. Phys.* **2011**, *212*, 643.

(101)    Cheng, D.; Hong, G.; Wang, W.; Yuan, R.; Ai, H.; Shen, J.; Liang, B.; Gao, J.; Shuai, X. *J. Mater. Chem.* **2011**, *21*, 4796.

(102)    Diao, Y.-Y.; Li, H.-Y.; Fu, Y.-H.; Han, M.; Hu, Y.-L.; Jiang, H.-L.; Tsutsumi, Y.; Wei, Q.-C.; Chen, D.-W.; Gao, J.-Q. *Int. J. Nanomed.* **2011**, *6*, 1955.

(103)    Yang, R.; Meng, F.; Ma, S.; Huang, F.; Liu, H.; Zhong, Z. *Biomacromolecules* **2011**, *12*, 3047.

(104)    Hong, G.-B.; Zhou, J.-X.; Yuan, R.-X. *Int. J. Nanomed.* **2012**, *7*, 2863.

(105)    Loverde, S. M.; Klein, M. L.; Discher, D. E. *Adv. Mater. (Weinheim, Ger.)* **2012**, *24*, 3823.

(106)    Miller, T.; Rachel, R.; Besheer, A.; Uezguen, S.; Weigandt, M.; Goepferich, A. *Pharm. Res.* **2012**, *29*, 448.

(107)    Zhao, Y.; Duan, S.; Zeng, X.; Liu, C.; Davies, N. M.; Li, B.; Forrest, M. L. *Mol. Pharmaceutics* **2012**, *9*, 1705.

(108)    Wang, Z.; Yu, Y.; Ma, J.; Zhang, H.; Zhang, H.; Wang, X.; Wang, J.; Zhang, X.; Zhang, Q. *Mol. Pharmaceutics* **2012**, *9*, 2646.

(109)    Rothemund, P. *Journal of the American Chemical Society* **1935**, *57*, 2010.

(110)    Adler, A. D.; Longo, F. R.; Finarelli, J. D.; Goldmacher, J.; Assour, J.; Korsakoff, L. *J. Org. Chem.* **1967**, *32*, 476.

(111)    Adler, A. D.; Longo, F. R.; Kampas, F.; Kim, J. *J. Inorg. Nucl. Chem.* **1970**, *32*, 2443.

(112)    Huang, L.; Chen, Y.; Gao, G.-Y.; Zhang, X. P. *J. Org. Chem.* **2003**, *68*, 8179.

(113)    Gale, P. A.; Twyman, L. J.; Handlin, C. I.; Sessler, J. L. *Chem. Commun. (Cambridge)* **1999**, 1851.

# Chapter 4

# Colloidosome microcapsules as potential vehicles for catalysis

# Chapter 4 – Colloidosome microcapsules as potential vehicles for catalysis

## 4.1 Introduction

My research has predominantly involved dendritic polymers. This chapter, however, will focus on a different type of system called a colloidosome. A colloidosome, at the simplest level, can resemble an enzyme, as it is able to control a microenvironment. Enzymes can also be referred to as biological catalysts and it is the area of catalysis which will be explored in this chapter. Although it is a different type of material to those explored in previous chapters, the principles of controlling an environment are maintained. This aspect of research was carried out in collaboration with Professor Steve Armes and Dr Kate Kirkham and this chapter will provide the reader with information about this particular chemical field. The reader will also be provided with an understanding into the synthesis and potential use of colloidosomes within the area of microencapsulation.

There has been a high level of interest in colloidosomes, attributable to their potential relevance in the area of microencapsulation. These microcapsules have the ability to both store and release a wide array of different materials, making them novel vehicles for a large range of therapeutic and industrial uses. A colloidosome is a type of microcapsule whose shell is made up of colloid particles, which have been merged together. The fusing of particles within the shell provides a level of control over permeability, not to mention additional stability.[1] Customarily, the synthesis of a colloidosome involves the self-assembly of colloidal particles at the interface of two liquids which are immiscible; namely water and oil. The preliminary structures formed by self-assembly are known as Pickering[2] or Ramsden[3] emulsions, and they have been known for over a century. For an amphiphilic surfactant at an oil/water interface, the hydrophobic-lipophile balance (HLB) is a key parameter in the determination of whether an oil-in-water (o/w) or water-in-oil (w/o) emulsion is stabilised.[4] Colloidal particles, adsorbed at a liquid-liquid interface, behave similarly to surfactant molecules and the HLB number is required to determine the oil or water susceptibility of a surfactant. The contact angle, formed at the oil/water interface, is used to determine the tendency for colloidal particles. The contact angle is a measure of the wettability of the particle and can consequently be used in the determination of whether an o/w or w/o emulsion will be stabilised. For hydrophilic particles, a contact angle less than 90°

will be observed, meaning that the greater part of the particle is located in the aqueous phase. For hydrophobic particles, the opposite is encountered and a w/o emulsion is preferred.[4] This principle is illustrated below in **figure 101**.



**Oil-in-water (θ<90˚)**                    **Water-in-oil (θ>90˚)**

**Figure 101**– Representation of the emulsion formed by particles at the interface for contact angles both below and above 90˚.[4]

Colloidosome preparation involves additional stabilisation at the interface of a Pickering emulsion. The resulting microcapsule is not only more robust, but also less penetrable. **Figure 102** is a schematic illustration of the formation of a colloidosome from the self-assembly of colloidal particles. The microcapsule template is upheld when the internal oil phase is removed, due to the merging of the colloidal particles.



**Figure 102** – Schematic representation of colloidosome formation via a Pickering emulsion step.

### 4.1.1 Synthetic approaches to the formation of colloidosome microcapsules

The primary organic colloidosome-type structures were first described by Velev *et al.*[5-7] In 1996, this group reported the assembly of hollow spherical microstructures. The assembly of latex particles was brought about by means of emulsion droplets as templates. These microstructures were subsequently entitled '*supraparticles.*'[5] Velev *et al.* showed that negatively charged sulphate stabilised polystyrene particles were not competent in the stabilisation of emulsion droplets. A solution to this drawback was to sensitise the particle surface using lysine. This amino acid provided partial hydrophobicity to the particles. Surface modification allowed the particles to adsorb at the interface. A strong coagulant was employed to lock the neighbouring particles together, within the microspheres. Introduction of a coagulant allowed the aggregation of the latex particles, which in turn provided additional stabilisation; this was sufficient to allow endurance of the microcapsules when the n-octanol droplets were removed by excess ethanol.[5] Velev *et al.* went on to develop an emulsion based technique to generate 'ball-like aggregates'.[6] These aggregates arise from permeation of particles into the greater part of the oil droplets. This is achieved by increasing the hydrophobicity of the particles. Sodium dodecyl sulphate is used to encourage adsorption into the body of the droplets. As a result, the droplets are sterically protected from coalescence and the particles, assembled within, are secure. This work, combined with the scheme for hollow particles[5], led to the development of composite particles. The cores of these particles comprised of ball-like aggregates of amidine latex particles which, were enclosed by a shell of negatively charged sulphate latex particles.[5] To conclude, the final paper in this series involved a reverse system, by which latex particles were assembled around water droplets; such that water-in-oil microspheres are formed.[7]

### 4.1.1.1 Thermal annealing

Following on from the pioneering work by Velev *et al.*, there has been a great deal of interest in the synthesis of organic latex based colloidosomes; with numerous contrasting synthetic techniques having been explored. The label 'colloidosome' was first suggested by Dinsmore *et al.*[8] Dinsmore took a different approach to synthesis. The colloidosomes were generated by the process of thermal annealing. The first stage involved the preparation of microcapsules by the self-assembly of carboxylate functionalised polystyrene latex particles at the outer layer of o/w emulsion droplets. The next stage was the formation of the colloidosome shell. This was accomplished by coalescing particles together by a process called sintering. This technique involved heating the emulsion at a slightly higher temperature than the $T_g$ of the

polystyrene latex particles at approximately 105˚C. Heating resulted in the fusion of the latex particles (**figure 103**). The outcome of sintering led to a colloidosome with a specific arrangement of '*uniform holes.*' The adjustment of the sintering time can also tune the size of these interstitial gaps present.[8]
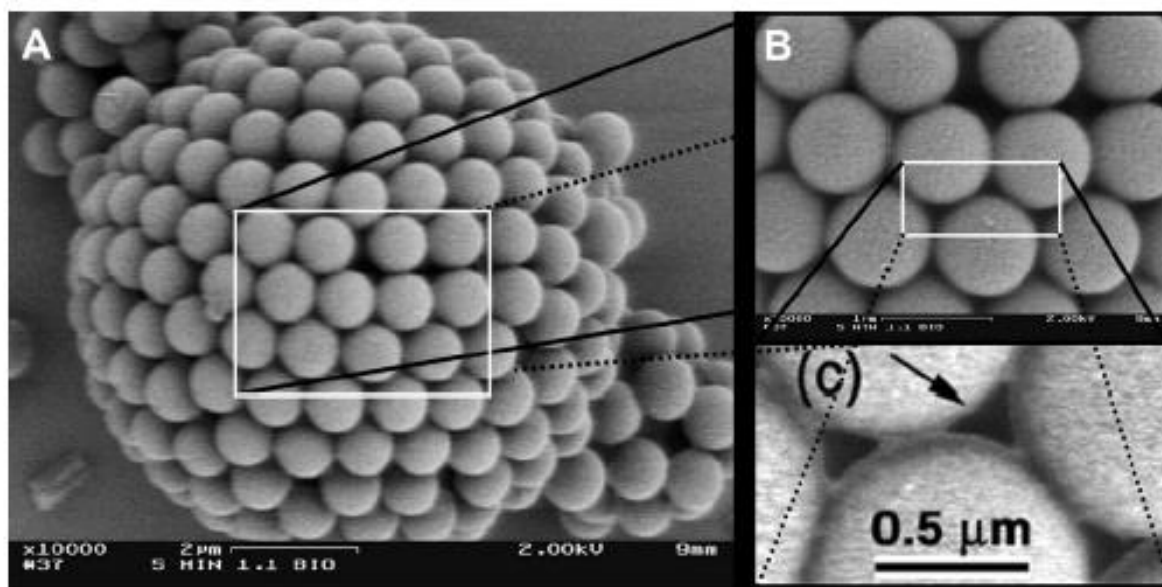


**Figure 103**– A scanning electron micrograph illustrating a 10μm '*colloidosome*' which has been assembled from an o/w emulsion droplet, comprising of 0.9μm polystyrene latex particles. The sintering procedure occurred at 105ºC for a period of 5 minutes, sufficiently fusing the particles.[8] Reprinted with permission from [Dinsmore, A. D.; Hsu, M. F.; Nikolaides, M. G.; Marquez, M.; Bausch, A. R.; Weitz, D. A., Science, **2002**, *298*, 1006-1009]. Copyright [2002] AAAS.

Progressing from this work, Routh *et al.* examined the potential in the use of copolymer colloidal particles in order to reduce the $T_g$, so as to reduce the sintering temperature required. Lowering the temperature would allow the successful encapsulation of sensitive materials. The research involved using poly (styrene-co-n-butylacrylate) colloidal particles in order to construct water-core colloidosomes under relatively mild conditions; with sintering temperatures ranging from 35 to 65ºC.[9] Following from this work, Routh *et al.* detailed the formation of colloidosomes at room temperature by exploiting colloidal instability. This was achieved by the incorporation of ethanol into the continuous oil phase. The latex particles used for this study were poly (methyl acrylate-co-n-butyl-acrylate). The addition of ethanol into the aqueous latex suspension allowed the latex particles to aggregate together.[10]

#### 4.1.1.2 Gel-trapping

Another technique which can be employed to assemble colloidosome microcapsules is gel-trapping. This approach exploits the use of an aqueous gel as the internal phase. The internal aqueous phased is gelled in order to produce a solid core. This will go on to provide support for the shell, not to mention enhance structural steadfastness and rigidity. Cayre *et al*. have employed this novel technique in the assembly of colloidosome microcapsules. Water-in-oil emulsions, stabilised by amine-functionalised polystyrene latex particles, were used to generate templates. In the aqueous phase a gelling agent was incorporated (1.5 wt.% agarose) and heating provided complete dissolution of the gel. The temperature was then lowered to room temperature, so as to set the gel. The gel core proved crucial in allowing the survival of the microcapsules during the transferral from diluted oil into water.[11] Work by Nobel *et al*. involved the same synthetic procedure, making use of agarose as a gelling agent. Research involved the synthesis of *'hairy'* colloidosomes, where the shells were comprised of microrod particles.[12] Duan *et al*. also exploited the use of gelation of an aqueous phase containing agarose in order to produce '*magnetic*´ colloidosomes from the directed self-assembly of magnetite ($Fe_3O_4$) nanoparticles.[13]

#### 4.1.1.3 Layer-by-layer deposition and polyelectrolyte complexation

As mentioned previously, Dinsmore *et al*. used thermal annealing to generate colloidosome microcapsules.[8] Work by this research group also included the use of a different technique, polyelectrolyte complexation. This work involved the electrostatic adsorption of an oppositely charged polyelectrolyte (poly-L-lysine) onto the anionic colloidosome surface. The poly-L-lysine molecules act as a bridge between neighbouring particles, therefore fixing them in place. A benefit to this synthetic approach, over sintering, is the improved flexibility in the colloidosome shell, leading to the production of microcapsules which are not only flexible, but also extremely robust.[8]

A similar approach was explored by Gordon *et al*., whereby cross-linked polystyrene latex particles were dispersed into toluene (the oil phase) and subsequently emulsified with an aqueous phase. Cationic poly-L-lysine was located in the aqueous phase and, after self-assembly of the emulsion droplets, the cationic polyelectrolyte could adsorb onto the polystyrene latex, connecting neighbouring particles together. It was then shown that these specific capsules could be inflated by osmotic pressure from the polyelectrolyte present in the aqueous droplet phase. In order to exploit this property, Gordon *et al*. used a range of

concentrations of sodium chloride solution to determine the concentration which leads to complete deflation of the microcapsule. It was shown that addition of 1M NaCl solution led to the full deflation of the microcapsules. The addition of salt therefore reduces the osmotic pressure of the polyelectrolyte in solution.[14]

There has also been work involving layer-by-layer deposition of enzyme multi-layered shells on latex particles, which could prove useful in the area of bio-catalysis.[15] Work by Fang *et al.* has followed on in this area by synthesising bio/nanoreactors through the incorporation of inorganic and magnetic nanoparticles, engulfed by multilayer polymer/enzyme shells. The enzyme used in these studies was glucose oxidase and Fang *et al* discovered that, the inclusion of silica layers on latex particles provided a higher surface area. An increase in the surface area means that adsorption of the enzyme will be increased, thus improving the catalytic activity of the bioreactor.[16]

## 4.1.1.4 Covalent cross-linking

The majority of techniques mentioned previously tend to involve the application of heat. Thermal annealing requires heat for sufficient stabilisation before emulsification. As stated earlier, Routh *et al.*[9,10] used copolymer colloidal particles in order to reduce the temperature required for sintering. In order for thermally sensitive compounds and biological materials to be successfully encapsulated within a colloidosome, without incurring any structural damage, heat is not optimal. Colloidosomes can be synthesised by covalent cross-linking which can provide sufficient locking of the structure at room temperature, without the need for any heat.

In 2003, Croll *et al.* reported the synthesis of '*tectocapsules*', which is one of the first reported examples of this method. These microcapsules involved the covalent cross-linking of poly (divinylbenzene-*alt*-maleic anhydride) microspheres with a range of polyamines. The amine functionality reacted with the anhydride group in order to generate both amide linkages and ammonium-carboxylate ionic linkages (**scheme 27**).[17]
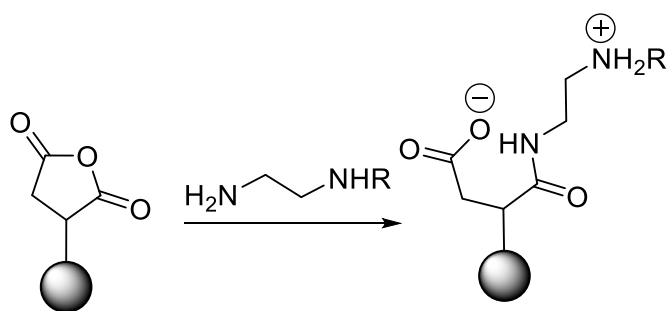
**Scheme 27** – Reaction scheme to illustrate the interaction between the anhydride functional group and the amine functional group, resulting in the formation of amide and ionic ammonium-carboxylate linkages.[17]

Recent work by Shah *et al.*, involved the fabrication of stimuli-responsive colloidosomes made from poly(N-isopropylacrylamide) microgels. Water-in-oil emulsions were prepared and were cross-linked by glutaraldehyde molecules. The amine functionalised microgels were interconnected by amine-aldehyde condensation reactions, owing to the reactive sites present at each end of a glutaraldehyde molecule[18] (**figure 104**).



**121**
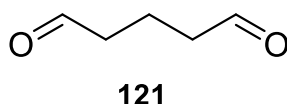
**Figure 104**– Figure to show the chemical structure of glutaraldehyde, which was used to cross-link water-in-oil emulsions of poly(N-isopropylacrylamide) microgel based colloidosomes developed by Shah and co-workers.[18]

In 2010, Thompson* *et al.* prepared poly (glycerol monomethacrylate)-based macromonomers to prepare sterically stabilised latex particles. These particles exhibited a suitable surface wettability to stabilise oil-in-water emulsions.[19] Colloidosome microcapsules were prepared by covalent cross-linking. The hydroxyl groups on the stabiliser chains within the oil droplet were cross-linked using an oil soluble cross-linker, polymeric diisocyanate (tolylene 2, 4-diisocyanate-terminated poly (propylene glycol) [PPG-TDI]. As the cross-linker was limited to the interior of the oil droplet, colloidosomes could be prepared at a high solid level (50 vol.%), without the occurrence of aggregation.[20]

*This project involved the collaboration with Dr Kate Kirkham (formally Kate Thompson) from the Armes research group at the University of Sheffield. These specific particles were utilised in research, therefore, more information regarding the preparation of these colloidosomes will be discussed in detail in section **4.3.6.4** of this chapter.*

Walsh *et al*. continued on from this work by the replacement of the hydroxyl-functionalised stabiliser with an amine-functionalised poly (ethylene imine) [PEI] stabiliser. This replacement showed that the PEI stabiliser chains could be cross-linked from both within the oil droplet (using an oil soluble cross-linker) and from the aqueous continuous phase (using a water soluble cross-linker).[21] As found in the initial study[20], use of an oil soluble cross-linker allowed colloidosome preparation to occur at 50 vol.% without aggregation. When covalent cross-linking took place from the aqueous continuous phase, similar results were observed. In both cases, colloidosome microcapsules could endure the extraction of the interior oil phase by washing with excess alcohol.[21] This project will focus on the potential novel uses of these microcapsules within the area of microencapsulation.

## 4.2 Aims and Objectives

### 4.2.1 Colloidosomes for Microencapsulation

As touched upon in the introductory section of this chapter, colloidosome microcapsules have attracted a great deal of attention owing to their promise in the area of microencapsulation. Microencapsulation is the process by which a core is confined by encircling said core in another material, termed the shell. The core can comprise of liquid droplets, solid particles or gases.[22] Microencapsulation is important in everyday life as it allows the controlled release of a variety of active ingredients in numerous sectors; some examples of these being medicine, agriculture, textiles, food and cosmetics.[23,24] The use of colloidal drug delivery systems in the biomedical field has advanced a great deal regarding diagnostics and treatment. Currently, colloidal carriers include liposomes, ethosomes, lipospheres and nanoparticles, which are used in a range of areas, such as gene delivery, tumour targeting and oral medication. A colloidosome is an alternative example of a vesicular system, offering promise in this area.[25] With a colloidosome microcapsule, one has the capability to control numerous factors such as size, permeability, mechanical strength and compatibility. The ability to control the size of microcapsules affords adaptability in applications, not to mention an option in the material which is to be enveloped. The colloidosome membrane has both an impenetrable phase (colloidal particle) and a penetrable phase (interstitial pores between particles). The ability to control the permeability of a microcapsule will enable both selective and targeted release of an active ingredient. Depending on the block co-polymer building block selected for synthesis, the mechanical strength of the colloidosome can also be governed. This will affect the mechanical load a microcapsule is able to endure. Finally, there is also the potential to manage the compatibility which facilitates the encapsulation of more sensitive entities, namely biological material. The ability to control these particular elements allows the design of specific release mechanisms, thus explaining why these microcapsules have become a prospective tool in this area.[8,25]

Encapsulation of live cells is an area which faces numerous challenges. Live probiotic bacteria, such as *Lactobacilli* and *Bifidobacteria*, have positive health effects which include competition with pathogens located in the intestine and improvement of the microbial balance.[26] In order for people to sustain a sufficient level of probiotic bacteria in the intestine, probiotics have been incorporated into food produce. A drawback to this is whether the

microorganisms sustain viability when passed through the gastrointestinal tract to the intestine, where they are required. If ingested orally, the bacteria need to be protected from the acidic conditions of the stomach, in order to have the desired effect.[26, 27] For this reason microencapsulation can be presented as a viable option and has subsequently received a considerable amount of attention. Routh *et al.* reported a method by which viable *Lactobacillus crispatus* could be encapsulated within water-core colloidosomes. The colloidosomes are made from poly (methyl methylacrylate-co-butyl acrylate) latex particles. These latex particles were fused together to form the microcapsule shell by the inclusion of a small amount of ethanol and salt to the oil continuous phase. Though slower than unencapsulated bacteria, metabolism of glucose to generate lactic acid did occur within the colloidosome. The microcapsule was subjected to conditions comparable to those within the stomach. After exposure to pH3 HCl for a period of 2 hours, the colloidosome proved effective in the protection of the live bacteria. A larger number of encapsulated bacteria remained viable under these conditions in comparison with unencapsulated bacteria.[26] Routh *et al*. also used this synthetic procedure to encapsulate yeast cells. The encapsulated baker yeast cells were able to metabolise glucose. A benefit of the colloidosome preparation, used in both cases presented, is that it does not involve high temperatures, meaning it is appropriate for encapsulation of biological material.[28]

Another application is the controlled release of active ingredients, such as dye molecules. Yow and Routh have described the preparation of colloidosomes from poly (styrene-co-n-butyl acrylate) latex particles and monitored the release of fluorescein sodium salt that has been successfully encapsulated. The sintering times were varied for water-core colloidosomes and the results showed that longer sintering times led to the fabrication of less porous shells. This gave rise to the slower release of the encapsulated active ingredients from the aqueous core. The dye release profiles show that there is not much difference for sintering times of 5 and 30 minutes. However, when the time is increased to 60 minutes, the dye was released within 24 hours, as opposed to merely a few. The dye release profiles for the water-core colloidosomes can be seen in **figure 105**. Though results show a notable improvement, this time period is not long enough for commercial applications, where months or even years would be desired retention time periods for industry.[22]
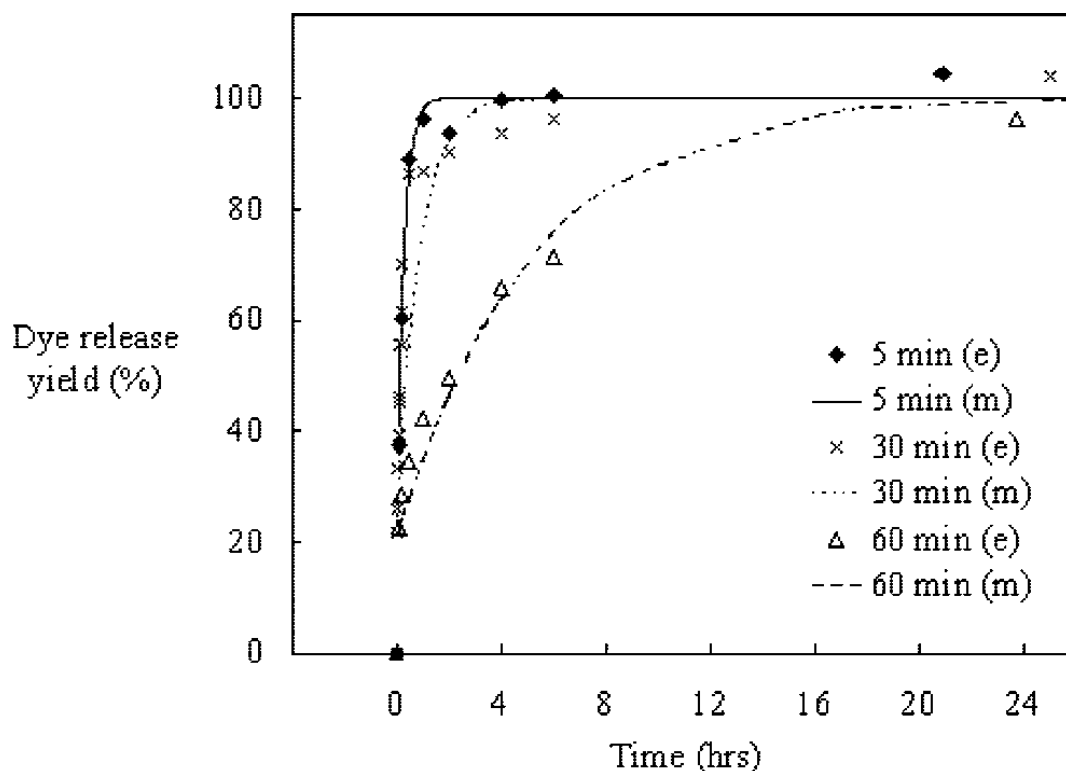
**Figure 105** – Figure to show the dye release profile for colloidosomes which have been prepared from poly (styrene-co-n-butyl acrylate) latex particles sintered at 50ºC for 5, 30 and 60 minutes. The dotted line for each time frame represents the release model (m) and the data points represent the experimental data (e).[22] Reprinted with permission from [Yow, H. N.; Routh, A. F., *Langmuir,* 2009, *25*, 159-166.] Copyright [2009] American Chemical Society.

There has been a high level of interest in using stabilisers that lead to microcapsule membranes which exhibit novel properties. For instance, as previously mentioned in the introductory section, Duan *et al.* showed the use of magnetic nanoparticles as stabilisers, meaning that colloidosome microcapsules fabricated could be influenced by an external magnetic field.[13] There has been a lot of interest in the development of colloidosome microcapsules which provide another possibility for the encapsulation and release of active ingredients, based on the chemistry of the microcapsule shell. Cayre *et al* have used pH as an external stimulus and fabricated pH responsive colloidosomes and thus reported the effect of pH upon release of actives. Cayre *et al.* have reported the use of PMMA-pDMAEMA to generate a pH responsive shell. At an acidic pH level, the amine groups, present on the pDMAEMA polymer, become protonated which subsequently leads to the extension of the polymer away from the particle surface. At an alkaline pH level, these groups become deprotonated and the chains collapse back onto the exterior of the particle. The particles were fused together by covalent cross-linking within the internal oil phase. Washing with alcohol allowed the removal of the internal oil phase and the shells were loaded with the

fluorescently labelled sugar, dextran. At low pH, as predicted, equilibrium of the sugar concentration between the microcapsule core and the continuous phase occurred. Under basic conditions, the sugar was held within the core of the microcapsule, with little seepage through the shell into the continuous phase taking place.[29] This technique has proved successful in the controlled encapsulation and release of larger molecules. One challenge which remains, however, is the retention of small molecules within colloidosome microcapsules.[30]

### 4.2.2 Colloidosomes in catalysis

As shown from the examples above, industrial and biomedical applications have received a great deal of interest. Another potential application for a colloidosome microcapsule, that is yet to be explored in detail, is catalysis. The research in this area predominantly concerns enzyme microencapsulation for bio-catalytic purposes. An enzyme is a potent biological catalyst and there is a wide variety is in existence with each one crucial to a specific organic reaction. Work by Wu *et al.*[31] has reported the use of hydrophobic silicon dioxide nanoparticles in the emulsification of aqueous solutions of various enzymes. A schematic representation of this can be seen in **figure 106**.
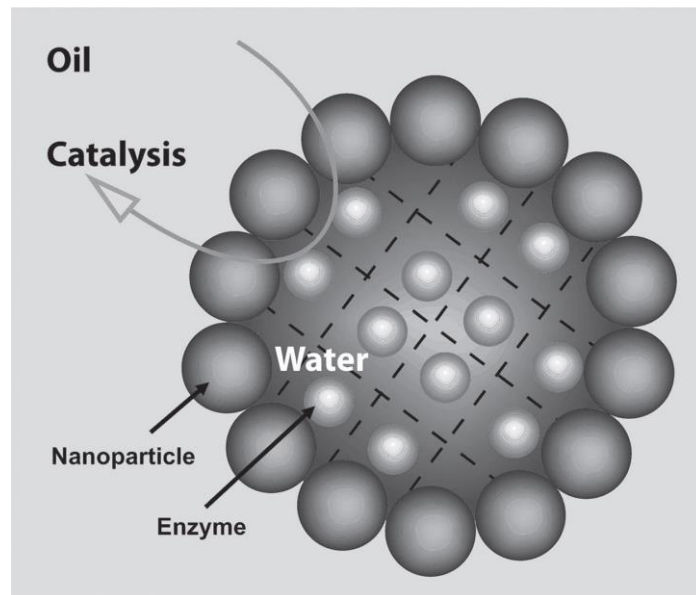


**Figure 106**– Schematic representation of a Pickering emulsion which has been stabilised by $SiO_2$ nanoparticles for enzyme catalysis. The grid is representative of the agarose gel network.[31] Reprinted with permission from [Wu, C.; Bai, S.; Ansorge-Schumacher, M. B.; Wang, D. *Adv. Mater. (Weinheim, Ger.)* **2011**, *23*, 5694] Copyright 2011 WILEY-VCH Verlag GmbH & Co. KGaA, Weinheim.

The catalytic activity of the Pickering emulsions was determined; the enzymes selected for inclusion in this study were Lipase A from *Candida antarctica* (CalA), Lipase B from *Candida antarctica* (CalB) and benzaldehyde lyase from *Pseudomonas fluorescens* Biovar I (BAL). Trimethoxy (octadecyl) silane (TMODS) was used to make the nanoparticles hydrophobic in nature so that they could be used to stabilise water-in-oil Pickering emulsions, where the aqueous core of the Pickering emulsion contained an enzyme. To facilitate fabrication and characterisation, gel-trapping with agarose gel was the synthetic technique used. CalB, when incorporated within a Pickering emulsion, showed activity of approximately 300 times more elevated than in its native state in a biphasic system. Cal A showed an enhanced catalytic performance of around 100 times compared to free enzyme, as demonstrated in the literature.[31-33] The most sensitive enzyme to be analysed, BAL, showed an enhancement in catalytic activity of around 4.5 times that of native BAL in a biphasic system. Though all enzymes tested display enhanced catalytic performance, the gel-trapping method utilised has a drawback. Though still higher than each enzyme in its native state, upon gelling with agarose, catalytic performance dropped, therefore synthetic modifications must be made in order to avoid the intraparticle diffusion constraints brought about by the agarose network.[31,34]

Wang *et al.*[35] continued work in this area by the investigation into stabilising Pickering emulsions through the use of hollow nanoparticles. The project involved the use of poly (ethylene glycol)-co-b-poly-(styrene-co-3-isopropenyl-α, α-dimethyl benzylisocyanate) (**figure 107**).
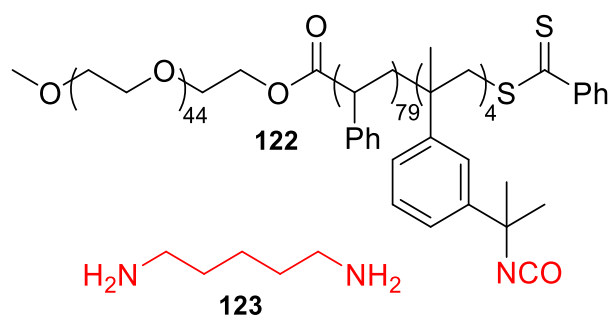
**Figure 107 –** Figure to show the chemical structure of the block copolymer building block (black) with the isocyanate moiety (red) and the chemical structure of the cross-linking agent (red).[35]

This polymer can be cross-linked through the isocyanate functionality present within the hydrophobic region. The enzyme selected for this study was CalB, which was encapsulated within the central cavity of the colloidosome. The enzyme was not only able to withstand purification in between each reaction cycle, but also sustain catalytic activity. An advantage to this method is the facilitation in separating the enzyme from both substrates and products, not to mention, the evident reusability of the enzyme. Furthermore, due to the particular arrangement of a polymersome stabilised Pickering emulsion, a system with different chambers is generated. Therefore, it is plausible that an array of different enzymes could be encapsulated, giving rise to the potential use of these systems for cascade reactions.[35] Previous work within the Twyman group has looked at the use of catalysis as a tool to probe encapsulation properties of dendritic polymers and we were interested, following discussions with Professor Steve Armes, to use this knowledge and study similar effects in colloidosomes.

### 4.2.3 Project motivation

Encapsulation has been described previously in chapter 3 and this theme is continued, in collaboration with Professor Steve Armes. The majority of research in the area of catalysis predominantly involves bio-catalysts; therefore, this project will focus on synthetic catalysts and using catalysis as a tool to probe the encapsulation properties of a colloidosome. As the control of a microenvironment is integral in a catalytic environment, a colloidosome appears to be a suitable tool for this purpose. This project involves the collaboration with Professor Steve Armes and Dr Kate Kirkham. Professor Armes works in the area of polymer and colloid chemistry at the University of Sheffield and has developed a prestigious reputation worldwide within this area of chemistry. Dr Kirkham played an integral role in the Armes

research group, specialising in covalently cross-linked colloidosomes.[19-21] Work within the Twyman group has involved the use of metalloporphyrin molecules as catalysts for a variety of chemical reactions[36-39] and so the expertise from both research groups was combined. Colloidosomes have proven to be successful in enzyme catalysis within an organic media.[31,35] As water is the most abundant solvent available and also non-toxic, it has been proposed to attempt catalysis using oil-in-water emulsions. The main objective for this project is to perform a reaction whereby the substrate is oil soluble but the product is water soluble, thus enabling it to pass out of the colloidosome and into the surrounding bulk water. A schematic representation of the ultimate aim of this project can be seen in **scheme 28**.
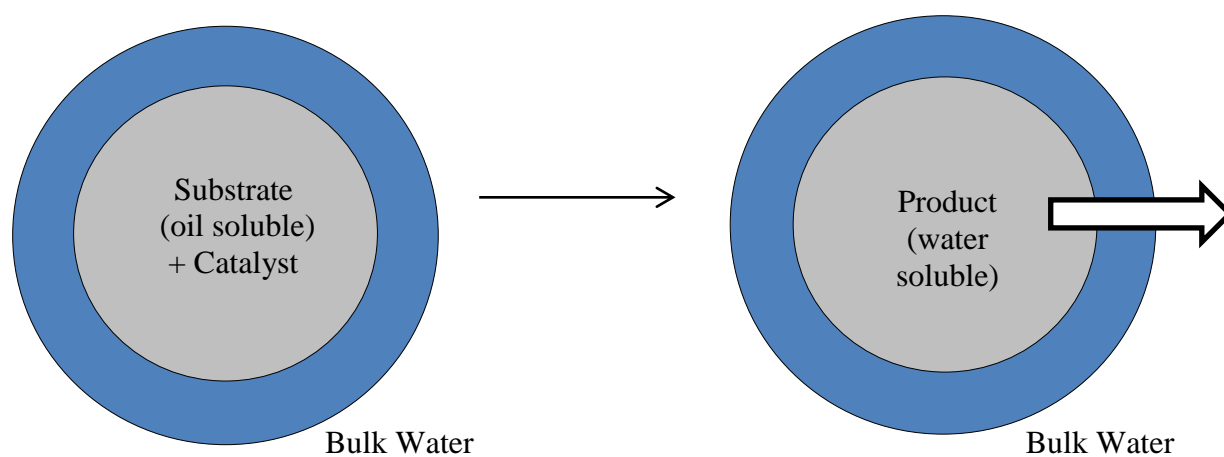


**Scheme 28 –** Schematic representation of the generation of a water soluble product from an oil soluble substrate, resulting in release of product into bulk water

## 4.3 Results & Discussion

### 4.3.1 Identification of a reaction and suitable catalyst

As identified in the aims and objectives of this research, catalysis will be used to probe encapsulation properties of a colloidosome structure. The ultimate goal is the development of a system where a substrate is oil soluble and, upon catalysis within the central cavity of the colloidosome, a water soluble product is fabricated and released into the aqueous phase.

The initial stage is to identify both a plausible reaction and appropriate catalyst, which fits the criteria set out in the aims of this project. As mentioned previously, there is a lot of experience in the Twyman group with porphyrin chemistry.[37, 38, 40-44] A porphyrin is a heterocyclic macrocycle, comprising of four pyrrole units. Each pyrrole unit is connected to another by the α-carbon atoms, interlinked by a methine bridge. The structure of porphine can be seen in **figure 108**. It depicts the heterocyclic ring structure made up of four pyrrole subunits and is the basic unit for a porphyrin macrocycle. Porphyrins possess 18 delocalised electrons, therefore obeying Hückels rule for aromaticity. This rule states that a cyclic molecule will exhibit aromatic behaviour when the number of Π electrons equates to $4n + 2$ (when $n \geq 0$).



**124**
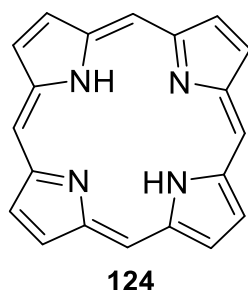
**Figure 108 –** Figure to show the chemical structure of Porphine, which is the basic unit of a porphyrin macrocycle.

Porphyrins have the ability to act as host molecules. This is a direct result of the central cavity present, which can accommodate a variety of metal ions. This host-guest potential allows metalloporphyrins to be applied as catalysts for a wide range of contrasting chemical reactions. There has been a vast level of interest in the area of catalysis using a wide array of metalloporphyrins. For further information, the reader is directed to the following pieces of literature which explore the recent development in this field.[45-49] Due to the extensive level of

experience and expertise in the synthesis and chemistry of this particular class of molecules, it was decided that this type of molecule would be used as a catalyst. Work by Evans and Smith showed oxidation of ethylbenzene using an iron porphyrin catalyst to generate a range of oxidation products; one of which was benzoic acid, which is water soluble (**scheme 29**).[50]
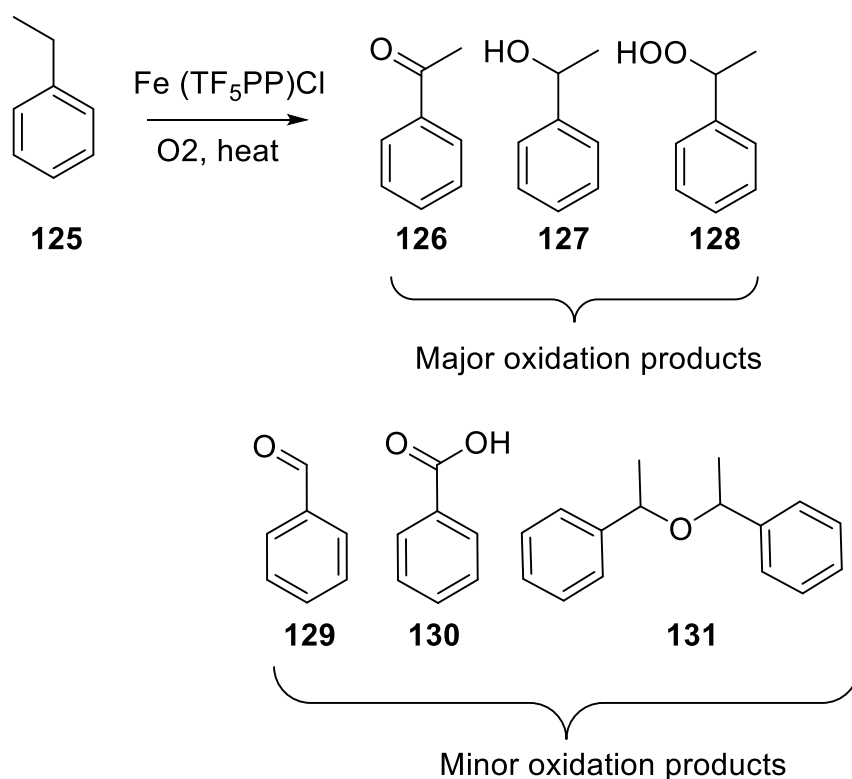


**Scheme 29 –** Oxidation of Ethyl benzene, indicating the major and minor oxidation products generated.[50]

Evans and Smith used a solvent free system, where ethylbenzene behaved as both substrate and solvent.[50] For the purpose of encapsulation within a colloidosome, the solvent needed is dodecane. Therefore, the porphyrin catalyst used must be oil soluble. It was hypothesised that, by adding long, non-polar alkyl chains to the periphery of a porphyrin, dissolution could be achieved. This would improve the lipophilicity, thus improving solubility of the macrocycle in oil. The proposed iron porphyrin catalyst is shown in **figure 109**.
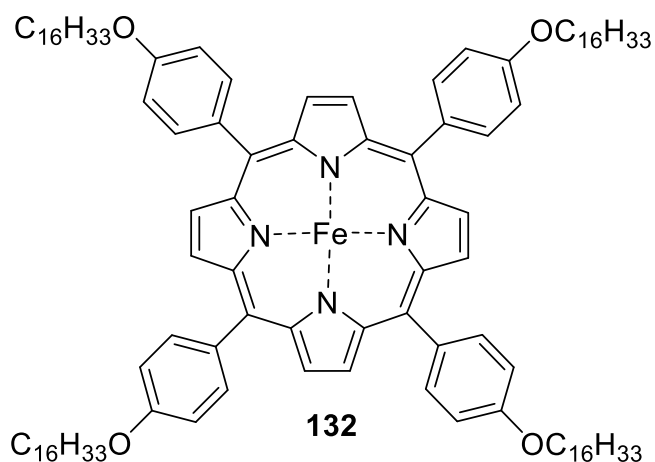
**Figure 109** – Figure to show the proposed chemical structure of the 5, 10, 15, 20-Tetra(4-hexadececycloxyphenyl)porphyrin iron catalyst.

### 4.3.2 Synthesis of 5, 10, 15, 20-Tetra(4-hexadececycloxyphenyl)porphyrin

### 4.3.2.1 Synthesis of 4-(hexadecyloxy) benzaldehyde

The initial stage in the synthesis of the oil soluble porphyrin is the preparation of the aldehyde starting material. The introduction of non-polar alkyl chains is accomplished by alkylating the aldehyde starting material, prior to porphyrin assembly. A hexadecyl chain is attached to 4-hydroxybenzaldehyde via the Williamson reaction. The reaction of an alcohol functional group with n alkyl halide to generate an ether bond is widely known as the Williamson ether synthesis.[51]

A mixture of 4-hydroxybenzaldehyde, bromohexadecane and potassium carbonate was dissolved in anhydrous acetonitrile and refluxed for a period of 3 days (**scheme 30**). Upon completion of reflux, the reaction mixture was concentrated, via rotary evaporation, and dissolved in diethyl ether and water (1:1). The organic layer was washed primarily with saturated sodium hydrogen carbonate solution followed by brine solution. The organic layer was collected and dried over magnesium sulphate prior to concentration, generating the crude product. Purification was accomplished by column chromatography using an eluent of petroleum ether 40-60 and ethyl acetate (20: 1).
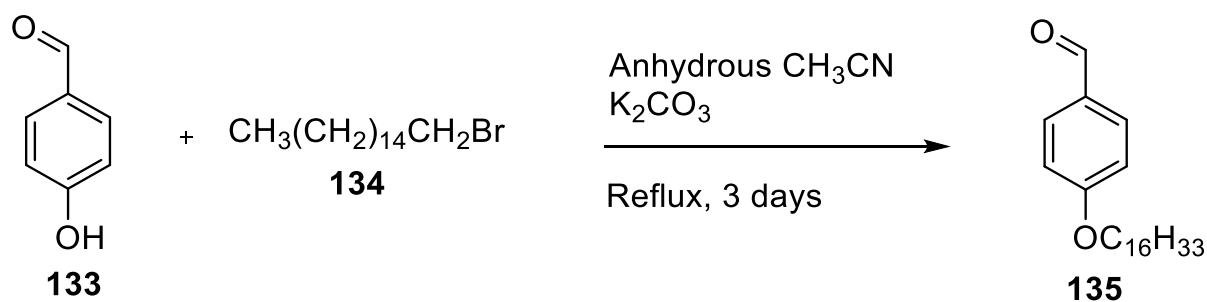
**Scheme 30** – Synthesis of 4-(hexadecyloxy) benzaldehyde.

The desired product could be visualised by UV due to the aromatic system present; under UV only one spot could be visualised. After staining with anisaldehyde a few impurities could be visualised. The desired product had an $R_f$ value of 0.83 and showed good separation from the impurities, facilitating purification.

Validation of the desired product was achieved from the use of a variety of analytical techniques. Elemental analysis showed results less than 0.5% of the expected values, giving confidence in the purity of the sample. $^1$HNMR was an essential tool in proof of the purity of the aldehyde (**figure 110**). The spectrum showed a singlet at 9.87 ppm, specific to an aldehyde functional group. Two doublets could be visualised at 6.97 and 7.81 ppm for the Phenylic ortho and meta protons respectively, with each doublet showing a coupling constant of $9H_z$. There is a triplet seen at 4.02 ppm which corresponds to the methylene group, neighbouring the oxygen atom on the $-OC_{16}H_{33}$ chain. The methylene group next to this gives a multiplet at 1.80ppm, integrating to 2 protons. The remaining 26 $CH_2$ protons in the alkyl chain show a series of multiplets from 1.20 to 1.50 ppm, attributable to the proximity in chemical shift of each pair and the coupling patterns generated. A triplet can be seen at 0.87ppm which integrates to 3 protons. This signal arises from the methyl group present at the end of the alkyl chain substituent.
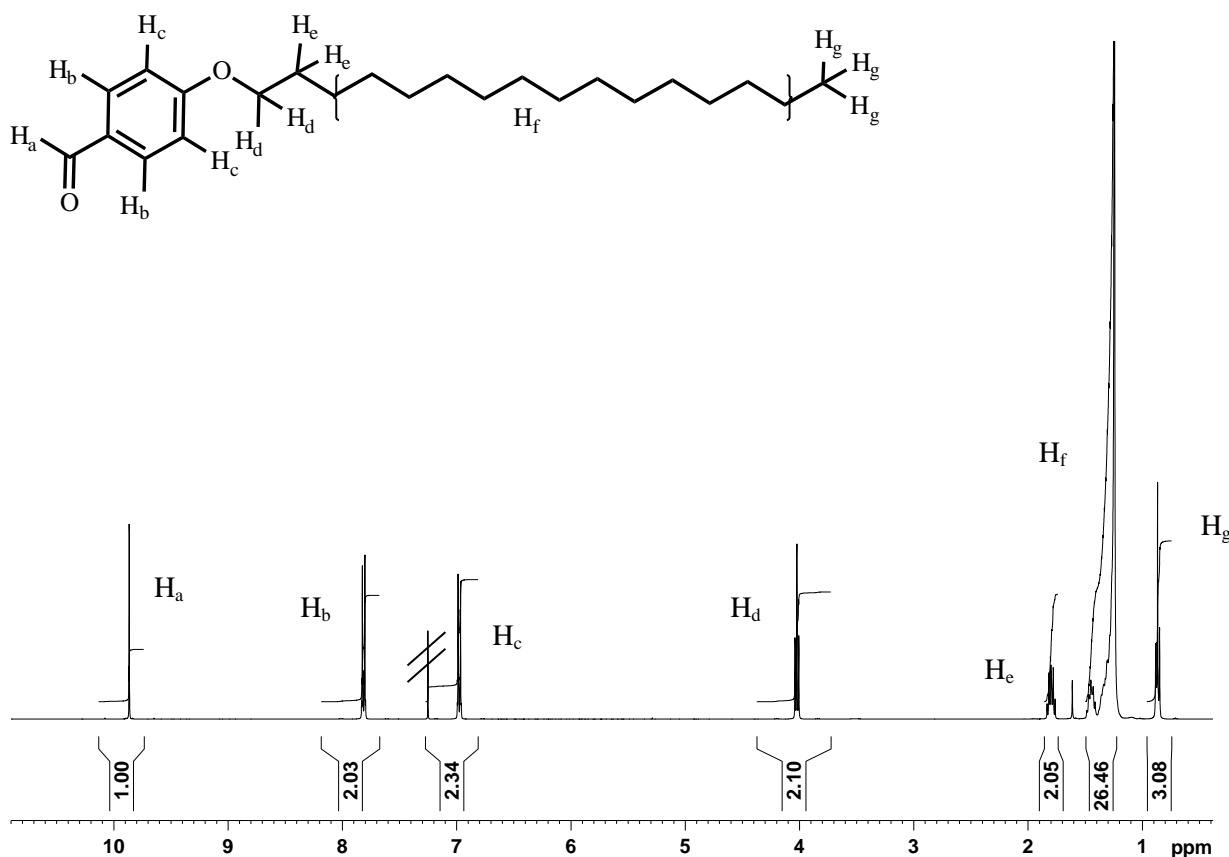
**Figure 110** – Figure to show the $^1$HNMR spectrum for 4-(hexadecyloxy) benzaldehyde showing the different proton environments present within the compound. Deuterated chloroform solvent gives a signal at 7.25ppn, which is highlighted.

In addition, the mass spectrum showed a peak at 347 which was indicative of the MH$^+$ ion. The combination of these techniques with $^{13}$C NMR and IR gave confidence in the success of the synthetic procedure and the purity of the aldehyde required for porphyrin assembly.

**4.3.2.2 Synthesis of 5, 10, 15, 20- tetrakis (4-hexadececycloxyphenyl) porphyrin**

With aldehyde preparation complete, the next step is the construction of the porphyrin macrocycle. There are numerous different approaches to porphyrin synthesis; the Lindsey method, the Rothemund method and the Adler method. The Rothemund and Adler methods will be discussed at a later point in this chapter for the synthesis of different porphyrin macrocycles. For this particular macrocycle the Lindsey method was adopted. In 1979, Lindsey and co-workers established a synthetic procedure for the assembly of a porphyrin under relatively mild reaction conditions. The initial stage of this approach is the acid catalysed condensation between the aldehyde in question and pyrrole at room temperature.[52] Lindsey investigated a variety of Lewis and Brønsted acid catalysts and discovered that the condensation step is highly sensitive to the catalyst used. A survey performed showed that 35

out of 45 acids tested produced TPP with a yield ranging from 5-58%.[53] Lindsey and co-workers also discovered the potential of co-catalysis with ethanol and Boron trifluoride diethyl etherate. Co-catalysis using these reagents showed enhanced yields in porphyrin assembly.[54] For the synthesis of 5, 10, 15, 20 – tetrakis (4-hexedececycloxyphenyl) porphyrin the co-catalysis approach was employed. Acid catalysis condensation results in the generation of a porphyrinogen intermediate. The next step of the synthetic procedure is the introduction of an oxidant. This results in the generation of the porphyrin via $6e^-/6H^+$ oxidative dehydrogenation of the intermediate.[52] The oxidant employed for the synthesis of the oil soluble polymer was 2, 3 – Dichloro-5, 6-dicyano- $p$-benzoquinone (DDQ). There are both advantages and disadvantages to this method. Whilst it gives a higher yield of porphyrin in comparison to other methods, it requires dilute concentrations of both aldehyde and pyrrole. Dilution is essential as it lessens the competition between the oligomerisation of pyrromethanes and cyclisation to yield the porphyrinogen intermediate. The synthetic steps for porphyrin formation can be found overleaf in **scheme 31**.
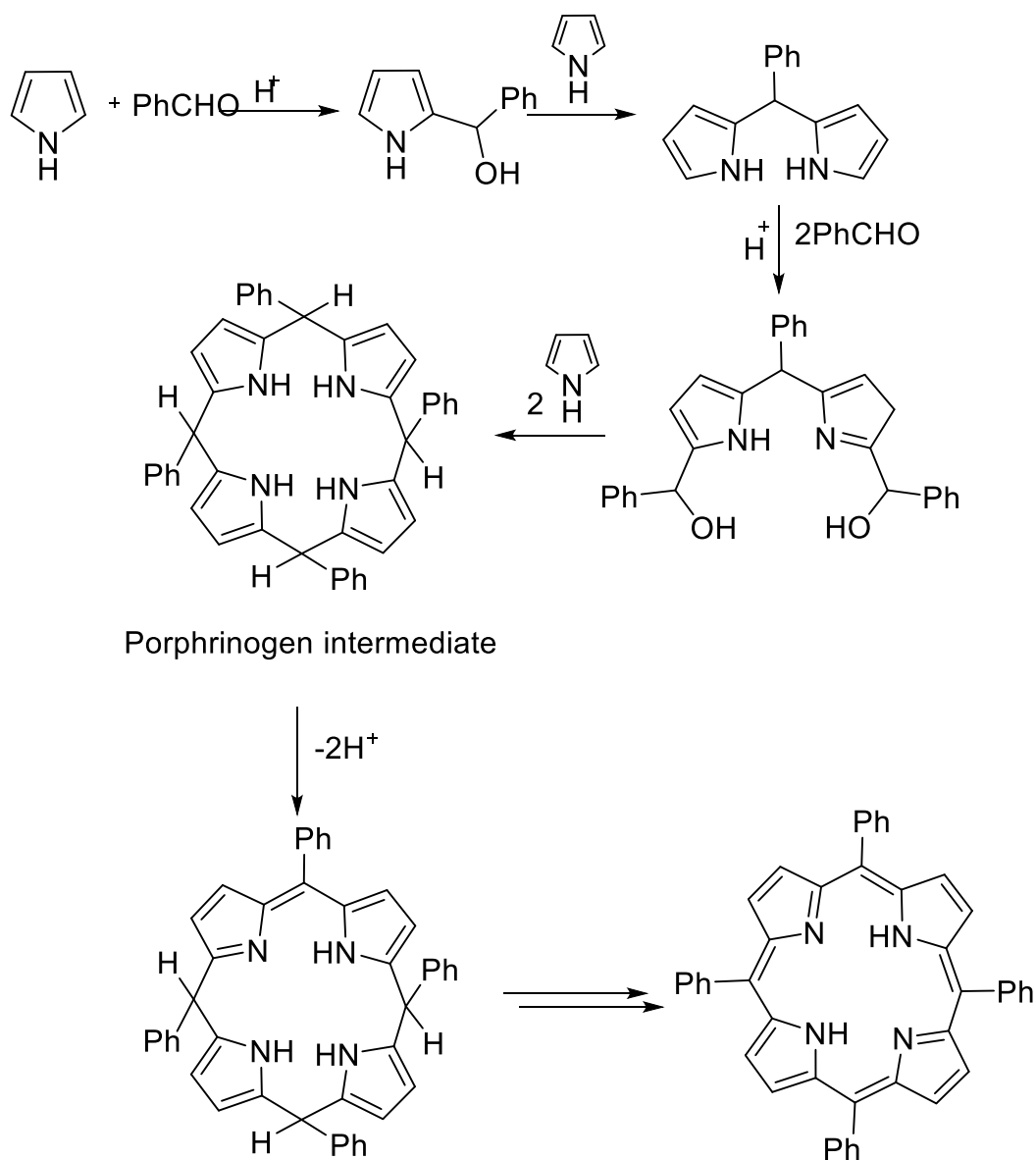
**Scheme 31**– Steps involved in the synthesis of a porphyrin

A 3-neck round bottom flask was charged with equal molar quantities of 5, 10, 15, 20 tetrakis (4-hexadececycloxyphenyl porphyrin) and pyrrole, dissolved in 300 mL of anhydrous dichloromethane at room temperature, under an atmosphere of Argon. Boron trifluoride diethyl etherate and a catalytic amount of anhydrous ethanol were added to the solution and stirred for 1 hour in an inert gas stream. This was followed by the addition of 2, 3-dichloro-5, 6-dicyano-*p*-benzoquinone (DDQ) at room temperature. The reaction mixture was then stirred for an additional hour. Purification was accomplished by, firstly, using flash chromatography and then column chromatography, eluting with chloroform, to generate the desired porphyrin. The synthetic procedure can be visualised in **scheme 32a**.
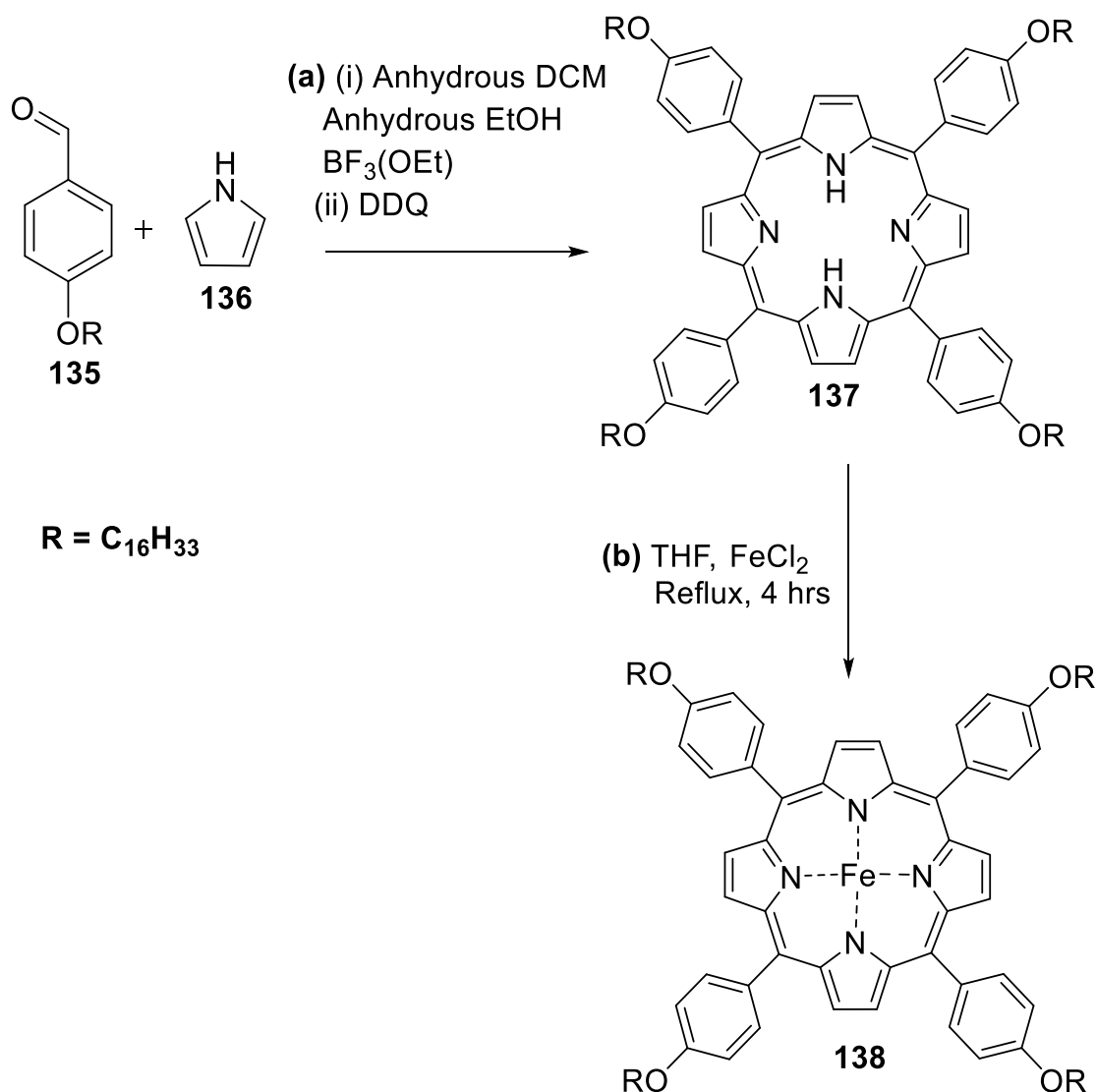
**Scheme 32** – (a) synthetic procedure for 5, 10, 15, 20 tetrakis (4-hexadececycloxyphenyl) porphyrin (b) synthetic procedure of 5, 10, 15, 20 – tetrakis (4-hexadececycloxyphenyl) – porphyrin complex, which is used as the catalyst for the oxidation of cyclooctene in dodecane solvent.

Authentication of the product was accomplished by use of a wide array of analytical techniques. Elemental analysis gave results less than 0.5% of the expected values, providing assurance in the purity of the sample. Another important tool used for the characterisation of this macrocycle was $^1$HNMR. The spectrum showed a singlet at 8.80 ppm, representative of the pyrrolic protons of the macrocycle. Two doublets can be seen at 7.30 and 8.14 ppm which denote the ortho and meta methylene protons present on the phenyl ring substituents. A triplet can be seen at 4.30 ppm, which relates to the methylene group, next to the oxygen atom on the $-OC_{16}H_{33}$ chain. The methylene group, neighbouring this methylene unit, gives a multiplet at 2.01 ppm, integrating to 2 protons. The remaining $CH_2$ protons in the alkyl chain

show a series of multiplets from 1.23 to 1.73 ppm, because of the closeness in chemical shift of each pair combined with the coupling patterns generated. A triplet can be seen at 0.91 ppm which integrates to 12 protons. This signal is indicative of the methyl groups present at the end of the alkyl chain substituent on each of the phenyl rings. Finally, a singlet can be seen at -2.72 ppm, representative of the highly shielded NH protons located at the centre of the macrocycle. MALDI-TOFF mass spectrometry showed a peak at 1575.4, which represents the MH$^-$ ion. This analytical data, in combination with a UV/Vis soret band at 423 nm and Q bands at 520, 557, 593 and 651 nm, confirms that the product is analytically pure.

## 4.3.2.3 Synthesis of 5, 10, 15, 20-tetrakis (4-hexadececycloxyphenyl)-porphyrin Iron(III) Complex

The porphyrin catalysis required for the epoxidation of cyclooctene requires a central iron atom in order to function. The insertion of iron into the porphyrin macrocycle was achieved by the reaction of a large excess iron (II) chloride (**scheme 32b**). The porphyrin, along with 2, 6-lutidine, were dissolved in anhydrous tetrahydrofuran and a large molar excess of iron (II) chloride was added and the reaction mixture was refluxed for a total of four hours. On completion, the mixture was exposed to air and cooled. This process allowed oxidation of Fe$^{(II)}$ to the desired Fe$^{(III)}$ oxidation state. The crude reaction mixture was filtered to remove unreacted iron (II) chloride and reduced via rotary evaporation. Following filtration, the mixture was dissolved in dichloromethane and washed repeatedly with 1M hydrochloric acid solution. After each wash impurities were formed at the solvent interface, these were subsequently removed via vacuum filtration. After performing an acid wash, purification was completed using column chromatography. The eluent used was a 3:1 ratio mixture of dichloromethane and methanol. The mass spectrum showed a molecular ion peak at 1631 which was indicative of the MH$^+$ ion. The product was validated by UV/Vis spectroscopy. The spectrum displayed noteworthy broadening of the soret band, at 412 nm, and a reduction in the number of Q bands, from four to two; both effects are anticipated for an iron porphyrin macrocycle. These effects can be seen from the UV spectra shown in **figure 111**.
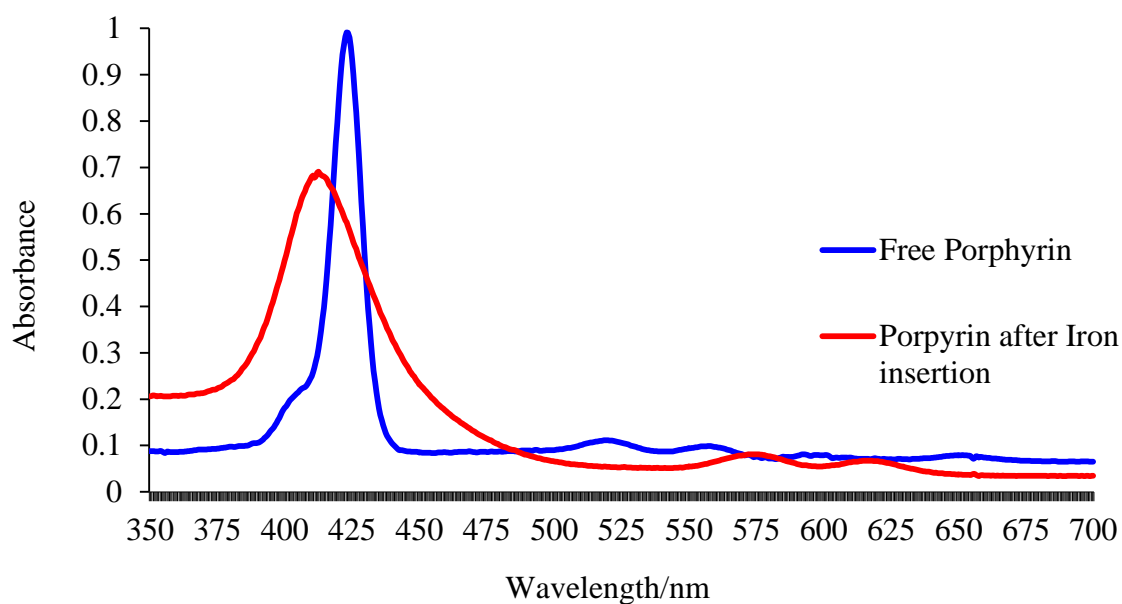
**Figure 111 –** Figure to show the UV/Vis spectral overlay of the free porphyrin (blue) and the porphyrin, after insertion of an iron metal centre (red).

Nuclear magnetic resonance spectroscopy was not possible for both proton and carbon. The spectrometer was not capable of locking the solvent, which was a result of the paramagnetic nature of the iron centre. The lack of complete characterisation, albeit not desirable, is not crucial to product identification. Consequently, the NMR spectra for both proton and carbon have been excluded from the experimental chapter.

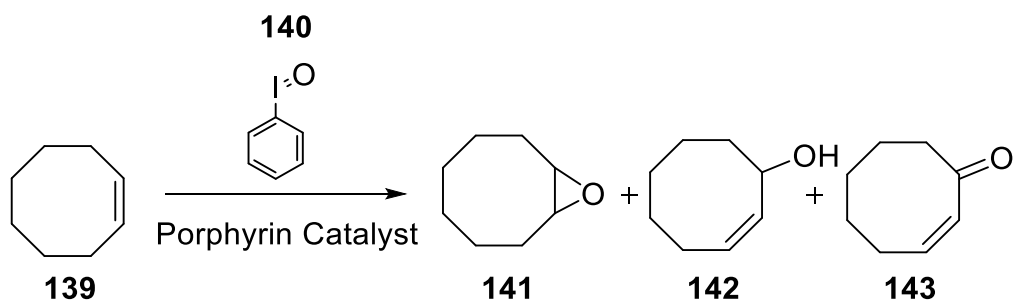### 4.3.3 Oxidation of ethylbenzene

### 4.3.3.1 Catalysis Quantification

As discussed in section **4.3.1**, the chemical reaction selected is the oxidation of ethylbenzene (**scheme 29, page 198**). Gas chromatography was the tool used to measure the extent of the oxidation reaction. Before the extent of reaction could be quantified, it was first important to run standards through the instrument. Highly pure GC grade products, purchased from Sigma Aldrich, were obtained. GC plots for each of the oxidation products and ethylbenzene starting material were attained at the appropriate concentration. This allowed the yield of each oxidation product to be calculated, as the area of each standard GC plot represents 100% of the relative product.

### 4.3.3.2 Control reaction in dodecane

An initial reaction was required to test the efficacy of the porphyrin catalyst and solvent for this type of oxidation reaction. A reaction flask was charged with ethylbenzene (20 mg, $2x10^{-4}$ mol), the iron porphyrin catalyst (3mg, $2x10^{-6}$ mol) and dodecane. The reaction was heated to 70 ºC and stirred in a constant stream of dioxygen for a period of 7 hours. Upon completion, the reaction mixture was filtered through a Whatman® GD/X syringe filter, with a pore size of 0.45 μm, directly into a GC vial. The sample was run through the chromatogram, where the procedure upheld a temperature of 50 ºC for five minutes. This then rose to 250 ºC over a period of 20 minutes. From analysis of the GC trace generated, the reaction did not appear to be successful. Ethylbenzene remained unreacted, suggesting that the catalyst and the solvent are not appropriate for this particular type of oxidation reaction.
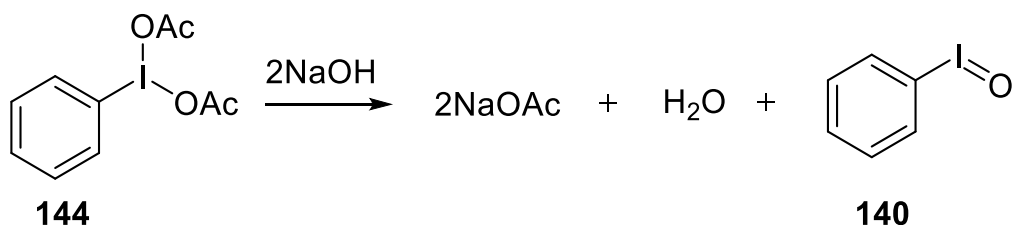
### 4.3.4 Oxidation of Cyclooctene

As the oxidation of ethylbenzene proved unsuccessful, another reaction was required to probe the encapsulation properties of colloidosomes. Previous work within the Twyman group has involved the use of an Iron porphyrin as a catalyst for the oxidation of cyclooctene[37], with iodosylbenzene as the oxygen source. In this reaction, oxygen is transported from iodosylbenzene to the iron porphyrin centre. This process results in the generation of a metal porphyrin oxo intermediate. The intermediate then reacts with the alkene substrate to generate the epoxide and various other oxidation by-products. The scheme for this reaction can be seen in **scheme 33**. Cyclooctene oxide is one of the oxidation products generated in this reaction. This work was based on work by Suslick *et al.* which involved the shape selective epoxidation of alkenes using metalloporphyrin dendrimer catalysts.[55] Though a water soluble product is not generated, there has been success within the Twyman group with regards to this reaction. It was decided that, despite the setback, this reaction could be used as a proof of principle that catalysis could occur within a colloidosome structure.

**Scheme 33**– Catalytic epoxidation of cyclooctene indicating the mixture of products obtained.

### 4.3.5 Synthesis of Iodosylbenzene

As the oil soluble catalyst has been prepared, the next stage is the synthesis of Iodosylbenzene, which is the oxygen source for the catalytic procedure. Iodosylbenzene was prepared by the reaction of iodobenzene diacetate with sodium hydroxide solution (**scheme 34**). The procedure involved stirring iodobenzene in a 3M solution of sodium hydroxide for a period of 45 minutes. The solution was filtered and the yellow powder obtained was washed thoroughly with water, followed by chloroform. Iodosylbenzene is highly sensitive and is easily decomposed when exposed to light. Therefore, due to the simplicity of the experimental procedure, iodosylbenzene was synthesised prior to each epoxidation reaction executed.



**Scheme 34** – Synthetic procedure of Iodosylbenzene, which is used as the oxygen source for the oxidation of cyclooctene.

A variety of analytical techniques were utilised to confirm successful preparation of iodosylbenzene. The mass spectrum confirmed the mass peak at 220 and also showed the presence of the fragment pattern at 204 and 205, resulting from the loss of the oxygen atom. This was in accordance with the Integrated Spectral Database System of Organic Compounds (AIST). The melting point showed decomposition at a temperature of 211 ℃, which is in agreement with results found in the literature.[56] Nuclear magnetic resonance for both proton and carbon were performed, confirming the identification of the product. The ^{1}HNMR

spectrum showed a multiplet at 8.05 ppm which was representative of the ortho protons and a multiplet at 7.58 ppm which was representative of the para and meta protons.

### 4.3.6 Catalysis Quantification

As discussed previously, when GC was first introduced in **4.3**, it is first necessary to run standards through the instrument. Neat samples of cyclooctene, cyclooctene oxide and iodobenzene, at appropriate concentrations, were run through the chromatograph. These compounds were purchased from Sigma Aldrich and this step of the procedure was imperative for determining the yield of the products obtained, upon completion of the reaction. An initial blank experiment was performed, so as to determine whether the alkene reacted with iodosylbenzene in the absence of the porphyrin catalyst. The GC traces obtained confirmed that there is a slight background reaction, but only to a minor extent. Though undesirable, this background reaction is inevitable and will be taken into consideration when deducing an accurate yield for cyclooctene oxide and the other oxidation products generated.

### 4.3.6.1 General Catalytic procedure – Control reaction

In a typical experiment 0.1 mmol of iodosylbenzene was added to a reaction vial, which was sealed and degassed thoroughly using low vacuum/$N_2$. A 2 mL solution of the solvent (dodecane) containing both 1 mmol cyclooctene substrate and 2.5 μmol porphyrin containing catalyst was then added via syringe. The suspension was then stirred in the dark for a period of thirty minutes under an atmosphere of nitrogen. After completion, the suspension was filtered using a Whatman® GD/X syringe filter, with a pore size of 0.45 μm, and transferred into a GC vial for analysis via manual injection. For the control reaction the yields obtained for cyclooctene oxide and all other oxidation products was very low. This procedure was repeated and similar results were obtained. As the yields obtained are low, it was advisable to test the efficiency of the oxygen source. The Twyman group performed this reaction with 4-acetoxyphenyl porphyrin and dichloromethane as the solvent and obtained yields of approximately 30-50%. In order to test the quality of the iodosylbenzene obtained, the reaction involving TAPP and dichloromethane was repeated.

### 4.3.6.2 Synthesis of 5, 10, 15, 20, tetrakis (4-acetoxyphenyl)-porphyrin (TAPP)

### 4.3.6.2.1 Synthesis of 4-acetoxybenzaldehyde

The initial task at hand, to carry out the repeat reaction, was the synthesis of TAPP. The initial step in the synthetic procedure of this porphyrin was the preparation of the 4-

acetoxybenzaldehyde. Although commercially available, 4-acetoxybenzaldehyde can be easily prepared via acetylation of 4-hydroxybenzaldehyde with acetyl chloride in an inert atmosphere (**scheme 35**).
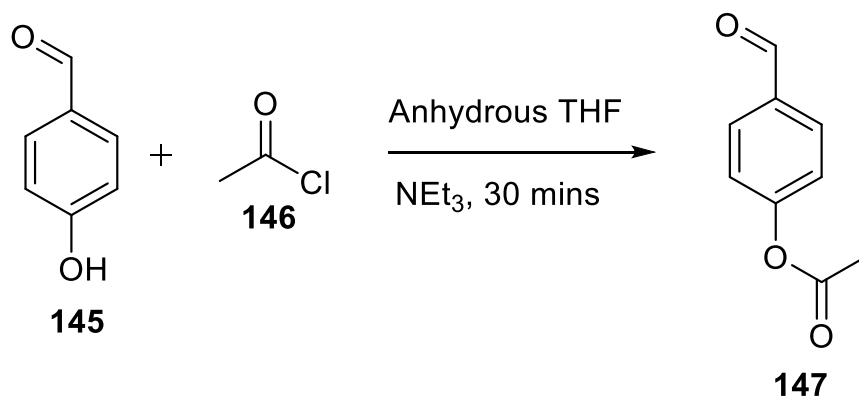


**Scheme 35** – Synthetic procedure of 4-acetoxybenzaldehyde.

A reaction flask, charged with 4-hydroxybenzaldehyde, anhydrous THF and anhydrous triethylamine, was degassed with argon and acyl chloride was added drop wise. The reaction mixture was stirred for a period of 30 minutes. The role of triethylamine in this reaction is that of a catalyst. The first step in the reaction is attack by the lone pair on the phenolic hydroxyl oxygen atom on the acyl carbon of acetyl chloride. Triethylamine present is then able to deprotonate the charged tetrahedral intermediate formed from the first step. This allows chloride to be ejected upon regeneration of the carbonyl double bond, generating the acetylated product. The chloride leaving group withdraws the hydrogen from the protonated amine species, restoring the catalyst. This mechanism can be visualised in **scheme 36**.
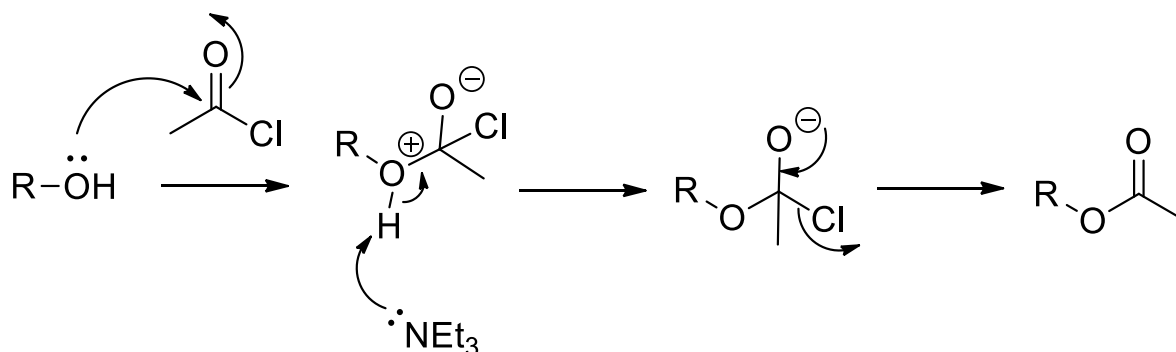


**Scheme 36** – Reaction mechanism for the acetylation of 4-hydroxybenzaldehyde, illustrating the role of triethylamine in the procedure.

Once the reaction is complete, the solid impurities generated were removed via filtration. The filtrate was reduced and the resulting brown oil was dissolved in chloroform and purified by washings with water and sodium hydrogen carbonate solution. The product was validated from the ^{1}HNMR spectrum which displayed a singlet at 2.36 ppm integrating to 3 protons, indicative of the methyl protons present on the acetoxy functional group. Utilisation of NMR and IR spectroscopy combined with mass spectrometry confirmed the product was sufficiently pure for the synthesis of 4-acetoxyphenyl porphyrin.

**4.3.6.2.2 Assembly of TAPP**

The simplicity of the production of the acetylated aldehyde enabled large quantities to be synthesised efficiently. With a sufficient amount of aldehyde, the next part was the construction of the porphyrin macrocycle. The porphyrin synthesis involved refluxing equal molar quantities of 4-acetoxybenzaldehyde and pyrrole in propionic acid for a period of 30 minutes (**scheme 37a**). This particular type of porphyrin synthesis differs to the Lindsey method, outlined previously. This alternate synthetic procedure was first considered by Rothemund in 1935.[57] Adler *et al.* went on to develop this method further towards the end of the 1960's.[58,59]
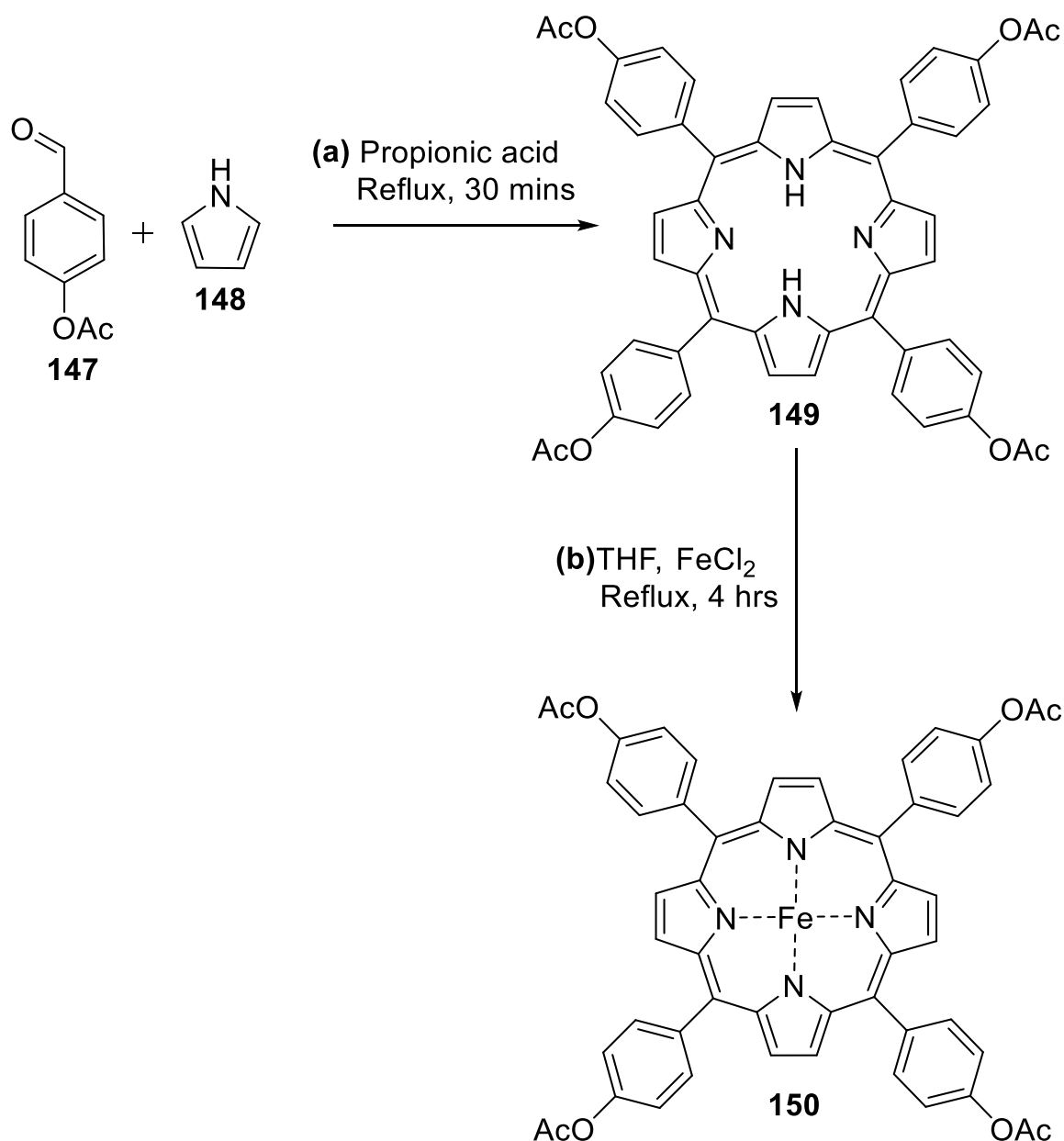
**Scheme 37** – (a) synthetic procedure of 4-acetoxyphenyl porphyrin (b) synthetic procedure for the 5, 10, 15, 20 – tetrakis (4-acetoxyphenyl)-porphyrin Iron (III) complex, which is used to catalyse the oxidation of cyclooctene in dichloromethane solvent.

Upon completion of reflux, a dark brown/black suspension remained in the reaction flask. This slurry was a mixture of numerous polypyrollic structures, incomplete porphyrin structures, other undesirable by-products and the desired porphyrin, 4-acetoxyphenyl porphyrin. The desired porphyrin was collected by vacuum filtration and purified by numerous washings with methanol. This workup was sufficient in generating analytically pure porphyrin. A notable disadvantage to using this specific method is the characteristically low yield associated with it. In order to explain this limitation, one must consider the

necessary prerequisites for total porphyrin assembly. In order to generate the complete macro-cyclic structure of the porphyrin, a succession of reactions must occur. The overall yield is inescapably poor, even if each individual successive reaction has a high yield. This is a result of accumulative negative effects present in macro-cyclic formation. The yield was typically between 15 and 20% for this experimental procedure.

The proton NMR displayed a singlet at 8.93 ppm which is representative of the pyrrolic protons on the porphyrin macrocycle. There are also doublets at 8.25 ppm and 7.54 ppm which are indicative of the ortho and meta protons of the phenyl ring. There is a singlet present at 2.53 ppm which corresponds to the methyl protons present in the acetoxy functional groups on the phenyl rings. The inner protons of the porphyrin are extremely shielded and therefore show a signal at -2.79 ppm. Electrospray mass spectrometry showed the molecular ion peak at 847, which is identical to the theoretical value. This analytical data, in combination with a UV/Vis soret band at 418 nm, confirms that the product synthesised is analytically pure.

### 4.3.6.2.3 Synthesis of 5, 10, 15, 20-tetrakis(4-acetoxyphenyl)-porphyrin Iron(III) Complex

As previously identified, the porphyrin catalysis required for the epoxidation of cyclooctene needs to have a central iron atom to operate. The insertion of iron into the porphyrin macrocycle was achieved using the same synthetic procedure as specified beforehand. The reaction scheme for iron insertion with TAPP is shown in **scheme 37b**. The product was verified by mass spectrometry and UV/Vis spectrometry. MALDI-TOFF gave a peak at 1631 which was indicative of an $MH^+$ ion. The UV/Vis spectrum showed notable broadening of the Soret band at 412 nm and a reduction in the number of Q bands, characteristic of iron insertion into a porphyrin.

### 4.3.6.3 Control reaction – test of purity of iodosylbenzene

As stated beforehand, in order to verify that the low yields are accurate and the iodosylbenzene used is analytically pure, a known reaction was to be repeated. The general catalytic procedure, described in **4.3.4**, was used and the yields obtained are tabulated overleaf in **table 6**.

| | Yield of total oxidation products (%) | Yield of cyclooctene oxide (%) |
|---|---|---|
| **TAPP-Fe(III)** | 27 ($\pm$1.6) | 20 ($\pm$1.5) |

**Table 6** – Table to show the percentage yields obtained for TAPP-Fe (III) in dichloromethane.

From the results tabulated, the percentage yield obtained for all oxidation products is approximately 30% which is in accordance for previous results obtained within the group, thus providing confidence in the analytical purity of iodosylbenzene synthesised. This confirms that dodecane and the oil soluble porphyrin synthesised are not the optimum solvent and catalyst for this procedure. Nevertheless, though the yields are inherently low, they are still measurable. For a proof of principle, a high yielding reaction is not a necessity; therefore this reaction will be suitable to determine the effect, if any, upon encapsulation within a colloidosome structure.
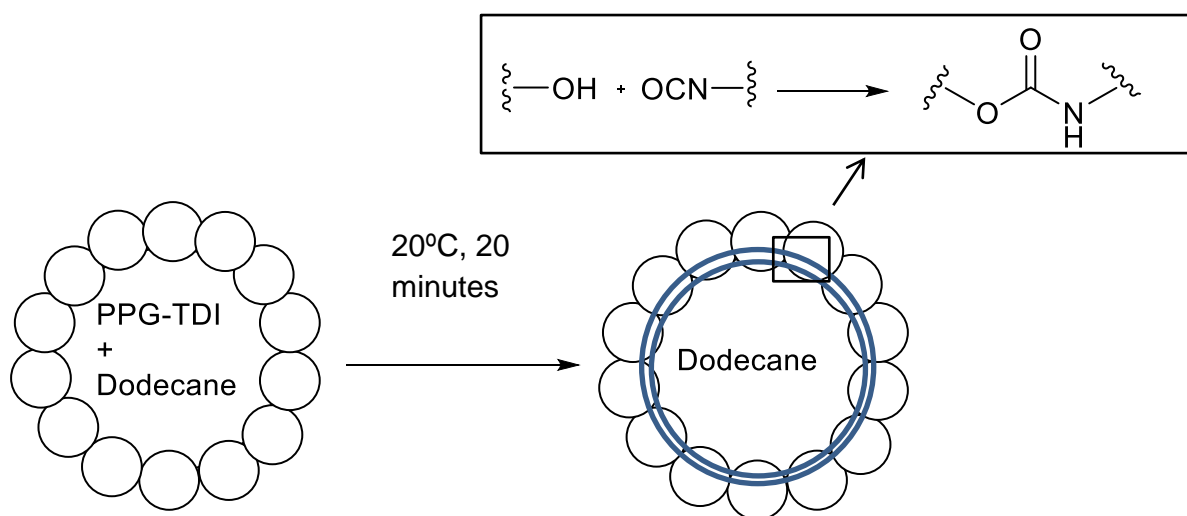
### 4.3.6.4 Colloidosome Encapsulation

The particles used for this study were provided by Dr. Kate Kirkham and were synthesised by an aqueous emulsification polymerisation using a PGMA$_{50}$ macromonomer.[19,60] The latex particles, provided by the Armes group, each have a hydroxyl rich surface as a result of PGMA$_{50}$ chains. These groups determine the hydrophilicity of the particle. It was also discovered that these PGMA$_{50}$ chains could be easily cross-linked to form urethane bonds.[20,61] For the purpose of this research, the cross-linker used was a polymeric diisocyanate (tolylene 2, 4-diisocyanate-terminated poly (propylene glycol) [PPG-TDI]. The structure of PPG-TDI can be seen in **figure 112**.[20]
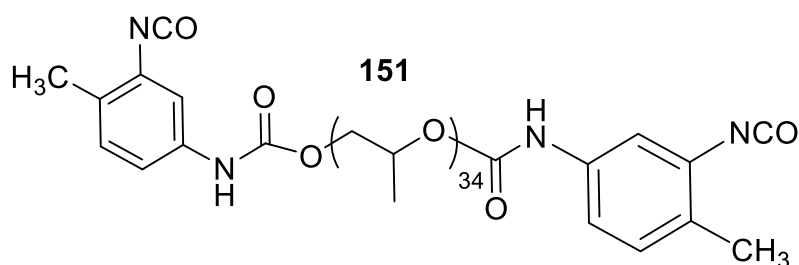
**Figure 112** – Figure to show the chemical structure of the oil soluble PPG-TDI cross-linker which is used in the covalent cross-linking of the colloidosomes used in this research.[18]

This is specifically oil soluble and commercially available. As this material is completely insoluble in water, cross-linking will be confined to the oil interior. Another added advantage to this cross-linking step is the mild conditions required. The cross-linker is dissolved in the oil phase and homogenised with the aqueous phase at room temperature and after a period of 20 minutes, covalent cross-linking is achieved. Cross-linking can be verified by optical microscopy, whereby the colloidosomes, after an alcohol challenge, remain intact. A schematic diagram for this step can be seen in **scheme 38**.[20]



**Scheme 38**– Schematic representation of covalent cross-linking of a colloidosome with the oil soluble cross-linker, PPG-TDI. The amide bond formation, which leads to crosslinking, is highlighted above.[20]

## 4.3.6.5 Encapsulation of porphyrin-Fe(III) complex into covalently cross-linked colloidosomes

Firstly, prior to carrying out the reaction, it was necessary to verify that encapsulation of the iron porphyrin did not interfere with the synthesis of the colloidosome. The oil phase

consisted of dodecane, the iron porphyrin catalyst and the cross linker, PPG-TDI. The aqueous phase was made up of 1% wt. aqueous solution of 125 nm $PGMA_{50}$-PS particles. Firstly the iron porphyrin complex and PPG-TDI were dissolved in dodecane and homogenised with the aqueous phase at 12,000 rpm for 2 minutes to generate the emulsion. The emulsion gave two distinct layers, the oil layer was coloured as a result of the brown iron porphyrin dissolved. The droplets were visualised by optical microscopy to verify that the initial emulsification was successful. The image from the microscope for the initial emulsification can be visualised in **figure 113**.
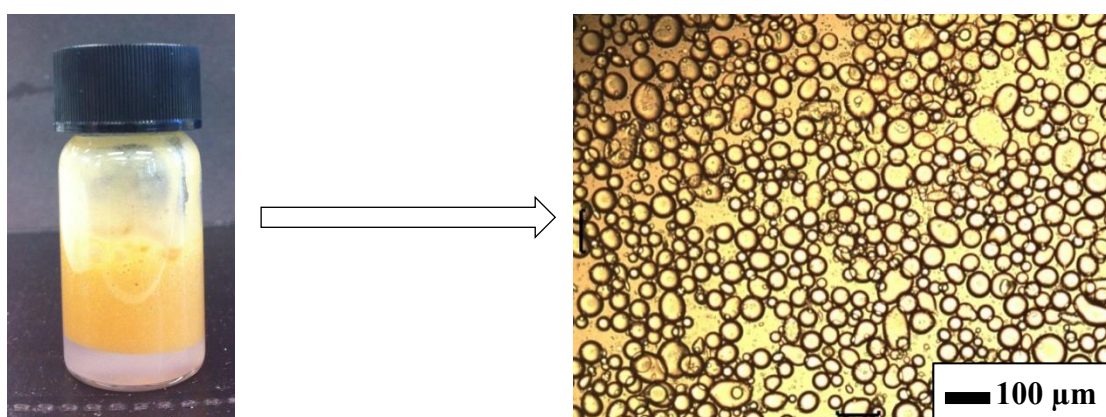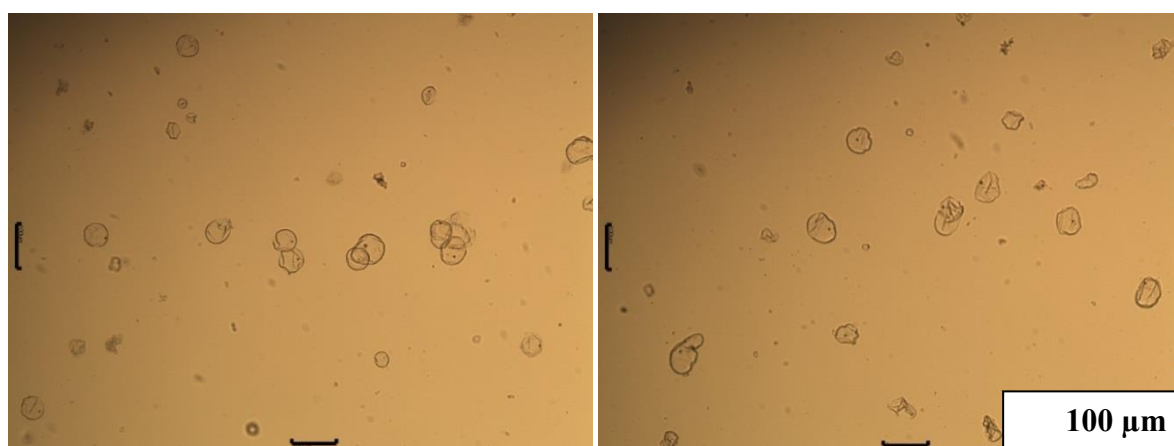


**Figure 113** – Figure to show the optical microscopic image of the emulsion containing the iron porphyrin complex.

The aqueous layer at the bottom of the vial remained clear, typical of successful homogenisation and the droplets, seen by microscopy, were similar to previous images without a porphyrin complex present. This provided confidence that the iron porphyrin catalyst is not reacting with the cross-linker in the oil phase. The droplet distribution was then measured via laser diffraction and the results can be seen in **figure 114** below.
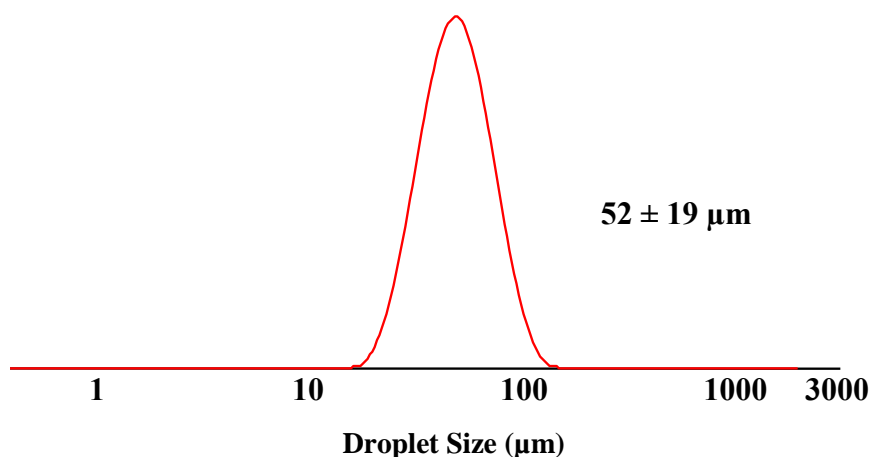


**Figure 114 – A g**raph to show the droplet distribution by laser diffraction.

A Gaussian distribution is desired as it means that there is no skew on droplet sizes, therefore, the presence of the iron porphyrin complex has not had an adverse effect upon distribution. The following stage was to confirm that cross-linking was successful. This was performed by an alcohol challenge; whereby a few drops of the emulsion were added to a vial of ethanol and shaken. This was then visualised by optical microscopy and the results of the alcohol challenge can be seen in **figure 115**.



**Figure 115** – Figure to show the optical microscope images of colloidosome shells after the alcohol challenge.

The next step was the encapsulation of the substrate and catalyst and, after homogenisation and crosslinking, the reaction could occur.

### 4.3.6.6 Background reaction

As mentioned previously in **4.3.6**, there is an unavoidable background reaction which occurs. The background reaction is a representation of how well the oxidation reaction proceeds without a catalyst present. Therefore, initial blank experiments within the colloidosome were performed. Blank experiments, without a catalyst, are required to determine the extent of the background reaction. These control reactions are important as all yields obtained will be quoted relative to the background reaction. After homogenisation and cross-linking, the colloidosome was injected into a vial, containing iodosylbenzene, under an atmosphere of nitrogen. The reaction mixture was then stirred in the dark for a period of 30 minutes (**scheme 39**).
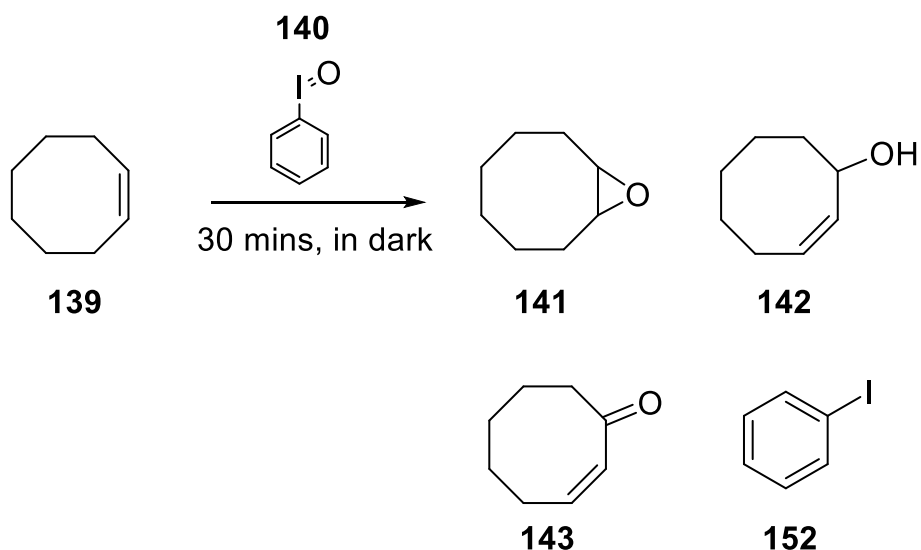
**Scheme 39 –** Reaction scheme for the background oxidation reaction which takes place in the absence of a catalyst.

The oil phase was removed by extraction with dichloromethane and filtered through a Whatman® GD/X syringe filter into a GC vial for analysis. The results, along with the control experiments (in dodecane), are tabulated overleaf in **table 7**. As mentioned previously in this section, the yields obtained in dodecane solvent were low, whereas, dichloromethane solvent gave a yield of total oxidation products of around 30%. Therefore, dodecane is not an optimum solvent for this particular reaction. However, we are restricted by the solvent applicable to colloidosome synthesis. The low yields predicted are disappointing, but are unavoidable. In dodecane, the yield of oxidation products was 2.2% whereas, in the colloidosome, this yield increased to 3.6%. The background reaction is faster within error and numerous repeats were performed which showed consistent results. This gave confidence that the colloidosome provided a better environment for the reaction. As yields are still measurable and repeatable, for a proof of principle, a reaction can be carried out regardless of low yields. The results tabulated overleaf have been normalised so that the control reaction in dodecane equates to 1.

| | Reaction in Dodecane (no porphyrin) | Reaction in Colloidosome (no porphyrin) | Colloidosome Enhancement |
|---|---|---|---|
| **Relative yield of all oxidation products** | 1.00 (±0.32) | 1.63 (±0.06) | 63% |

**Table 7**– A Table to show the relative yields of the background reaction for all oxidation products in both dodecane and the colloidosome without porphyrin catalyst.

From the blank experiment, it is evident that the colloidosome is having a positive effect upon the yield of the background reaction. Therefore; once the catalyst is incorporated, it is important to see if a similar effect is observed.

### 4.3.6.7 General catalytic procedure - Colloidosome

In a typical experiment 0.1 mmol of iodosylbenzene was added to a reaction vial, which was sealed and degassed thoroughly using low vacuum/$N_2$. A colloidosome was synthesised by the homogenisation of a 2 mL solution of the solvent (Dodecane) containing both 1 mmol cyclooctene substrate, 2.5 μmol porphyrin containing catalyst and the PPG-TDI cross-linker and a 2 mL solution of the aqueous phase (1 wt. % aqueous solution of 125 nm PGMA$_{50}$-PS particles). Homogenisation took place for a period of 2 minutes at 12000 rpm. The colloidosome was injected via a syringe and the suspension was then stirred in the dark for a period of thirty minutes under an atmosphere of nitrogen. After completion, the suspension was extracted using dichloromethane (3 mL) and the organic layer was collected and filtered using a Whatman® GD/X syringe filter with a pore size of 0.45 μm. The filtrate was transferred into a GC vial for analysis via manual injection.
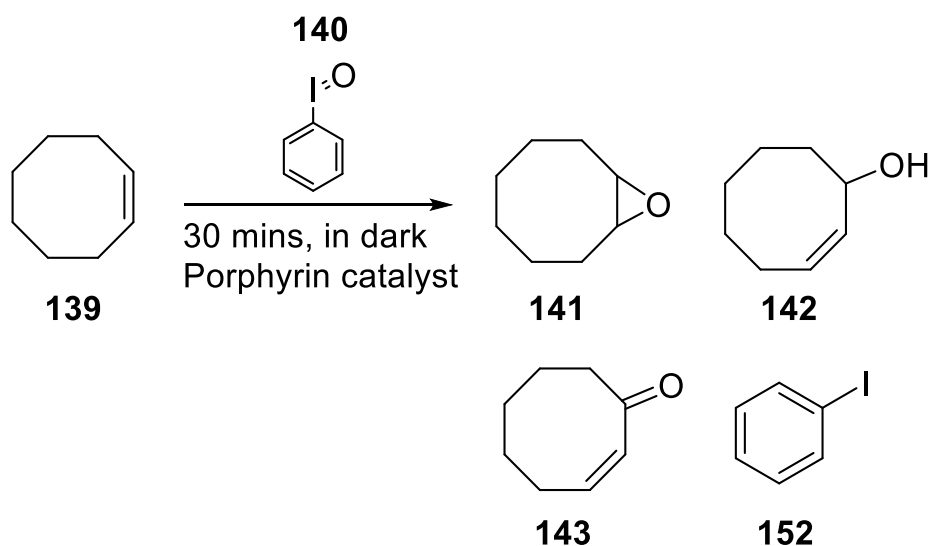
**Scheme 40** – Reaction scheme for cyclooctene in the presence of an iron porphyrin catalyst and the yields obtained after encapsulation within a colloidosome.
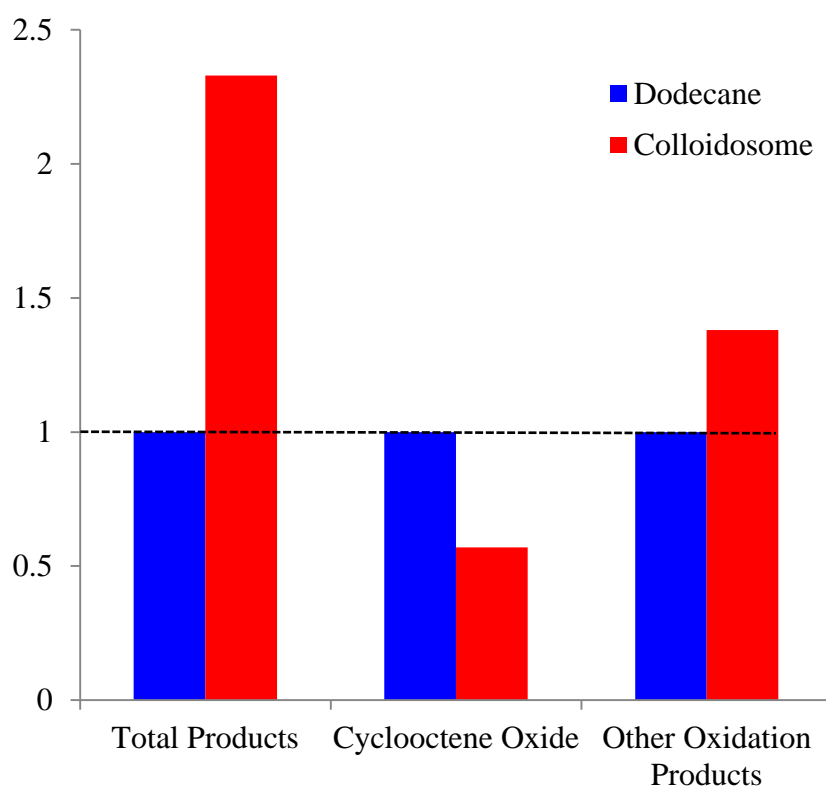
### 4.3.6.8 The effect of encapsulation within a colloidosome upon catalysis

With addition of the iron porphyrin catalyst, a similar enhancement effect was observed within the colloidosome compared to the reaction in dodecane alone. The results for all oxidation products, both the raw data and taking into account the background reaction, are tabulated below in **table 8**.

| | Total Product (i.e. data including the background reaction) | | | Porphyrin catalysis (i.e. Data minus background reaction) | | |
|---|---|---|---|---|---|---|
| | Dodecane | Colloidosome | Colloidosome Enhancement | Dodecane | Colloidosome | Colloidosome Enhancement |
| **All Oxidation Products** | 1.00 (±0.16) | 2.33 (±0.10) | 233% | 1.00 (±0.34) | 3.99 (±0.17) | 399% |

**Table 8** - A Table to show the relative percentage yields for all oxidation products when porphyrin catalyst is added, both the raw data and the data accounting for the background reaction is shown (in all cases final data normalised to the result obtained in dodecane).

Results have also shown that the oxidation reaction, in the presence of a catalyst, is also faster in a colloidosome. Numerous repeats were performed and consistent results were obtained. The estimated error is lower than the difference, meaning yields are both valid and measurable, and also lie within the limits of the technique. In terms of all possible oxidation products, there is a definite enhancement effect with encapsulation in a colloidosome. Specifically looking at cyclooctene oxide, the yields for the background reaction were immeasurable. Therefore, in order to gain a basic understanding upon the effect on the yield of this particular oxidation product, the raw data was contrasted for both dodecane and the colloidosome. The results are shown below in both **figure 116** and **table 9**.



**Figure 116** – A chart to show the effect of the colloidosome upon the relative yields of oxidation products. The dotted line indicates the result if there is no effect upon encapsulation within the colloidosome.

|  | Total Products | Cyclooctene oxide | Other oxidation products |
|---|---|---|---|
| **Relative yield in dodecane** | 1.00 | 1.00 | 1.00 |
| **Relative yield in colloidosome** | 2.33 | 0.57 | 1.38 |
| **Colloidosome effect** | (+) 233% | (-) 43% | (+) 38% |
| **Change in product distribution** | / | | 81% |

**Table 9 –** Table to show the relative yields (using raw data) and the product distributions for the porphyrin catalysed reactions in dodecane and colloidosome. The shift in product distribution is calculated by taking the difference in the colloidosome effect for the cyclooctene and the other oxidation products.

From analysis of the raw data it appears that, whilst there is an increase in yield of all oxidation products when the reaction occurs within the colloidosome, the yield of cyclooctene oxide is reduced. There are a few potential reasons for this result. A possible explanation for this outcome is that cyclooctene oxide generated could react with the polymeric structure of the colloidosome, thereby leading to a lower yield. In order to confirm whether this is taking place, a control reaction is performed. Cyclooctene oxide is dissolved into the dodecane phase, prior to homogenisation, and the reaction conditions are implemented. Upon completion, the reaction mixture is extracted with dichloromethane and filtered, as before, into a GC vial and analysed. The area present for cyclooctene oxide on both initial and final GC plots is contrasted. The result for the control reaction is shown in **scheme 41**.
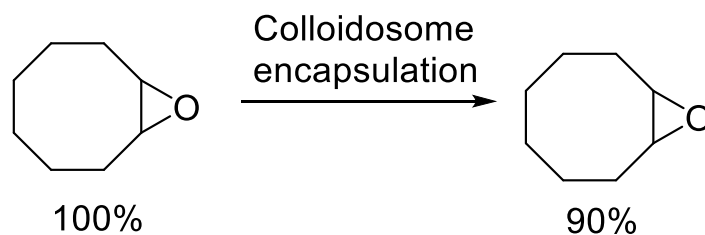
**Scheme 41** – Control reaction to demonstrate whether cyclooctene interacts with the colloidosome.

From the control reaction, 90% of cyclooctene was present within the dodecane phase of the colloidosome. This means that one should consider a 10% error in the extraction procedure with dichloromethane to extract the internal oil phase. As the results displayed show selectivity greater than 10%, this error does not affect the trends seen above. From the data obtained it is evident that cyclooctene oxide is not interacting with the colloidosome, meaning that the colloidosome is having an effect on the product distribution of the reaction. It was initially hypothesised that the effect of the colloidosome, if any, would not alter the product distribution. Though the yields for this reaction in dodecane are low, it is evident that there are significant changes to the yields and relative product distribution. The change in selectivity experienced is highly significant.

Upon documentation of the results, it was postulated that there were numerous possibilities to explain the increase in yield of products. The initial hypothesis is that the reaction is taking place within dodecane core. However, the yield could be elevated as a result of stabilisation of the reaction by the polystyrene (PS) particles of the colloidosome. It is possible that the PS could provide a different environment. As mentioned beforehand, catalysis of oxidation involves an iron porphyrin. In order to deduce the likelihood that the porphyrin catalyst is soluble in polystyrene, initial solubility tests involving toluene were performed. Toluene is similar in structure to polystyrene so can be presumed to have similar solvent properties. The porphyrin catalyst was found to be highly soluble in toluene, so it can be postulated that the PS is acting as an additional solvent system. The PS could be providing a more efficient solvent system for oxidation to that of dodecane, thus resulting in an enhanced yield of products. Consequently, a third location for catalysis to take place would be at the oil/particle interface. The results show that the use of a colloidosome leads to an enhanced total yield; however, the exact reasoning behind this is still unknown. The possible locations for oxidation, stated above, can be visualised in **figure 117**
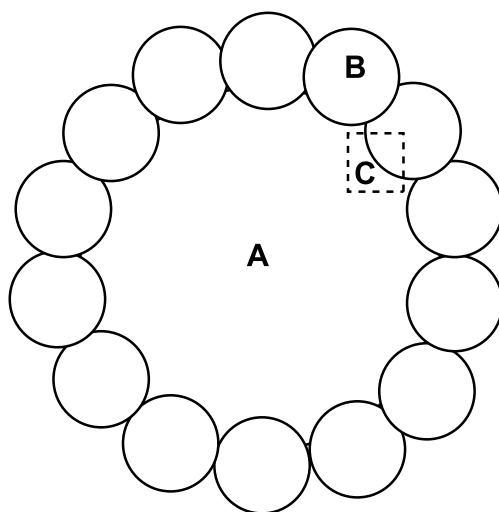
**Figure 117** – Figure to show the possible locations within a colloidosome structure where oxidation of cyclooctene could potentially take place. (A) within the dodecane oil core (B) within the PS particle, and (C) at the dodecane oil/PS particle interface.

The colloidosome was also affecting the product distribution of this particular oxidation reaction. The porphyrin catalyst used for this research contains iron (III) and there are several possible pathways for epoxidation which are presented below in **scheme 42**. [62]
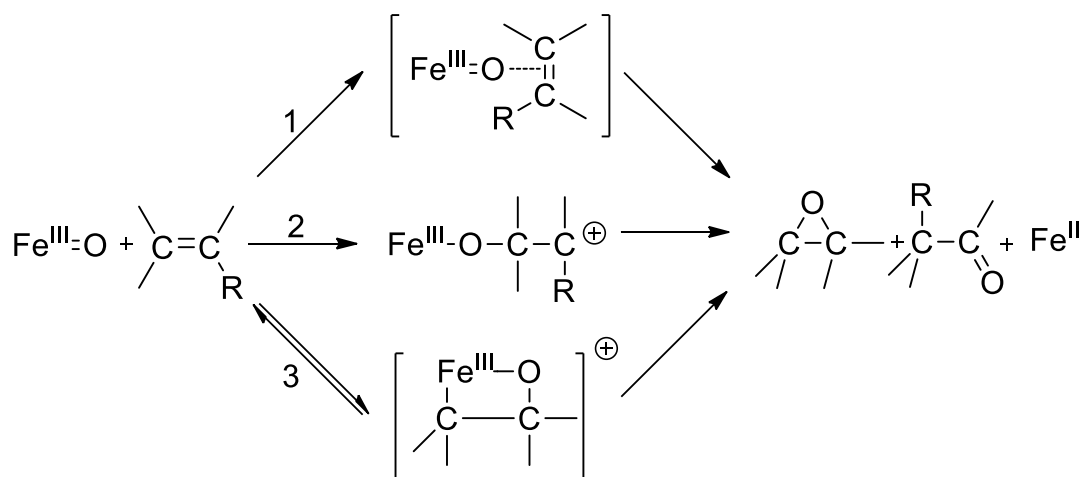


**Scheme 42** – Representation of the possible pathways possible for the epoxidation of an alkene. Pathway 1 represents the direct insertion of an oxygen atom, pathway 2 represents electrophilic addition followed by ring closure and pathway 3 represents the reversible formation of an electrocyclic metallooxetane followed by dissociation to generate the epoxide or other oxidation products.[62]

The epoxide can result from numerous pathways and, although not shown in **scheme 42**, there can also be other intermediates generated, which could possibly be influenced by the

colloidosome.[62] Therefore, it is evident that alkene oxidation involves a complicated mechanism with numerous viable routes to the products. A possible explanation for the change in product distribution could be a result of stabilisation by some aspect/region of the colloidosome of a particular intermediate, giving rise to the alcohol. Stabilisation could occur through cation-π interactions between the positively charged intermediate and the face of an electron rich benzene ring present within the colloidosome structure. Furthermore, if the reaction is taking place within the PS particles instead of the dodecane core, the different solvent environment could account for the stabilisation of a different intermediate.

As mentioned beforehand, in addition to an epoxide and an alcohol, another product which can be generated is a ketone. In 1989, Ostović and Bruice[63] carried out research on the catalysed epoxidation of alkenes by use of a sterically hindered iron (III) porphyrin macrocycle. This work demonstrated that the presence of a heavy iron atom within the porphyrin macrocycle can allow the mixing of spin states. This work showed that, following formation of a charge transfer complex and the subsequent change in spin state, there are two possible oxidation pathways possible; the first being concerted oxygen insertion to give an epoxide and the second being electron transfer to the porphyrin π-cation radical moiety to give a ketone. These two pathways are illustrated overleaf in **scheme 43**.
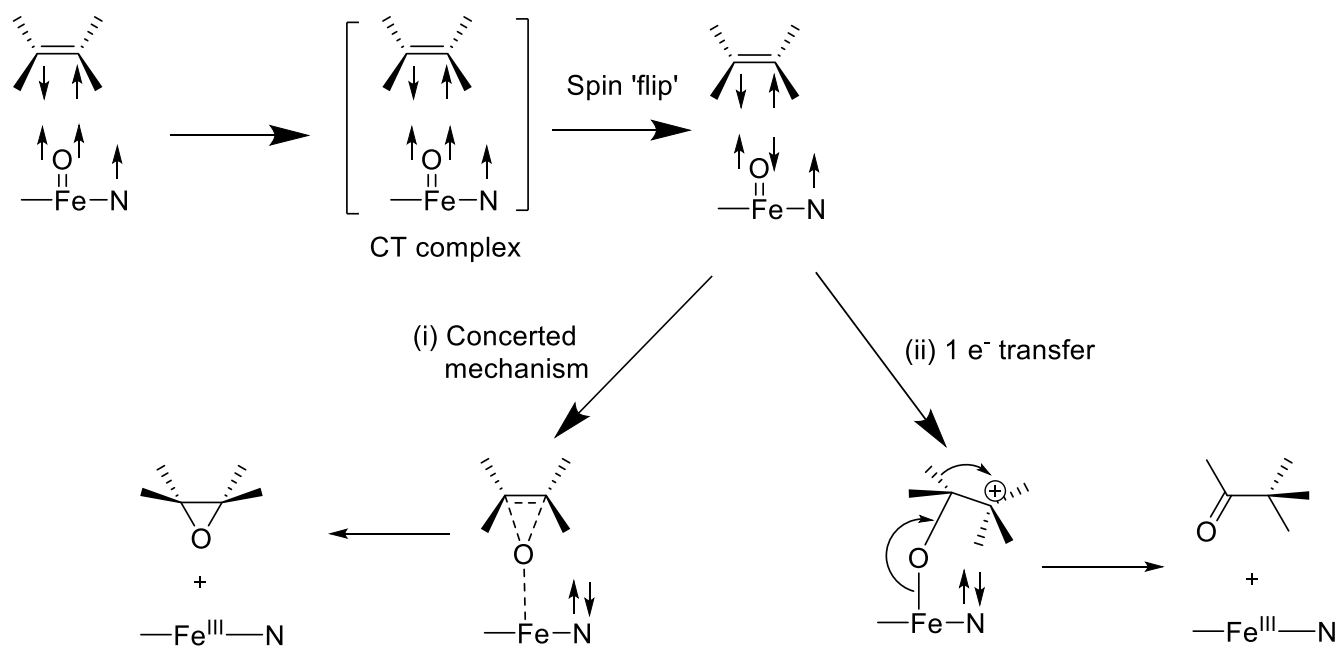
**Scheme 43** – Representation of the two possible pathways for the oxidation of an alkene via an iron porphyrin catalyst. Route (i) shows a concerted mechanism for the insertion of an oxygen atom and route (ii) represents the electron transfer to the porphyrin π-cation radical moiety.[63]

It can be postulated that, within a colloidosome, pathway (ii) is preferred over pathway (i), meaning the ketone would be the dominant product. Finally, another explanation for the change in product distribution could be that the environment within the colloidosome promotes the rearrangement of the epoxide into the ketone. Each of these explanations could account for the reduction in the level of cyclooctene oxide compared to other oxidation products, when catalysis takes place within a colloidosome.

Unfortunately, due to time restraints, control reactions involving the use of PS particles, prior to emulsification, could not be attempted. Future work, relating to this project, would be to investigate the ability of PS as a solvent. This would provide more insight into the role of the PS particles during this reaction. Furthermore, future work in this area would involve finding a suitable reaction for dodecane as a solvent, and also investigating different types of catalysis reactions to examine whether similar effects are observed. In addition to this, similar micelle structures could be investigated. Furthermore, if the product distribution is altered for other reactions, colloidosome catalysis could be a useful tool in selectivity of a desired product which, under usual condition, is perhaps a minor product, giving rise to a potential novel use for these microcapsules.

## 4.4 References

(1)     Yow, H. N.; Routh, A. F. *Soft Matter* **2006**, *2*, 940.

(2)     Pickering, S. U. *J. Chem. Soc., Trans.* **1907**, *91*, 2001.

(3)     Ramsden, W. *Proc. Royal Soc. London* **1903**, *72*, 156.

(4)     Aveyard, R.; Binks, B. P.; Clint, J. H. *Adv. Colloid Interface Sci.* **2003**, *100-102*, 503.

(5)     Velev, O. D.; Furusawa, K.; Nagayama, K. *Langmuir* **1996**, *12*, 2374.

(6)     Velev, O. D.; Furusawa, K.; Nagayama, K. *Langmuir* **1996**, *12*, 2385.

(7)     Velev, O. D.; Nagayama, K. *Langmuir* **1997**, *13*, 1856.

(8)     Dinsmore, A. D.; Hsu, M. F.; Nikolaides, M. G.; Marquez, M.; Bausch, A. R.; Weitz, D. A. *Science (Washington, DC, U. S.)* **2002**, *298*, 1006.

(9)     Laib, S.; Routh, A. F. *J. Colloid Interface Sci.* **2008**, *317*, 121.

(10)    Nomura, T.; Routh, A. F. *Langmuir* **2010**, *26*, 18676.

(11)    Paunov, V. N.; Cayre, O. J. *Adv. Mater. (Weinheim, Ger.)* **2004**, *16*, 788.

(12)    Noble, P. F.; Cayre, O. J.; Alargova, R. G.; Velev, O. D.; Paunov, V. N. *J. Am. Chem. Soc.* **2004**, *126*, 8092.

(13)    Duan, H.; Wang, D.; Sobal, N. S.; Giersig, M.; Kurth, D. G.; Moehwald, H. *Nano Lett.* **2005**, *5*, 949.

(14)    Gordon, V. D.; Chen, X.; Hutchinson, J. W.; Bausch, A. R.; Marquez, M.; Weitz, D. A. *J. Am. Chem. Soc.* **2004**, *126*, 14117.

(15)    Caruso, F.; Fiedler, H.; Haage, K. *Colloids Surf., A* **2000**, *169*, 287.

(16)    Fang, M.; Grant, P. S.; McShane, M. J.; Sukhorukov, G. B.; Golub, V. O.; Lvov, Y. M. *Langmuir* **2002**, *18*, 6338.

(17)    Croll, L. M.; Stoever, H. D. H. *Langmuir* **2003**, *19*, 5918.

(18)    Shah, R. K.; Kim, J.-W.; Weitz, D. A. *Langmuir* **2010**, *26*, 1561.

(19)    Thompson, K. L.; Armes, S. P.; York, D. W.; Burdis, J. A. *Macromolecules (Washington, DC, U. S.)* **2010**, *43*, 2169.

(20)    Thompson, K. L.; Armes, S. P.; Howse, J. R.; Ebbens, S.; Ahmad, I.; Zaidi, J. H.; York, D. W.; Burdis, J. A. *Macromolecules (Washington, DC, U. S.)* **2010**, *43*, 10466.

(21)    Walsh, A.; Thompson, K. L.; Armes, S. P.; York, D. W. *Langmuir* **2010**, *26*, 18039.

(22)    Yow, H. N.; Routh, A. F. *Langmuir* **2009**, *25*, 159.

(23)    Gibbs, B. F.; Kermasha, S.; Alli, I.; Mulligan, C. N. *Int. J. Food Sci. Nutr.* **1999**, *50*, 213.

(24)    Chang, T. M. S.; Prakash, S. *Mol. Biotechnol.* **2001**, *17*, 249.

(25)    Saraf, S.; Rathi, R.; Kaur, C. D.; Saraf, S. *Asian J. Sci. Res.* **2011**, *4*, 1.

(26)    Keen, P. H. R.; Slater, N. K. H.; Routh, A. F. *Langmuir* **2012**, *28*, 16007.

(27)    Islam, M. A.; Yun, C.-H.; Choi, Y.-J.; Cho, C.-S. *J. Microbiol. Biotechnol.* **2010**, *20*, 1367.

(28)    Keen, P. H. R.; Slater, N. K. H.; Routh, A. F. *Langmuir* **2012**, *28*, 1169.

(29)    Cayre, O. J.; Hitchcock, J.; Manga, M. S.; Fincham, S.; Simoes, A.; Williams, R. A.; Biggs, S. *Soft Matter* **2012**, *8*, 4716.

(30)    Williams, M.; Armes, S. P.; York, D. W. *Langmuir* **2012**, *28*, 1142.

(31)    Wu, C.; Bai, S.; Ansorge-Schumacher, M. B.; Wang, D. *Adv. Mater. (Weinheim, Ger.)* **2011**, *23*, 5694.

(32)    Buthe, A.; Kapitain, A.; Hartmeier, W.; Ansorge-Schumacher, M. B. *J. Mol. Catal. B: Enzym.* **2005**, *35*, 93.

(33)    Wu, C.-Z.; Kraume, M.; Ansorge-Schumacher, M. B. *ChemCatChem* **2011**, *3*, 1314.

(34)    Klibanov, A. M. *Science (Washington, D. C., 1883-)* **1983**, *219*, 722.

(35)    Wang, Z.; van, O. M. C. M.; Rutjes, F. P. J. T.; van, H. J. C. M. *Angew. Chem., Int. Ed.* **2012**, *51*, 10746.

(36)    Twyman, L. J.; King, A. S. H. *J. Chem. Res., Synop.* **2002**, 43.

(37)    Zheng, X.; Oviedo, I. R.; Twyman, L. J. *Macromolecules (Washington, DC, U. S.)* **2008**, *41*, 7776.

(38)    Twyman, L. J.; Ellis, A.; Gittins, P. J. *Macromolecules (Washington, DC, U. S.)* **2011**, *44*, 6365.

(39)    Kirkorian, K.; Ellis, A.; Twyman, L. J. *Chem. Soc. Rev.* **2012**, *41*, 6138.

(40)    Twyman, L. J.; King, A. S. H. *Chem. Commun. (Cambridge, U. K.)* **2002**, 910.

(41)    Ballester, P.; Gomila, R. M.; Hunter, C. A.; King, A. S. H.; Twyman, L. J. *Chem. Commun. (Cambridge, U. K.)* **2003**, 38.

(42)    Twyman, L. J.; The University of Sheffield, UK . 2005, p 25 pp.

(43)    Twyman, L. J.; Ge, Y. *Chem. Commun. (Cambridge, U. K.)* **2006**, 1658.

(44)    Twyman, L. J.; Ge, Y.; Gittins, P. J. *Supramol. Chem.* **2006**, *18*, 357.

(45)    Yamazaki, S.-i.; Ioroi, T.; Tanimoto, K.; Yasuda, K.; Asazawa, K.; Yamaguchi, S.; Tanaka, H. *J. Power Sources* **2012**, *204*, 79.

(46)    Gao, B.; Chen, Y.; Lei, Q. *J. Inclusion Phenom. Macrocyclic Chem.* **2012**, *74*, 455.

(47)    Adilina, I. B.; Hara, T.; Ichikuni, N.; Shimazu, S. *J. Mol. Catal. A: Chem.* **2012**, *361-362*, 72.

(48)    Chatterjee, C.; Chisholm, M. H. *Inorg. Chem.* **2011**, *50*, 4481.

(49)    Chatterjee, C.; Chisholm, M. H. *Inorg. Chem.* **2012**, *51*, 12041.

(50)    Evans, S.; Lindsay, S. J. R. *Perkin 2* **2000**, 1541.

(51)    Chen, J.; Franking, R.; Ruther, R. E.; Tan, Y.; He, X.; Hogendoorn, S. R.; Hamers, R. J. *Langmuir* **2011**, *27*, 6879.

(52)    Lindsey, J. S. *Acc. Chem. Res.* **2010**, *43*, 300.

(53)    Geier, G. R., III; Ciringh, Y.; Li, F.; Haynes, D. M.; Lindsey, J. S. *Org. Lett.* **2000**, *2*, 1745.

(54)    Lindsey, J. S.; Wagner, R. W. *J. Org. Chem.* **1989**, *54*, 828.

(55)    Bhyrappa, P.; Young, J. K.; Moore, J. S.; Suslick, K. S. *J. Mol. Catal. A: Chem.* **1996**, *113*, 109.

(56)    Wei, J.-F.; Shi, X.-Y. *Indian J. Chem., Sect. A: Inorg., Bio-inorg., Phys., Theor. Anal. Chem.* **2005**, *44A*, 2240.

(57)    Rothemund, P. *Journal of the American Chemical Society* **1935**, *57*, 2010.

(58)    Adler, A. D.; Longo, F. R.; Finarelli, J. D.; Goldmacher, J.; Assour, J.; Korsakoff, L. *J. Org. Chem.* **1967**, *32*, 476.

(59)    Adler, A. D.; Longo, F. R.; Kampas, F.; Kim, J. *J. Inorg. Nucl. Chem.* **1970**, *32*, 2443.

(60)    Thompson, K. L. PhD, Univesity of Sheffield, 2011.

(61)    Mookhoek, S. D.; Blaiszik, B. J.; Fischer, H. R.; Sottos, N. R.; White, S. R.; van, d. Z. S. *J. Mater. Chem.* **2008**, *18*, 5390.

(62)    Traylor, T. G.; Nakano, T.; Dunlap, B. E.; Traylor, P. S.; Dolphin, D. *J. Am. Chem. Soc.* **1986**, *108*, 2782.

(63)    Ostovic, D.; Bruice, T. C. *J. Am. Chem. Soc.* **1989**, *111*, 6511.

# Chapter 5

## Experimental

# Chapter 5 - Experimental

## 5.1 Instrumentation

### Infrared (IR) Spectroscopy
IR spectra were recorded using a Perkin-Elmer UATR Infrared spectrometer. Spectra were analysed with Spectrum100 software and positions of peaks are stated as wave numbers $(cm^{-1})$.

### NMR Spectroscopy
All NMR samples were prepared using deuterated solvents supplied by Sigma Aldrich. $^1H$ NMR and $^{13}C$ NMR spectra were recorded using a Brucker AV1400 MHz machine. Chemical shifts are quoted using ppm, coupling constants are quoted in Hertz and anomalous impurity and solvent peaks are labelled and referenced to residual solvent signals, with Tetramethylsilane $\delta=0$ at $=0$ as the reference. The NMR spectra were analysed using Topspin 3.0 NMR software.

### NMR Titrations
The anion receptor, N, N'- Bis-(3-acetoxy-phenyl)-isophthalamide, and the three hyperbranched polymers of varying molecular weight, bearing this receptor as a core molecule, were each titrated against a variety of anionic guests. Each titration began with 0.7 mL of the host species at the correct concentration in deuterated chloroform in an NMR tube. The anionic guest, at the correct concentration in deuterated chloroform, was added in aliquots (10-25 μL) to the host. NMR scans (32) were run following each addition and the position of the NH chemical shift (ppm) was monitored. Solutions were made up fresh and used immediately after preparation and anionic guests were added as tetrabutylammonium salts. Topspin 2.6 software was used to process the NMR spectra generated.

### Mass Spectrometry
The form of ionisation used was dependent on the molecular weight of the sample in question. For samples with a low molecular weight, an Electrospray ionisation (ES) was used to record spectra. The instrument used was a WATERS LCT mass spectrometer. For samples with a high molecular weight, Matrix assisted laser desorption ionisation (MALDI) was required. The instrumentation used was a BRUKER REFLEX III MALDI-ToF mass spectrometer.

### Gel Permeation Chromatography
Analytical THF GPC data was obtained at room temperature using either a high molecular weight column (3x300 mm PL gel 10 μm mixed-B), or a low molecular weight column (2x600 mm PL gel 5um (500 Å)). Calibration was achieved by using polystyrene standards (Mn 220-1, 1,000,000 Da) and molecular weights are thus reported relative to these specific standards used. The samples were run using Fisher GPC grade THF as a solvent stabilised with 0.025 % BHT (which was supplied to the columns by a Waters 515 HPLC Pump at 1.00 mLmin$^{-1}$). Toluene was added to prepared sample as a flow marker, before injection through a 200 μL sample loop with a Gilson 234 Auto Injector. The concentration of a sample was studied using an Erma ERC-7512 refractive index detector and, where applicable, by UV using a Waters Millipore Lambda Max 481 LC Spectrophotometer. Aqueous GPC data was acquired using a Millipore Waters Lambda-Max 481 LC spectrometer with a LMW/HMW column. The eluent which was used was $NaNO_3/NaH_2PO_4$ (pH=7) buffer solution (unless stated otherwise). The data attained was then analysed using cirrus GPC-online software. Samples were filtered using Whatman® GD/X syringe filters with a pore size of 0.45 μm prior to analysis.

### UV/Vis spectroscopy
The ultraviolet absorbance was recorded on an Analytik Jena AG Specord s600 UV/Vis Spectrometer and analysed using its attached Software (WinASPECT).

## Gas Chromatography

Gas chromatography results were obtained using a PerkinElmer Clarus 400 Gas Chromatograph. Samples were performed using a hydrogen gas flow and by means of an Altech AT1 non-polar column (length 30 metres, ID: 0.32 mm, Film Thickness: 5.00 um). The injection temperature was 250 ˚C; the temperature of the oven remained at 50 ˚C for 5 minutes and then subsequently increased to 250 ˚C over a period of 20 minutes. All data was processed using Total Chrome Nav software.

## Fluorescence Spectroscopy

Fluorescence results were obtained using a HORIBA Scientific Fluoromax-4 spectrofluorometer using its attached software (FluorEssence V3).

## Fluorescence Titrations

Fluorescence labelled PAMAM dendrimers, **33** and **34**, were each titrated against cytochrome-c (from equine heart). Each $10^{-6}$ M solution of the fluorescence labelled dendrimers was prepared using ultra-pure water. A solution containing a large excess ($5x10^{-3}$ M) of the guest, cytochrome-c, was then prepared using the corresponding dendrimer solution to ensure constant concentration of dendrimer throughout the titration. The dendrimer solution was accurately measured (3 mL) into a quartz cuvette and aliquots of ligand solution (between 10 μL and 50 μL) were added. Fluorescence emission scans were taken after each addition, monitoring the quenching of the emission spectrum of the labelled dendrimer (508 nm). Solutions were made fresh and used immediately after preparation.

## Dynamic light scattering (DLS)

DLS results were obtained using the Brookhaven instrument 90 Plus Particle Size Analyser (Holtsville, NY, USA) 35 mW solid state standard laser. This instrumentation was used to determine the hydrodynamic diameter of nanoparticles. Particle sizing software 9kpsdw32.exe.ver.3.80 was used for characterisation. Light was scattered at an angle of 90 ° with each run lasting 2 minutes at a temperature of 37.5 °C. Samples were filtered using Whatman® GD/X syringe filters with a pore size of 0.45 μm, prior to analysis. Results reported are based upon volume distribution.

## pH measurement

The pH of the buffer solutions prepared was substantiated using a pH 210 Microprocessor pH Meter from Hanna Instruments Ltd. (Leighton Buzzard, UK). The device was calibrated using pH 4.0 and pH 7.0 standard solutions, prepared with buffer tablets (Sigma-Aldrich, Poole, UK).

## 5.2 Synthetic procedures for Protein binding
The PAMAM dendrimers were synthesised in collaboration with a 4th year project student.

### 5.2.1 General procedures for synthesis of PAMAM dendrimers

#### 5.2.1.1 General procedure for synthesis of half generation PAMAM dendrimers
Methyl acrylate was added drop-wise over a period of 30 minutes to a solution of the previous diamine intermediate (or ethylene diamine (EDA) in the case of G-0.5) dissolved in methanol (various amounts) in a 500 mL round bottom flask at 0 °C. The reaction was then stirred at room temperature for a given amount of time depending on the generation of dendrimer in question. The excess methyl acrylate and solvent were then removed by rotary evaporation at 40 °C and then placed under a high vacuum to give the desired half generation PAMAM dendrimer.

#### 5.2.1.2 General procedure for synthesis of whole generation PAMAM dendrimers
The ester terminated intermediate generated previously was dissolved in methanol (various amounts) and added drop-wise over period of 30 minutes to EDA in a 500 mL round bottom flask at 0 °C. The reaction was subsequently stirred at room temperature for a given amount of time depending on the generation of dendrimer in question. The solvent was removed via rotary evaporation at 40 °C and then excess EDA was removed by washing the product with an azeotropic mixture of toluene: methanol in the ratio 9:1. The purification, by way of an azeotropic wash, was repeated until no further trace of EDA could be detected analytically, generating the desired whole generation PAMAM dendrimer.

### 5.2.2 Synthesis of a PAMAM dendrimer holding 4 terminal OMe terminal groups (28)
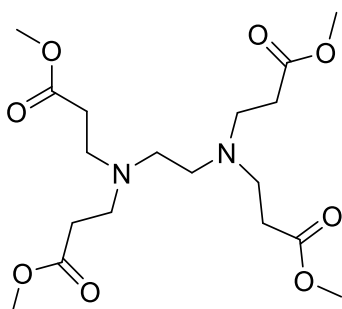


The general procedure was followed where methyl acrylate (25.10 g, 0.29 moles) was added to EDA (2.56 g, 0.04 moles) dissolved in methanol (20 mL). The reaction was then stirred at room temperature for 24 hours. Purification yielded a light yellow oil.

Figure 27 page 61
Scheme 6 page 64

Yield 14.12 g, 82% ^{1}HNMR (CD$_3$OD, 400 MHz) $\delta_H$ 3.68 (s, 12H, C$\underline{H}_3$), 2.79 (t, 8H, NC$\underline{H}_2$CH$_2$C=O, J=7.0), 2.54 (s, 4H, NC$\underline{H}_2$C$\underline{H}_2$N), 2.49 (t, 8H, OC=OC$\underline{H}_2$, J=7.0) ^{13}CNMR (CD$_3$OD, 400 MHz) $\delta_C$ 173.18, 49.51, 47.74, 32.01 FTIR (cm$^{-1}$) 2952 (C-H-sp$^2$), 1731 (ester carbonyl), 1436 (CH$_2$ bend), 1357, 1329, 1194, 1171, 1042 ES-MS 405 (MH+), 427 (MNa+)
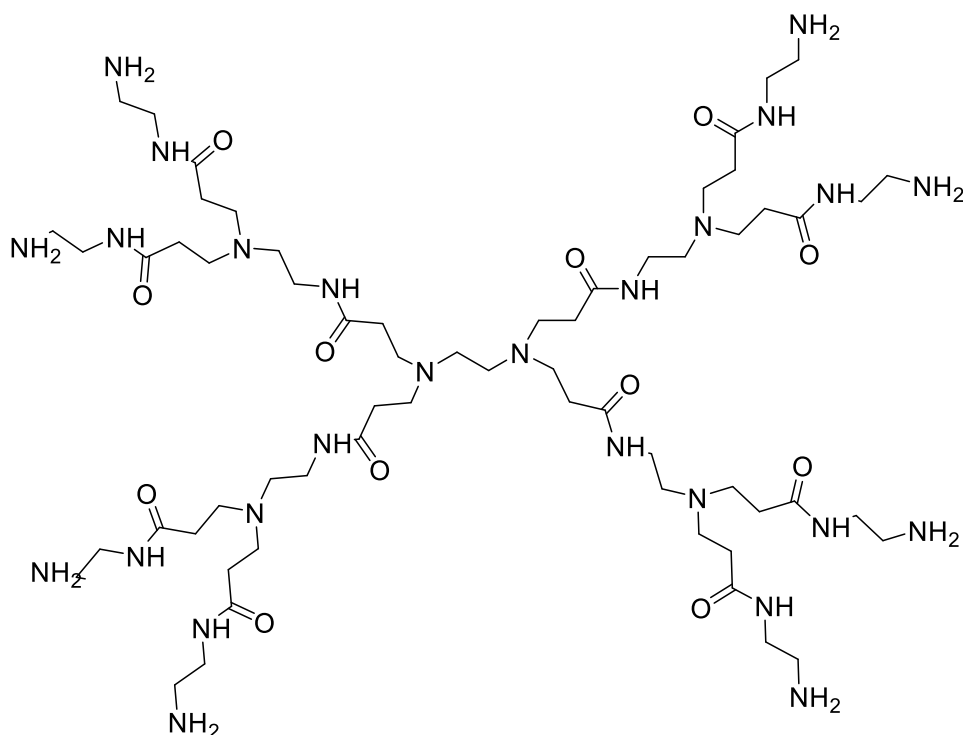
### 5.2.3 Synthesis of a PAMAM dendrimer holding 4 terminal NH2 terminal groups
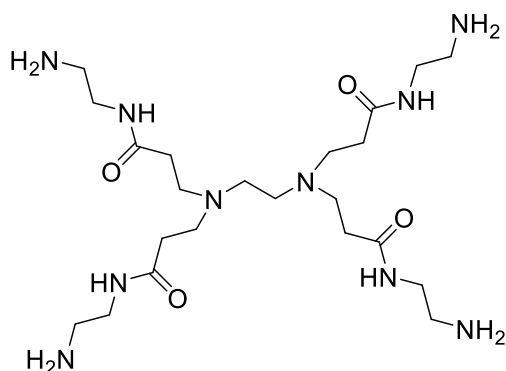


The general procedure was followed where the ester terminated intermediate (6.7 g, 0.02 moles) was dissolved in methanol (20 mL) and added, drop wise, to EDA (48.88 g, 0.82 moles). The reaction was allowed to react for 5 days. Purification yielded a yellow/brown oil

Yield 6.34 g, 74 % ^{1}HNMR (CD$_3$OD, 400 MHz) $\delta_H$ 4.92 (s, 4H, N$\underline{H}$), 3.69 (S, 8H, N$\underline{H}_2$), 3.33-3.27 (mm, 16H, H$_2$NC$\underline{H}_2$ + C$\underline{H}_2$NH), 2.81-2.41 (m, 20H, C=OC$\underline{H}_2$C$\underline{H}_2$ + NC$\underline{H}_2$C$\underline{H}_2$N) ^{13}CNMR (CD$_3$OD, 400 MHz) $\delta_C$ 173.32, 52.36, 49.10 , 48.04, 37.08, 32.18 FTIR (cm$^{-1}$) 3274 (amide N-H stretch), 3072, 2926 (CH-sp$^2$), 2865 (CH-sp$^3$), 1637 (amide C=O stretch), 1547, 1438, 1358, 1258, 1194, 112 ES-MS 517 (MH+)

### 5.2.4 Synthesis of a PAMAM dendrimer holding 8 terminal OMe terminal groups
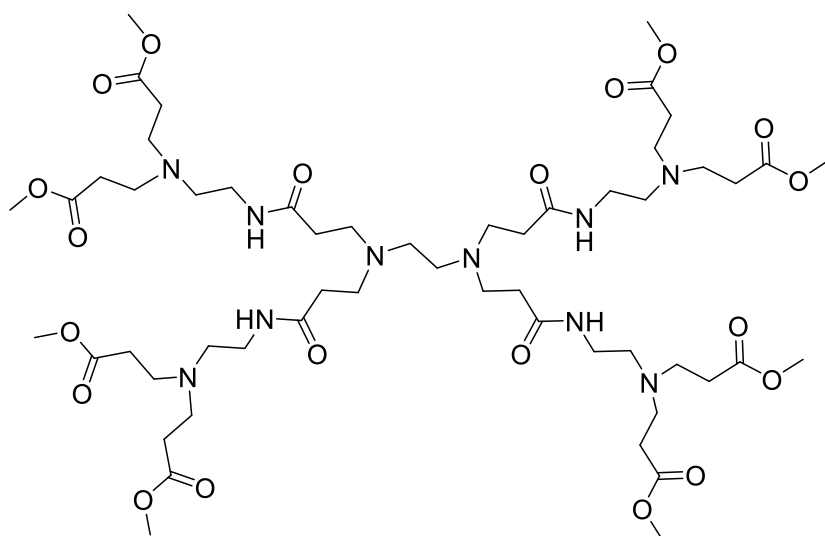


The general procedure was followed where methyl acrylate (7.32 g, 0.09 moles) was added to the diamine intermediate (2.51 g, 4.86 mmoles) dissolved in methanol (30 mL). The reaction was then stirred at room temperature for 24 hours. Purification yielded a viscous yellow/brown oil.

Yield 3.23 g, 72 %^{1}HNMR (CD$_3$OD, 400 MHz) $\delta_H$ 4.91 (s, 4H, N$\underline{H}$), 3.69 (s, 24H, C$\underline{H}_3$), 3.33-3.28 (m, 24H, NHC$\underline{H}_2$ + NHCH$_2$CH$_2$NC$\underline{H}_2$) , 2.87- 2.48 (mm, 44H, NC$\underline{H}_2$C$\underline{H}_2$N + NC$\underline{H}_2$C$\underline{H}_2$C=ONH + NHCH$_2$C$\underline{H}_2$N + CH$_3$OC=OC$\underline{H}_2$)^{13}C-NMR (CD$_3$OD, 400 MHz) $\delta_C$ 173.35, 173.04, 52.35, 50.71, 49.42, 49.10, 37.09, 32.19 31.89 FTIR (cm$^{-1}$) 3274 (Amide N-H stretch), 2952 (C-H-sp$^2$), 2825 (C-H-sp$^3$), 1730 (ester C=O stretch), 1643 (amide C=O stretch), 1536, 1436, 137, 1195, 1175, 1042 ES-MS 1206 (MH+)

**5.2.5 Synthesis of a PAMAM dendrimer holding 8 terminal NH₂ terminal groups**



The general procedure was followed where the ester terminated intermediate (6.62 g, 5.49 mmoles) was dissolved in methanol (30 mL) and added, drop wise, to EDA (51.21 g, 0.85 moles). The reaction was allowed to react for 7 days. Purification yielded a deep orange viscous oil.

Yield 7.12 g, 90 % $^1$HNMR (CD$_3$OD, 400 MHz) $\delta_H$ 4.91 (s, 12H, N$\underline{H}$), 3.37 (s, 14H , N$\underline{H}_2$), 3.33-3.27 (m, 24H , NHC$\underline{H}_2$CH$_2$N + NH$_2$CH$_2$C$\underline{H}_2$NH) 2.83-2.16 (mm, 76H, NH$_2$C$\underline{H}_2$CH$_2$NH + NC$\underline{H}_2$CH$_2$C=O + NC$\underline{H}_2$CH$_2$NH + NC$\underline{H}_2$C$\underline{H}_2$N) $^{13}$CNMR (CD$_3$OD, 400 MHz) $\delta_C$ 176.53, 52.53, 50.17, 49.74, 44.40, 43.42, 40.00, 35.90 FTIR (cm$^{-1}$) 3274 (amide N-H stretch), 3064, 2932 (C-H-sp$^2$), 2824 (C-H-sp$^3$), 1638 (amide C=O), 1546, 1440, 1365, 1280, 1195, 1126 ES-MS 1430 (MH+) MALDI-TOF MS 1430 (MH+), 1452 (MNa+), 1468 (MK+)

## 5.2.6 Synthesis of a PAMAM dendrimer holding 16 terminal OMe terminal groups
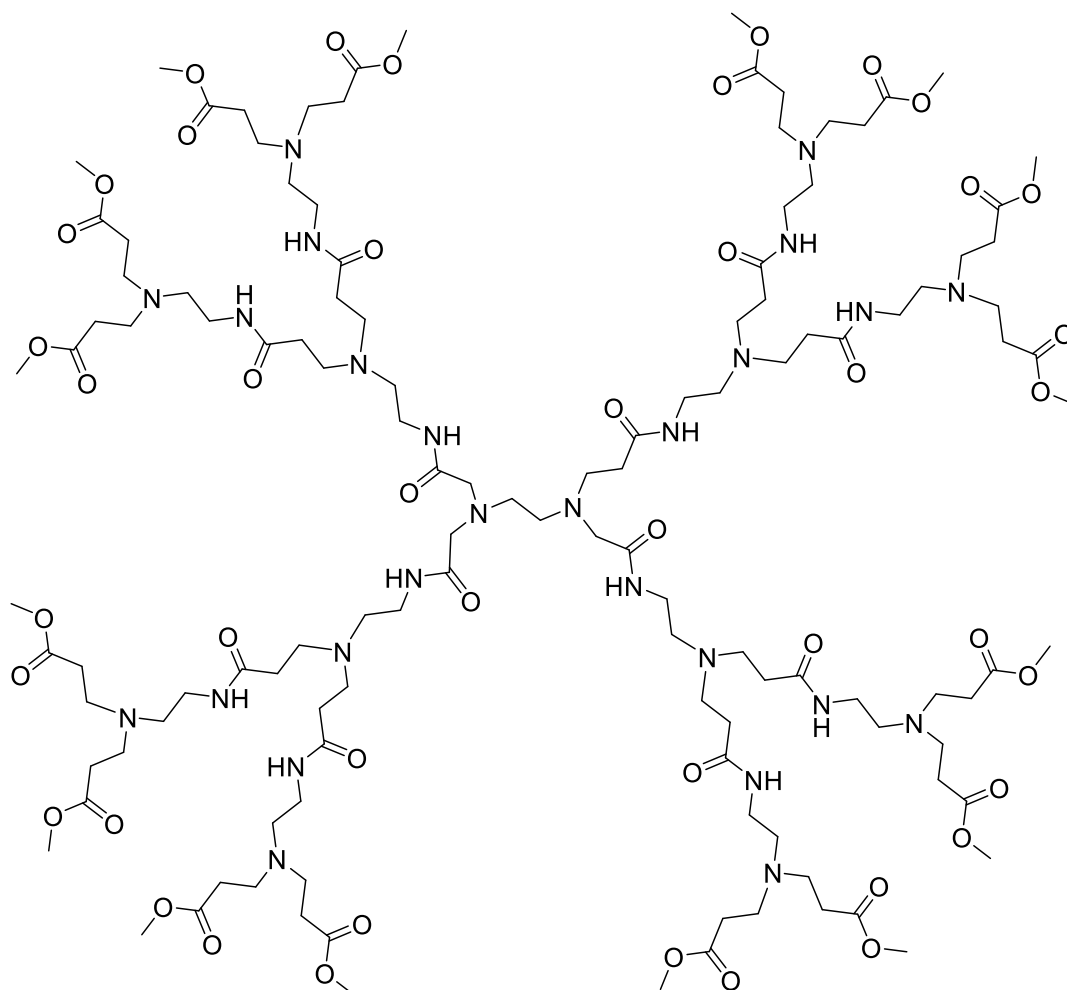


The general procedure was followed where methyl acrylate (2.81 g, 0.03 moles) was added to the diamine intermediate (1.25 g, 0.87 mmoles) dissolved in methanol (30 mL). The reaction was then stirred at room temperature for 2 days. Purification yielded a honey coloured, extremely viscous oil.

Yield 1.82 g, 73 % $^1$HNMR (CD$_3$OD, 400 MHz) $\delta_H$ 4.92 (s, 12H, N$\underline{H}$), 3.69 (s, 48H, C$\underline{H}_3$), 3.30 (m, 12H, NHC$\underline{H}_2$CH$_2$N), 2.80-2.41 (mm, 152H, OC=OC$\underline{H}_2$C$\underline{H}_2$N + NC$\underline{H}_2$CH$_2$NH + NHC=OC$\underline{H}_2$C$\underline{H}_2$N + NC$\underline{H}_2$C$\underline{H}_2$N) $^{13}$CNMR (CD$_3$OD, 400 MHz) $\delta_C$ 173.34, 173.23, 52.38, 52.08, 50.82, 49.66, 49.09, 48.03, 37.25, 33.33 32.18 FTIR (cm$^{-1}$) 3293 (amide N-H stretch), 2950 (C-H-sp$^2$), 2834 (C-H-sp$^3$), 1731 (ester C=O stretch), 1640 (amide C=O stretch), 1536, 1436, 1357, 1196, 1177, 1043 MALDI-TOF MS 2807 (MH+), 2829 (MNa+), 2845 (MK+)

## 5.2.7 Synthesis of a PAMAM dendrimer holding 16 terminal NH₂ terminal groups
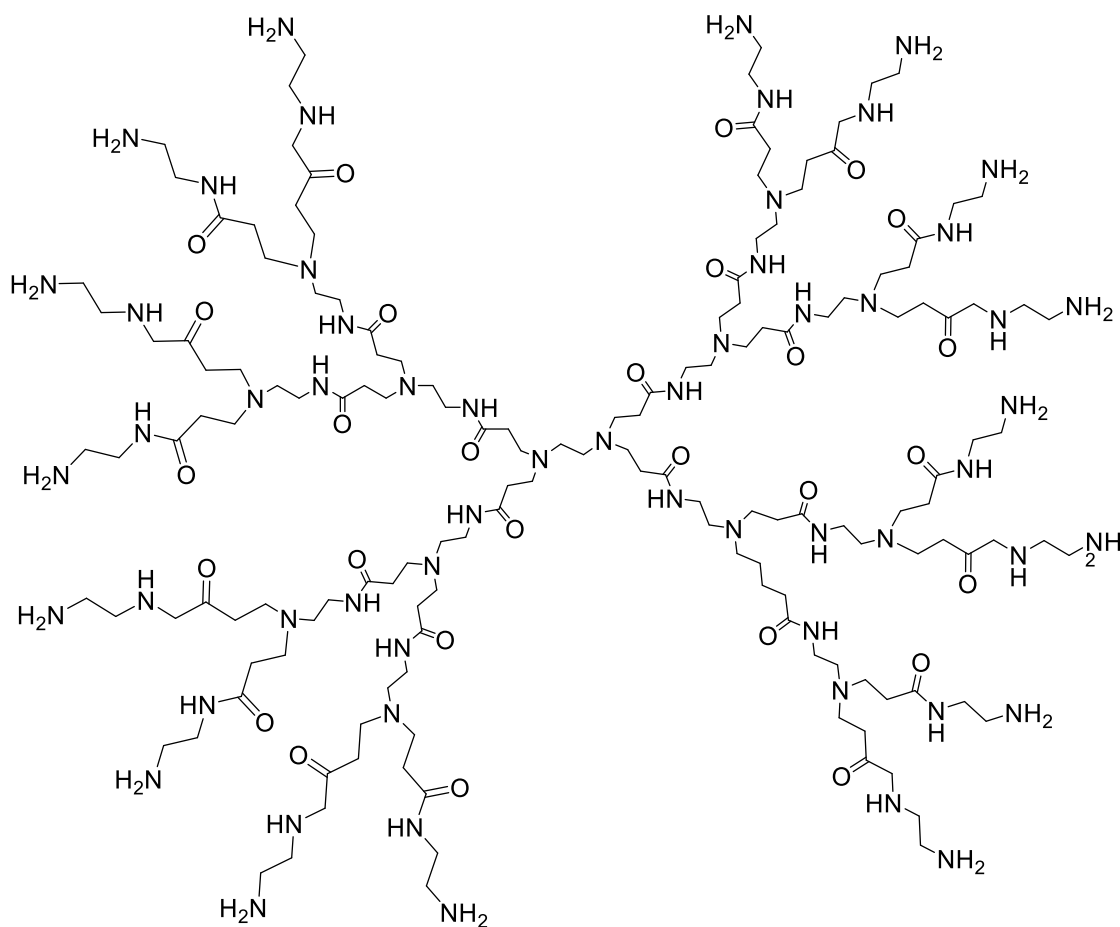


The general procedure was followed where the ester terminated intermediate (1.71 g, 0.62 mmoles) was dissolved in methanol (30 mL) and added, drop wise, to EDA (7.20 g, 0.12 moles). The reaction was allowed to react for 7 days. Purification gave a deep orange and extremely viscous oil.

Yield 1.01 g, 52 % $^1$HNMR (CD$_3$OD, 400 MHz) $\delta_H$ 4.93 (s, 28H, N$\underline{H}$), 3.6873 (s, 32H, N$\underline{H}_2$), 3.34-3.28 (m, 56H, NHC$\underline{H}_2$CH$_2$N + NH$_2$CH$_2$C$\underline{H}_2$NH) 2.85-2.41 (mm, 172H, NH$_2$C$\underline{H}_2$CH$_2$NH + NC$\underline{H}_2$CH$_2$C=O + NC$\underline{H}_2$CH$_2$NH + NC$\underline{H}_2$C$\underline{H}_2$N) $^{13}$CNMR (CD$_3$OD, 400 MHz) $\delta_C$ 173.33, 52.39, 50.84, 49.64, 48.03, 37.23, 33.32, 32.19 FTIR (cm$^{-1}$) 3278 (amide N-H stretch), 3074, 2928 (C-H-sp$^2$), 2864 (C-H-sp$^3$), 1637 (amide C=O), 1548, 1435, 1359, 1285, 1194, 1110, 1032 MALDI-TOF MS 3260

**5.2.8 Synthesis of a PAMAM dendrimer holding 32 terminal OMe terminal groups**
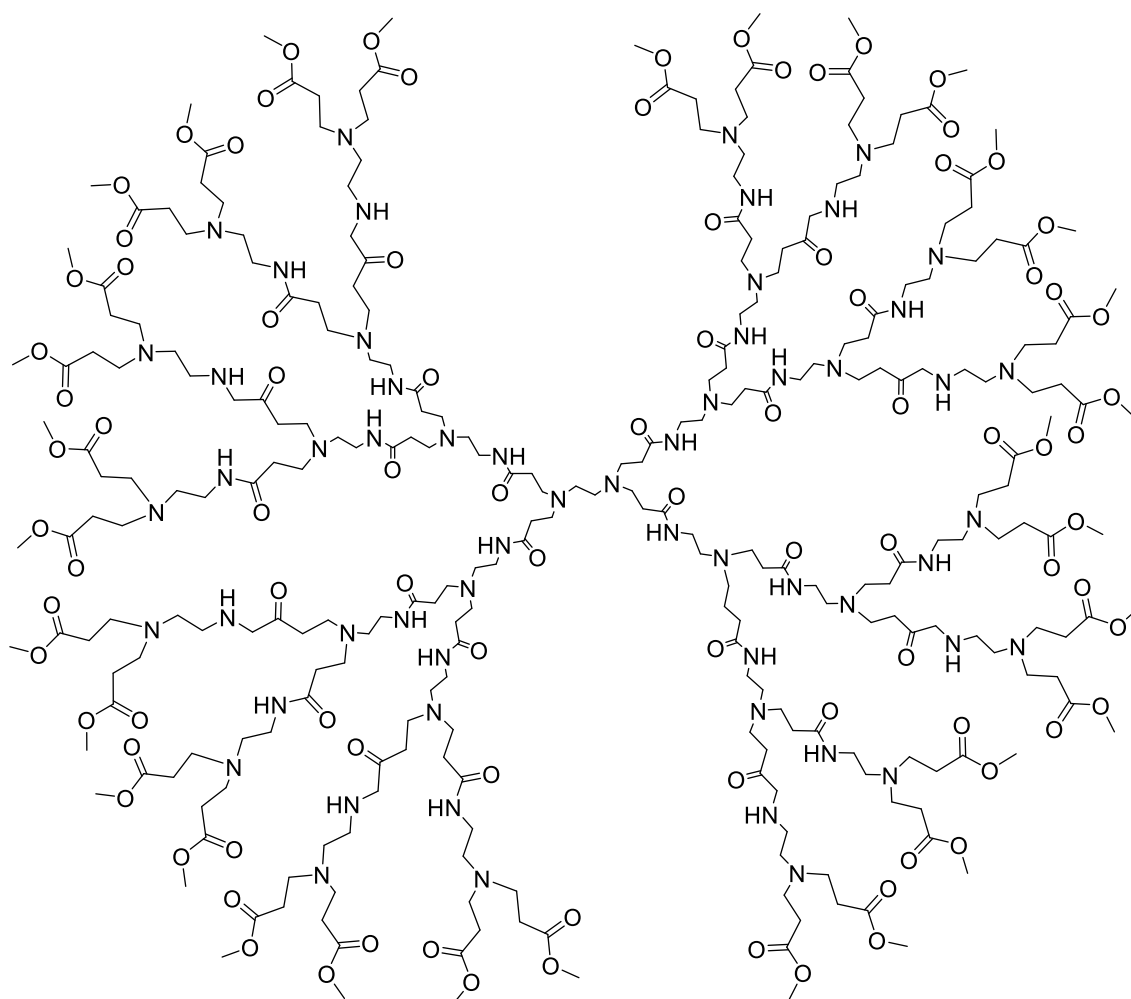


The general procedure was followed where methyl acrylate (1.92 g, 0.02 moles) was added to the diamine intermediate (1.03 g, 0.30 mmoles) dissolved in methanol (40 mL). The reaction was then stirred at room temperature for 3 days. Purification yielded a Viscous yellow/orange oil.

Yield 0.92 g, 47 % $^1$HNMR (CD$_3$OD, 400 MHz) $\delta_H$ 4.92 (s, 28H, N$\underline{H}$), 3.87 (s, 96H, C$\underline{H}_3$), 3.34-3.28 (m, 120H, OC=OCH$_2$C$\underline{H}_2$N + NHC$\underline{H}_2$CH$_2$N), 2.85-2.41 (mm, 236H, OC=OC$\underline{H}_2$CH$_2$N + NHC=OC$\underline{H}_2$C$\underline{H}_2$N + NHCH$_2$C$\underline{H}_2$N, NC$\underline{H}_2$C$\underline{H}_2$N) $^{13}$CNMR (CD$_3$OD, 400 MHz) $\delta_C$ 173.33, 173.23, 52.39, 52.09, 50.84, 49.64, 48.03, 37.22, 33.33 32.19 FTIR (cm$^{-1}$) 3274 (amide N-H stretch), 2951 (C-H-sp$^2$), 2825 (C-H-sp$^3$), 1731 (ester C=O stretch), 1640 (amide C=O stretch), 1544, 1436, 1357, 1196, 1043 MALDI-TOF MS 6034 (MNa+)

## 5.3 Protein Binding Assay -The inhibition of α-Chymotrypsin using PAMAM dendrimers

### 5.3.1 Preparation for α-Chymotrypsin binding assay

#### 5.3.1.1 Preparation of Buffer Solution
1.75 g monosodium dihydrogen phosphate and 14.48 g of disodium hydrogen phosphate were dissolved in 1000 mL of distilled water. This gave a buffer of concentration 0.1M and pH 7.4.

#### 5.3.1.2 Preparation of Protein Solution
2.6 mg α-chymotrypsin was dissolved in 100 mL ($1 \times 10^{-6}$ M) phosphate buffer (pH=7.4, 0.1 M).

#### 5.3.1.3 Hydrolysis of PAMAM dendrimers
Each dendrimer was dissolved in 10mL of methanol and 1 mL of distilled water was added with a stoichiometric amount (relative to the number of end groups) of NaOH and ammonium chloride added to a 50 mL round bottom flask equipped with a magnetic flea and reflux condenser. The mixture was heated at 30 ºC for 24 hours. Upon completion, the solvent was removed by rotary evaporation.

### 5.3.2 Assay of Chymotrypsin Activity
45.4 mg BTNA was added in 10 mL MeOH. For each run the cuvette began with 50 μL BTNA, in addition to1 2 mL protein-buffer background solution. Hydrolysis was followed by monitoring product formation at 410 nm over a time period of 7500 s at RT. All absorption readings are recorded at least three times.

## 5.4 Protein Binding Assay for Circular Dichroism (CD) Spectroscopy

### 5.4.1 Preparation of Buffer Solution
1.75 g monosodium dihydrogen phosphate and 14.48 g of disodium hydrogen phosphate were dissolved in 1000 mL of distilled water. This gave a buffer of concentration 0.1M and pH 7.4.

### 5.4.2 Preparation of dendrimer solutions for Circular Dichroism analysis
Various PAMAM dendrimer solutions, G1.5, G2.5, G3.5 and G4.5 were made up in buffer solution to create a stock solution of concentration $1 \times 10^{-5}$ M. These dendrimer stock solutions were used to prepare dendrimer solutions of a concentration $2 \times 10^{-6}$ M by extracting 2 mL of each solution into 4 respective 10 mL volumetric flasks and diluting down with buffer solution.

### 5.4.3 Preparation of protein solutions

#### 5.4.3.1 Chymotrypsin: 5.2 mg Chymotrypsin was dissolved in 100 mL buffer to give a solution with a concentration $2 \times 10^{-6}$ M. 1 mL of this was extracted and dissolved in 10 mL buffer solution giving a second diluted solution of $1 \times 10^{-6}$ M.

#### 5.4.3.2 Cytochrome-C: 2.5 mg Cytochrome-c was dissolved in 100 mL buffer to give a solution with concentration $2 \times 10^{-6}$ M. 1 mL of this was extracted and dissolved in 10 mL buffer solution giving a second diluted solution of $1 \times 10^{-6}$ M.

A CD spectrum for each protein at concentration $1 \times 10^{-6}$ M was run.

**5.4.4 CD Analysis of Protein-Dendrimer solutions in a 1:1 ratio of concentration**

**5.4.4.1 Chymotrypsin:** The various dendrimer solutions (G1.5, G2.5, G3.5 and G4.5 $2 \times 10^{-6}$M) and Chymotrypsin solution ($2 \times 10^{-6}$ M) were mixed in equal volume (1 mL: 1 mL) to four respective sample vials. Each sample was transferred into a 10 mm quartz cuvette and a CD spectrum was generated for each at 37 °C.

**5.4.4.2 Cytochrome-C:** The various dendrimer solutions (G1.5, G2.5, G3.5 and G4.5 $2 \times 10^{-6}$M) and Cytochrome-c solution ($2 \times 10^{-6}$ M) were mixed in equal volume (1 mL: 1 mL) to four respective sample vials. Each sample was transferred into a 10 mm quartz cuvette and a CD spectrum was generated for each at 37 °C.

**5.4.5 CD Analysis of Protein-Dendrimer solutions in a 1:5 concentration ratio**

**5.4.5.1 Chymotrypsin:** The various dendrimer solutions (G1.5, G2.5, G3.5 and G4.5 $1 \times 10^{-5}$M) and Chymotrypsin solution ($2 \times 10^{-6}$ M) were mixed in equal volume (1 mL: 1 mL) to four respective sample vials. Each sample was transferred into a 10 mm quartz cuvette and a CD spectrum was generated for each at 37 °C.

**5.4.5.2 Cytochrome-C:** The various dendrimer solutions (G1.5, G2.5, G3.5 and G4.5 $1 \times 10^{-5}$M) and Cytochrome-c solution ($2 \times 10^{-6}$ M) were mixed in equal volume (1 mL: 1 mL) to four respective sample vials. Each sample was transferred into a 10 mm quartz cuvette and a CD spectrum was generated for each at 37 °C.

**5.4.6 Circular Dichroism Analysis involving temperature variation**

**5.4.6.1 Chymotrypsin:** To carry out a variable temperature CD spectrum, the appropriate absorption wavelength for Chymotrypsin was selected, which was determined from previous CD analysis. The wavelength of choice was found to be 230 nm, and the protein in buffer solution (2 mL), giving a concentration of $1 \times 10^{-6}$ M, was transferred to a 10 mm quartz cuvette and heated by 1 °C per minute from 37 °C to approximately 85 °C. The next stage was to put 1 mL Chymotrypsin in buffer solution ($2 \times 10^{-6}$ M) and 1 mL G3.5 PAMAM Dendrimer in buffer solution ($1 \times 10^{-5}$ M) into a 10 mm quartz cuvette and place it into the CD spectrometer. This was then heated by 1 °C per minute from 37 °C to approximately 85 °C.

**5.4.6.2 Cytochrome-C:** To carry out a variable temperature CD spectrum, the appropriate absorption wavelength for Cytochrome-C was selected, which was determined from previous CD analysis. The wavelength of choice was found to be 222 nm, and the protein in buffer solution (2 mL), giving a concentration of $1 \times 10^{-6}$ M, was transferred to a 10 mm quartz cuvette and heated by 1 °C per minute from 37 °C to approximately 95 °C. The next stage was to put 1 mL Cytochrome-C in buffer solution ($2 \times 10^{-6}$ M) and 1 mL G2.5 PAMAM Dendrimer in buffer solution ($1 \times 10^{-5}$ M) into a 10 mm quartz cuvette and place it into the CD spectrometer. This was then heated by 1 °C per minute from 37 °C to approximately 95 °C.

**5.4.7 Presentation of CD data**

The CD spectrometer displayed spectra with temperature in degrees Celsius (°C) along the x-axis and CD in millidegrees along the y-axis. The data along the y-axis was converted into percentage unfolding for data analysis.
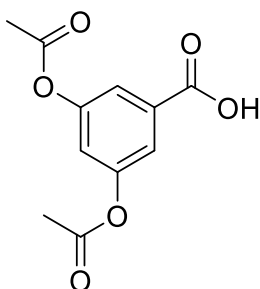
This was performed using the following formula:
Percentage unfolding for $n^{th}$ data point = $[(P_N - P_I) / (P_F - P_I)] \times 100$
Where $P_N = n^{th}$ CD data point, $P_I$ = initial CD data point and $P_F$ = final CD data point.
CD data was transferred into a database and this calculation was performed using Microsoft Excel.

## 5.5 Synthetic procedures for Anion Binding

### 5.5.1 Synthesis of 3,5diacetoxybenzoic acid (91)

A 250 mL round bottom flask was equipped with a magnetic stirrer bar and charged with 3, 5-dihydroxybenzoic acid (50.02 g, 0.32 moles) and acetic anhydride (150 mL) and fitted with a reflux condenser. There was a large quantity of acid being used, therefore efficient stirring was essential to complete dissolution. The reaction mixture was heated to reflux (160 °C) and left to reflux for 5-6 hours, giving rise to a brown solution. Excess acetic anhydride and acetic acid by-product was removed under high vacuum via vacuum distillation, ensuring that the solution is not heated above 80 °C at all times, to avoid polymerisation of the monomer.

Scheme 12 page 120
Scheme 16 page 132
Scheme 17 page 133

The compound was dissolved in 130 mL of refluxing chloroform and then filtered hot. This was followed by the addition of 45 mL of Petroleum ether 40:60 to the mother liquor, precipitating a white solid. The mixture was then left overnight to further the recrystalisation process.

The white solid was isolated by filtration and thoroughly washed with ice cold petroleum ether. The product obtained was then left in a vacuum desiccator overnight to dry thoroughly. Mother liquor obtained from filtration was rotary evaporated and re-disolved in refluxing chloroform and the recrystalisation process was repeated further to obtain as much 3,5-diacetoxybenzoic acid as possible.

Yield 41.23 g, 34 % ^{1}H NMR (CDCl$_3$, 400 MHz) $\delta_H$ 10.32 (br s, 1H, COO$\underline{H}$), 7.75 (d, 2H, *Ar o*-C$\underline{H}$, J=2.0), 7.20 (t, 1H, *Ar p*-C$\underline{H}$, J=2.0), 2.32 (s, 6H, -C$\underline{H_3}$) ^{13}CNMR (CDCl$_3$, 400 MHz) $\delta_C$ 170.24, 168.79, 151.02, 131.37, 120.82, 121.03, 121.12, 21.00 FTIR (cm$^{-1}$) 3400-2400, 1764 (COOR), 1688 (COOH), 1603,  EA %: Carbon (Expected value: 55.47 %) Found: 55.17 % Hydrogen (Expected value: 4.23 %) Found: 3.86 % ES-MS 237 (MH$^-$) m.p. 161-162 ˚C

### 5.5.2 Synthesis of N, N'- Bis-(4-hydroxy-phenyl)-isophthalamide (94)
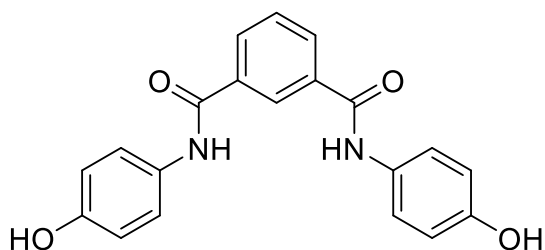
Triethylamine was vacuum distilled in the presence of the drying agent calcium hydride. A 100 mL 2 necked round bottom flask was oven dried, to this 4-aminophenol (0.59 g, 5.41 mmol) was added and the flask was cooled under nitrogen. When cool, dry triethylamine (0.76 mL, 7.51 mmol) and NMP (30 mL), were added via syringe and hypodermic needle through a fresh suba seal.

Scheme 14 page 123

A second 100 mL 2 neck round bottom flask was oven dried and isophthaloyl chloride (0.51 g, 2.51 mmol) was added and the flask was allowed to cool under nitrogen; when cool NMP (30 mL) was added. 4-aminophenol, NMP and triethylamine were stirred together and the flask was heated to 60 °C. Isophthaloyl chloride solution was then added via a syringe, dropwise, over a period of 10 minutes and the reaction was left to stir for 30 minutes. The temperature was then raised to 80 °C and left for an additional 20 minutes. The solution was filtered and the crystals (salt by-product) were washed with cold methanol. The mother liquor was vacuum distilled in order to remove the NMP solvent (NB. NMP has a boiling point of 202 ºC).  Once all the solvent had been removed, methanol

was added to the reaction flask and swirled. The white solid produced was filtered off and washed thoroughly with ice cold methanol and finally placed in a vacuum desiccator to ensure complete dryness is achieved.

Yield 2.71 g, 31 % ^{1}HNMR (CD$_3$SOCD$_3$, 400 MHz) $\delta_H$ 10.21 (s, 2H, O<u>H</u>) 9.33 (s, 2H N<u>H</u>) 8.48 (s, 1H, Ar-C=OCC<u>H</u>CC=O) 8.09 (dd, 2H, Ar-C<u>H,</u> J=8.0, 1.5) 7.66 (t, 1H, Ar-C<u>H,</u> J =8.0) 7.58 (d, 4H, Phenol NHCC<u>H</u>, J= 9.0) 6.80 (d, 4H, Phenol C<u>H</u>COH, J=9.0) ^{13}CNMR (CD$_3$SOCD$_3$, 400 MHz) $\delta_C$ 164.99, 154. 27, 135.82, 131.05, 130.71, 128.95, 127.20, 122.71, 115.50 FTIR (cm$^{-1}$) 3276 (OH) 3000-3020 (aromatic C-H stretch) 1644 (amide C=O stretch) 1610 (aromatic C=C bend), 1522, 1540, 1422, 1240 EA %: Carbon (Expected value: 68.96 %) Found: 66.15 % Hydrogen (Expected value: 4.63 %) Found: 4.63 % Nitrogen (Expected value: 8.04%) Found: 7.84 ES-MS 349 (MH$^+$) m.p. 317-319 ˚C

### 5.5.3 Acetylation of N, N'- Bis-(4-hydroxy-phenyl)-isophthalamide (93)
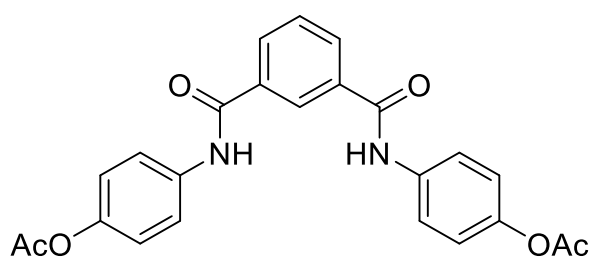


Figure 67 page 122
Scheme 14 page 123
Figure 69 page 124
Scheme 17 page 133

An oven dried round bottom flask was charged with N, N'- Bis-(4-hydroxy-phenyl)-isophthalamide (0.5 g, 1.4 mmol) and dissolved in anhydrous pyridine (75 mL). The flask was degassed with Argon before addition of acetyl chloride (0.61 mL, 7.8 mmol). The mixture was then stirred at room temperature for a period of 4 hours. Pyridine was then removed via vacuum distillation and the crude product was purified by column chromatography. The crude product was loaded in a minimum amount of chloroform and eluted with ethyl acetate (R$_f$ = 0.84)

Yield: 192 mg, 31% ^{1}HNMR (d$^6$-DMSO, 400 MHz) $\delta_H$ 10.53 (s, 2H. N<u>H</u>) 8.54 (s, 1H, Ar-COCC<u>H</u>CCO) 8.16 (dd, 2H, Ar-COCC<u>H</u>, J=2.0, 8.) 7.83 (m, 4H, Ar-CH$_3$COOCC<u>H</u>) 7.72 (t, 1H, Ar-COCCHC<u>H</u>CHCCO J=8.0) 7.17-7.13 (m, 4H, Ar-CH$_3$COOCCHC<u>H</u>) 2.28 (s, 6H, C<u>H$_3$</u>) ^{13}CNMR (d$^6$-DMSO, 400 MHz) $\delta_C$ 169.8, 165.5, 146.8, 137.1, 135.5, 131.2, 129.1, 127.5, 122.4, 121.8 FTIR (cm$^{-1}$) 3000.1-3030.6 (aromatic region) 1703.2 (amide CO) 1610.9 (aromatic C=C) 1561, 1510, 1427, 1229 ES-MS 433 (MH$^+$) EA %: Carbon (Expected value: 66.66 %) Found: 66.32 % Hydrogen (Expected value: 4.66 %) Found: 4.47 % Nitrogen (Expected value: 6.48 %) Found: 6.42 % m.p. 258-260 ˚C

### 5.5.4 Synthesis of N, N'- Bis-(3-hydroxy-phenyl)-isophthalamide (101)
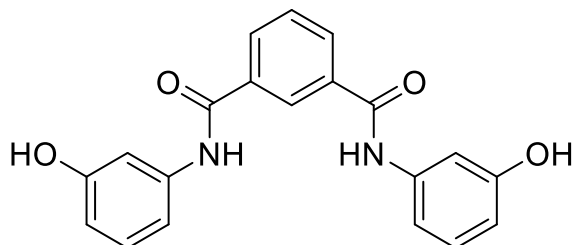


Scheme 18 page 134
Figure 72 page 135

3-Aminophenol (13.10 g, 0.119 mol) and anhydrous N, N'-Dimethylacetamide (75 mL) was added to a 250 mL round bottom flask under an inert atmosphere of argon. Isophthaloyl chloride (12.18 g, 0.060 mol) was added after cooling the solution to 0 ºC. The reaction was stirred for 6 hours, during which the temperature was allowed to rise to room temperature. The reaction mixture was then poured into 1 L of ice cold distilled water and filtered.

248

The filtrate was washed several times with distilled water and the pH of the filtrate was monitored using litmus paper. Purification was achieved by dissolving the crude product in a minimum amount of hot ethanol followed by a hot filtration. The filtrate was subsequently added to an excess of ice cold distilled water and filtered. The crystals were dried under vacuum at 100 °C.

Crude yield 17.5186 g ,84 % Pure Yield 11.14 g, 64% $^1$HNMR (CD$_3$SOCD$_3$, 400 MHz) $\delta_H$ 10.31 (s, 2H, O$\underline{H}$) 9.47 (s, 2H, N$\underline{H}$) 8.47 (s, 1H, *Ar*-OCCC$\underline{H}$CCO) 8.11 (dd, 2H, *Ar*-COCC$\underline{H}$, J=8.0, 2.0) 7.68 (t, 1H, *Ar*-COCCHC$\underline{H}$, J=8.0) 7.39 (m, 2H, *Ar*-NHCC$\underline{H}$COH) 7.20-7.12 (bm, 4H, *Ar*-NHCCHC$\underline{H}$) 6.53 (bm, 2H, *Ar*-NHCCHCOHC$\underline{H}$) $^{13}$ CNMR (CD$_3$SOCD$_3$, 400 MHz) $\delta_c$ 107.9, 111.4, 111.6, 127.4, 129.0, 129.8, 131.1, 135.7, 140.5, 158.0, 165.5 FTIR (cm$^{-1}$) 3364 (N-H stretch), 3188 (OH stretch), 1646, 1604 (amide C=O stretch), 1547, 1489, 1450, 1266, 683 EA %: Carbon (Expected value: 68.96 %) Found: 68.53 % Hydrogen (Expected value: 4.63 %) Found: 4.81 % Nitrogen (Expected value: 8.04%) Found: 7.89 % ES-MS 349.1 (MH$^+$) m.p. 247-249 ˚C

### 5.5.5 Acetylation of  N, N'- Bis-(3-hydroxy-phenyl)-isophthalamide (100)
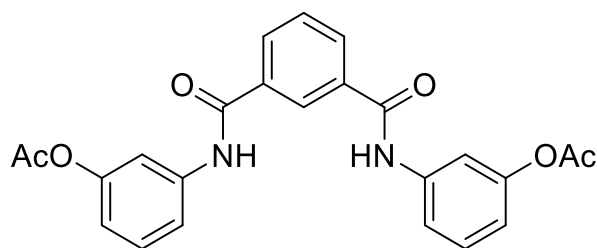


An oven dried round bottom flask was charged with N, N'- Bis-(3-hydroxy-phenyl)-isophthalamide (1.0 g, 2.9 mmol) and dissolved in anhydrous pyridine (75 mL). The flask was degassed with Argon before addition of acetyl chloride (1.22 mL, 17.2 mmol). The mixture was then stirred at room temperature for a period of 4 hours.

Scheme 18 page 134
Figure 73 page 136
Figure 74 page 137

Pyridine was then removed via vacuum distillation and dissolved in dichloromethane. This was followed by washings with saturated sodium hydrogen carbonate solution and distilled water to remove any trace amounts of acid. The organic layer was then reduced down and dissolved again in chloroform and filtered by gravity. A cream solid was collected and purified by recrystalisation. The crude cream solid was dissolved in a minimum amount of hot dichloromethane and petroleum ether (40:60) was added drop wise until the yellow solution remained cloudy. The solvent was left to evaporate slowly yielding cream coloured crystals.

Yield 800 mg, 65% $^1$HNMR ((CD$_3$)$_2$CO, 400 MHz) $\delta_H$ 9.86 (s, 2H, N$\underline{H}$) 8.55 (s, 1H, *Ar*-OCCC$\underline{H}$CCO) 8.20 (dd, 2H, *Ar*-COCC$\underline{H}$, J=8.0, 2.0) 7.81 (t, 1H, *Ar*-COCCHC$\underline{H}$CHCCO J=2.0) 7.70-7.66 (bm, 4H, *Ar*-CONHCC$\underline{H}$CHCHCO, *Ar* -CONHCC$\underline{H}$CO) 7.40-7.38 (bm, 2H, *Ar*-CONHCCHC$\underline{H}$CHCO) 6.92 (dd, 2H, *Ar*-CONHCCHCHC$\underline{H}$CO, J=8.0, 1.0) 2.30 (s, 6H, OC$\underline{H_3}$) 13 CNMR ((CD$_3$)$_2$CO, 400 MHz) $\delta_c$ 168.8, 164.9, 151.3, 140.3, 135.4, 130.6, 129.3, 128.8, 126.5, 117.2, 117.2, 117.0, 113.6, 20.1 FTIR (cm$^{-1}$) 3050-3100 (aromatic C-H stretch), 1764 (acetate C=O stretch), 1646, 1603 (amide C=O), 1543, 1483, 1433, 1196, 681 EA %: Carbon (Expected value: 66.66 % ) Found: 65.88 % Hydrogen (Expected value: 4.66 %) Found: 4.45 % Nitrogen (Expected value: 6.48%) Found: 6.40 %  ES-MS 433.1406 (MH$^+$) m.p. 178-180 ˚C

## 5.6 Synthetic procedures involving the polymerisation of 3, 5-diacetoxybenzoic acid

### 5.6.1General procedure for the polymerisation of 3, 5-diacetoxybenzoic acid

3, 5-Diacetoxy benzoic acid (various amounts) and diphenyl ether (various amounts) were dispensed into a 250 mL round bottom flask, which was then thoroughly degassed and flushed with nitrogen. The mixture was heated to 225 °C and stirred for a period of 45 minutes. The temperature was reduced to 180 °C and the reaction was subsequently placed under reduced pressure for 4 hours. The crude mixture was dissolved in refluxing THF and precipitated into ice cold methanol (800 mL) and placed in a freezer overnight to maximise precipitation. The resulting solid was filtered off and washed with ice cold methanol, yielding the polymer.

### 5.6.2 Polymerisation of 3, 5-diacetoxybenzoic acid (97)
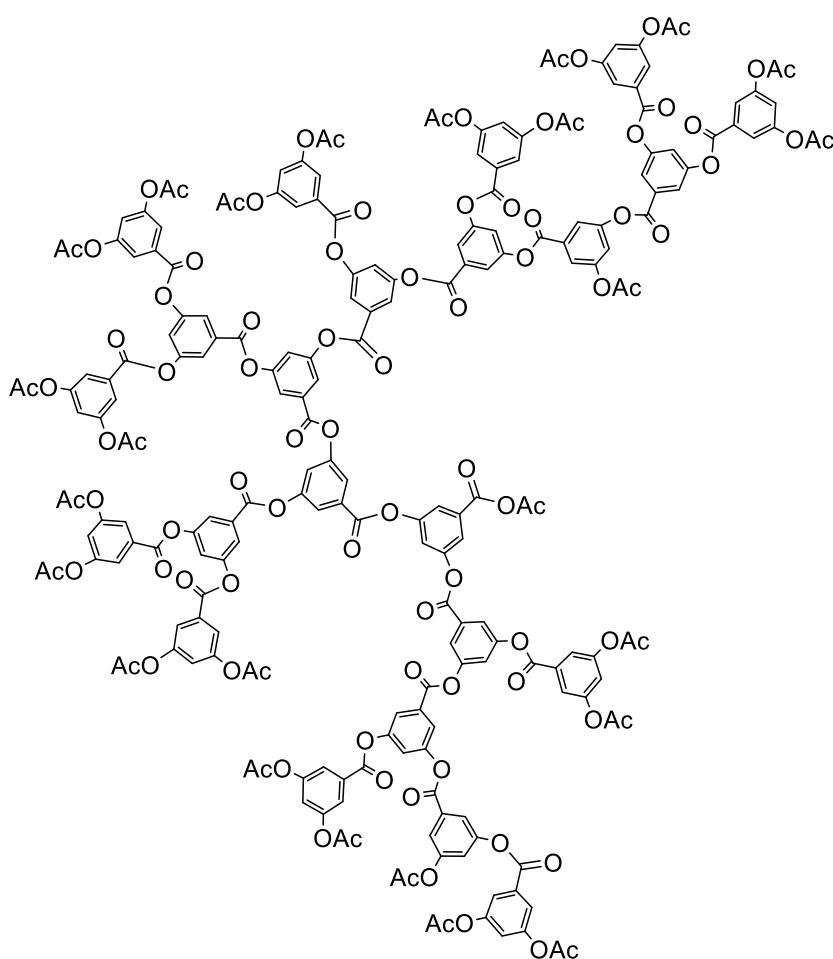


Scheme 16 page 132
Scheme 17 page 133

The general procedure was followed where 3, 5-Diacetoxy benzoic acid (3.95 g, 0.02 mol) and diphenyl ether (3.95 g, 0.02 mol) were reacted together, yielding the polymer (white solid powder).

Yield 2.42 g, 61 % (by mass) $^1$HNMR (CD$_3$SOCD$_3$, 400 MHz) $\delta_H$ 8.20-8.02 (br d, 1H, [Polymer] Ar $p$-C$\underline{H}$) 7.96-7.79 (br d, 2H, [Polymer] Ar $o$-C$\underline{H}$) 2.38 (br s, 3H [Polymer] C$\underline{H}_3$) $^{13}$CNMR (CDCl$_3$, 400 MHz)  $\delta_C$ 168.8, 162.8, 151.2, 130.9, 130.7, 121.3, 120.9, 21.0 FTIR (cm$^{-1}$) 2972, 2209, 2039 (aromatic C-H stretch) 1742 (ester C=O stretch) 1367, 1276 GPC M$_n$ = 23535 M$_w$ = 59502 PD = 2.53

**5.6.3 Polymerisation of 3, 5-diacetoxybenzoic acid with 4-Nitrophenyl acetate core using a 1:20 ratio**
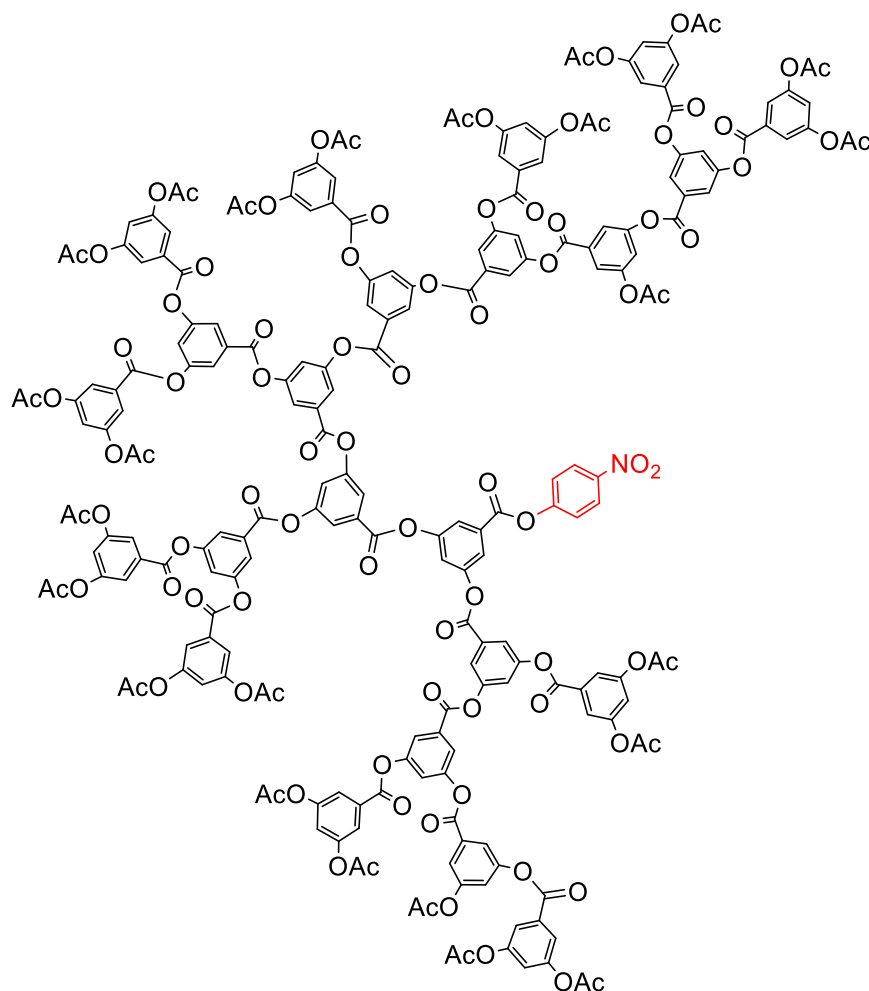


The general procedure was followed where 3, 5-Diacetoxy benzoic acid (3.95 g, 0.02 mol), 4-Nitrophenyl acetate (150.0 mg, 0.83 mmol) and diphenyl ether (4.10 g, 0.02 mol) were reacted together, yielding the polymer (white solid powder).

Yield 3.23 g, 79% (by mass) ^{1}HNMR (CDCl$_3$, 400 MHz) $\delta_H$ 8.39-8.31 (br d, 2H, [Core] Ar C$\underline{H}$CNO$_2$) 8.09-7.93 (br d, 1H, [Polymer] Ar $p$-C$\underline{H}$) 7.92-7.77 (br d, 2H, [Polymer] Ar $o$-C$\underline{H}$) 2.39 (br s, 3H, [Polymer] C$\underline{H}_3$) ^{13}CNMR (CDCl$_3$, 400 MHz) $\delta_C$ 168.74, 162.78, 151.18, 130.92, 121.32, 21.02 FTIR (cm$^{-1}$) 2972, 2930, 2505 (aromatic C-H stretch) 1743 (ester C=O stretch) 1593, 1443, 1369, 1277, 755 (C-H aromatic $ortho$) GPC M$_n$ = 8992 M$_w$ = 21745 PD = 2.42

**5.6.4 Polymerisation of 3, 5-diacetoxybenzoic acid with N, N'- Bis-(4-acetoxy-phenyl)-isophthalamide core using a 1:20 ratio (98)**
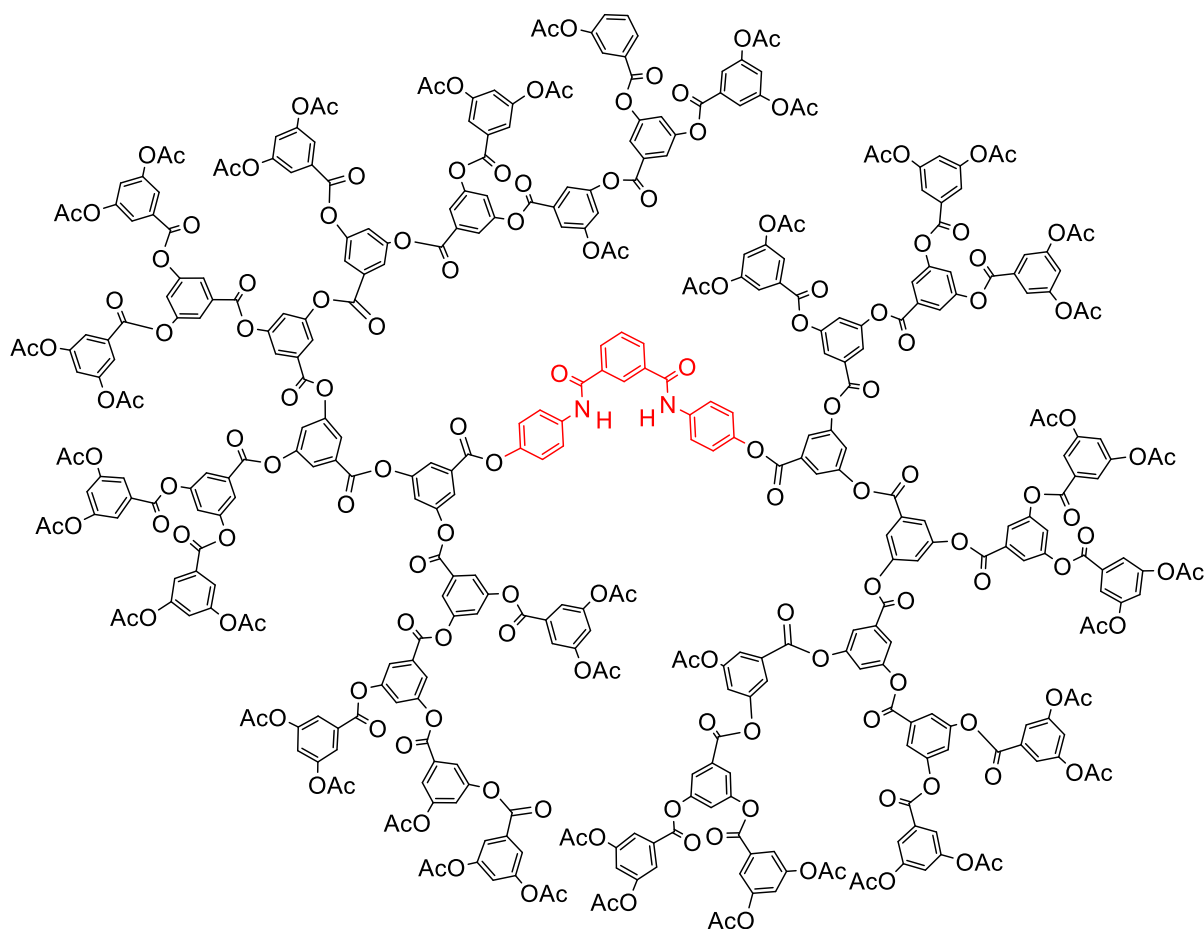


Scheme 17 page 133
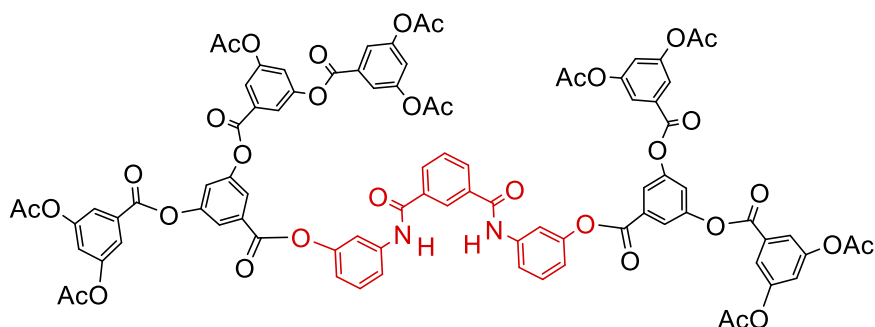
The general procedure was followed where 3, 5-Diacetoxy benzoic acid (2.18 g, 9.15 mmol), 4- N, N'- Bis-(4-acetoxy-phenyl)-isophthalamide (0.25 g, 0.72 mmol) and diphenyl ether (3.01 g, 17.68 mmol) were reacted together, yielding the polymer (cream coloured solid powder).

Yield 462 mg, 19 % (by mass) HNMR (C$_4$D$_8$O, 400 MHz) $\delta_H$ 7.76 (br s, 1H, [Core] C=OCC$\underline{H}$CC=O) 7.17 (br s, 1H, [Core] Ar-C$\underline{H}$) 6.68 (br s, 2H, [Core] Ar-C$\underline{H}$) 6.37-6.16 (br d, 1H, [Polymer] Ar $p$-C$\underline{H}$) 6.12-5.96 (br d, 2H, [Polymer] Ar $o$-C$\underline{H}$) 0.44 (br s, 3H, [Polymer] C$\underline{H}_3$) $^{13}$CNMR (C$_4$D$_8$), 400 MHz) $\delta_C$ 166.09, 160.78, 149.75, 129.37, 118.61, 22.48 FTIR (cm$^{-1}$) 2972, 2931, 2505 (aromatic C-H stretch) 1742 (ester C=O stretch) 1442, 1277, 754 GPC M$_n$ = 2934 M$_w$ = 4801 PD = 1.64

## 5.7 Polymerisation of 3, 5-diacetoxybenzoic acid with N, N'- Bis-(3-acetoxy-phenyl)-isophthalamide core

### 5.7.1 Polymerisation of 3, 5-diacetoxybenzoic acid with N, N'- Bis-(3-acetoxy-phenyl)-isophthalamide core using a 1:1 ratio (104)



Figure 81 page 149
Figure 82 page 150

The general procedure was followed where 3, 5-Diacetoxy benzoic acid (171.10 mg, 0.72 mmol), 4-N, N'- Bis-(3-acetoxy-phenyl)-isophthalamide (0.25 g, 0.72 mmol) and diphenyl ether (421.0 mg, 2.48 mmol) were reacted together, yielding the polymer (light brown/grey solid powder).

Yield 93 mg, 54 % (by mass) $^1$HNMR (CDCl$_3$, 400 MHz) $\delta_H$ 8.57-8.74 (bm, 2H, [Core] N$\underline{H}$) 8.06-8.33 (bm, 1H, [Core] *Ar*-OCCC$\underline{H}$CCO, 2H, [Core] *Ar*-COCC$\underline{H}$) 7.67-8.04 (bm, 1H [Core] *Ar*-COCCHC$\underline{H}$CHCCO, 2H [Polymer] *Ar p*-C$\underline{H}$) 7.47-7.66 (bm, 4H, [Core] *Ar*-CONHCC$\underline{H}$CHCHCO, *Ar* –CONHCC$\underline{H}$CO2H) 7.04-7.46 (bm, 2H, [Core] *Ar*-CONHCC$\underline{H}$CO, 2H, [Polymer] *Ar o*-C$\underline{H}$) 6.71-6.94 (bm, 2H, [Core] *Ar*-CONHCCHCHC$\underline{H}$CO) 2.34 (bs, 3H, [Polymer] C$\underline{H}_3$) $^{13}$CNMR (CDCl$_3$, 400 MHz) $\delta_C$ 169.7, 168.8, 164.5, 163.8, 163.5, 162.8, 151.2, 139.0, 133.3, 131.3, 130.7, 129.5, 129.2, 128.3, 125.6, 121.3, 120.9, 117.5, 113.9, 21.0 FTIR (cm$^{-1}$) 2000-2050 (aromatic C-H) 1740 (ester C=O stretch) 1370, 1287, 757 GPC M$_n$ = 1554 M$_w$ = 2390 PD = 1.54 M$_n$ (NMR estimation) = 2034

## 5.7.2 Polymerisation of 3, 5-diacetoxybenzoic acid with N, N'- Bis-(3-acetoxy-phenyl)-isophthalamide core using a 1:5 ratio (103)
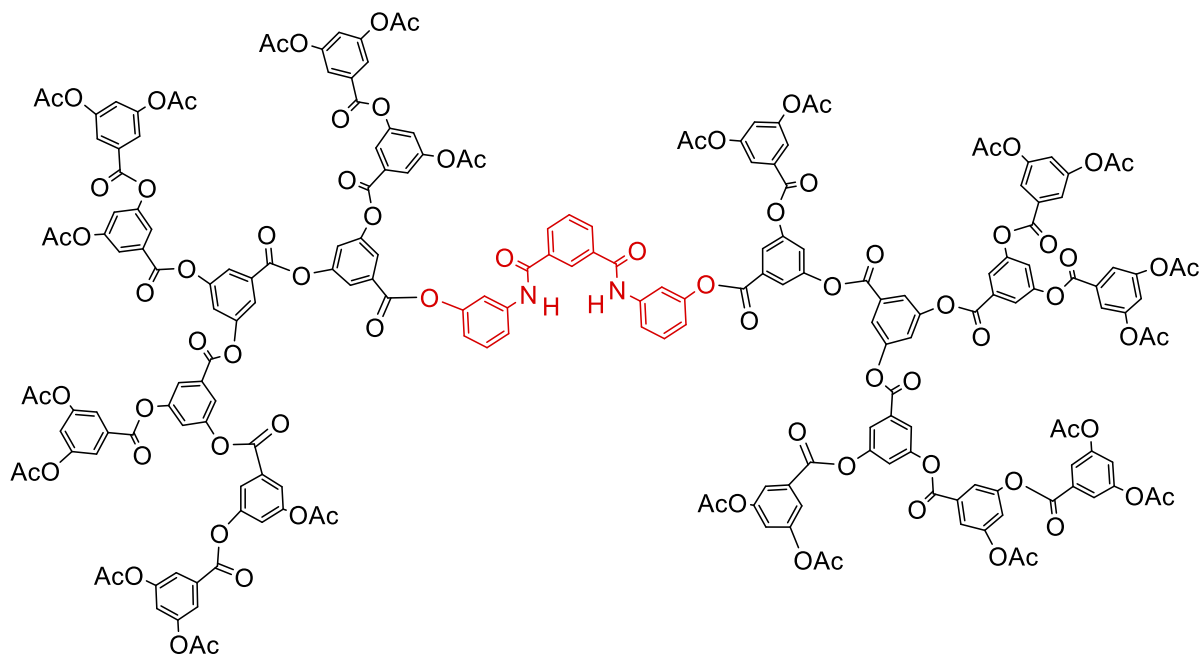


Figure 76 page 140
Figure 77 page 141

The general procedure was followed where 3, 5-Diacetoxy benzoic acid (688 mg, 2.89 mmol), 4- N, N'- Bis-(3-acetoxy-phenyl)-isophthalamide (0.25 g, 0.72 mmol) and diphenyl ether (0.95 g, 5.58 mmol) were reacted together, yielding the polymer, which was a light brown/grey solid powder in appearance.

Yield 488.2 mg, 71 % (by mass) $^1$HNMR (CDCl$_3$, 400 MHz) $\delta_H$ 8.55-8.67 (bm, 2H, [Core] N$\underline{H}$) 8.20-8.33 (bm, 1H, [Core] *Ar*-OCCC$\underline{H}$CCO, 2H, [Core] *Ar*-COCC$\underline{H}$) 7.65-8.08 (bm, 1H [Core] *Ar*-COCCHC$\underline{H}$CHCHCCO, 2H [Polymer] *Ar p*-C$\underline{H}$) 7.40-7.64 (bm, 4H, [Core] *Ar*-CONHCC$\underline{H}$CHCHCO, *Ar* -CONHCC$\underline{H}$CO2H) 7.19-7.39 (bm, 2H, [Core] *Ar*-CONHCC$\underline{H}$CO, 2H, [Polymer] *Ar o*-C$\underline{H}$) 6.72-6.90 (bm, 2H, [Core] *Ar*-CONHCCHCHCH$\underline{H}$CO) 2.25 (bs, 3H, [Polymer] C$\underline{H}_3$) ) $^{13}$CNMR (CDCl$_3$, 400 MHz) $\delta_C$ 168.8, 163.8, 162.8, 151.2, 139.1, 130.9, 130.7, 129.7, 121.3, 120.9, 117.5, 114.0, 21.0 FTIR (cm$^{-1}$) 2009-2158 (aromatic C-H) 1741 (ester C=O stretch) 1369, 1286, 757 GPC M$_n$ = 4009 M$_w$ = 12973 PD = 3.2 M$_n$ (NMR estimation) = 4670

### 5.7.3 Polymerisation of 3, 5-diacetoxybenzoic acid with N, N'- Bis-(3-acetoxy-phenyl)-isophthalamide core using a 1:20 ratio (105)
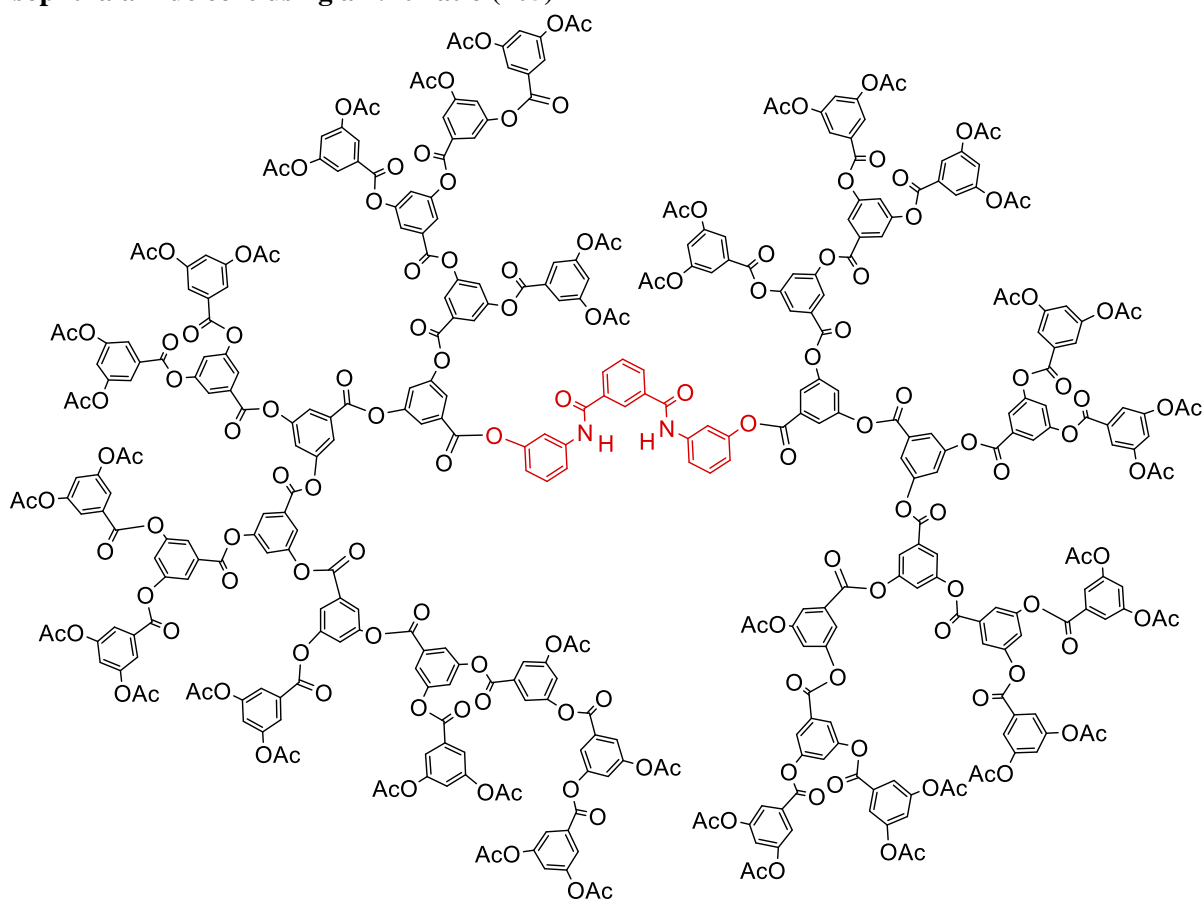


Figure 83 page 151
Figure 84 page 152

The general procedure was followed where 3, 5-Diacetoxy benzoic acid (2.18 g, 9.15 mmol), 4- N, N'- Bis-(3-acetoxy-phenyl)-isophthalamide (0.25 g, 0.72 mmol) and diphenyl ether (3.01 g, 17.68 mmol) were reacted together, yielding the polymer (white solid powder).

Yield 1.42 g, 65% (my mass) ^{1}HNMR (CDCl$_3$, 400 MHz) $\delta_H$ 8.50-8.71 (bm, 2H, [Core] N$\underline{H}$) 8.22-8.43 (bm, 1H, [Core] *Ar*-OCCC$\underline{H}$CCO) 8.09-8.19 (bm, 2H, [Core] *Ar*-COCC$\underline{H}$) 7.75-8.11 (bm, 1H [Core] *Ar*-COCCHC$\underline{H}$CHCCO, 2H [Polymer] *Ar p*-C$\underline{H}$) 7.19-7.62 (bm, 4H, [Core] *Ar*-CONHCC$\underline{H}$CHCHCO, *Ar* -CONHCC$\underline{H}$CO2H, [Core] *Ar*-CONHCC$\underline{H}$CO, 2H, [Polymer] *Ar o*-C$\underline{H}$) 6.72-6.89 (bm, 2H, [Core] *Ar*-CONHCCHC$\underline{H}$CHCO) 2.31 (bs, 3H, [Polymer] C$\underline{H_3}$) ^{13}CNMR (CDCl$_3$, 400 MHz) $\delta_C$ 168.8, 162.8, 151.2, 130.9, 130.7, 129.7, 123.2, 121.3, 120.9, 118.9, 21.0 FTIR (cm$^{-1}$) 2972, 2931, 2505 (aromatic C-H stretch), 1742 (ester C=O stretch), 1442, 1277, 754 GPC M$_n$ = 10343 M$_w$ = 42137 PD = 4.07 M$_n$ (NMR estimation) = 12,299

## 5.7.4 Synthesis of Polyglycidol with 4-Nitrophenol core (109)
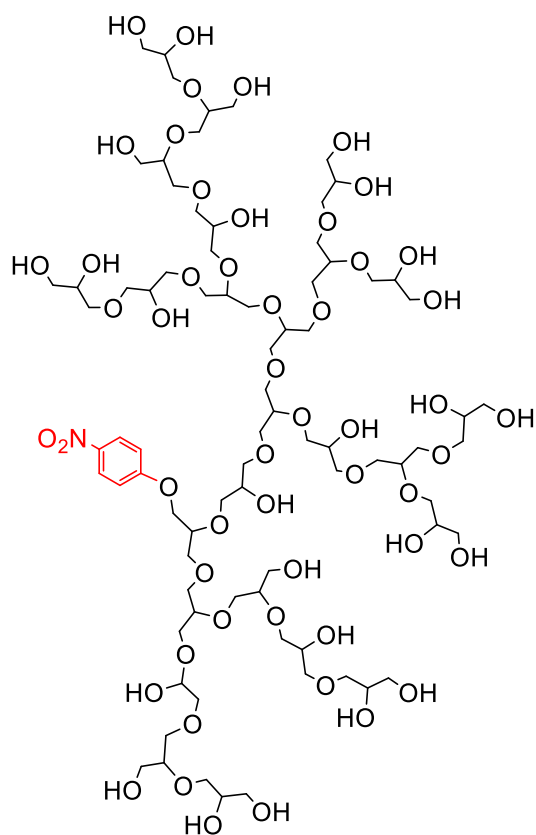


Scheme 22 page 166

Para-nitro phenol (0.25 g, 2.29 mmol) was added to Diethylene glycol dimethyl ether (20 mL) in a 100mL round bottomed flask. The solution was heated to 50 ºC until all the Nitro phenol was dissolved before raising the temperature to 90 ºC. After 20 minutes, sodium hydride (14.4 mg, 0.6 mmol) was added to the solution (the solution turned from colourless to yellow). The solution was left stirring for a period of 90 minutes. Glycidol (3.03 mL, 0.05 moles) was added, drop-wise, over a period of 12 hours using a syringe pump. The reaction mixture was then left to react for a further 5 hours. The reaction mixture was cooled to room temperature and then the solvent was decanted off. Methanol (50 mL) was added to the reaction mixture and left stirring until dissolution was complete. The solution was then added, drop-wise, to ice cold acetone (400 mL). Once addition was complete, the mixture was covered with tin foil and left stirring for 1 hour before decanting the solvent. Acetone (400 ml) was added to the product again, before covering with aluminium foil and stirring for a further hour. The acetone was disposed and the product was dried overnight in a vacuum oven to give hyperbranched polyglycidol as golden brown, viscous oil.

Yield 473 mg, 14 % (by mass) $^1$HNMR (D$_2$O, 400 MHz) $\delta_H$ 8.20 (s, 1H, [Core] C$\underline{H}$CNO$_2$) 3.95-3.20 (bm, 4H [Polymer] O$\underline{H}$, C$\underline{H}$, C$\underline{H_2}$) (D$_2$O, 400 MHz) $\delta_C$ 79.37, 72.09, 62.53 FTIR (cm$^{-1}$) 3360 (O-H stretch) 2869-2970 (C-H stretch) GPC M$_n$ = 12715 M$_w$ = 52970 PD = 4.17

## 5.8 Di-block encapsulation studies
### 5.8.1 Synthesis of mPEG-b-PCL di-block copolymer (112) †
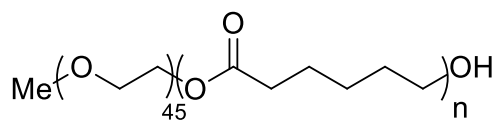


(i)   n = 5
(ii)  n = 10
(iii) n = 20
(iv) n = 60

Scheme 23 page 171

Oven-dried mPEG (3.001 g, 1.501 mmol) was added to a 50 mL two-neck round-bottom flask and stirred for 1 h at 130 °C under vacuum. Then the apparatus was refilled with nitrogen and ε-caprolactone (varied in ratio to the mPEG monomer units) was added using 10 mL syringe followed tin(II)2-ethyl hexanoate (0.05 % w/w). The reaction mixture was stirred for 24 hours at 130 °C to yield white solid at ambient temperature which was dissolved in dichloromethane and precipitated into petroleum ether 40-60 to yield methyl polyethylene glycol-*block*-poly(ε-caprolactone) as a white solid.

(i)

mPEG (3.001 g, 1.501 mmol) was reacted with PCL (0.97 mL) to give mPEG-*b*-PCL5 (14.606 g, 99 %) $^1$HNMR (CDCl$_3$, 400 MHz$_Z$) $\delta_H$ 4.24 (2H, m, OCH$_2$CH$_2$OCO), 4.07 ( 12H, t, CH$_2$OH J=6.5), 3.65 (180H, s, OCH$_2$CH$_2$O), 3.39 (3H, s, CH$_3$O), 2.32 (11H, t, α-CH$_2$ J=7.5), 1.66 (21H, m, β and δ-CH$_2$), 1.39 ( 10H, m, γ-CH$_2$) $^{13}$CNMR (CDCl$_3$, 400 MHz$_Z$) $\delta_C$ 173.6, 70.5, 64.1, 34.1, 28.3, 25.5, 24.6 FTIR (cm$^{-1}$) 3417, 1721, 1239, 1106, 732 GPC (LMW, THF) (n=5) Mn = 1921 PD = 1.20

(ii)

mPEG (3.001 g, 1.501 mmol) was reacted with PCL (1.83 mL, 16.5 mmol) to give mPEG-*b*-PCL10 (4.151 g, 85 %) $^1$HNMR (CDCl$_3$, 400 MHz$_Z$) $\delta_H$ 4.24 (2H, m, OCH$_2$CH$_2$OCO), 4.07 (23H, t, CH$_2$OH, J = 6.5) 3.66 (181H, s, OCH$_2$CH$_2$O), 3.39 (3H, s, CH$_3$O), 2.32 (25H, t, α-CH$_2$, J = 7.5), 1.66 (49H, m, β and δ-CH$_2$), 1.39 (25H, m, γ-CH$_2$) $^{13}$CNMR (CDCl$_3$, 400 MHz$_Z$) $\delta_C$ 173.6, 70.5, 64.1, 34.1, 28.3, 25.5, 24.6 FTIR (cm$^{-1}$) 3417, 1722, 1240, 1104, 731 GPC (LMW, THF) (n=10) Mn = 2506 PD = 1.18

(iii)

mPEG (3.001 g, 1.501 mmol) was reacted with PCL (1.83 mL, 16.5 mmol) to give mPEG-*b*-PCL10 (4.151 g, 85 %) $^1$HNMR (CDCl$_3$, 400 MHz$_Z$) $\delta_H$ 4.23 (2H, m, OCH$_2$CH$_2$OCO), 4.07 (44H, t, CH$_2$OH, J = 6.5) 3.66 (182H, s, OCH$_2$CH$_2$O), 3.39 (3H, s, CH$_3$O), 2.32 (46H, t, α-CH$_2$, J = 7.5), 1.66 (96H, m, β and δ-CH$_2$), 1.39 (48H, m, γ-CH$_2$) $^{13}$CNMR (CDCl$_3$, 400 MHz$_Z$) $\delta_C$ 173.6, 70.5, 64.1, 34.1, 28.3, 25.5, 24.6 FTIR (cm$^{-1}$) 3417, 1723, 1240, 1104, 731 GPC (LMW, THF) (n=20) Mn = 4344 PD = 1.23

(iv)

mPEG (3.001 g, 1.501 mmol) was reacted with PCL (1.83 mL, 16.5 mmol) to give mPEG-*b*-PCL10 (4.151 g, 85 %) $^1$HNMR (CDCl$_3$, 400 MH$_Z$) $\delta_H$ 4.23 (2H, m, OCH$_2$CH$_2$OCO), 4.07 (138H, t, CH$_2$OH, J = 6.5) 3.65 (172H, s, OCH$_2$CH$_2$O), 3.39 (3H, s, CH$_3$O), 2.32 (140H, t, α-CH$_2$, J = 7.5), 1.66 (290H, m, β and δ-CH$_2$), 1.39 (146H, m, γ-CH$_2$) $^{13}$CNMR (CDCl$_3$, 400 MH$_Z$) $\delta_C$ 173.6, 70.5, 64.1, 34.1, 28.3, 25.5, 24.6 FTIR (cm$^{-1}$) 3417, 1722, 1239, 1106, 732 GPC (LMW, THF) (n=60) Mn = 7772 PD = 1.34

† The synthesis of mPEG-b-PCL di-block copolymers of varying chain length were prepared and analysed by Caroline Glover, a 4$^{th}$ year project student

### 5.8.2 Micelle formation
Micelle samples of di-block copolymers were prepared by direct dissolution method in which an aqueous solution of polymer (1 mg mL$^{-1}$) was vigorously stirred on the shaker for 30 minutes.

### 5.8.3 HBP loaded micelle formation
HBP loaded polymeric micelles were prepared by an oil-in-water emulsion method for the slightly water soluble mPEG-PCL di-block copolymer. This method involved dropwise addition of HBP dissolved in a suitable organic solvent to the preformed micelle solution. The mixture was stirred for 1.5 hours to remove organic solvent by evaporation. Un-loaded HBP was removed by filtration through Whatman® GD/X syringe filter.

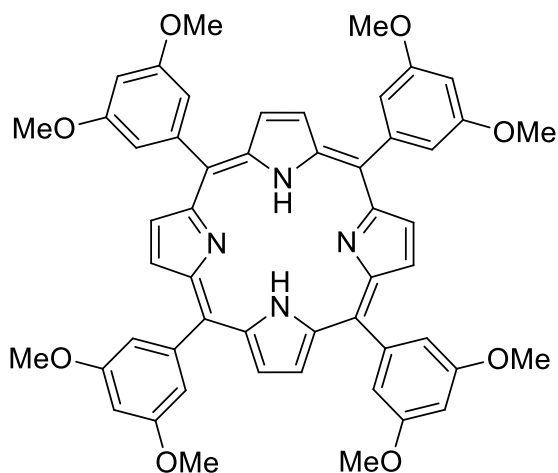### 5.8.4 Synthesis of tetraphenyl porphyrin (115)
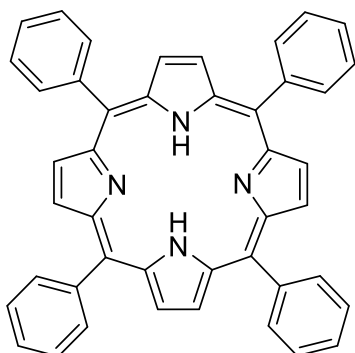


Pyrrole (7.00 mL, 0.101 mol) was added to a refluxing solution of benzaldehyde (10.0 mL, 0.0985 mol) in propionic acid (375 mL) and stirred for 30 minutes under reflux. The reaction mixture was left to cool to ambient temperature and then filtered under vacuum to give meso-tetraphenyl porphyrin (2.8 g, 18%) as a purple powder;

Scheme 24 page 173

Yield 2.92 g, 19 % $^1$HNMR (CDCl$_3$, 400 MH$_Z$) $\delta_H$ 8.90 (s, 8H, Pyrrolic-C$\underline{H}$) 8.27 (8H, dd, Phenylic *o*-C$\underline{H}$ J = 2, 7.5) 7.81 (m, 12H, Phenylic *m*-C$\underline{H}$, Phenylic *p*-C$\underline{H}$) -2.71 (s, 2H, N$\underline{H}$) $^{13}$CNMR (CDCl$_3$, 400 MH$_Z$) $\delta_C$ 142.2, 134.6, 132.3, 127.7, 126.7, 120.2 FTIR (cm$^{-1}$) 3315 (amine N-H stretch) 3030-3054 (aromatic and alkene C-H stretch) 1594, 1441, 795, 695 EA %: Carbon (Expected value: 85.97 %) Found: 85.34 % Hydrogen (Expected value: 4.92 %) Found: 4.61 % Nitrogen (Expected value: 9.11 %) Found: 8.96 % ES-MS 615 MH$^+$ (expected 616) UV absorbance (CHCl$_3$) $\lambda_{max}$ (nm) 418.5, 515.0, 550.5, 590.5, 645.0

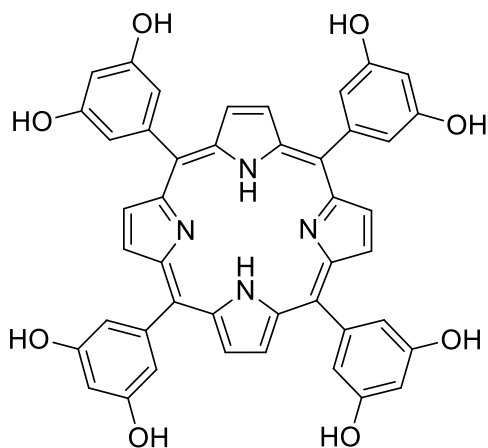### 5.8.2 Synthesis of 5, 10, 15, 20-tetrakis(3, 5-dimethoxyphenyl)-21H, 23H-Porphyrin (118)



Freshly distilled pyrrole (5.54 mL, 80 mmol) and 3, 5-dimethoxybenzaldehyde (13.28 g, 80 mmol) was added to refluxing propionic acid (300 mL). The mixture was refluxed for 30 minutes, allowed to cool to room temperature and obtained via vacuum filtration. The product collected was subsequently washed with ice cold methanol until washings were colourless.

Scheme 25 page 175
Scheme 26 page 176

Yield 2.45 g, 14% $^1$H NMR (CDCl$_3$, 400 MHz) $\delta_H$ 8.97 (s, 8H, pyrrolic β-C$\underline{H}$) 7.43 (d, 8H, phenylic $o$-C$\underline{H}$, J=2.0) 6.93 (t, 4H, phenylic $p$-C$\underline{H}$, J=2.0) 3.99 (s, 24H, OC$\underline{H}_3$) -2.80 (s, 2H, N$\underline{H}$) $^{13}$C NMR (CDCl$_3$, 400 MHz) $\delta_C$ 158.9, 114.0, 119.8, 113.8, 100.2, 55.3 FTIR (cm$^{-1}$) 1157 ES-MS 855 (MH$^+$) UV absorbance (CH$_3$OH) $\lambda_{max}$ (nm) 421, 515, 550, 589, 649.5

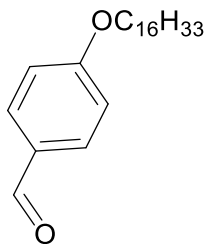### 5.8.3 Synthesis of 5, 10, 15, 20-tetrakis (3, 5-dihydroxyphenyl)-21H, 23H-porphyrin (119)



A round bottom flask was charged with 5, 10, 15, 20-tetrakis (3, 5-dimethoxyphenyl) porphyrin (300 mg, 0.35 mmol), anhydrous dichloromethane (10 mL) and degassed. Boron tribromide (1.14 mL, 11.83 mmol) was added via a syringe and the reaction mixture was gently stirred under nitrogen at room temperature for 5 hours. The reaction was then quenched carefully with distilled water (1.5 mL, 0.08 mol) and stirred further for a period of 20 minutes. The crude reaction mixture was then transferred to a separation funnel along with ethyl acetate and water, and neutralised with sodium hydrogen carbonate. The resulting insoluble impurities which formed at the solvent interface were removed by filtration of the entire solution. The organic layer was collected and the solvent was removed to yield the porphyrin.

Scheme 26 page 176

Yield 216 mg, 72%; $^1$H NMR (CD$_3$OD, 400 MHz) $\delta_H$ 9.03 (s, 8H, pyrrolic β-C$\underline{H}$) 7.20 (d, 8H, phenylic $o$-C$\underline{H}$, J=2.0) 6.76 (t, 4H phenylic $p$-C$\underline{H}$, J=2.0) $^{13}$C NMR (CD$_3$OD, 400 MHz) $\delta_C$ 156.5, 143.7, 120.0, 114.4, 101.8 FTIR (cm$^{-1}$) 3205 (O-H stretch) UV absorbance (CH$_3$OH) $\lambda_{max}$ (nm) 417.5, 513, 546.5, 587.5, 645 ES-MS 743 (MH$^+$)

## 5.9 Synthetic procedures for Colloidosome Catalysis
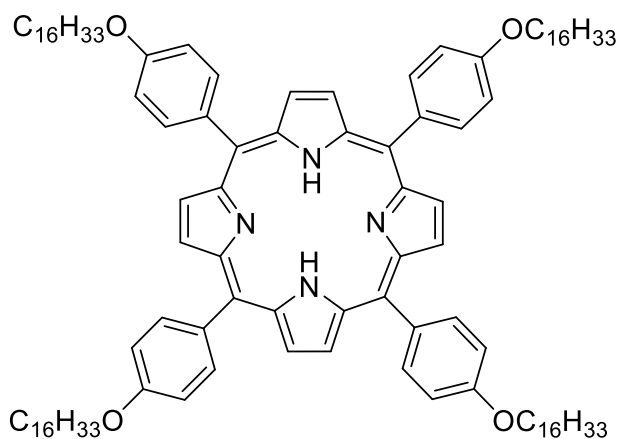### 5.9.1 Synthesis of 4-(hexadecyloxy) benzaldehyde via the Williamson reaction (135)

A mixture of bromohexadecane (5.50 g, 18.0 mmol), 4-hydroxybenzaldehyde (2.0 g, 16 mmol), potassium carbonate (2.72 g, 19.6 mmol) and a crystal of 18-crown-6 in anhydrous acetonitrile was refluxed for 3 days. The reaction mixture was concentrated in vacuo and the residue was dissolved in diethyl ether/water (1:1). The organic layer was washed three times with saturated aqueous sodium hydrogen carbonate, once with saturated brine solution and subsequently dried over magnesium sulphate. Evaporation of the solvent under vacuo affords the crude product. The product was purified by column chromatography and eluted with 20:1 petroleum ether 40-60: ethyl acetate. (Rf = 0.83,TLC was visualised using anisaldehyde staining).

Scheme 30 page 207
Figure 110 page 208
Scheme 32 page 211

Yield 3.26 g, 57% $^1$H NMR (CDCl$_3$, 400 MH$_z$) $\delta_H$ 9.86 (s, 1H, R-C$\underline{H}$O), 7.81 (d, 2H, phenylic $m$-C$\underline{H}$, J=9.0), 6.97 (d, 2H, phenylic $o$-C$\underline{H}$, J=9.0), 4.02 (t, 2H, OC$\underline{H}_2$C$_{15}$H$_{31}$, J=7.0), 1.80 (m, 2H, OCH$_2$C$\underline{H}_2$C$_{14}$H$_{29}$) 1.50-1.20 (bm, 26H, OCH$_2$CH$_2$C$_{14}$$\underline{H}_{26}$CH$_3$), 0.87 (t, 3H, OC$_{15}$H$_{30}$C$\underline{H}_3$, J=7.0); $^{13}$C NMR (CDCl$_3$, 400 MH$_z$) $\delta_C$ 190.8, 164.3, 132.0, 129.7, 114.7, 68.4, 32.0, 29.6, 29.4, 26.0, 22.7, 14.2, ) FTIR (cm$^{-1}$) 2916, 2848, 2738 (alkyl C-H stretch), 1683 (aldehyde C=O stretch), 1603, 1578, 1509, 1241 EA %: Carbon (Expected value: 79.71 %) Found: 79.42 % Hydrogen (Expected value: 11.05 %) Found: 11.38 % ES MS 347 (MH$^+$) m.p. 42-44 ˚C

### 5.9.2 Synthesis of 5, 10, 15, 20-Tetra(4-hexadececycloxyphenyl)porphyrin via the Lindsay method (137)

Boron trifluoride diethyl etherate (37.30 μl, 0.3 mmol) and a catalytic amount of anhydrous ethanol (1.95 mL, 30 mmol) were added to a solution of 4-hexadececycloxybenzaldehyde (1.05g, 3.0 mmol) and pyrrole (210.2 μL, 3.0 mmol) in anhydrous dichloromethane (300 mL, 4.68 mol, 15.6 mol/L) at room temperature under argon. The reaction mixture was then stirred for 1hr in an inert gas stream at room temperature; 2, 3-dichloro-5, 6-dicyano-1.4 benzoquinone (619.0 mg, 2.7 mmol) was added and the mixture was stirred for another 1hr. The reaction products were separated by flash chromatography and eluted with chloroform. The target product was purified by column chromatography and eluted with chloroform.

Scheme 32 page 211

Yield 1.27 g, 25 % $^1$H-NMR (CDCL$_3$, 400 MH$_Z$) $\delta_H$ 8.88 (s, 8H, pyrrolic β-$\underline{H}$), 8.14 (d, 8H, phenylic $o$-C$\underline{H}$ J=8.0), 7.30 (d, 8H, phenylic $m$-C$\underline{H}$ J=8.5), 4.30 (t, 8H, OC$\underline{H}_2$C$_{15}$H$_{31}$, J=6.0), 2.01 (bm, 8H, OCH$_2$C$\underline{H}_2$C$_{14}$H$_{29}$) 1.72-1.23 (bm, 104H, OCH$_2$CH$_2$C$_{14}$$\underline{H}_{26}$CH$_3$), 0.91 (t, 12H, OC$_{15}$H$_{30}$C$\underline{H}_3$, J=6.5), -2.72 (s, 2H, N$\underline{H}$), $^{13}$C-NMR (CDCL$_3$, 400 MH$_Z$) $\delta_C$ 159.0, 158.3, 144.1, 135.6, 134.6, 119.9, 114.3, 112.71, 100.9, 68.4, 32.0, 29.7, 29.4, 26.3, 22.7, 14.1 FTIR (cm$^{-1}$) 2918, 2850 (alkyl C-H stretch), 1509, 1241 EA %: Carbon (Expected value: 82.28 %) Found: 81.94 % Hydrogen (Expected value: 10.10 %) Found: 9.97 % Nitrogen (Expected value: 3.55 %) Found: 3.41 % MALDI TOFF MS 1575.4 (MH$^-$) UV absorbance (CHCl$_3$) $\lambda_{max}$ (nm) 423.0, 520.0, 557.0, 593.0, 651

### 5.9.3 Synthesis of 5, 10, 15, 20-Tetra(4-hexadececycloxyphenyl)porphyrin Iron(III) complex (132)
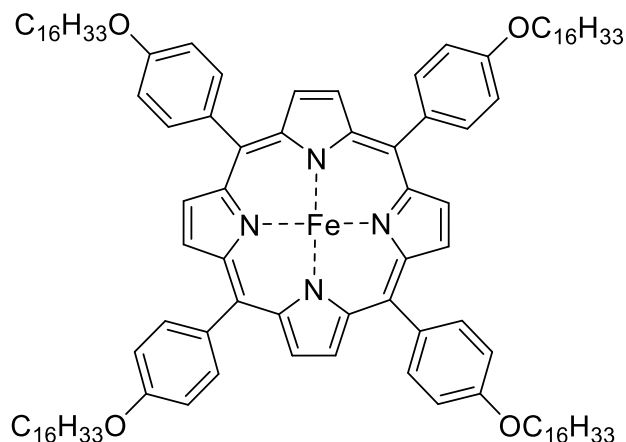


Figure 109 page 206
Scheme 32 page 211

5, 10, 15, 20-Tetra(4-hexadececycloxyphenyl)porphyrin (50 mg, $3.17\times10^{-2}$ mmol) was dissolved in THF (25 mL) with Iron (II) chloride (80.4 mg, 0.634 mmol) and 2, 6-lutidine (9.2 μL, $7.93\times10^{-2}$ mmol). The solution was warmed to 50 ℃ under reflux and stirred for 3 hours. Solvent was then removed via rotary evaporation and a 1:1 mix of chloroform and water was added to the flask. After vigorous shaking many insoluble impurities formed at the solvent interface and were removed via vacuum filtration. The organic layer was collected and solvent was removed via rotary evaporation and eluted through a silica column with 1:1 chloroform and methanol.

Yield 25 mg, 50 % FTIR (cm$^{-1}$) 2917, 2849 (alkyl C-H stretch), 1511 (aromatic C=C stretch), 1242 (C-O) MS-MALDI 1631(MH$^+$) UV absorbance (CHCl$_3$) λmax (nm) 412.0, 573.5, 616

### 5.9.4 Synthesis of Iodosylbenzene (140)
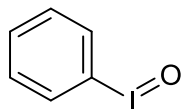


Scheme 33 page 215
Scheme 34 page 215
Scheme 39 page 225
Scheme 40 page 227

3M sodium hydroxide (15 mL) was added over 3 minutes to a beaker containing (Diacetoxyiodo) benzene (3.22 g, 0.01 mol) with vigorous stirring. The reaction was then left to stand for a period of 45 minutes. Distilled water (15 mL) was then added with continual stirring and the solid collected via vacuum filtration. The solid was then stirred in excess distilled water for a period of 30 minutes and the solid was collected. The final step of purification was performed by stirring the collected yellow solid in chloroform for a period of 30 minutes. The titled product was collected via vacuum filtration and dried in a vacuum desiccator.

Yield 1.47 g, 67 %, $^1$HNMR (CD$_3$OD, 400 MHz) δ$_H$ 8.05 (m, 2H, *Ar o*-C$\underline{H}$) 7.58 (m, 3H, *Ar p*-C$\underline{H}$, *Ar m*-C$\underline{H}$) $^{13}$CNMR (CDCl$_3$, 400 MHz) δ$_C$ 131.9, 130.8, 130.6 FTIR (cm$^{-1}$) 3038 (aromatic C-H stretch) 1566, 1434, 733, 689 ES-MS 220 (M$^+$) 205, 204 (M - O$^{2-}$) accurate mass spec: calculated mass 220.9463 formula: C$_6$H$_6$OI m.p. 211 ˚C (decomposed)

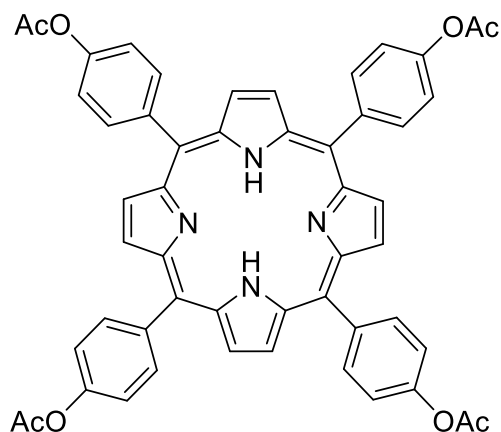### 5.9.5 Synthesis of 4-acetoxybenzaldehyde (147)
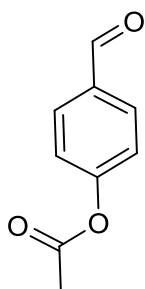


Scheme 35 page 217
Scheme 37 page 219

A round bottomed flask was charged with 4-hydroxybenzaldehyde (20.00 g, 167 mmol), triethylamine (30 mL), and anhydrous THF (600 mL). The flask was degassed with argon and stirred under a flow of nitrogen for 10 minutes before the addition of acetyl chloride (30 mL, 422 mmol) drop-wise via a syringe. The reaction mixture was then stirred for a period of 30 minutes. The white solid formed was filtered off via vacuum filtration and the brown filtrate was then reduced down using a rotary evaporator. The remaining brown oil was dissolved in dichloromethane (100 mL) and washed with saturated sodium hydrogen carbonate solution (200 mL), then distilled water (200 mL). The washing process was repeated; the organic layer was collected and dried over magnesium sulphate. Solvent removal yielded a brown oil.

Yield 16.42 g, 61 %, $^1$HNMR (CDCl$_3$, 400 MH$_Z$) $\delta_H$ 10.00 (s, 1H, CO$\underline{H}$) 7.94 (d, 2H, *Ar*-$\underline{H}$ J = 8.5) 7.30 (d, 2H, *Ar*-$\underline{H}$, J = 8.5) 2.36 (s, 3H, C$\underline{H_3}$) $^{13}$CNMR (CDCl$_3$, 400 MH$_Z$) $\delta_C$ 190.9, 168.7, 155.3, 134.0, 131.3, 122.37, 21.13 FTIR (cm$^{-1}$) 3072 (aromatic C-H stretch) 2830, 2743 (aldehyde C-H stretch) 1760 (ester C=O stretch) 1699 ( aldehyde C=O) 1595, 1156, 1187 ES-MS 165 (MH$^+$)

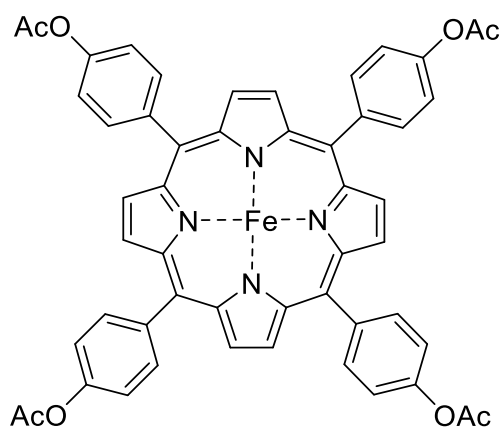### 5.9.6 Synthesis of 5, 10, 15, 20- tetrakis (4-acetoxyphenyl)-21H, 23H-porphyrin (149)



Freshly distilled pyrrole (5.54 mL, 80 mmol) and 4-acetoxybenzaldehyde (13.13 g, 80 mmol) were added to refluxing propionic acid (300 mL). The mixture was refluxed for 30 minutes and then allowed to cool to room temperature. The reaction mixture was filtered and washed with methanol until washings were colourless.

Scheme 37 page 219

Yield 4.27 g, 25 % $^1$HNMR (CDCl$_3$, 400 MH$_Z$) $\delta_H$ 8.93 (s, 8H, Pyrrolic β-$\underline{H}$) 8.25 (d, 8H, Phenylic *o*-C$\underline{H}$, J = 8.5) 7.54 (d, 8H, Phenylic *m*-C$\underline{H}$, J = 8.5) 2.53 (s, 12H, C$\underline{H_3}$) -2.79 (s, 2H, N$\underline{H}$) $^{13}$CNMR (CDCl$_3$, 400 MH$_Z$) $\delta_C$ 169.7, 150.6, 139.6, 135.4, 119.9, 119.3, 21.5 FTIR (cm$^{-1}$) 2925-3000 (aromatic C-H stretch) 1749 (ester C=O stretch) 1602 (NH bend) 1365, 1185, 1165 ES-MS 847 (M$^+$) UV absorbance (CHCl$_3$) $\lambda_{max}$ (nm) 418.0, 514.5, 549.5, 590.5, 646.0

**5.9.7 Synthesis of 5, 10, 15, 20-tetrakis(4-acetoxyphenyl)-porphyrin Iron(III) Complex (150)**



Scheme 37 page 219

5, 10, 15, 20- tetrakis (4-acetoxyphenyl)-21H, 23H-porphyrin (750 mg, 0.89 mmol) was added to a round bottomed flask equipped with a reflux condenser, evacuated and flushed with nitrogen. Anhydrous THF (80 mL) and 2, 6 lutidine (0.77 mL, 6.54 mmol) were added via syringe. Iron (II) chloride (1.12g, 13mmol) was added to the reaction flask and the solution was then refluxed for 4 hours. The solution was exposed to air as it was allowed to cool to room temperature. Unreacted Iron (II) chloride was removed via vacuum filtration and the crude product was dissolved in dichloromethane and washed with 1 M HCL followed by distilled water. Purification was performed by column chromatography with a solvent system of dichloromethane: methanol (75:25).

Yield 645 mg, 81% FTIR (cm$^{-1}$) 2918 (aromatic C-H stretch) 1753 (ester C=O) 119, 1163 (ester C-O stretch) 1603 (N-H bend), 1494, 1367 ES-MS 900 (MH$^+$) UV absorbance (CHCl$_3$) $\lambda_{max}$ (nm) 413.5, 566.5, 609.0

**5.9.8 General catalytic procedure (control reactions)**
In a typical experiment 0.1 mmol of iodosylbenzene was added to a reaction vial, which was sealed and degassed thoroughly using low vacuum/N$_2$. A 2 mL solution of the solvent (dichloromethane/Dodecane) containing both 1 mmol cyclooctene substrate and 2.5 μmol porphyrin containing catalyst was then added via syringe. The suspension was then stirred in the dark for a period of thirty minutes under an atmosphere of nitrogen. After completion, the suspension was filtered using a Whatman® GD/X syringe filter, with a pore size of 0.45 μm, and transferred into a GC vial for analysis via manual injection.

**5.9.9 General catalytic procedure – Colloidosome**
In a typical experiment 0.1 mmol of iodosylbenzene was added to a reaction vial, which was sealed and degassed thoroughly using low vacuum/N$_2$. A colloidosome was synthesised by the homogenisation of a 2 mL solution of the solvent (Dodecane) containing 1 mmol cyclooctene substrate, 8mg of PPG-TGI cross-linker and 2.5 μmol porphyrin containing catalyst and a 2 mL solution of the aqueous phase (1 wt. % aqueous solution of 125 nm PGMA$_{50}$-PS particles). Homogenisation took place for a period of 2 minutes at 12,000 rpm. The colloidosome was injected via a syringe and the suspension was then stirred in the dark for a period of thirty minutes under an atmosphere of nitrogen. After completion, the suspension was extracted using dichloromethane (5 mL) and the organic layer was collected and filtered using a Whatman® GD/X syringe filter with a pore size of 0.45 μm. The filtrate was transferred into a GC vial for analysis via manual injection.

*The PGMA$_{50}$ – PS particles were prepared by Dr Kate Kirkham and the procedures can be found in the literature.[270,271]

264